



# University of HUDDERSFIELD

## University of Huddersfield Repository

Elmekawy, Ahmed

Bifunctional supported catalysts for fine chemical synthesis

### Original Citation

Elmekawy, Ahmed (2014) Bifunctional supported catalysts for fine chemical synthesis. Doctoral thesis, University of Huddersfield.

This version is available at <http://eprints.hud.ac.uk/id/eprint/23325/>

The University Repository is a digital collection of the research output of the University, available on Open Access. Copyright and Moral Rights for the items on this site are retained by the individual author and/or other copyright owners. Users may access full items free of charge; copies of full text items generally can be reproduced, displayed or performed and given to third parties in any format or medium for personal research or study, educational or not-for-profit purposes without prior permission or charge, provided:

- The authors, title and full bibliographic details is credited in any copy;
- A hyperlink and/or URL is included for the original metadata page; and
- The content is not changed in any way.

For more information, including our policy and submission procedure, please contact the Repository Team at: [E.mailbox@hud.ac.uk](mailto:E.mailbox@hud.ac.uk).

<http://eprints.hud.ac.uk/>

# **Bifunctional Supported Catalysts for Fine Chemical Synthesis**

By

**Ahmed Abdalla Ahmed Elmekawy**



*University of*  
**HUDDERSFIELD**

A thesis submitted to the University of Huddersfield  
in partial fulfilment of the requirements for  
the degree of Doctor of Philosophy

May 2014

The Department of Chemical and Biological Sciences  
University of Huddersfield  
Queensgate  
Huddersfield HD1 3DH

# Dedication

“This dissertation is lovingly dedicated to my mother for her support, encouragement,  
and constant love throughout my life”.

# Acknowledgments

First and foremost, my sincere thanks go to Allah almighty through divine direction and inspiration which helped me to attain and accomplish this academic level. I wish to express my sincere appreciation and deepest gratitude to my supervisor and advisor, Professor Robert Brown, to whom I am indebted for his guidance, motivation and support throughout this study.

I would like to express my heartfelt thanks to all those individuals whose wisdom, support and encouragement made my work possible, including Dr Lisa Dawson, Dr Gareth Parkes, my friends in the research office and our research group.

Last, but not least, I gratefully acknowledge Huddersfield University's financial support for this work.

# Abstract

The objective was to prepare and optimise solid acid and solid base catalysts for liquid phase reactions. The approach has been to functionalize porous silica support materials with acid and base catalytic groups. Solid acid, solid base and bifunctional solid acid/base catalysts were studied. Evidence for acid-base cooperative catalytic mechanisms was found, suggesting that these bifunctional catalysts could show significant advantages over singly functionalized materials or mixtures thereof.

Silicas functionalized with tethered aminopropyl groups were prepared by both a grafting method and a sol-gel method. The solids were fully characterized and were tested in the nitroaldol condensation between nitromethane and benzaldehyde to afford nitrostyrene and the aldol reaction between 4-nitrobenzaldehyde and acetone to afford 4-(4-nitrophenyl)-4-hydroxy-2-butanone. The catalytic activities of these materials were found to be dependent on the dispersion and accessibilities of the active sites which, in turn, depend on the methods utilized for the catalyst preparation.

Solid acid catalysts were prepared by grafting silica with mercaptopropyl-trimethoxysilane (MPTS) followed by oxidation. The influence of the oxidation procedure on the acidity of the catalyst is described. The use of concentrated  $\text{HNO}_3$  optimizes the oxidation process and increases the concentration of active sites in comparison to  $\text{H}_2\text{O}_2$ . The activities of these catalysts were tested in the deacetalization of benzaldehyde dimethyl acetal to benzaldehyde.

The use of solid acid and solid base catalysts in the same system was examined, in a two-stage acid-catalyzed deacetalization and base-catalyzed Henry reaction.

Solid bifunctional acid-base catalysts were prepared by grafting on amorphous silica in two ways: 1) by grafting propylsulfonic acid and aminopropyl groups to the silica surface ( $\text{NH}_2\text{-SiO}_2\text{-SO}_3\text{H}$ ) and 2) by grafting aminopropyl groups and then partially neutralizing with phosphotungstic acid, relying on the  $\text{H}_2\text{PW}_{12}\text{O}_{40}^-$  ion for surface acidity ( $\text{NH}_2\text{-SiO}_2\text{-}$

$\text{NH}_3^+[\text{H}_2\text{PW}_{12}\text{O}_{40}]^-$ . These two bifunctional catalysts were compared with each other and with the singly functionalised catalysts described above. Surface acidities and basicities were characterized by adsorption calorimetry, using  $\text{SO}_2$  as a probe for surface basicity and  $\text{NH}_3$  for surface acidity. Catalytic activities were measured in the tandem deacetalization/Henry reaction described above, and in an aldol reaction in which a cooperative acid-base catalytic mechanism is thought to be effective. Overall  $\text{NH}_2\text{-SiO}_2\text{-SO}_3\text{H}$  catalysts showed higher concentrations and strengths of both acid and base sites, and higher activities. Both catalysts showed evidence of cooperative acid-base catalytic sites. Even in the deacetalization/Henry reaction, the bifunctional catalysts exhibited a catalytic advantage over physical mixtures of singly functionalized catalysts.

A further bifunctional acid-base catalyst was prepared and studied by tethering proline to silica. In this case, the catalyst was chiral and was tested in the asymmetric aldol reaction between acetone and 4-nitrobenzaldehyde. Grafting methods with and without protecting groups for the active sites on proline were investigated. Remarkably the optimised supported proline catalysts showed higher activities and higher enantioselectivities than proline in homogeneous solution, and showed minimal loss in activity with time. Both activity and enantioselectivity depended strongly on the nature of the reaction solvent.

## Table of contents

<b>Abstract.....</b>	<b>iii</b>
<b>Chapter 1 .....</b>	<b>1</b>
<b>Introduction.....</b>	<b>1</b>
1.1. Immobilized catalysts .....	2
1.2. Immobilization methods for hybrid catalysts .....	4
1.2.1. Immobilized catalysts: Adsorption .....	5
1.2.2. Immobilized catalysts: Entrapment.....	5
1.2.3. Immobilized catalysts: Direct Incorporation.....	6
1.2.4. Immobilized catalysts: Covalent grafting .....	6
1.3. Catalyst support materials.....	6
1.3.1. Non-ordered mesoporous silica gel.....	7
1.3.2. Ordered mesoporous MCM-41 silica.....	10
1.4. Cooperative catalysis .....	11
1.5. Heterogeneous cooperative catalysis in the literature .....	13
1.6. Catalytic reactions used to study the catalytic activity in this work.....	14
1.7. Thesis structure.....	15
1.8. Thesis goals .....	16
1.9. References.....	17
<b>Chapter 2 .....</b>	<b>19</b>
<b>Instrumental techniques (background theory) .....</b>	<b>19</b>
2. Introduction.....	20
2.1. Catalyst characterization.....	20
2.2. Powder X-Ray Diffraction (p-XRD) .....	21
2.3. Nitrogen Adsorption .....	23
2.4. Adsorption isotherm models.....	24

2.5.	Adsorption in pores.....	28
2.6.	Adsorption Calorimetry .....	29
2.6.1.	Measuring the heat of adsorption.....	31
2.6.2.	Types of Calorimeter .....	32
2.6.3.	Gases Used for Adsorption .....	32
2.6.4.	Adsorption Microcalorimetry Measurements .....	32
2.7.	High pressure liquid chromatography (HPLC).....	35
2.8.	Gas Chromatography (GC).....	35
2.9.	References.....	37
<b>Chapter 3</b>	<b>.....</b>	<b>38</b>
	<b>Cooperative acid-base catalysis using physical mixture of amine/sulfonic acid-functionalized silica.....</b>	<b>38</b>
3.	Introduction.....	39
3.1.	Acid catalysis.....	39
3.2.	Base catalysis.....	41
3.3.	Acid-base bifunctional catalysis .....	43
3.4.	Experimental.....	53
3.4.1.	Materials.....	53
3.4.2.	Activation of silica gel (SiO <sub>2</sub> ).....	53
3.4.3.	Synthesis of amorphous mesoporous silica base catalyst (SiO <sub>2</sub> -NH <sub>2</sub> ) .....	53
3.4.4.	Synthesis of silylated mesoporous silica base catalyst (SiO <sub>2</sub> -NH <sub>2</sub> -CH <sub>3</sub> ) .....	53
3.4.5.	Synthesis of supported propylsulfonic acid catalysts (SiO <sub>2</sub> -SO <sub>3</sub> H).....	54
3.4.6.	Synthesis of mesoporous ordered silica (MCM-41) .....	54
3.4.7.	Synthesis of MCM-41-NH <sub>2</sub> (G) by grafting method .....	54
3.4.8.	Direct synthesis of MCM-41-NH <sub>2</sub> (C) by co-condensation method.....	55
3.5.	Catalyst characterization.....	55
3.6.	Catalytic activity measurement.....	57
3.6.1.	Aldol reaction.....	57

3.6.2.	Deacetalization reaction and deacetalization-nitroaldol reaction .....	57
3.7.	Results and discussion .....	58
3.7.1.	Characterization of base catalysts .....	58
3.7.2.	Study of surface basicity by calorimetric adsorption of SO <sub>2</sub> .....	61
3.7.3.	Characterization of solid acid catalysts.....	62
3.8.	Catalytic activity of base catalysts.....	64
3.8.1.	Nitroaldol reaction (Henry reaction).....	64
3.8.2.	Activity of solid base catalyst (SiO <sub>2</sub> -NH <sub>2</sub> ) in repeat reactions .....	66
3.8.3.	Effect of acid treatment of SiO <sub>2</sub> on the activity of supported amine catalysts.....	67
3.8.4.	Effect of silanol groups on the catalytic activity of solid base catalysts.....	68
3.9.	Catalytic activity of acid catalysts .....	70
3.10.	Physical mixture of acid and base solid catalysts as bifunctional catalyst .....	71
3.11.	Conclusion .....	76
3.12.	References.....	79
<b>Chapter 4</b>	<b>.....</b>	<b>82</b>
<b>Co-operative acid base bifunctional catalyst.....</b>	<b>.....</b>	<b>82</b>
4.	Introduction.....	83
4.1.	Experimental Section.....	88
4.1.1.	Materials.....	88
4.2.	Catalyst synthesis.....	88
4.2.1.	Supported propylamine catalysts .....	88
4.2.2.	Supported propylsulfonic acid catalysts .....	88
4.2.3.	Supported propylsulfonic acid-propylamine bifunctional catalysts.....	89
4.2.4.	Simultaneous method.....	89
4.2.5.	Sequential methods .....	90
4.2.6.	Supported propylamine/phosphotungstic acid bifunctional catalysts .....	91
4.3.	Catalyst characterization.....	91
4.4.	Catalytic activities .....	92

4.4.1.	Nitroaldol (Henry) reaction.....	92
4.4.2.	One-pot deacetalization–Henry reaction.....	93
4.4.3.	Aldol condensation reaction.....	93
4.5.	Results and discussion .....	94
4.6.	Characterization of the silica structures.....	94
4.7.	Catalytic activity.....	103
4.7.1.	One-pot deacetalization–Henry reaction.....	103
4.7.1.1.	Silica-supported amine/sulphonic acid catalysts.....	103
4.7.1.2.	Silica-supported amine/phosphotungstic acid catalysts .....	105
4.8.	Aldol condensation catalytic activity.....	108
4.9.	Conclusion .....	110
4.10.	References.....	112
<b>Chapter 5 .....</b>		<b>114</b>
<b>Cooperative acid-base catalysis using amine/ carboxylic acid-functionalized silica with potential for chiral synthesis .....</b>		<b>114</b>
5.	Introduction.....	115
5.1.	Organocatalysis.....	116
5.2.	Proline as a powerful chiral catalyst.....	116
5.3.	Immobilization of proline .....	120
5.3.1.	Polymer-supported proline.....	121
5.3.2.	Silica-supported proline .....	123
5.4.	Experimental section .....	128
5.4.1.	Materials.....	128
5.4.2.	Synthesis of catalyst materials .....	129
5.4.3.	Chloropropyl functionalized silica gel (SiO <sub>2</sub> -Cl).....	129
5.4.4.	Proline-functionalized silica gel (SiO <sub>2</sub> -Pr) by direct route .....	129
5.4.5.	Proline-functionalized silica gel by amine protecting/deprotecting route ....	129

5.4.6. Proline-functionalized silica gel by both amine and carboxylic acid groups protecting/deprotecting route .....	130
5.4.7. Proline-functionalized MCM-41 silica by direct route (MCM-41-Pr) .....	130
5.5. Catalyst characterization:.....	130
5.6. Catalytic activities .....	131
5.6.1. Development of a suitable analytical method for reactants and products.....	132
5.7. Results and discussion .....	135
5.7.1. Characterization of L-proline functionalized silica materials.....	135
5.8. Catalytic activity.....	141
5.8.1. Supported-proline catalytic activity in polar aprotic solvent.....	146
5.8.2. Supported-proline catalytic activity with various aromatic aldehydes .....	146
5.9. Conclusion .....	147
5.10. References.....	148
<b>Chapter 6 .....</b>	<b>150</b>
<b>Summary and conclusion .....</b>	<b>150</b>
<b>Chapter 7 .....</b>	<b>154</b>
<b>Future consideration.....</b>	<b>154</b>
<b>Appendixes .....</b>	<b>156</b>

## List of figures

Figure 1.1 – Immobilization methods for hybrid catalysts: (a) adsorption, (b) entrapment, (c) covalent grafting and (d) encapsulation. ....	4
Figure 1.2 – Surface modification of silica oxide with alkoxy silanes .....	8
Figure 1.3 – Reaction of trimethoxysilanes with (a) one, (b) two, or (c) three surface hydroxyl groups .....	9
Figure 1.4 – Synthesis of MCM-41 mesoporous silica .....	10
Figure 2.1 – Powder x-ray diffraction, lattice planes. ....	22
Figure 2.2 – Typical powder x-ray diffraction pattern of MCM-41 .....	22
Figure 2.3 – Types of physisorption isotherms.....	23
Figure 2.4 – Nitrogen adsorption isotherm typical of that of mesoporous silica.....	28
Figure 2.5 – irreversible chemisorption and reversible physisorption.....	30
Figure 2.6 – Adsorption calorimetry: a typical heat signal recorded by a differential calorimeter as a series of pulses of probe gas is passed over the sample. ....	31
Figure 2.7 – An example of the heat signal obtained from the calorimeter (top) and the mass spectrometer signal obtained when probe gas (in this case ammonia). ....	34
Figure 3.1 – Acid and base groups shielded by star-shaped polymers for one-pot multistep catalysis. ....	46
Figure 3.2 – Individually recoverable acid and base catalysts for one-pot cascade reactions. ....	46
Figure 3.3 – Bifunctionalized mesoporous silica nanosphere (MSN) materials with ureidopropyl (udp) group, and 3-[2-(2-aminoethylamino)ethylamino]- propyl (aep) group. ....	50
Figure 3.4 – N <sub>2</sub> adsorption isotherms at 77 K for SiO <sub>2</sub> and SiO <sub>2</sub> -NH <sub>2</sub> and MCM-41, MCM-41-NH <sub>2</sub> (g) and MCM-41-NH <sub>2</sub> (c) .....	58
Figure 3.5 – XRG patterns of MCM-41, MCM-41-NH <sub>2</sub> (g), MCM-41-NH <sub>2</sub> (c) .....	60
Figure 3.6 – The FT-IR spectrum of SiO <sub>2</sub> -NH <sub>2</sub> (a) and MCM-41-NH <sub>2</sub> (g) (b).....	61
Figure 3.7 – $\Delta H^{\circ}_{ads}$ (SO <sub>2</sub> ) vs. Amount adsorbed at 120 °C.....	62

Figure 3.8 – $\Delta H^{\circ}_{ads}$ ( $\text{NH}_3$ ) vs. Amount adsorbed at 120 °C, for supported acid catalysts. .....	63
Figure 3.9 – Reactivity of nitromethane (5 mL) with benzaldehyde (1.0 mmol) over $\text{SiO}_2\text{-NH}_2$ , MCM-41- $\text{NH}_2$ (g) and MCM-41- $\text{NH}_2$ (c) (all with equivalent number of supported propylamine, 0.08 mmol) at 70 °C as a function of time.....	65
Figure 3.10 – Reactivity of nitromethane with benzaldehyde in the presence of nitrostyrene over $\text{SiO}_2\text{-NH}_2$ with repeated addition of the reactants. ....	66
Figure 3.11 – Activity of $\text{SiO}_2\text{-NH}_2$ in nitroaldol reaction at 50 °C.....	67
Figure 3.12 – Water sorption isotherm obtained at 298 K on $\text{SiO}_2$ , $\text{SiO}_2\text{-NH}_2$ and $\text{NH}_2\text{-SiO}_2\text{-CH}_3$ .....	68
Figure 3.13 – Activity of $\text{SiO}_2\text{-NH}_2$ (0.03 g) and $\text{NH}_2\text{-SiO}_2\text{-CH}_3$ (0.03 g) in nitroaldol reaction at 50 °C. ....	69
Figure 3.14 – Reactivity of $\text{SiO}_2\text{-SO}_3\text{H}$ [ $\text{HNO}_3$ ] and $\text{SiO}_2\text{-SO}_3\text{H}$ [ $\text{H}_2\text{O}_2$ ] in deacetalization of benzaldehyde dimethyl acetal reaction at 90°C for 2 hr.....	71
Figure 3.15 – Composition of the reaction mixture vs. time for the deacetalization-henry reaction, catalyzed by a physical mixture of $\text{SiO}_2\text{-SO}_3\text{H}$ (0.03 g) and $\text{SiO}_2\text{-NH}_2$ (0.03 g) at 90 °C. ....	72
Figure 3.16 – Composition of the reaction mixture vs. time for the deacetalization-henry reaction, catalyzed by a physical mixture of $\text{SiO}_2\text{-SO}_3\text{H}$ (0.03 g) and $\text{SiO}_2\text{-NH}_2$ (0.09 g) at 90 °C. ....	73
Figure 3.17 – Composition of the reaction mixture vs. time for the deacetalization-henry reaction, catalyzed by a physical mixture of $\text{SiO}_2\text{-SO}_3\text{H}$ (0.06 g) and $\text{SiO}_2\text{-NH}_2$ (0.03 g) at 90 °C. ....	73
Figure 3.18 – Composition of the reaction mixture vs. time for the deacetalization-henry reaction, catalyzed by physical mixtures of $\text{SiO}_2\text{-SO}_3\text{H}$ (0.03 g) and $\text{CH}_3\text{-SiO}_2\text{-NH}_2$ (0.03 g) at 90 °C.....	74
Figure 3.19 – Composition of the reaction mixture vs. time for the deacetalization-henry reaction, catalyzed by physical mixtures of $\text{SiO}_2\text{-SO}_3\text{H}$ (0.06 g) and $\text{CH}_3\text{-SiO}_2\text{-NH}_2$ (0.09 g).....	75
Figure 4.1 – $\text{N}_2$ adsorption–desorption isotherms at 77 K for $\text{SiO}_2$ , $\text{SiO}_2\text{-NH}_2$ , $\text{NH}_2\text{-SiO}_2\text{-SH}$ (sequential) and $\text{NH}_2\text{-SiO}_2\text{-SO}_3\text{H}$ (sequential). ....	94
Figure 4.2 – $\text{N}_2$ adsorption–desorption isotherms at standard temperature of catalysts ( $\text{SiO}_2\text{-NH}_2$ , $\text{NH}_2\text{-SiO}_2\text{-PTA}$ 0.1 and $\text{NH}_2\text{-SiO}_2\text{-PTA}$ 0.5.....	95

Figure 4.3 – $^{13}\text{C}$ CP mas nmr spectra of silica catalysts bearing a) aminopropyl groups, b) aminopropyl and mercaptopropyl groups and c) aminopropyl and mercaptopropyl groups following nitric acid oxidation.....	98
Figure 4.4 – $^{31}\text{P}$ mas-nmr spectrum of $\text{NH}_2\text{-SiO}_2\text{-NH}_3^+[\text{H}_2\text{PW}_{12}\text{O}_{40}^-]$ (0.9). ....	99
Figure 4.5 – a) $\Delta\text{H}^\circ_{\text{ads}}$ ( $\text{SO}_2$ ) vs. amount adsorbed at 120 °C and b) $\Delta\text{H}^\circ_{\text{ads}}$ ( $\text{NH}_3$ ) vs. Amount adsorbed at 120 °C, for supported catalysts.....	100
Figure 4.6 – IR spectra of samples $\text{SiO}_2$ (black line), $\text{SiO}_2\text{-NH}_2$ (green line), $\text{NH}_2\text{-SiO}_2\text{-SH}$ (sequential) (blue line) and $\text{NH}_2\text{-SiO}_2\text{-SO}_3\text{H}$ (red line). ....	102
Figure 4.7 – Composition of the reaction mixture versus time for the deacetalization Henry reaction between benzaldehyde dimethyl acetal and nitromethane at 90 °C to form nitrostyrene, catalyzed by a) $\text{NH}_2\text{-SiO}_2\text{-SO}_3\text{H}$ (sequential) and b) $\text{NH}_2\text{-SiO}_2\text{-SO}_3\text{H}$ (simultaneous).....	104
Figure 4.8 – Composition of the reaction mixture versus time for the deacetalization-Henry reaction between benzaldehyde dimethyl acetal and nitromethane at 90 °C to form nitrostyrene, catalyzed by a physical mixture of $\text{SiO}_2\text{-SO}_3\text{H}$ and $\text{SiO}_2\text{-NH}_2$ . ....	105
Figure 4.9 – Composition of the reaction mixture vs. time for the reaction between benzaldehyde dimethyl acetal (1) and water to form benzaldehyde (2) and the subsequent reaction with nitromethane to form nitrostyrene (3), catalyzed by $\text{NH}_2\text{-SiO}_2\text{-PTA}$ with acid/amine ratios of 0.9, 0.5, 0.1 and 0.05 at 90 °C .....	106
Figure 4.10 – Proposed catalytic cycle for aldol condensation. ....	110
Figure 5.1 – Structure of the bifunctional organocatalyst l-proline.....	116
Figure 5.2 – Structures of polymer-supported proline.....	122
Figure 5.3 – Structure of MCM-41 supported proline.....	123
Figure 5.6 – Standard HPLC chromatogram with the components deriving from a cross-aldol reaction between 4-nitro-benzaldehyde and acetone plus the internal standard (i.s). . .....	133
Figure 5.7 – Chiral HPLC chromatogram of hydroxyl aldol product (B) deriving from a cross-aldol reaction between 4-nitro-benzaldehyde and acetone in presence of $\text{SiO}_2\text{-Pr}$ (h). Standard HPLC chromatograms of  B as racemic mixture. ....	134
Figure 5.8 – X-ray diffraction pattern of MCM-41, MCM-41-Cl and MCM-41-Pr. ....	135
Figure 5.9 – $\text{N}_2$ adsorption–desorption isotherms at 77 K for MCM-41, MCM-41-Cl and MCM-41-Pr (a) and $\text{SiO}_2$ (l), $\text{SiO}_2\text{-Cl}$ (l), $\text{SiO}_2\text{-Pr}$ (l), $\text{SiO}_2\text{-Pr-boc}$ and $\text{SiO}_2\text{-Pr-boc,me}$ (b). ....	136

Figure 5.10 – TGA-curves of hybrid silica samples with different organic groups in nitrogen atmosphere.....	138
Figure 5.11 – FT-IR spectra of hybrid silica samples.....	140
Figure 5.12– Comparison of aldol reaction of the studied catalysts over time .....	141
Figure 5.13 – First-order kinetic model of aldol reaction for the studied catalysts.....	142
Figure 5.14 – Simplified representation of the competition between the silanol and COOH groups. ....	144

## List of schemes

Scheme 1.1 – Synthesis of polysilicic acid.....	7
Scheme 1.2 – Dehydration of n-butanol via “concerted mechanism” .....	11
Scheme 1.3 – Tsuji–trost reaction via “concerted mechanism” .....	12
Scheme 1.4 – Tandem deacetalization-henry reaction. ....	12
Scheme 1.5 – Tandem deacetalization-henry reaction. ....	14
Scheme 1.6 – Aldol condensation: a = 4-nitrobenzaldehyde; b = 4-hydroxy-4-(p-nitrophenyl)butan-2-one; c = 4-(4-nitrophenyl)but-3-en-2-one. ....	15
Scheme 3.1 – “One-pot” synthesis of dual-functionalized mesoporous catalyst sba-15-acid/base. ....	47
Scheme 3.2 – Synthesis of mesoporous materials with acid and base sites. <sup>[67]</sup> .....	48
Scheme 3.3 – Syntheses of bifunctional mesoporous silica nanoparticles having sulfonic acid groups on the internal surface and organic amine groups on the external surface.....	49
Scheme 3.4 – Synthesis of bifunctional mesoporous catalysts with grafted amino and phosphotungstic acid moieties.....	51
Scheme 3.5 – Imine catalytic mechanism for henry reaction catalyzed by amines on silica .....	70
Scheme 3.6 – Tandem deacetalization-henry reaction. ....	72
Scheme 4.1 – NH <sub>2</sub> -SiO <sub>2</sub> -SO <sub>3</sub> H and NH <sub>2</sub> -SiO <sub>2</sub> -PTA bifunctional catalysts. ....	83
Scheme 4.2 – Tandem deacetalization-henry reaction. ....	85
Scheme 4.3 – Cross-aldol reaction between 4-nitrobenzaldehyde (a) and acetone to give 4-hydroxy-4-(p-nitrophenyl)butan-2-one (b) and (e)-4-(4-nitrophenyl)but-3-en-2-one (c) products. ....	85
Scheme 4.4 – Reaction mechanism for base-catalyzed aldol reaction. ....	85
Scheme 4.5 – Reaction mechanism for base-catalyzed aldol reaction. ....	86
Scheme 4.6 – Synthesis of supported base catalyst. ....	88
Scheme 4.7 – Synthesis of supported acid catalyst.....	89
Scheme 4.8 – Synthesis of acid-base bifunctional catalyst by the simultaneous method. 90	

Scheme 4.9 – Synthesis of acid-base bifunctional catalyst by the sequential method. ....	90
Scheme 4.10 – Synthesis of acid-base bifunctional catalyst by the partial neutralization method. ....	91
Scheme 5.1 – Proposed mechanism of the proline-catalyzed asymmetric aldol reaction... ..	117
Scheme 5.2 – First proline-catalyzed intramolecular aldol reaction.....	118
Scheme 5.3 – Preparation of polystyrene-supported hydroxyproline.....	122
Scheme 5.4 – Direct aldol reaction of acetone with aromatic aldehydes using mcm-41-pro.....	124
Scheme 5.5 – Preparation of porous sba-15-proline.....	125
Scheme 5.6 – Preparation of porous silica-supported proline .....	127
Scheme 5.7 – Cross-aldol reaction between 4-nitrobenzaldehyde (a) and acetone to give the aldol addition (b) and aldol condensation (c) products. ....	128

## List of tables

Table 3.1 – Materials of solid base catalysts .....	42
Table 3.2 – Textural parameters and level of functionalization for supported base catalysts. ....	59
Table 3.3 – Textural parameters and level of functionalization for supported acid catalysts. ....	63
Table 3.4 – Summary calorimetric NH <sub>3</sub> adsorption data.....	64
Table 3.5 – One-pot deacetalization–Henry reaction over different catalysts.....	76
Table 4.1 – Textural parameters for supported acid, supported base and amine/sulfonic acid samples.....	94
Table 4.2 – Textural parameters for supported amine and supported amine/phosphotungestic acid catalysts.....	95
Table 4.3 – Elemental analysis data for supported amine, supported sulfonic acid and bifunctional catalysts. ....	96
Table 4.4 – Summary calorimetric SO <sub>2</sub> adsorption data.....	103
Table 4.5 – Catalytic activities in the aldol condensation between 4-nitrobenzaldehyde (A) and acetone to form 4-hydroxy-4-(p-nitrophenyl)butan-2-one (B) and 4-(4-nitrophenyl)but-3-en-2-one (C). ....	108
Table 5.1 – Enantioselective aldol reaction catalyzed by L-proline, between acetone and a variety of aldehydes.....	119
Table 5.2 – Amino acid derivatives tested as catalysts for the asymmetric aldol reaction of acetone with 4-nitrobenzaldehyde.....	120
Table 5.3 – Textural parameters for studied catalysts. ....	137
Table 5.4. TGA and elemental analysis for the synthesized materials. ....	139
Table 5.5 – Pseudo-first-order rate constant the studied catalysts at pseudo-first-order condition aldol condensation reaction. ....	142
Table 5.6 – Catalytic activities in the aldol condensation between 4-nitrobenzaldehyde and acetone. ....	143
Table 5.7 – Catalytic activities in the aldol condensation between 4-nitrobenzaldehyde and acetone in DMSO at room temperature. ....	146

Table 5.8 – Catalytic activities in the aldol condensation between acetone and a range of aldehydes. .... 147

## LIST OF SYMBOLS AND ABBREVIATIONS

SiO<sub>2</sub> - Silica gel

MCM-41 - Mobil researchers, hexagonally ordered mesoporous oxide molecular sieve

SBA-15 - Stucky et al, hexagonally ordered mesoporous material

HMS - Pinnavaia et al, hexagonally ordered mesoporous silicas

MPTMS - 3-mercaptopropyltrimethoxysilane

C16TAB - hexadecyltrimethylammonium

TEOS - tetraethoxysilane

H<sub>2</sub>O<sub>2</sub> - hydrogen peroxide

MeOH - methanol

EtOH - ethanol

H<sub>2</sub>O - water

N<sub>2</sub> - nitrogen

HCl - Hydrochloric acid

NaOH - sodium hydroxide

NH<sub>3</sub> - ammonia

SO<sub>2</sub> - Sulfur dioxide

ATR - Attenuated Total Reflectance

BJH - Barret Joyner Halenda

BET - Brunauer Emmett Teller

DVS - Dynamic Vapour Sorption

FTIR - Fourier Transform Infra Red

GC - Gas Chromatography

HPLC - High-performance liquid chromatography

XRD - X-ray Diffraction

# Chapter 1

## Introduction

---

In this chapter, the background and the objectives of this research are described. The structure of this thesis and a brief overview of individual chapters are also summarized.

### 1.1. Immobilized catalysts

Catalysis study is a core aspect of chemical engineering. Prior to the design of any industrial process, the catalytic requirement must be examined.<sup>[1]</sup> The choice of catalyst has major ramifications for reactor design and product purification steps.<sup>[1]</sup> Even minor changes to the catalyst can have consequences for an overall process. Hence, researchers in industry and academia are continuously seeking innovative catalysts and new methods of altering the performance of current catalysts.<sup>[2-3]</sup>

Homogeneous catalysts are those used in the same phase as the reactants. Broadly, this applies to either liquid or soluble solid catalysts in a liquid solution. Examples include the mineral acids and bases that are used extensively in industry.<sup>[4]</sup> In contrast, heterogeneous catalysts exist in a different phase to the reactants. These are usually solid catalysts in liquid or gas phase reactants. An everyday example may be found in the catalytic converters of automobiles. Platinum alloys convert pollutants in the exhaust to more benign compounds, drastically reducing emissions of harmful pollutants into the environment.<sup>[5]</sup> Heterogeneous catalysis has secured Nobel prizes for Fritz Haber and Carl Bosch in 1918, Irving Langmuir in 1932, Ziegler and Natta in 1963, and Gerhard Ertl in 2007.<sup>[6-7]</sup>

Homogeneous and heterogeneous catalysts each have advantages and disadvantages. Homogeneous catalysts are usually single-sited, with a single, specific site on which the catalysis occurs. By applying advanced synthesis methods and characterization techniques, these catalysts can be designed to be highly active and selective for a particular reaction. Selectivity in catalysis can be observed in nature through cellular enzymes. Enzymes show high specificities to reactants consumed and products formed within a cell, even in the presence of all other cellular components. Although synthetic, non-biological catalysts seldom reproduce the selectivity and specificity of enzymatic biocatalysts, enzyme performance serves as a motivation for homogeneous catalyst design.<sup>[8-9]</sup> Regardless of the high activity and selectivity possessed by homogeneous catalysts, their use in industry has been troubled by the difficulty of separation from the

final product.<sup>[10]</sup> From an economic and environmental point of view, it is often very important to recover and recycle the catalysts, especially in the case of expensive and/or toxic transition metal catalysts.<sup>[11]</sup> For instance, in the pharmaceuticals industry, where homogeneous organometallic catalysts are used to synthesize some chiral chemicals, removal of the metals to ppm levels is of vital importance for product purity, as specified by the United States Food and Drug Administration.<sup>[12]</sup> However, in many other cases, the catalyst is never recovered, either because the catalyst is extremely active or because only small concentrations are required (as can be the case of olefin polymerization catalysts)<sup>[13]</sup> or because it is simply cheaper to use the catalyst once rather than to separate and recover it (as can be the case with mineral acid/base catalysts).<sup>[14]</sup>

In contrast, heterogeneous catalysts are multi-sited catalysts that exist in a different phase from the reaction medium. Multi-sited catalysts may have several different chemical environments on the surface of the material, which promote activity.<sup>[14]</sup> These catalysts tend to be less active and less selective than homogeneous catalysts. However, the majority of industrial-scale catalysts are heterogeneous because they can easily be reused in continuous processes.<sup>[15]</sup> Therefore, heterogeneous catalysis is considered green. Against this, many solid catalysts require the use of homogeneous catalysts, reagents and high calcination temperatures for their synthesis, all factors that detract from their environmental attractiveness.<sup>[16]</sup>

An alternative way of making it easier to separate catalysts from a reaction mixture is through immobilization of organic catalysts on solid supports. There are many ways of immobilizing a homogeneous catalyst on an insoluble support. These include polymer encapsulation,<sup>[17]</sup> covalent tethering to a polymer backbone,<sup>[18]</sup> and covalently tethering to an inorganic framework such as silica to form an organic/inorganic hybrid material.<sup>[19]</sup> The last case is advantageous because of the low cost and thermal stability of silica materials and the wide variety of low-cost organosilanes available for covalent surface modification. More recently, materials such as nylon have been used as supports for organic catalysts.<sup>[20]</sup> The behavior of organic groups tethered to the surface are similar to their behavior when they are used in solution, but the factors controlling surface reactions

apply, such as diffusion of reactants towards the surface, migration of the reactants to the active catalytic sites and desorption of products from the surface. Understanding these principles, along with the organic chemistry of the tethered groups, is necessary to design supported catalysts of that type. There are innumerable reports in the literature of functionalizing silica materials with a single organic functionality for use in catalysis. The most common groups used for this purpose are acids and bases, although more complex molecules such as cinchona alkaloids<sup>[21]</sup> or enzymes have also been immobilized on silica for use in heterogeneous catalysis.<sup>[22]</sup> In some instances, the heterogeneous catalyst outperforms its homogeneous analogue, due either to solid/liquid partitioning which concentrates reactants near the catalytic sites, to interactions with the support, or to other concentration-dependent effects linked to the concentration of the active catalytic sites on a two-dimensional surface.

## 1.2. Immobilization methods for hybrid catalysts

A number of methods may be used to immobilize catalysts to form hybrid materials (Figure 1.1). The specific reaction conditions may dictate which method is best suited to the particular circumstance.

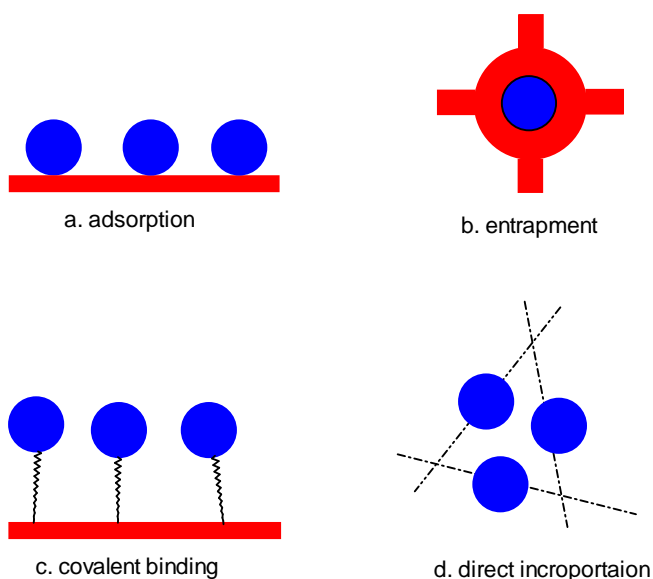


Figure 1.1 – Immobilization methods for hybrid catalysts: (a) adsorption, (b) entrapment, (c) covalent grafting and (d) encapsulation.

### 1.2.1. Immobilized catalysts: Adsorption

The simplest method of immobilizing homogeneous catalysts on solid supports involves adsorption of the homogeneous catalyst onto a solid support. This type of catalyst is created by first synthesizing the solid support and then contacting it with the catalyst. The catalyst can be weakly bound via physisorption or more strongly bound via electrostatic interactions or metal coordination. In all cases, there is no covalent linkage between the support and the catalyst. As such, these materials are prone to leaching and may be restricted to mild reaction conditions.<sup>[23]</sup>

### 1.2.2. Immobilized catalysts: Entrapment

A second immobilization method involves encapsulation of the catalyst and requires no bonding between the catalyst and support. Two types of encapsulated catalysts commonly appear. The first involves synthesis of the support material with the catalyst present in the reaction mixture. Two examples include sol-gel and polymeric materials. In either case, the polymerizable unit (commonly alkoxysilanes or sodium silicates with sol-gels or olefins or other polymerizable monomers in the case of polymers) and catalyst are mixed together in one pot while the solid support forms. Catalyst selection is limited to those that can survive the support synthesis conditions.<sup>[23]</sup> These materials may also be prone to leaching as the sol-gel or polymer may be subject to swelling in certain solvents. The active catalyst may diffuse out of the swollen solid support. This swelling can also be problematic in fixed volume reactors.

A second type of encapsulated catalyst utilizes a ship-in-the-bottle synthesis.<sup>[23]</sup> A rigid, microporous support is synthesized first, generally zeolites or MCM-type materials. The solid support is then impregnated with catalyst precursors by diffusion into the porous network. The catalyst is then “assembled” from the precursors within the network. If the catalyst is larger than the pore channels, it cannot diffuse out of the support, and is entrapped within the solid matrix. These materials also present disadvantages, including decreased activities due to slow molecular diffusion of reactants and products into and out of the porous solid and, often, low catalyst loadings.

### 1.2.3. Immobilized catalysts: Direct Incorporation

The third common type of hybrid catalyst incorporates the active catalyst directly within the support framework. These can be polymeric<sup>[24]</sup> or silica-based<sup>[25]</sup>. Like sol-gel or polymer-encapsulated materials, the catalyst and polymerizable monomers are combined together in the support synthesis. However, in this case, the catalyst contains a polymerizable unit as well. When the support forms, the catalyst site is directly incorporated into the solid structure.<sup>[25]</sup> The resulting catalyst can be more stable than the previous two types due to the covalent linkage to the support. In addition, ordered materials can be created through use of structure-directing agents during the synthesis, as is the case with pre-modified mesoporous silicas. Non-ordered directly incorporated catalysts such as sol-gel silicas or polymers can be subject to solvent swelling/shrinkage. However, they are less prone to leaching due to the covalent linkage to the support, unlike encapsulated or adsorbed catalysts where no covalent bonding is present.

### 1.2.4. Immobilized catalysts: Covalent grafting

The fourth and most common type of hybrid catalyst utilizes covalent grafting to immobilize single-sited catalysts on insoluble, solid supports. In this technique, the solid support is synthesized, and the surface is modified with chemical functional groups. Using this method, the catalyst may be immobilized in one step or in a step-by-step fashion as commonly utilized in solid phase synthesis.<sup>[26]</sup> Since the catalyst and support are synthesized in different steps, the catalyst choice is not limited by the reaction conditions of the solid support synthesis. The covalent nature of the bonding between the support and the catalyst can generate a more stable catalyst and may prevent leaching. Due to these positive attributes, the majority of the work in this thesis will focus on this covalent grafting method to generate immobilized catalysts. A range of organic grafted silica gel catalysts have been prepared, characterized, and tested.

## 1.3. Catalyst support materials

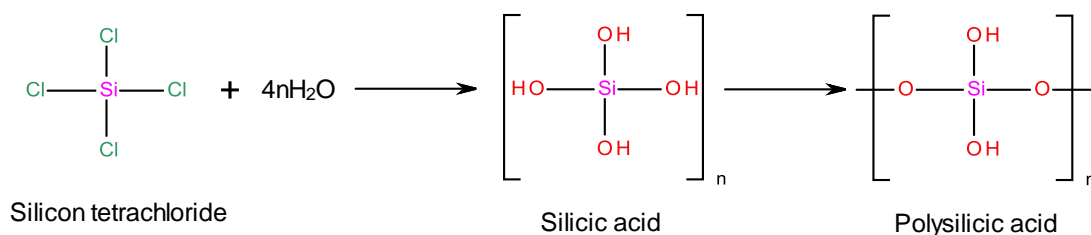
Covalent grafting of homogeneous catalyst analogues on solid supports offers numerous possibilities in terms of flexibility for a wide range of synthesis and/or reaction conditions. Consequently, a discussion on the various support materials that may be used is presented here. Although post-grafting techniques are possible on organic polymeric

supports (such as Wang resins),<sup>[27]</sup> this introduction will primarily focus on the most common inorganic oxide support (porous silica) due to its high thermal, chemical, and mechanical stability.

### 1.3.1. Non-ordered mesoporous silica gel

The usual form of silica is a tetrahedral structure in which four oxygen atoms surround each silicon atom. Usually, silica appears in nature as a crystalline phase, which is present in plants such as rice, bamboo and barley, and in minerals such as quartz. However, the majority of the silica used in chemical applications has a synthetic source.<sup>[28]</sup> Synthesized silica is usually in an amorphous form. Porous amorphous silica provides a large surface which lends it superiority over crystalline counterparts for chemical and physical applications.

Amorphous silica is usually formed as silica gel. The formation involves two main steps: formation of a wet gel, then drying the wet gel to generate numerous forms of silica. Wet gels can be produced by the aqueous condensation of sodium silicate, or perhaps, analogous materials. Though this method works well, the reaction produces salts inside the gel which need to be removed by repeated rinsing of the material, which is a very long, time-consuming procedure.<sup>[29]</sup> Silica gel, a polysilicic acid, can be made when silicon tetrachloride is hydrolyzed (Scheme 1.1).<sup>[29]</sup>



**Scheme 1.1** – Synthesis of polysilicic acid

The polysilicic acid condenses further to form a cross-linked gel. Alkoxysilanes such as  $\text{Si}(\text{OR})_4$  can also be used where R is  $\text{CH}_3$ ,  $\text{C}_2\text{H}_5$  or  $\text{C}_3\text{H}_7$ . However, several other alkoxides, with various organic functional groups, can often provide altered properties to the gel. The advantage of using alkoxide-based sol-gel chemistry is that it reduces the possibility of formation of unfavorable salt by-products. In addition, it permits a high

degree of control over the final products. The gel is referred to as hydrogel or alcogel if an alcohol has been used as the solvent.<sup>[30]</sup> The nature of the gel and the solid silica formed from it is controlled by temperature, the pH of the reaction medium, the nature of the solvent and any present electrolyte, as well as the starting materials.<sup>[31]</sup> Control of pore size, pore volume, and specific surface area can be obtained through these variables.<sup>[31-32]</sup>

The surface chemistry of silica gel was studied by Hofmann<sup>[33]</sup>, Kiselev<sup>[34]</sup> and Carman<sup>[35]</sup>. They showed that hydroxyl (silanol) groups, Si-OH, are present on the surface. Yaroslavsky<sup>[36]</sup> proved for the first time the existence of hydroxyl groups on the silica surface (porous glass) by infrared spectroscopy. The acidic nature of the silanol groups is responsible for the adsorption properties of these materials and is exploited for the chemical modifications in several different fields including catalysis. The enhanced acidity of silica surface gives it a high degree of chemical reactivity; thus, it can react with many coupling agents to immobilize organo-functionalized alkoxy silanes (Figure 1.2),

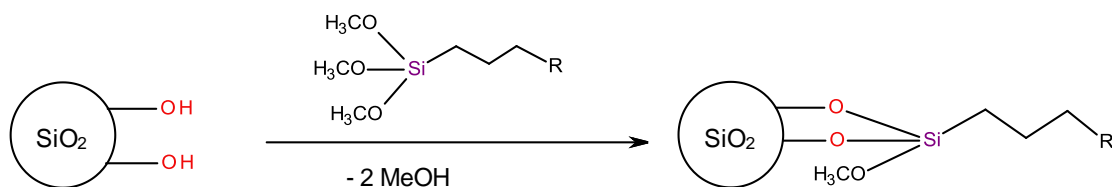


**Figure 1.2** – Surface modification of silica oxide with alkoxy silanes

This reaction generally uses methoxy or ethoxy silanes, as C<sub>3</sub> or higher alkoxy groups tend to be less reactive due to their increased bulkiness. This reaction forms a covalent Si-O-Si bond between the solid support and functional group. The functional group on the alkoxy silane can be any number of chemically reactive species. Common commercially available examples include amines, alcohols, carbonyls, halogens, thiols, olefins, etc.

Reaction of typical trialkoxysilanes with solid supports can result in the condensation of one, two, or three surface hydroxyl groups (Figure 1.3).

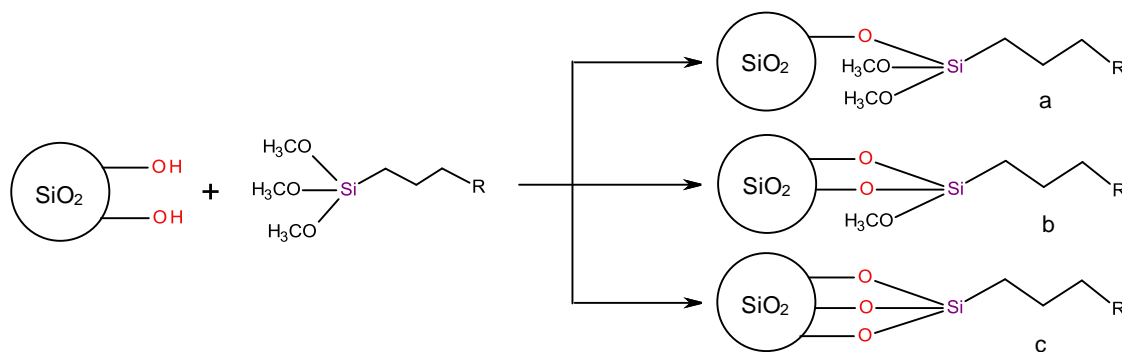


**Figure 1.3** – Reaction of trimethoxysilanes with (a) one, (b) two, or (c) three surface hydroxyl groups

It has been found that if water is present during the reaction, it can hydrolyze the alkoxy groups of the silane, forming hydroxyl groups. These hydroxyl groups can react with other alkoxy silanes, thus forming multi-layers of functional groups instead of monolayers of functional groups. Depending on the user's desire for a material with higher loading and less uniform surface coverage, or a material with lower loading and a better-defined monolayer coverage, water may or may not be included in the grafting procedure. Should monolayer coverage be desired, the inorganic oxide must be pre-dried at a high temperature to remove all water, as these materials tend to be highly hygroscopic.

Finally, silica-immobilized organic materials have certain advantages:

- The physical rigidity of their structures;
- Negligible swelling in both aqueous and organic solutions;
- High biodegradation, photochemical and thermal stability;
- Slower poisoning by irreversible side reactions;
- Readily modified by a variety of functional groups.

However, there are some notable drawbacks of silica-immobilized organic materials such as leaching of the functional groups from the support surface into the solution upon treatment with acidic solutions, as the surface bonds are hydrolyzed.

### 1.3.2. Ordered mesoporous MCM-41 silica

In 1992, the synthesis of a new family of silicate mesoporous molecular sieves, denoted as M41S, was reported. MCM-41, which stands for Mobil Composition of Materials number 41, is one member of this family; it has uniform hexagonal pores and is produced using rod-like micelles of cationic surfactant molecules as a template (Figure 1.4). The pore size of MCM-41 can be varied from 2 to 10 nm depending on the template used in the synthesis process. According to the definition of the International Union of Pure and Applied Chemistry (IUPAC), mesoporous materials are those that have pore diameters between 2 and 50 nm. Therefore, MCM-41 is considered to be within the mesoporous category. A full review of this material can be found in the literature.<sup>[37]</sup> Due to the highly porous nature of the material, surface areas in excess of 800 m<sup>2</sup>/g can be achieved. This material makes a promising catalyst support due to its high surface area for chemical modifications, its thermal and structural stability, its well defined and characterized nature, and its chemical inertness to most reaction conditions.<sup>[38]</sup>

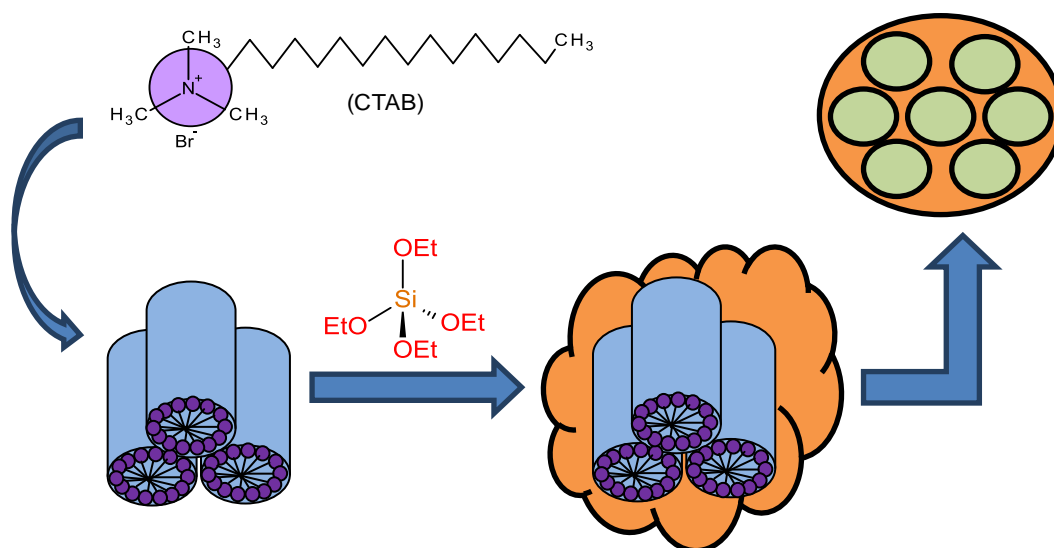


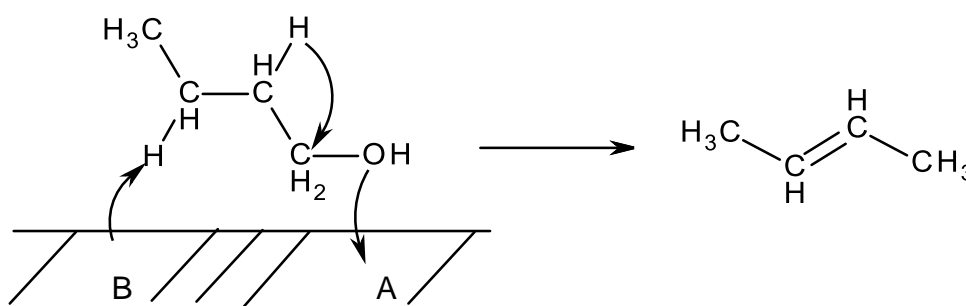
**Figure 1.4** – Synthesis of MCM-41 mesoporous silica

In aqueous solution, a surfactant such as hexadecyltrimethylammonium (C<sub>16</sub>TAB) and dodecyltrimethylammonium ions are used as a structure-directing agent (Typically, the bromide salts are dissolved to form micelles). In fact, the micelle formation in this synthesis is thought to occur at unexpectedly low surfactant concentration.

Tetraethylorthosilicate (TEOS) is added to the solution, which polymerizes around the organic micelles forming the pore walls of the material. After filtration and washing, the material is calcined to combust the organic structure-directing agent, leaving the mesoporous MCM-41 silica. The MCM-41 can now be reacted with alkoxy silanes to covalently graft surface functional groups as seen in Figure 1.4. MCM-41 is utilized in Chapters 3 and 5 as a catalyst support for propylaminesilane and L-proline catalysts.<sup>[37-38]</sup>

#### 1.4. Cooperative catalysis

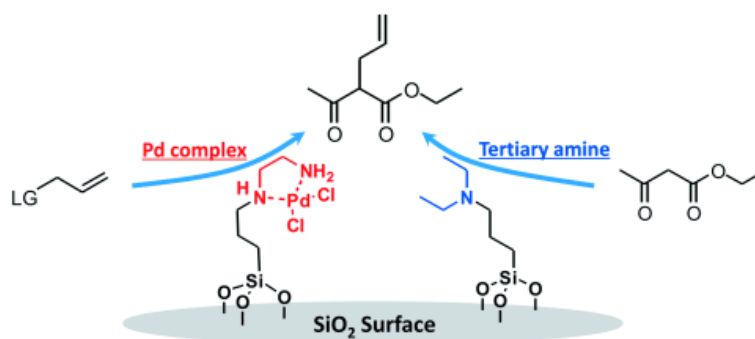
While catalysts functionalized with a single functional group are sufficient for many purposes, bifunctionalized materials allow for cooperative catalysis between the two different functionalities. Cooperative catalysis in this thesis is categorized into two types depending on whether the interaction of the two different functional groups with the substrate takes place simultaneously or successively. In simultaneous cooperative catalysis, the two functional groups act together to increase the rate of a reaction beyond the sum of the rates achievable from the individual functional groups alone. Simultaneous cooperative catalysis can be further divided into two types. One type involves the two functional groups interacting simultaneously with one molecule at different positions. The dehydration of 1-butanol on Na-doped alumina is an example of a reaction involving a concerted mechanism. An acid and a base site simultaneously activate the alcohol (Scheme 1.2).



**Scheme 1.2** – Dehydration of n-butanol via “concerted mechanism”

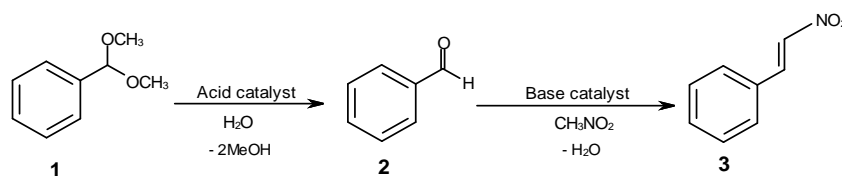
The other type is where one functional group interacts with one substrate molecule and the other functional group interacts with a second substrate molecule. Both interactions

occur simultaneously but independently. The substrate activated by one functional group reacts with the substrate activated by the other functional group. The synergistic catalysis by a Pd complex and an organic amine on a silica surface for the acceleration of the Tsuji–Trost reaction is a typical example of a reaction involving this type of interaction. The Tsuji–Trost reaction proceeds in the presence of a Pd species and a base. The role of the base is as an electron donor for the activation of the nucleophile (R-H) to enhance addition to the  $\eta^3$ -allylpalladium species (Scheme 1-3).<sup>[39]</sup>



**Scheme 1.3** – Tsuji–Trost reaction via “concerted mechanism” (LG is a leaving group).<sup>[39]</sup>

In successive cooperative catalysis, one functional group interacts with a substrate to form an intermediate which successively interacts with the other functional group to form another intermediate or final product. A good example of cooperative catalysis can be found in the deacetalization of benzaldehyde dimethyl acetal to benzaldehyde by acid sites. Then benzaldehyde reacts with nitromethane in the presence of base sites to form nitrostyrene. Each site has its own role in the independent reaction step (Scheme 1-4).



**Scheme 1.4** – Tandem deacetalization-Henry reaction.

Binding two, or more, catalysts to the same support raises several questions. Will each catalyst react as it does individually or will the catalysts interfere with one another? Can

such systems be recycled? Where catalysts do react or interfere with each other, can this be avoided by anchoring in such a way that contact between them is prevented? Finally, will one catalyst intervene in the reaction path, or be destroyed by the reaction which the second catalyst promotes? There are a number of important design parameters which must be investigated. Of primary importance is the identity of the different functional groups. Once a set of two or more cooperating functional groups is chosen for a given reaction, the second design parameter is the arrangement of these groups on the surface of the catalyst. The first of these challenges has its foundation in homogeneous catalysis, in which combinatorial approaches are well suited to finding combinations of catalysts which are effective at catalyzing a given reaction. Most of the reported examples of cooperative heterogeneous catalysis utilize a set of functional groups determined by solution-phase experiments.

The second of these challenges, the effect of the type and positioning of cooperative functional groups, is unique to heterogeneous catalysis. In solution, there is no well-defined arrangement; the reacting molecules are constantly diffusing and rearranging, and at any given time there is a broad distribution of distances. On the surface of a solid catalyst particle, on the other hand, the catalytic species are fixed locally with respect to the surface and to one another. In order to determine the ideal way to obtain the maximum efficiency of the cooperating groups, one must first devise a synthetic methodology by which to produce the right arrangement of functional groups on the surface. Second, one must be able to vary this arrangement methodically. This dissertation is primarily focused on describing new methods of generating paired bifunctional surfaces and studying their catalytic behavior.

### **1.5. Heterogeneous cooperative catalysis in the literature**

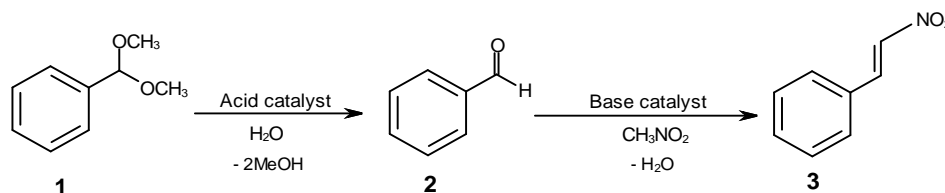
There have been several reports of bifunctional catalysts in which cross-linked polymers have been decorated with two different types of functionalities and used as a cooperative catalyst. The cross-linking eliminates catalyst solubility but still allows the flexible catalyst particles to swell and change shape in different solvents. To avoid this, most heterogeneous cooperative organocatalysts reported in the literature use some form of

silica as a rigid insoluble support.<sup>[40]</sup> These include acid/thiol bifunctionalized mesoporous silica for bisphenol A synthesis and aldol catalysts containing amine and urea groups or acid and base groups.<sup>[41]</sup> The first report in which two antagonistic functional groups were grafted onto a silica surface was published by Davis in 2006.<sup>[40]</sup> A critical review of acid-base bifunctional catalysts is presented in Chapter 3.

In this dissertation, the synthesis and catalytic activity of hybrid inorganic/organic mesoporous silica catalysts functionalized with pairs of acid and base groups are reported. The activity of the paired catalysts is compared to that of catalysts in which the two groups are immobilized on different surfaces. In some instances, the method of grafting these two groups in the paired catalysts is varied, thus providing an insight into the dependence of the catalytic reaction on the methodology used to create the cooperating catalytic moieties.

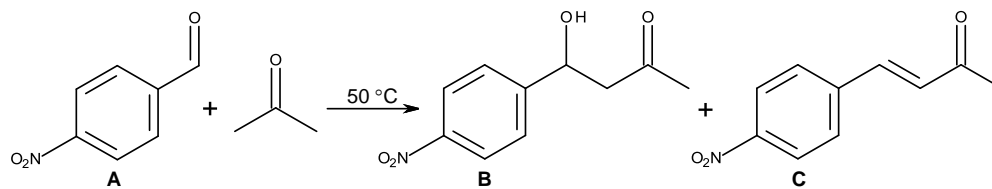
### 1.6. Catalytic reactions used to study the catalytic activity in this work

As test reactions for bifunctional cooperative catalysis, two test reactions were chosen, each with literature precedents for bifunctional cooperativity. The first, the tandem deacetalization-Henry reaction shown in Scheme 1.5, is a two-step reaction requiring first acid and then base catalysis. The first step is the acid-catalyzed deacetalization of benzaldehyde dimethyl acetal in the presence of water, to give benzaldehyde. The benzaldehyde then reacts with nitromethane in a base-catalyzed step, giving nitrostyrene.



**Scheme 1.5** – Tandem deacetalization-Henry reaction.

The second test reaction (Scheme 1.6) is the Aldol condensation between 4-nitrobenzaldehyde and acetone to produce 4-hydroxy-4-(p-nitrophenyl)butan-2-one (product B).



**Scheme 1.6** – Aldol condensation: A = 4-nitrobenzaldehyde; B = 4-hydroxy-4-(p-nitrophenyl)butan-2-one; C = 4-(4-nitrophenyl)but-3-en-2-one.

This reaction can proceed by the conventional base-catalyzed mechanism in which alpha hydrogen is abstracted from the ketone, but it is thought that the simultaneous activation of the aldehyde by a neighbouring acid site increases the reaction rate.<sup>[42-43]</sup> It therefore provides a test for the proximity of the acid and base catalytic sites.<sup>[42, 44]</sup> The subsequent dehydration of B to form 4-(4-nitrophenyl) but-3-en-2-one (product C) is acid-catalyzed and therefore not dependent on acid/base cooperativity. Kinetic selectivity to B over C can therefore be regarded as an indicator of the presence of catalytic acid-base pairs.<sup>[45]</sup>

### 1.7. Thesis structure

This report is divided into seven chapters. Chapter 1, the introduction, explains the background of the study, the literature review, the report structure and the research objectives. In chapter 2, the characterization methods used in this thesis are explained. In chapter 3, different routes to preparing monofunctional supported acid and supported base catalysts are reported and the activities of the resultant catalysts are tested. Then physical mixtures of acid and base catalyst are prepared and tested in the deacetalization-Henry reaction and compared. In chapter 4, supported bifunctional acid-base catalysts are prepared and compared with one another along with the physical mixtures described in chapter 3. All types of bifunctional acid-base catalysts in this chapter are tested in cooperative catalytic mechanisms in which acid and base sites act in concert (aldol condensation) and in successive cooperative reactions (the tandem deacetalization-Henry reaction). The relationships between catalyst composition and activity are used to optimize catalytic performance. This study highlights the potential benefits in overall activity, for some reactions at least, achievable through supporting acidic and basic functional groups on the same support. In chapter 5, acid-base bifunctional catalysts with chiral potential are prepared where L-proline is grafted on silica support. This study

shows that some grafting methods result in heterogeneous catalysts with activity similar to the homogeneous L-proline and in some cases higher when large surface area with large pore size mesoporous silica is used as a support. The enantioselectivities of the catalysts were also measured along with the solvent effect. Chapter 6 summarizes the overall results, and chapter 7 offers recommendations for future work.

### **1.8. Thesis goals**

The project is aimed directly at reducing the environmental impact of the chemical syntheses that are currently used in industry. The challenge is to develop solid catalysts with activities sufficiently high to make them viable alternatives to liquid catalysts. This will have to be achieved if the chemical industry is to consider replacing liquid with solid catalysts. The research described above provides an innovative way of increasing the relative activity of solid catalysts for this purpose and is therefore of immediate interest to the chemical industry.

The overall theme is the development of novel hybrid organic/inorganic bifunctional catalysts for the synthesis of chemicals relevant to the fine chemical and pharmaceutical industries. They are designed to catalyze two rather than one chemical process. In order to do this, the surfaces of the solid catalysts are designed to hold two types of catalytic centre. The two types, an acidic and a basic centre, are often antagonistic; therefore, a specific goal is to graft acidic and basic groups onto the same porous silica support material in such a way that the acidic and basic properties are retained.

## 1.9. References

- [1] D. Richard, D. Schweich, M. A. Al Sawah, C. de Bellefon, *Comptes Rendus Chimie* **2010**, *13*, 488-493.
- [2] Z. Liu, Y. Wang, Z. Xie, *Chinese Journal of Catalysis* **2012**, *33*, 22-38.
- [3] A. T. Bell, *Chemical Engineering Science* **1990**, *45*, 2013-2026.
- [4] E. G. Garrido-Ramírez, B. K. G. Theng, M. L. Mora, *Applied Clay Science* **2010**, *47*, 182-192.
- [5] D. N. Belton, K. C. Taylor, *Current Opinion in Solid State and Materials Science* **1999**, *4*, 97-102.
- [6] C. T. Campbell, *Surface Science* **2007**, *601*, ix.
- [7] J. Ross, *Applied Catalysis A: General* **1992**, *92*, N3-N4.
- [8] R. Breslow, *Science* **1982**, *218*, 532-537.
- [9] J. A. Gladysz, *Chemical Reviews* **2002**, *102*, 3215-3216.
- [10] R. Mat, R. A. Samsudin, M. Mohamed, A. Johari, *Bulletin of Chemical Reaction Engineering and Catalysis* **2012**, *7*, 142-149.
- [11] D. J. Cole-Hamilton, *Science* **2003**, *299*, 1702-1706.
- [12] A. Thayer, *Chemical & Engineering News* **2005**, *83*, 55-58.
- [13] X. J. Yin, S. L. Lu, *Xiandai Huagong/Modern Chemical Industry* **2013**, *33*, 9-13.
- [14] D. Rosenthal, *Physica Status Solidi (A) Applications and Materials Science* **2011**, *208*, 1217-1222.
- [15] I. Fecheté, Y. Wang, J. C. Védrine, *Catalysis Today* **2012**, *189*, 2-27.
- [16] A. Shanaghi, *Surface Review and Letters* **2012**, *19*.
- [17] W. F. Liu, Z. X. Guo, J. Yu, *Gaofenzi Cailiao Kexue Yu Gongcheng/Polymeric Materials Science and Engineering* **2009**, *25*, 67-70.
- [18] Y. Xiao, D. Chen, N. Ma, Z. Hou, M. Hu, C. Wang, W. Wang, *RSC Advances* **2013**, *3*, 21544-21551.
- [19] X. S. Zhao, X. Y. Bao, W. Guo, F. Y. Lee, *Materials Today* **2006**, *9*, 32-39.
- [20] J.-W. Lee, T. Mayer-Gall, K. Opwis, C. E. Song, J. S. Gutmann, B. List, *Science* **2013**, *341*, 1225-1229.
- [21] K. M. Kacprzak, N. M. Maier, W. Lindner, *Tetrahedron Letters* **2006**, *47*, 8721-8726.
- [22] D. Moelans, P. Cool, J. Baeyens, E. F. Vansant, *Catalysis Communications* **2005**, *6*, 307-311.
- [23] P. McMorn, G. J. Hutchings, *Chemical Society Reviews* **2004**, *33*, 108-122.
- [24] P. Mastrolilli, C. F. Nobile, *Coordination Chemistry Reviews* **2004**, *248*, 377-395.
- [25] F. Hoffmann, M. Cornelius, J. Morell, M. Fröba, *Angewandte Chemie International Edition* **2006**, *45*, 3216-3251.
- [26] A. Bhattacharya, B. N. Misra, *Progress in Polymer Science* **2004**, *29*, 767-814.
- [27] H. J. Lee, B. Ramaraj, S. M. Lee, K. R. Yoon, *Journal of Polymer Science Part A: Polymer Chemistry* **2008**, *46*, 1178-1184.
- [28] in *Studies in Surface Science and Catalysis, Vol. Volume 93* (Eds.: P. V. D. V. E.F. Vansant, K. C. Vrancken), Elsevier, **1995**, pp. 3-30.
- [29] I. M. El-Nahhal, N. M. El-Ashgar, *Journal of Organometallic Chemistry* **2007**, *692*, 2861-2886.
- [30] V. A. Fenelonov, V. Y. Gavrillov, L. G. Simonova, in *Studies in Surface Science and Catalysis, Vol. Volume 16* (Eds.: P. G. G. Poncelet, P. A. Jacobs), Elsevier, **1983**, pp. 665-674.
- [31] B. Handy, K. L. Walther, A. Wokaun, A. Baiker, in *Studies in Surface Science and Catalysis, Vol. Volume 63* (Eds.: P. A. J. P. G. G. Poncelet, B. Delmon), Elsevier, **1991**, pp. 239-246.
- [32] J. Limpo, M. C. Bautista, J. Rubio, J. L. Oteo, in *Studies in Surface Science and Catalysis, Vol. Volume 87* (Eds.: F. R.-R. K. S. W. S. J. Rouquerol, K. K. Unger), Elsevier, **1994**, pp. 429-437.
- [33] U. Hofmann, K. Endell, D. Wilm, *Angewandte Chemie* **1934**, *47*, 539-547.
- [34] A. V. Kiselev, *Kolloidn. Zh.* **1936**, *2*, 17-26.
- [35] P. C. Carman, *Transactions of the Faraday Society* **1940**, *36*, 964-973.
- [36] N. G. Yaroslavsky, A. N. Terenin, *Dokl. Akad. Nauk SSSR* **1949**, *66*.
- [37] X. S. Zhao, G. Q. Lu, G. J. Millar, *Industrial & Engineering Chemistry Research* **1996**, *35*, 2075-2090.
- [38] D. J. Macquarrie, D. B. Jackson, B. L. King, A. Watson, in *Studies in Surface Science and Catalysis, Vol. Volume 142* (Eds.: G. G. R. Aiello, F. Testa), Elsevier, **2002**, pp. 1125-1132.
- [39] H. Noda, K. Motokura, A. Miyaji, T. Baba, *Angewandte Chemie International Edition* **2012**, *51*, 8017-8020.

- [40] R. K. Zeidan, S.-J. Hwang, M. E. Davis, *Angewandte Chemie* **2006**, *118*, 6480-6483.
- [41] D. Das, J.-F. Lee, S. Cheng, *Journal of Catalysis* **2004**, *223*, 152-160.
- [42] S. L. Hruby, B. H. Shanks, *Journal of Catalysis* **2009**, *263*, 181-188.
- [43] R. K. Zeidan, M. E. Davis, *Journal of Catalysis* **2007**, *247*, 379-382.
- [44] F. Shang, J. Sun, S. Wu, H. Liu, J. Guan, Q. Kan, *Journal of Colloid and Interface Science* **2011**, *355*, 190-197.
- [45] X. Yu, Y. Zou, S. Wu, H. Liu, J. Guan, Q. Kan, *Materials Research Bulletin* **2011**, *46*, 951-957.

## Chapter 2

# Instrumental techniques (background theory)

---

In this chapter, the techniques used to characterize and test the catalysts are covered.

## 2. Introduction

The main goal of this chapter is to show the physical techniques applied in this work to characterize solid materials. The first goal is to establish the identity card of the material, including its structure, morphology, porosity, and chemical composition, while the second is to obtain the characteristics of the surface related to its reactivity (nature and number of surface sites).

### 2.1. Catalyst characterization

The characterization methods used in this thesis are explained. Nitrogen adsorption measurements were performed to determine porosities and surface areas. Powder X-ray diffraction (p-XRD) was used to confirm crystal structures for some catalysts studied. Elemental analysis (C, H, N and S) was used to estimate the loading of active sites on the catalyst surface. Dynamic vapour sorption (DVS) was used to investigate the hydrophilicity and hydrophobicity character of the catalysts. Flow adsorption microcalorimetry was used to determine the number and strength of surface basic and acid sites.  $^{13}\text{C}$  and  $^{31}\text{P}$  magic angle spinning NMR was used to investigate the nature of organic groups on the surface of the catalyst. Infra-red spectroscopy was used to confirm the presence of functional organic groups on the catalyst surface. Gas chromatography (GC) was used to monitor reaction rates by quantitative analysis of reactants and products in the deacetalization-Henry reaction. Gas chromatography-Mass spectrometry (GC-MS) was used to confirm the final product in the deacetalization-Henry reaction. High-pressure liquid chromatography (HPLC) reverse and normal phase were used to monitor the aldol condensation reaction and estimate the enantioselectivity of the catalysts.  $^1\text{H}$  NMR spectroscopy was used to confirm the aldol condensation reaction products. It is worth mentioning that, in some techniques such as HPLC and flow adsorption microcalorimetry, the development of a suitable method and validation was a time-consuming process requiring extensive laboratory work. Moreover, as far as we are aware, there are not any previously reported data on flow adsorption microcalorimetry analysis of antagonistic organic groups grafted on the same solid support. In the following sections, the theory and the applied methods of the major techniques used in this work are covered.

## 2.2. Powder X-Ray Diffraction (p-XRD)

Powder X-Ray Diffraction (p-XRD) has been used to characterize some catalysts in this thesis when the ordered mesoporous silica (MCM-41) was used as support. p-XRD was discovered in 1912 by Laue, Friederich and Knipping and later developed by W. H. Bragg and W. L. Bragg.<sup>[1-2]</sup>

A monochromatic beam of x-rays can be diffracted by atoms in a crystal. The angle at which intense reflections are detected is governed by interferences between x-ray beams reflected by adjacent planes of atoms in the crystal. From these angles, the spacing between the various planes of atoms can be determined. Diffraction patterns (intensity of reflections vs.  $2\theta$ , where  $\theta$  is both the incident and reflected angle between the x-ray beam and the planes of the atoms) recorded for individual crystalline materials can be interpreted in terms of the crystal structure of the material.

Reflected x-rays from a set of planes interfere constructively when the Bragg condition is met, (Equation 2.1 and Figure 2.1).

$$n\lambda = 2d_{hkl} \sin \theta \quad \text{Equation 2.1}$$

Where  $d$  is the spacing between the planes,  $\theta$  the angle between both incident and reflected beams and the plane, and  $n$  is an integer, the order of reflection.  $h$ ,  $k$  and  $\ell$  are Miller indices associated with the set of planes in the basis of the reciprocal lattice vectors.

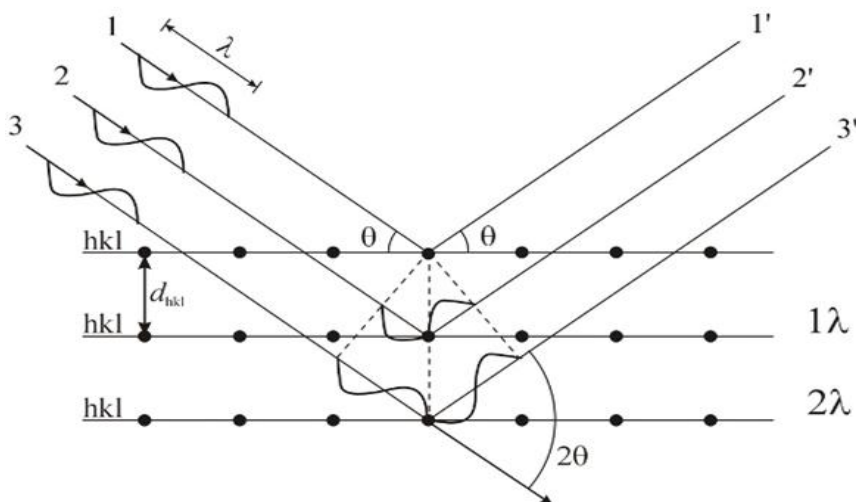


**Figure 2.1** – Powder X-ray diffraction, lattice planes.

There are many sets of planes of atoms in a crystal that give rise to diffraction. Each set of planes is defined by Miller indices,  $h$ ,  $k$  and  $l$ . These relate how planes intersect the three axes,  $x$ ,  $y$  and  $z$  relative to the dimensions of the crystal unit cell. Diffraction patterns recorded from powdered (polycrystalline) samples contain less information than those collected from single crystals but sometimes give information on specific lattice spacings which help characterize the powdered material. Powder XRD patterns are routinely used to fingerprint crystal structures. The p-XRD pattern of a typical MCM-41 is quite characteristic and can be seen in Figure 2.2.

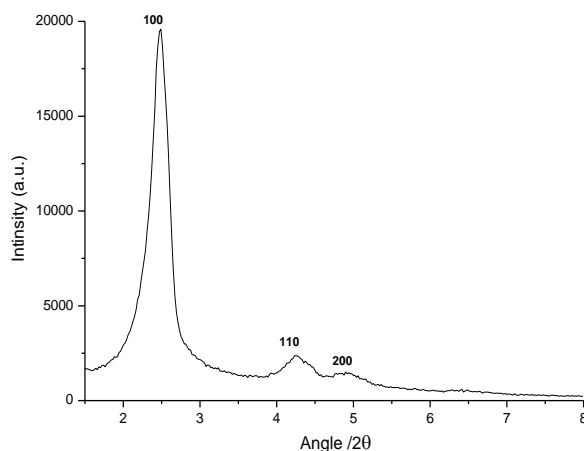


**Figure 2.2** – Typical powder X-ray diffraction pattern of MCM-41

Generally, the typical powder X-ray diffraction pattern of MCM-41 with long-range order shows three peaks that can be indexed on a hexagonal unit cell to (100), (110) and (200) by analogy with literature reports.<sup>[3]</sup> The level of crystallization of MCM-41 can be judged through the diffraction intensities of these peaks. The more highly is the ordered hexagonal structure, the higher the intensities.

### 2.3. Nitrogen Adsorption

By using the adsorption of an inert gas onto a solid surface we can calculate the surface area of the solid. Typically, nitrogen is used as an adsorbate, and an adsorption isotherm is generated by measuring the amount of nitrogen adsorbed by a solid as a function of the pressure of nitrogen in equilibrium with the solid. The pressure is conventionally expressed as  $P/P_0$  where  $P$  is the pressure of nitrogen and  $P_0$  is the saturated vapour pressure at the adsorption temperature. Adsorption isotherms are normally reported over  $P/P_0$  range of zero to 1.0. With nitrogen, adsorption isotherms are usually collected at 77 K when the saturated vapour pressure  $P_0$  is 1.0 atmosphere.

Adsorption of a gas onto a solid can be either via van der Waals (physical) or covalent (chemical) interactions. There are six identified types of adsorption isotherm that are classified in terms of the nature (porosity) of the adsorbent (Figure 2.3).

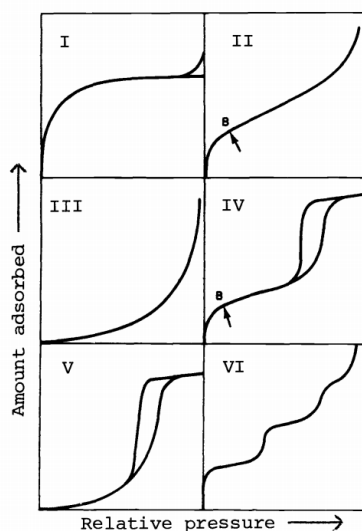


**Figure 2.3** – Types of physisorption isotherms.<sup>[4]</sup>

Type I isotherms are apparent when a monolayer forms on the surface. It is typically observed for microporous adsorbents (where pore widths do not exceed 2 nm). The adsorption takes place at relatively low pressure and the isotherm flattens off when a monolayer of adsorbate forms, only rising again when  $P/P_0$  approaches 1.0 and condensation occurs. Type II isotherms are typical of non-porous (or macroporous) solids for which multilayer adsorption occurs. Type III isotherms do not show any point at which a monolayer is formed. These are seen when the heat of adsorption is less than that of liquefaction. This type of isotherm is very uncommon. The type IV isotherm is characteristic of mesoporous solids (pore widths 2 nm – 50 nm). Hysteresis loops are apparent because the capillary condensation that occurs in mesoporous solids is not replicated at the same pressures during the desorption process. Pores appear to fill at higher pressure during adsorption and then at lower pressure during desorption. Type IV isotherms are initially similar to type I isotherms as a monolayer is formed but gradually multilayer formation can be seen as the pores fill up. Type V isotherms are not common and are obtained when there is very little interaction between the adsorbent and the adsorbate. Type VI isotherms are also uncommon because the sites involved are usually non-uniform in size and energetics. The steps that are seen in this isotherm show that there are groups of different sized pores.

#### 2.4. Adsorption isotherm models

The simplest model for the adsorption process of gas molecules onto a surface was derived by Langmuir in 1918.<sup>[5]</sup> This model assumes the following:

- Adsorption cannot form more than one molecular layer on the surface.
- All adsorption sites are uniform and equivalent.
- The probability of a site adsorbing a molecule is the same, irrespective of whether the adjacent sites are vacant or not.
- Every adsorption site can accommodate only one molecule of adsorbate.
- Molecules of the adsorbate do not interact with one another.

- Equilibrium is achieved between the rate at which species adsorb and desorb from the surface.

Hence, adsorption is a dynamic process. The Langmuir isotherm equation can be derived by looking at the processes of adsorption and desorption of a gas on a uniform solid surface. At equilibrium, the rate of adsorption is equal to the rate of desorption. The rate of adsorption of gas A on the surface is proportional to the pressure of gas and the concentration of vacant sites, expressed as the fraction of sites on the surface that are available for adsorption (when  $\Theta$  = the fraction of surface sites occupied by gas A), (Equation 2.3).

$$rate_{ads} = k_{ads} P_A (1 - \Theta) \quad \text{Equation 2.3}$$

The rate of desorption of gas A is proportional to the concentration of sites occupied by gas A on the surface, expressed as the fractional coverage of gas A on the surface  $\Theta$ , (Equation 2.4).

$$rate_{des} = k_{des} \Theta \quad \text{Equation 2.4}$$

At equilibrium:

$$k_{ads} P_A (1 - \Theta) = k_{des} \Theta \quad \text{Equation 2.5}$$

Therefore:

$$\frac{k_{des}}{k_{ads}} = \frac{P_A (1 - \Theta)}{\Theta} \quad \text{Equation 2.6}$$

If “b” is defined as  $k_{ads}/k_{des}$  then from Equation 2.6 it can be shown that:

$$\Theta = \frac{bP}{1+bP} \quad \text{Equation 2.7}$$

Now,  $\Theta = V/V_m$ , where  $V$  is the volume of gas A (at STP) adsorbed at equilibrium and  $V_m$  is the volume of gas required to complete a monolayer of A on the surface of the adsorbent, so:

$$\frac{V}{V_m} = \frac{bP}{1+bP} \quad \text{Equation 2.8}$$

We can rearrange this equation:

$$\frac{P}{V} = \frac{1}{bV_m} + \frac{P}{V_m} \quad \text{Equation 2.9}$$

Therefore, if Langmuir's model isotherm is obeyed, a plot of  $P/V$  against  $P$  over the equilibrium pressure range studied will give a straight line. The intercept will be equal to  $1/bV_m$  with a gradient of  $1/V_m$ . If the surface area occupied by one molecule of the adsorbate is known then the volume  $V_m$  can be used to calculate the surface area of the solid. The value of  $b$  gives an indication of the "strength" of the adsorption of gas A on the surface. If  $V_m$  is the volume of gas at STP required to form a monolayer on the sample used (of known weight),  $N_A$  is Avogadro's number and  $\sigma$  is the cross-sectional area of one molecule of adsorbant, in this case  $N_2$  ( $1.6 \text{ nm}^2$ ), the surface area of the surface sample ( $S$ ) is given by:

$$S = \frac{101325}{8.314 \times 298} V_m \times N_A \times \sigma \quad \text{Equation 2.10}$$

The assumptions made by Langmuir are not appropriate for many porous materials and there have been several attempts to develop a model that does not rely so heavily on them, one of which is the BET (Braunauer, Emmett and Teller) model.<sup>[6]</sup> The BET equation is based on the Langmuir model but with the following additional assumptions:

- The adsorbate may form more than a single layer on the surface.
- The initial monolayer heat of adsorption has a specific value.

- The heat of adsorption of the second and subsequent layers of adsorbed gas molecules is equal to the heat of condensation of the gas.
- Interactions between the vapour and surface only correspond to adsorption and desorption.
- Adsorbed molecules are not free to migrate from one layer to another.

The BET equation is:

$$\frac{P}{V(P_0 - P)} = \frac{1}{V_m c} + \frac{(c-1)}{V_m c} \cdot \frac{P}{P_0} \quad \text{Equation 2.11}$$

$P$  is the equilibrium pressure of the adsorbate and  $P_0$  is the saturated vapour pressure.  $V$  is the volume of gas adsorbed at  $P/P_0$ .  $V_m$  is the volume of gas adsorbed to form a monolayer and the constant  $c$  is associated with the net heat of adsorption. A straight line, usually between  $P/P_0$  values of 0.05-0.35, is obtained by plotting:

$$\frac{P}{V(P_0 - P)} \text{ vs. } \frac{P}{P_0} \quad \text{Equation 2.12}$$

The intercept,  $\frac{1}{V_m c}$  and the slope,  $\frac{(c-1)}{V_m c}$  can be used to calculate  $V_m$  and then the surface area of the solid can be calculated as before.

$$V_m = \frac{1}{\text{slope} + \text{intercept}} \quad \text{Equation 2.13}$$

An example of a nitrogen adsorption/desorption isotherm of a mesoporous silica structure can be seen in Figure 2.4 – a type IV isotherm. The surface area is normally calculated using the desorption isotherm.

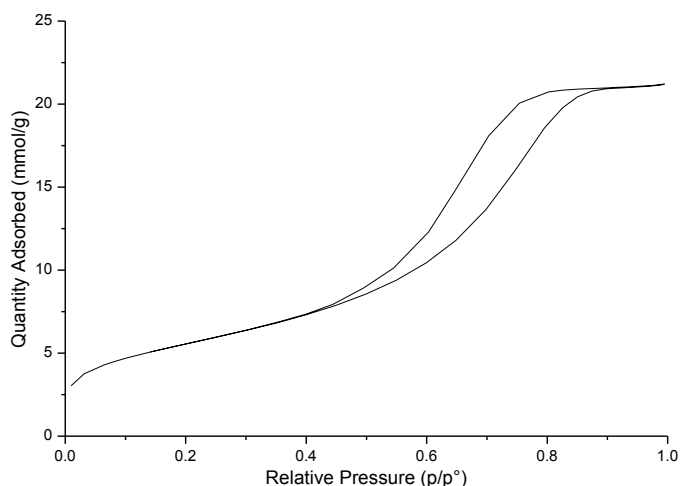


**Figure 2.4** – Nitrogen adsorption isotherm typical of that of mesoporous silica.

### 2.5. Adsorption in pores

In this thesis the BJH (Barrett, Joyner and Halenda) method is used to calculate the pore size distribution of porous solid samples.<sup>[7]</sup> This method is used conventionally to analyse mesoporous materials and is based on the Kelvin equation. There are assumptions made, which are:

- The pores are of a uniform shape.
- All pores are in the mesoporous range (pore widths between 2 nm and 50 nm).
- The presence of pores in an adsorbent solid can affect the shape of an adsorption/desorption isotherm because the equilibrium vapour pressure above condensed liquid in a (cylindrical) pore, in which the surface of the liquid is curved, is lower than that above a liquid with a flat surface.

The Kelvin equation relates the equilibrium vapour pressure of a liquid in a small cylindrical pore where the surface of the liquid takes up a regular curvature. The Kelvin equation describes the dependence of the equilibrium vapour pressure of a liquid in the pore on the radius of the pore,  $r$ , and the contact angle,  $\theta$ . Because the equilibrium vapour pressure above a curved surface is lower than above a flat surface, vapour condenses in pores at lower  $P/P_0$  values than on a flat surface, with narrow pores filling at lower pressures than wide pores. From the pressure at which condensation occurs, the radius of the pores can be calculated. The Kelvin equation is given below. In the equation,  $P/P_0$  is

the relative vapour pressure at which condensation occurs in pores of radius  $r$  with contact angle of the condensed liquid with the pore walls  $\theta$ . ( $\theta$  is assumed to be zero for pores in the size range studied here). Other constants are  $\gamma$ , the surface tension of the condensed liquid,  $V_{\text{molar}}$ , the molar volume of the liquid,  $R$  and  $T$ .

$$\ln \frac{P}{P_0} = \frac{-2\gamma \cdot V_{\text{molar}}}{r \cdot R \cdot T} \cos \theta \quad \text{Equation 2.14}$$

The BJH method involves a correction of the pore radius given by the Kelvin equation to allow for a film of condensed vapour on the pore walls which means that the pore radius is slightly larger than the radius of curvature of the meniscus. Data shown in this thesis is BJH corrected pore diameter.

## 2.6. Adsorption Calorimetry

Adsorption calorimetry is a technique which measures the amount of heat given out when a gas molecule adsorbs on the surface of a solid adsorbent. Catalysts can be characterised using adsorption calorimetry with suitable probe adsorbate compounds, where enthalpies of adsorption can be linked to the “strength” of active sites. The adsorption of a probe acid or base gas onto an adsorbent surface is via either a physical or chemical interaction. A physical interaction (physisorption) between a gas and adsorbate is generally reversible and is usually through van der Waals forces of attraction. In calorimetric terms, the enthalpy of this adsorption is usually  $<70 \text{ kJ mol}^{-1}$  for the relatively polar and reactive gases used in this thesis.<sup>[8]</sup>

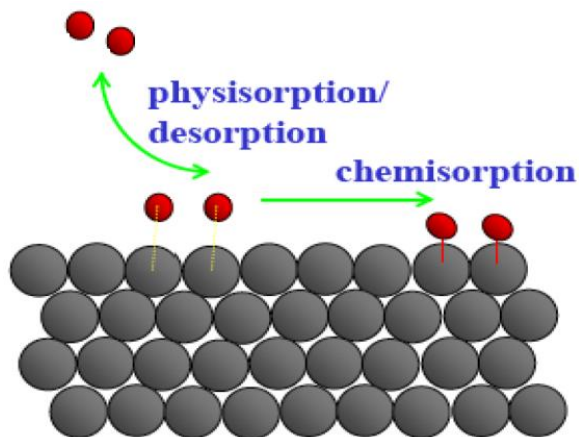


**Figure 2.5** – Irreversible chemisorption and reversible physisorption.

A chemical interaction (chemisorption) involves the gas attaching to the surface and forming a chemical bond (Figure 2.5). Usually, chemisorption is restricted to monolayer formation because of the nature of the interaction. In adsorption calorimetry it is necessary to relate the amount of gas adsorbed in an experiment to the amount of heat released in the adsorption process. The latter is measured calorimetrically. There are a number of ways of introducing and measuring the probe gas on a solid surface. The amount of gas adsorbed as a function of the equilibrium pressure of gas above the sample can be measured using a volumetric system of gas burette linked directly to the calorimeter cell holding the adsorbent. Another way of monitoring adsorbed gas is by using a gravimetric method, monitoring increases/decreases in mass before and after adsorption/desorption.

A flowing system can also be used where a probe gas is introduced to a carrier gas flow over the solid, monitoring the concentration of probe gas downstream of the sample by a mass spectrometer. The flow system largely removes ambiguity about whether the adsorption is reversible or irreversible because only irreversible adsorbed gas contributes to the measurement.

Figure 2.6 shows a typical heat signal recorded by a differential heat flow calorimeter in a flow adsorption calorimetry system. A series of pulses of probe gas is passed over the

sample and the size of the heat signal (heat flow vs. time) is a measure of the extent and strength of adsorption, and the shape gives information on the rate at which adsorption occurs. Irreversible adsorption in the early stages is replaced by reversible adsorption.

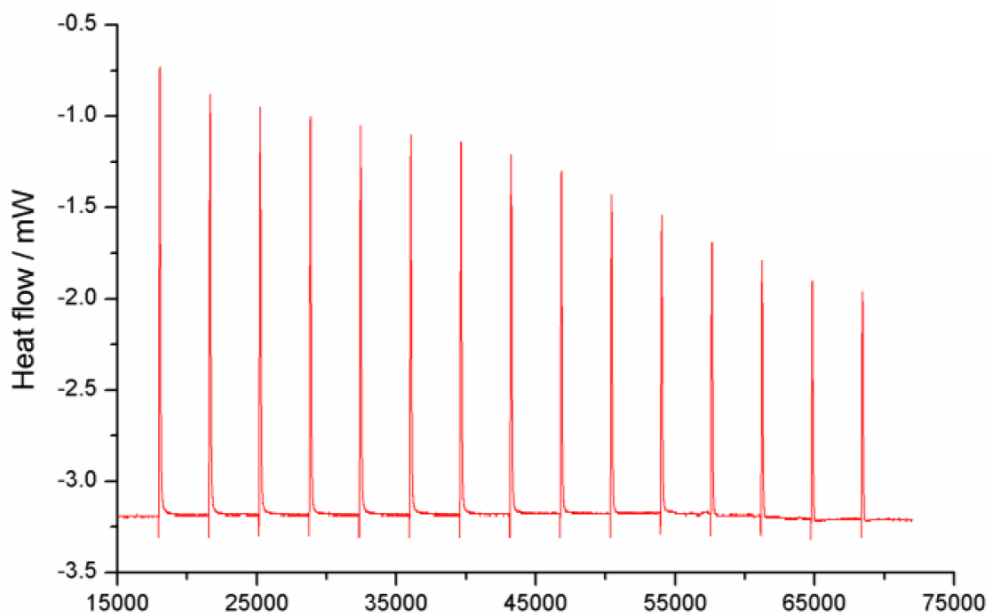


**Figure 2.6** – Adsorption calorimetry: a typical heat signal recorded by a differential calorimeter as a series of pulses of probe gas is passed over the sample.

### 2.6.1. Measuring the heat of adsorption

When heat,  $q$ , is added to a system at constant pressure then the enthalpy change in the system is equal to  $q$ :

$$\Delta H_{\text{sys}} = q \quad \text{Equation 2.15}$$

A calorimeter records the heat released by the system:

$$\Delta H_{\text{sys}} = -q_{\text{calorimeter}} \quad \text{Equation 2.16}$$

The change in enthalpy of a system is equal to the change in the internal energy of the system, corrected for any pressure/volume work that the system may do. As such it

broadly reflects the formation and the breaking of bonds, the former resulting in negative values of  $\Delta H$  (exothermic processes) and the latter positive values (endothermic processes). Heat changes are measured at constant pressure (atmospheric pressure) so  $q_{\text{sys}} = \Delta H_{\text{sys}}$ . It is useful to rely on  $\Delta H_{\text{sys}}$  to describe the energy change associated with gas adsorption.

### 2.6.2. Types of Calorimeter

There are three most commonly used calorimeters, heat accumulation, heat exchange and heat conduction (isothermal) calorimeters. In this work a heat flux (heat flow) calorimeter has been used, a form of heat conduction calorimeter. In this instrument heat emitted by the sample in the sample cell is conducted through a thermopile which surrounds the sample cell, to a large thermal sink. When heat is produced in the cell, it is conducted to the heat sink through the sensitive thermocouple which records a transient signal which returns to zero as soon as thermal equilibrium is re-established. The thermopile is connected to a similar thermopile around the reference cell in such a way that voltage differences between the two thermopiles are sensitive to differences between the two. As the heat flow from the sample cell rises and falls, so does the signal. This signal is the differential of the heat output and can be interpreted to give the heat output itself.

### 2.6.3. Gases Used for Adsorption

There are many gaseous probe compounds that can be used to study the basicities and acidities of solids. In general, ammonia ( $\text{NH}_3$ ) (base strength in water  $\text{pK}_a$  9.4) is most commonly used for studying acidity. Basicity measurements are commonly studied using  $\text{SO}_2$  and  $\text{CO}_2$ .  $\text{SO}_2$  is a stronger acid than  $\text{CO}_2$ , with  $\text{pK}_a$  values of 1.89 and 6.37 respectively in water.

### 2.6.4. Adsorption Microcalorimetry Measurements

Flow-through adsorption calorimetry using carbon dioxide and ammonia under flow conditions was performed using an indigenously developed system based on a flow-through Setaram 111 differential scanning calorimeter (DSC) and an automated gas flow and switching system, with a mass spectrometer detector for the down-stream gas flow (Hiden HPR20) connected via a heated capillary (at 175 °C).<sup>[9]</sup> The powdered sample was

held on a porous frit in the middle of a silica sample tube located in the DSC sample cell. In a typical experiment, the sample (~30-50 mg) was activated under dried nitrogen (5 ml min<sup>-1</sup>) for one hour at 150 °C. When using carbon dioxide, the sample was cooled to 120 °C for adsorption measurements. The adsorption temperature when using ammonia was 150 °C. Small pulses (typically 1 ml but depending of the volume of the sample loop) of the probe gas (1 % carbon dioxide or ammonia in nitrogen) were then injected at regular intervals into the carrier gas stream from a gas sampling valve. Both gases were passed through drying tubes before exposing to the sample.

The concentration of carbon dioxide or ammonia downstream of the sample was monitored with the mass spectrometer. The interval between pulses was chosen to ensure that the carbon dioxide or ammonia concentration in the carrier gas (including that adsorbed and then desorbed after the pulse has passed) returned to zero and the DSC heat flow baseline re-established itself. An important feature of the flow calorimetric technique is that net heat measurements relate only to carbon dioxide or ammonia bound irreversibly to the samples. Weakly bound (physisorbed) carbon dioxide or ammonia desorbs immediately the gas flow reverts to the carrier gas (Figure 2.7). The net amount of carbon dioxide or ammonia irreversibly adsorbed from each pulse was determined by comparing the mass spectrometer signal during each pulse with a signal recorded during a control experiment through an empty sample tube. Net heat released for each pulse was calculated from the DSC thermal curve.

The Setaram 111 was connected to a computer using Setaram Setsoft 2000 software by which the heat flow signal could be integrated to obtain a heat value. An example of the data obtained is shown in Figure 2.7 and is the differential heat flow (mW) vs. time (s).

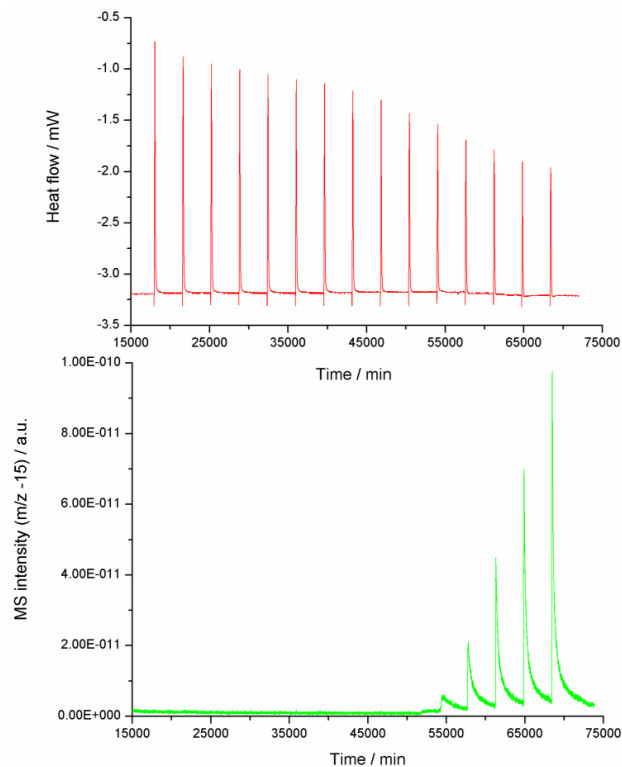


**Figure 2.7** – An example of the heat signal obtained from the calorimeter (top) and the mass spectrometer signal obtained (down).

The heat flow signal can be seen to decrease in area as more pulses are applied to the sample. This is indicative of the strongest sites adsorbing ammonia initially, followed by the weaker sites. The energy (in Joules) produced by the adsorption of the probe gas is obtained by the integration of a peak via the software. To determine if the sample has fully adsorbed the gas, ammonia was monitored during the experiment by the mass spectrometer. The mass spectrometer signal throughout the experiment corresponding to ammonia ( $m/z = 15$ ) is shown in Figure 2.7. This  $m/z$  ratio was chosen to avoid simultaneous detection of water ( $m/z = 18, 17, 16$ ). In this example, ammonia is seen to be adsorbed fully by the sample up to the final five pulses. It worth saying that attempts were made to gain data using a gas burette system in which probe gas reached equilibrium with the sample but experimental difficulties meant it was not possible to collect enough data on which to draw meaningful conclusions.

## 2.7. High pressure liquid chromatography (HPLC)

Chromatographic methods utilize partitioning a sample between two phases, one of which is the stationary phase and the other one is the mobile phase. Equipment for liquid chromatography includes a column, where separation takes place, pump, which generates a mobile phase flow, and detector, where the separated compounds are detected. Chromatography is a method which separates molecules based on differences in their structures, namely in size, in presence of charged, polar, and non-polar groups or moieties interacting specifically with an affinity column. After separation in the column, particles are eluted to the detector and they are detected as chromatograms peaks. More information about this technique is provided in Chapter 5.

## 2.8. Gas Chromatography (GC)

Gas chromatography (GC) is an analytical technique by which mixtures of organic compounds in the vapour at gas are separated and their components quantified. A small amount of sample is introduced to an injector which is set to a temperature hot enough to vaporize the sample. The vaporized mixture is then swept into the column by a carrier gas. The column inner walls are coated by an adsorbent material, the stationary phase. Interactions between the sample and the stationary phase cause the individual compounds in the mixture to pass through the column at different rates and to reach the detector at different times; the stronger the interaction between the compound and the stationary phase, the longer it takes for the compound to reach the detector. The column can be subjected to a temperature program if there is a requirement to separate materials with widely different boiling points. Stationary phases are chosen depending on the compounds that require separation. In general, polar compounds will interact strongly with polar stationary phases and therefore will have longer retention times. As well as temperature, other variables which affect separation include the column length, injection volume and the nature and flow rate of the carrier gas. There are several types of detector, e.g. flame ionization (FID), thermal conductivity (TCD), and electron capture (ECD). For all experiments in this thesis FID was used. An FID can be used to detect organic compounds with significant hydrocarbon content, and is used with a hydrogen-air flame. Organic compounds emerging from the column are burnt in the flame and the ions

generated in the flame are detected via increased electrical conductivity across the gas flow. A potential difference of 200-300 V is applied across the flowing gas and the current that flows is measured, amplified and seen as a peak on a chromatograph.

## 2.9. References

- [1] W. H. Bragg, *Journal of the Franklin Institute* **1930**, 210, 9-14.
- [2] W. L. Bragg, *Journal of the Franklin Institute* **1925**, 199, 761-772.
- [3] M. Mokhonoana, N. Coville, *Journal of Sol-Gel Science and Technology* **2010**, 54, 83-92.
- [4] K. S. W. Sing, D. H. Everett, R. A. W. Haul, L. Moscou, R. A. Pierotti, J. Rouquerol, T. Siemieniewska, in *Handbook of Heterogeneous Catalysis*, Wiley-VCH Verlag GmbH & Co. KGaA, **2008**.
- [5] I. Langmuir, *Journal of the American Chemical Society* **1918**, 40, 1361-1403.
- [6] S. Brunauer, P. H. Emmett, E. Teller, *Journal of the American Chemical Society* **1938**, 60, 309-319.
- [7] E. P. Barrett, L. G. Joyner, P. P. Halenda, *Journal of the American Chemical Society* **1951**, 73, 373-380.
- [8] J. Bars, A. Auroux, *Journal of Thermal Analysis* **1993**, 40, 1277-1284.
- [9] P. F. Siril, A. D. Davison, J. K. Randhawa, D. R. Brown, *Journal of Molecular Catalysis A: Chemical* **2007**, 267, 72-78.

## Chapter 3

# Cooperative acid-base catalysis using physical mixture of amine/sulfonic acid-functionalized silica

---

In this chapter, an introduction covering work by others on acid/base bifunctional solid catalysts is presented. The preparation, characterization and catalytic testing of solid base catalyst, solid acid catalysts and physical mixture of solid acid and solid base catalysts for co-operative catalysis are presented and discussed.

### 3. Introduction

Acid and base catalysts are probably the most ubiquitous catalysts in modern chemistry and chemical engineering. Liquid mineral acids and bases are widely utilized in industry, even though they present ecological disadvantages. These catalysts cannot be easily recovered and, in many instances, the waste streams are neutralized and treated, producing waste water. This process can be inefficient and costly. Therefore, numerous solid acids and bases have been produced to overcome such issues. Solid acids and bases have several advantages over liquid acids and bases. They are easily separated, non-corrosive, recyclable, and therefore environmentally benign compared to liquid acids and bases.<sup>[1]</sup> As such, their use in industry is prevalent. A current survey quoted the use of 180 different types of solid acid and base catalysts in 127 commercial industrial processes.<sup>[2]</sup>

#### 3.1. Acid catalysis

The most prevalent solid acids are zeolites along with other inorganic oxides because of their widespread use in alkylation, isomerization, and catalytic cracking procedures.<sup>[2]</sup> Because these materials are inorganic and crystalline, they have thermal as well as mechanical stability, making them especially suited to high temperature and pressure reactions. However, many of these materials, especially zeolites, are limited by their small pore diameters, as bulky compounds have difficulty accessing internal active sites.

Some solid acids have been prepared that do not exhibit most of these problems, notably acidic ion-exchange polymer resins. Most of these non-crystalline, copolymer resins are made up of styrene, divinylbenzene (cross-linking agent), and also vinylbenzenesulfonic acid monomers.<sup>[3]</sup> By using a porogen such as xylene, it is possible to synthesize these macroporous resins with average pore diameters of 30 nm or larger.<sup>[4]</sup> Since they are organic and non-crystalline, most of these polymer resins are less thermally and chemically stable than zeolites, and they are susceptible to swelling/shrinking in some solvents. Nonetheless, they are appropriate for use in aqueous solutions, unlike almost all other solid acids.<sup>[5]</sup>

Another type of solid acid catalyst that does not suffer from swelling and shrinkage is based on mesoporous silica-based materials. There are efforts to use mesoporous silica materials to produce solid-state acids analogous to Brønsted acidic zeolites.<sup>[6]</sup> Because they possess bigger pores, they will incorporate larger substrates. Frequently, sulfonic acid derivatives are tethered to the surface using one- and two-step functionalization approaches.<sup>[7]</sup>

There are two types of mesoporous silica: amorphous mesoporous silica and ordered mesoporous silica. The most frequently used ordered mesoporous silica-based materials have been the ordered hexagonal molecular sieve MCM-41 and the cubic ordered MCM-48,<sup>[8]</sup> both featuring large surface areas ( $>1000 \text{ m}^2/\text{g}$ ), high pore volumes ( $>0.7 \text{ cm}^3/\text{g}$ ) and a very uniform pore structure of unidirectional channels (pore diameter 2–3 nm).<sup>[8-9]</sup> Other types of ordered mesoporous silica such as SBA-15 (Santa Barbara Amorphous type material) with a surface area and pore size of up to  $1500 \text{ m}^2/\text{g}$  and 25 nm respectively<sup>[10]</sup> and FSM-16 (Folded Sheets Mesoporous) have also been used.<sup>[11]</sup>

Macquarrie<sup>[12]</sup> introduced a range of mesoporous solid sulphonic acid catalysts by incorporating propylthiol groups into a silica framework by using a sol-gel condensation and then converting them under mild oxidative conditions with  $\text{H}_2\text{O}_2$  to propylsulfonic acid groups. Meanwhile, Das et al.<sup>[13-14]</sup> functionalized ordered MCM-41 and MCM-48 with propylsulfonic acid groups by grafting propylthiol groups and converting them to propylsulfonic acid groups using  $\text{H}_2\text{O}_2$ . These pathways were pursued for the corresponding functionalization of FSM-16<sup>[15]</sup> (Folded Sheets Mesoporous) and SBA-15 (Santa Barbara Amorphous) materials.<sup>[16]</sup>

Another interesting approach to obtaining sulfonic acid groups tethered to SBA-15 material was pursued by Dufaud et al.<sup>[17]</sup> SBA-15 was functionalized with a bis-silylated disulfide reagent followed by cleavage of the disulfide bridges and oxidation of the thiols to sulfonic acid groups. This results in sulfonic acid groups with a specific spatial separation from one another in the material. Mbaraka and Shanks<sup>[18]</sup> grafted hydrophobic alkyl residues to the residual free silanol groups to create a hydrophobic surface to repel

water produced during an esterification reaction of fatty acids away from the neighbourhood of the catalytic active centre. Remarkably, Alvaro et al.<sup>[19]</sup> produced MCM-41 and SBA-15 phases with perfluorosulfonic acid groups similar to Nafion which is a sulfonated tetrafluoroethylene based fluoropolymer-copolymer discovered in the late 1960s.<sup>[19-20]</sup>

Two main synthesis routes were used to obtain functionalized acid materials. The first was a grafting or post-synthesis functionalization with 3-mercaptopropyltrimethoxysilane (MPTS) onto an ordered or amorphous silica support.<sup>[21]</sup> The second was through a direct co-condensation reaction of different organosilanes in the presence of a surfactant solution.<sup>[22]</sup> The latter method has the advantages of requiring one step and incorporating a higher number of functional groups. However, the grafting method usually results in the more active catalyst. Therefore, the grafting method was used in this work. The sulfonic form of these functionalized mesoporous materials is usually obtained through the oxidation of the precursor  $\text{SiO}_2\text{-SH}$ . The oxidation of thiol to sulfonic groups in these materials has been described by using different oxidizing agents such as nitric acid or hydrogen peroxide.<sup>[23-24]</sup> The nature and number of the final acid groups depend on the agent used and it is closely related to the catalytic performance of the material. An incomplete oxidation of the thiol groups can produce sulphur species partially oxidized<sup>[25]</sup> which are not active in the acid catalyzed reactions. Therefore, a better knowledge of the oxidation process would be useful in order to optimize this process.

### 3.2. Base catalysis

Solid bases have also received interest over the years, albeit to a lesser degree than solid acids.<sup>[2, 26]</sup> In 1955, Pines et al. reported that sodium metal dispersed on alumina acted as an efficient catalyst for double bond migration in alkenes.<sup>[27]</sup> Sodium metal dispersed on alumina will act as a solid base catalyst because of the strong tendency of sodium to donate electrons. In the 1970s, studies of solid base catalysts became more popular.<sup>[28]</sup> A number of single component metal oxides were found to act as solid base catalysts in the absence of alkali metals. In addition to the single-component metal oxides, alkali ion-exchanged X and Y type zeolites were found to be catalysts for base-catalyzed reactions.

Following these findings, a wide variety of solid base catalysts have been identified.<sup>[28]</sup> The most common types of solid base catalysts are listed in Table 3.1.

**Table 3.1** – Materials of solid base catalysts

Metal oxides <sup>[29]</sup>	MgO, CaO, Al <sub>2</sub> O <sub>3</sub> , ZrO <sub>2</sub> , Rare earth oxides (La <sub>2</sub> O <sub>3</sub> etc.), Alkali metal oxides
Mixed oxides <sup>[30]</sup>	SiO <sub>2</sub> -MgO, SiO <sub>2</sub> -CaO, Al <sub>2</sub> O <sub>3</sub> -MgO (calcined hydrotalcite)
Alkali or alkaline earth oxides loaded on support <sup>[31-32]</sup>	MgO/SiO <sub>2</sub> , Cs <sub>2</sub> O on zeolites
Alkali compounds on Al <sub>2</sub> O <sub>3</sub> <sup>[33]</sup>	KF/Al <sub>2</sub> O <sub>3</sub> , K <sub>2</sub> CO <sub>3</sub> /Al <sub>2</sub> O <sub>3</sub> , KNH <sub>2</sub> /Al <sub>2</sub> O <sub>3</sub> , NaOH/Al <sub>2</sub> O <sub>3</sub> , KOH/Al <sub>2</sub> O <sub>3</sub>
Amides and imines loaded on support <sup>[34-35]</sup>	KNH <sub>2</sub> /Al <sub>2</sub> O <sub>3</sub> , K, Y, Eu supported on zeolites from ammoniacal solution, silica supported imines
Alkali metals loaded on support <sup>[33]</sup>	Na/Al <sub>2</sub> O <sub>3</sub> , K/Al <sub>2</sub> O <sub>3</sub> , K/MgO, Na/zeolite
Anion exchangers <sup>[36]</sup>	Anion exchange resins. Hydrotalcite and modified hydrotalcites
Zeolites <sup>[31]</sup>	K, Rb, Cs-exchanged X-zeolites, ETS-10,
Clays <sup>[31-32, 37]</sup>	Sepiolite
Phosphates <sup>[38]</sup>	Hydroxyapatite, natural phosphates
Amines or ammonium ions tethered to support <sup>[39]</sup>	Aminopropyl group /silica or MCM-41 Alkylammonium group/MCM-41

The breakthrough in base catalysis was the recognition that many materials act as solid base catalysts if properly pretreated. Before the 1970s, catalysts were normally pretreated at higher temperatures of around 723 K at which the surfaces of basic materials are covered with carbon dioxide, water, oxygen, etc., and show low activities for base-catalyzed reactions. Removal of the carbon dioxide, water and oxygen etc. on the surfaces by pretreatment at high temperature allowed the surfaces to exhibit basic properties and promote catalyzed reactions. Pretreatment of the catalysts at a high temperature is crucial for solid base catalysts.<sup>[28, 40]</sup>

The most common solid bases include supported alkali metals,<sup>[29]</sup> alkaline oxides, and hydrotalcites.<sup>[41]</sup> Due to the porous nature of these materials, they can suffer from diffusion limitations and size restrictions of products and reactants. They also tend to be strongly basic and can suffer from lower selectivities than those of weaker organic bases.<sup>[26]</sup> These weaker, organic bases may consist of supported amines on polymer

resins. As mentioned previously, polymer resin-supported catalysts are less thermally and chemically stable and are also prone to swelling in solvents. However, they are highly tunable in terms of the basicity and selectivity based on the choice of amine for each application. They have widespread application in industry for a variety of organic transformations: Michael additions,<sup>[42]</sup> transesterifications,<sup>[43]</sup> aldol additions,<sup>[44-45]</sup> hydrogenations, aminations, Knoevenagel condensations,<sup>[46]</sup> alkylations,<sup>[47]</sup> etc.

Mesoporous silica materials have also been employed in the development of heterogeneous base catalysts. A comprehensive survey of work up to 2000 may be found in a review by Weitkamp et al.<sup>[48]</sup> Corma et al.<sup>[49]</sup> have studied MCM-41 samples functionalized with 1,8-bis (dimethylaminonaphthalene) which have proven to be highly efficient catalysts in the Knoevenagel condensation of benzaldehyde with activated methylene compounds and in the Claisen–Schmidt condensation of benzaldehyde with 2-hydroxyacetophenone. Macquarrie et al.<sup>[50]</sup> investigated the distribution of aminopropyl groups in correspondingly functionalized MCM-41 phases in the catalysis of classical C–C coupling reactions such as the nitroaldol condensation of nitromethane with benzaldehyde, and the Michael addition of nitromethane with 2-cyclohexene-1-one.

Recently, a number of research groups have pursued new and creative approaches to incorporating acid and base functional groups into the same heterogeneous catalysts, which can catalyze multistep reaction cascades in one system or work in a cooperative manner.<sup>[51]</sup>

### 3.3. Acid-base bifunctional catalysis

In modern synthetic chemistry, researchers often try to emulate nature, as it easily masters highly selective reactions in complex systems and the construction of structurally advanced and functional molecules. Today, drugs and synthetic or biomimetic macromolecules with very complex structures and with specific functions can be prepared by multistep synthesis owing to great progress in catalysis and the development of highly selective reactions under mild reaction conditions.<sup>[52]</sup> A limiting factor, or at least one that determines costs, however, is the necessary isolation and purification of

intermediates between reaction steps when the reactive components of one reaction step quench or deactivate the reagents of the subsequent step. If multistep reactions could be carried out in a single reactor in high yield without complex reactor design or specific purification procedures, synthetic approaches to the production of organic compounds would strongly profit.<sup>[52]</sup>

Thirty years ago, Patchornik et al.<sup>[53]</sup> defined the principle and requirements of sequential multistep one-pot reactions, involving insoluble polymeric reagents. They investigated two-stage reactions in which a starting material was modified successively by two polymeric transfer reagents. The analogous soluble reagents reacted with each other rapidly in solution, but they were rendered mutually inactive upon attachment to the respective polymeric phases. Thus, multipolymer systems of insoluble polymeric reagents were identified; they were unique in that reactions can only take place within the matrix of the polymeric reagent. Since then, polymers with more than one functional site have been used widely.<sup>[54]</sup> This approach goes back to the groundbreaking work by Astle and Zaslowsky<sup>[55]</sup> and Manecke and Storck<sup>[56]</sup> on polymeric reagents, where they showed the first examples of sequential multistep organic reactions carried out over polymer-anchored homogeneous catalysts. However, it is not possible to have the same polymer material with two incompatible reagents as the internal mobility of such swollen resins would allow these reagents to come into contact with and destroy each other. In the last ten years,<sup>[57]</sup> the concept of incompatible one-pot reactions has been rediscovered and has emerged as a powerful tool for probing “site-isolation” effects in cross-linked solid materials in the work by Gelman et al.<sup>[57-58]</sup>, who investigated sol-gel processes with encapsulated opposing reagents.

Sol-gel entrapment was found to be a good way of placing acids and bases in a reaction mixture together without their mutual destruction, while still allowing them to activate or participate in desired reactions.<sup>[58]</sup> In several studies, it has been proven that reagents entrapped within a sol-gel framework maintain their physical and chemical properties<sup>[59]</sup> and that external reactant molecules can diffuse into the pore network, react with the entrapped reagent, and emerge from the pores as products. One of the more successful

uses of doped sol-gel materials has been in the field of pH sensors<sup>[60]</sup>. This approach is not suitable for placing acid and base reagents inside the same material, as they will deactivate each other. However, if the acid and the base are entrapped in two different materials, they become protected from each other but are still available for useful reactions. Gelman<sup>[61]</sup> has introduced silica sol-gel entrapped acids, bases and organometallic catalysts which were used successfully in one-pot reactions without interfering with each other.

There are many studies on metal oxides, such as alumina, which contain both acidic and basic sites on their surfaces.<sup>[2]</sup> These oxides lack the versatility of tailoring the acid/base properties by demand as offered by sol-gel materials, which can be used to entrap practically any of the thousands of known acids and bases (except, of course, those which destroy the matrix itself). However, the only industrial catalysts that are covalently used as bifunctional acid base solid catalysts as described in the recent review<sup>[2]</sup> are mixed metal oxides, used in 14 kinds of commercial processes.

Recently, three new, remarkably successful, concepts for site isolation in one-pot multistep reactions have been reported that are very different in their details. First, layered clays, such as  $\text{Mg}_6\text{Al}_2(\text{OH})_{16}\text{CO}_3$  hydrotalcite and  $\text{Ti}^{4+}$ -exchanged montmorillonite, are known to be strong Brønsted bases and acids respectively, in organic synthesis.<sup>[62]</sup> Kaneda et al.<sup>[63]</sup> utilized both in a single reactor without mutual destruction as acid and base in one-pot reaction sequences, since the large hydrotalcite particles cannot penetrate the narrow spaces between the layers of the  $\text{Ti}^{4+}$ -exchanged montmorillonite. Second, Frechet and Hawker et al.<sup>[64]</sup> used core-confined catalytic sites, again acid and base, shielded by a star-shaped polymer architecture in one-pot multistep homogeneous catalysis (Figure 3.1).

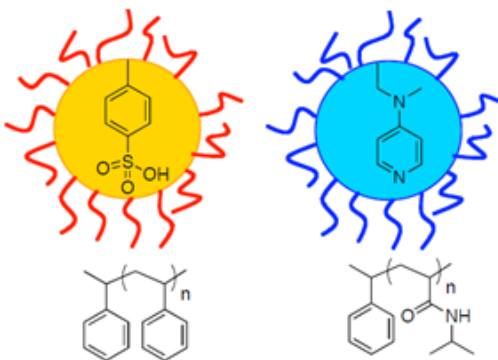


**Figure 3.1** – Acid and base groups shielded by star-shaped polymers for one-pot multistep catalysis.<sup>[64]</sup>

Third, Jones<sup>[65]</sup> introduced another approach by combining base catalysts that are magnetically recoverable with acid catalysts that can be recovered gravimetrically. In his work, magnetic ferrite nanoparticles were functionalized through silane chemistry with N-[3-(trimethoxysilyl)propyl]ethylenediamine to create surface base sites. The basic nanoparticle solids were then used in conjunction with a sulfonic acid polymer resin in a cascade reaction (Figure 3.2).

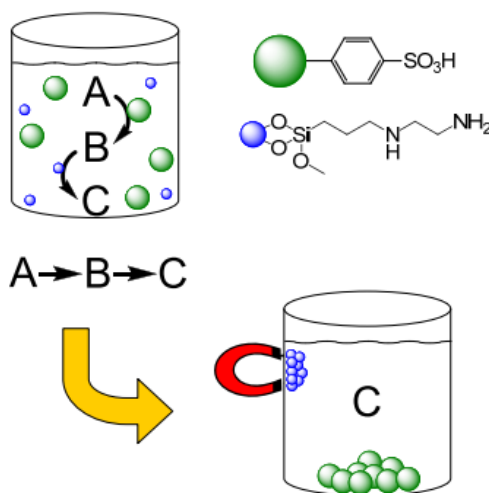
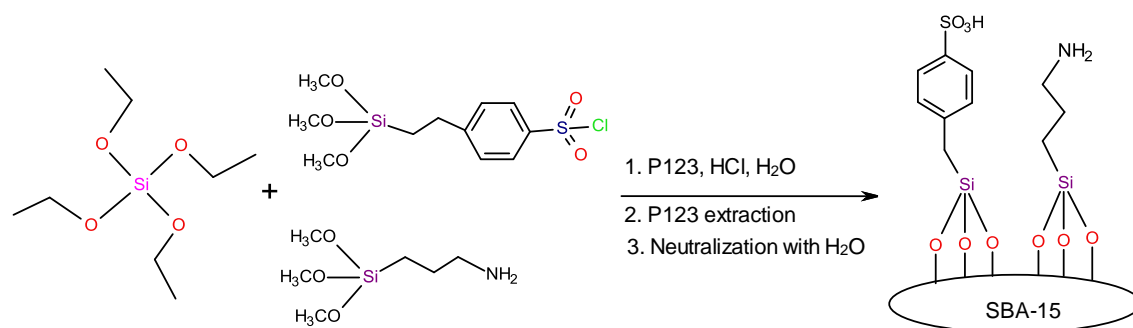


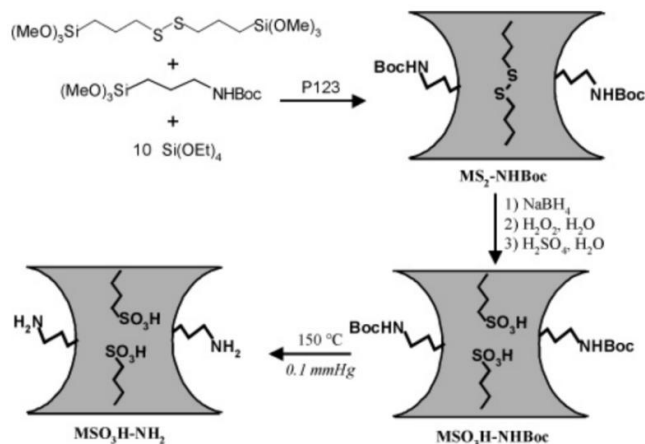
**Figure 3.2** – Individually recoverable acid and base catalysts for one-pot cascade reactions.<sup>[65]</sup>

All these approaches to obtaining acid-base catalysts for one-pot tandem organic reactions involved physical mixtures of acid and base materials. Another approach is to have both groups on the same support. Davis<sup>[51]</sup> reported the first mesoporous material functionalized with acid and base groups on the same support that showed activity not achievable by the acid and base organic groups tethered to different supports. A sulfonic acid and amine were incorporated into SBA-15 through a “one-pot” synthesis as shown in Scheme 3.1.



**Scheme 3.1** – “One-pot” synthesis of dual-functionalized mesoporous catalyst SBA-15-acid/base.<sup>[66]</sup>

Since then, interest in materials bearing sulfonic acids and amine groups has been rising. Corriu et al. reported mesoporous materials with an acidic framework and basic pores.<sup>[67]</sup> They found that both antagonist organic groups can co-habit independently without mutual destruction in aprotic solvents. In contrast, in protic solvents, there is protonation of the NH<sub>2</sub> group (which is clear evidence of the existence of both antagonist groups on the same materials). However, they had to protect the base groups during the synthesis of the catalyst until the acid sites were generated. After that, the protecting groups were removed by heating under vacuum. Synthesis procedures are shown in Scheme 3.2.

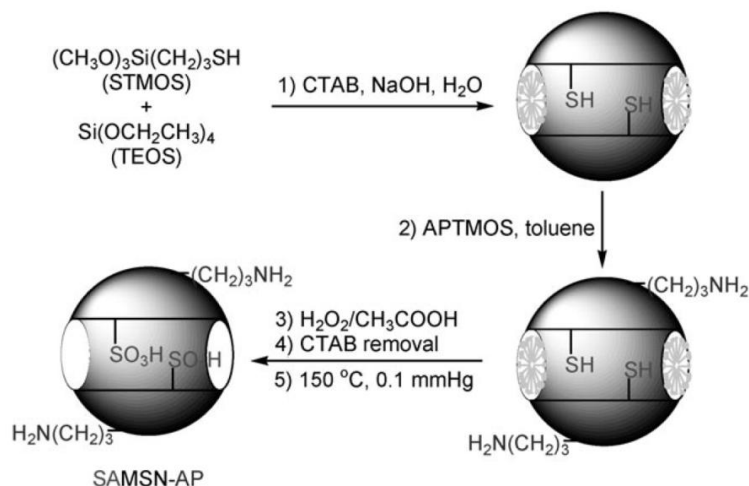


**Scheme 3.2** – Synthesis of mesoporous materials with acid and base sites.<sup>[67]</sup>

The synthesis of multifunctional hybrid materials containing both acids and bases is not an easy task, due to the incompatible nature of these functional groups. Frequently, amine base groups are protected using di-tert-butyl-dicarbonate (BOC)<sup>[67-69]</sup> during the acid treatment necessary to convert the precursor of acid groups, usually thiols or disulfide moieties, into the corresponding sulfonic acids. Then, a deprotection of the amine groups by thermal treatment is needed to restore the base properties of the hybrid. However there are disadvantages to this method in terms of its efficiency and effect on other surface species.

New approaches have been applied to eliminate the protecting/deprotecting steps. Lin et al.<sup>[70]</sup> reported mesoporous silica nanoparticles in which one group was attached to the internal surface through co-condensation and the second group was tethered onto the external surface by post-synthesis grafting. Both of these functional groups showed significant activity in a two-step reaction sequence that cannot be achieved when the catalysts are combined in a one-pot homogeneous system. These materials were synthesized by co-condensation of tetraethyl orthosilicate and 3-mercaptopropyltrimethoxysilane in the presence of cetyltrimethylammonium bromide (CTAB) as a template under basic reaction conditions, and subsequent post-treatment for grafting 3-aminopropyltrimethoxysilane (APTMS) onto the external surface. This was

followed by oxidation of thiols groups to sulfonic acid groups using  $\text{H}_2\text{O}_2/\text{CH}_3\text{COOH}$  without protecting the amine groups (Scheme 3.3).<sup>[70]</sup>



**Scheme 3.3** – Syntheses of bifunctional mesoporous silica nanoparticles having sulfonic acid groups on the internal surface and organic amine groups on the external surface.<sup>[70]</sup>

More recently, bifunctional mesoporous hybrid materials, containing both proton sponges and acid groups, have been prepared by different synthetic routes: co-condensation processes (sol–gel or micellar one-pot routes) and post-synthetic grafting of the organic functionalities.<sup>[71]</sup> 1,8-bis(dimethylamino)naphthalene (DMAN), a proton sponge with high pKa, was used as an organic builder base and 3-mercaptopropyltriethoxysilane (MPTES) as a pendant precursor of sulfonic acids located on the surface of the mesoporous channels. DMAN has previously been modified in order to have two terminal reactive silyl groups able to perform co-condensation with a conventional organosilane (TMOS), through sol–gel or micellar one-pot routes. This method has allowed the direct introduction of the functionalized DMAN builders into mesoporous silica walls by direct synthesis. Sulfonic acid groups were obtained by oxidation of thiol groups using  $\text{H}_2\text{O}_2$  without protection of the DMAN base molecules.

The cooperation of general acid and base groups has been demonstrated by Lin et al.<sup>[72]</sup> They prepared a cooperative catalytic system comprising a series of bifunctionalized

mesoporous silica nanosphere materials with various relative concentrations of a general acid, the ureidopropyl (UDP) group, and a general base, the 3-[2-(2-aminoethylamino)ethylamino]-propyl (AEP) group (Figure 3.3).

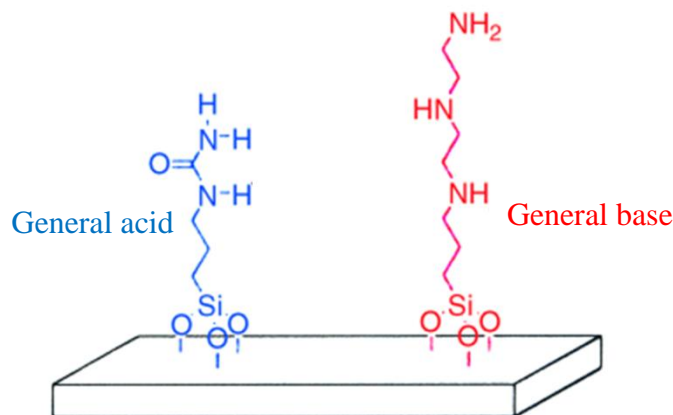
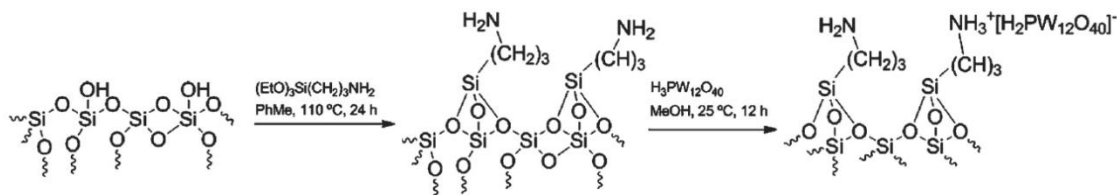


**Figure 3.3** – Bifunctionalized mesoporous silica nanosphere (MSN) materials with ureidopropyl (UDP) group, and 3-[2-(2-aminoethylamino)ethylamino]-propyl (AEP) group.<sup>[72]</sup>

Heteropoly acids as acid sites on bifunctional catalysts have been introduced recently. To date, there are only a very few reports on heteropolyacid (HPA) acid–base bifunctional systems. N. R. Shiju and co-workers reported mesoporous silica with site-isolated amine and phosphotungstic acid groups, which showed tunable antagonistic functions for one-pot tandem reactions.<sup>[73]</sup> As far as we know, this is the first published work on antagonistic functional HPAs with acidic and basic sites for one-pot cooperative catalysis. Organized mesoporous silicas with site-isolated amino and phosphotungstic acid groups were synthesized through two successive post-grafting steps (Scheme 3.4) in which aminopropyl groups were tethered to SBA-15 silica and acidity was added by reacting phosphotungstic acid ( $\text{H}_3\text{PW}_{12}\text{O}_{40}$ ) with a fraction of the amine groups on the surface, leaving  $\text{H}_2\text{PW}_{12}\text{O}_{40}^-$  as the source of acidity, and unreacted amine groups to provide basicity.



**Scheme 3.4** – Synthesis of bifunctional mesoporous catalysts with grafted amino and phosphotungstic acid moieties<sup>[73]</sup>

Mizuno's group<sup>[74]</sup> designed acid–base catalysts by incorporating rare-earth metals (RE) into a lacunary  $[\gamma\text{-SiW}_{10}\text{O}_{36}]^{8-}$ . These materials exhibited Lewis acidity from rare-earth metals and basicity from the nucleophilic surface of anion of HPAs. Recently, Wang's group<sup>[75]</sup> reported the synthesis of Schiff base structured acid–base catalysts  $[\text{PySAIm}]_3\text{PW}_{12}\text{O}_{40}$  using Schiff base ionic liquid (IL) and  $\text{Na}_3\text{PW}_{12}\text{O}_{40}$ .

More recently, Jiang reported a new catalytic system including acid–base bifunctional heteropolyacids (HPAs) nanocatalyst for the simultaneous transesterification of oil and esterification of free fatty acids (FFAs), to directly convert low-quality feedstocks to biodiesel in a one-pot process. Phosphotungstic acid  $\text{H}_3\text{PW}_{12}\text{O}_{40}$  was used as the inorganic part and lysine as the organic group to self-assemble lysine-dodecaphosphotungstate (HPW-LY) hybrid particles. The acid and base characteristics of this material could be modulated by varying the amounts of HPW and lysine.<sup>[76]</sup>

To conclude this literature review, there have been many papers published over the last ten years describing different routes to preparing mesoporous silica acid-base bifunctional catalysts. However, despite this large number of papers, results from the literature are somewhat conflicting and do not allow an easy choice of the best approach to preparing mesoporous silica with acid-base bifunctional catalyst. This is mainly due to the fact that these materials were applied in different model reactions and tested under different experimental conditions. In the work represented here, we add to the general understanding of acid/base bifunctional solid catalysts through a comparative study.

The strategy used in this work has been to prepare supported base catalysts, supported acid catalysts and supported bifunctional acid-base catalysts as the basis for the comparative study. This chapter will be divided into three main sections. The first section covers supported base catalysts which have been prepared by grafting of aminopropyl trimethoxysilane on two silica supports, amorphous silica ( $\text{SiO}_2$ ) and ordered silica (MCM-41), in order to compare the effect of support physical properties on the catalytic activity. The co-condensation method has also been used and compared with the grafting method in order to find the best method of preparing the base catalysts. The effect of support silanol ( $\text{Si-OH}$ ) groups on the catalytic activity has been investigated by capping the silanol groups by methyl groups using a grafting method.

The effect of acid pretreatment of amorphous silica with concentrated acid has also been investigated. In the second section, supported acid catalysts have been prepared by grafting mercaptopropyl trimethoxysilane on amorphous silica support. Two oxidation routes to obtaining sulfonic acid groups have been investigated. In the third section, a physical mixture of supported base and acid catalysts has been studied in tandem with the deacetalization-Henry reaction to investigate the ability to house opposing functional groups by immobilizing the catalysts on heterogeneous supports. The advantage of this method over those of other groups who prepared such mixtures of acid and base groups is that all of them tend to trap the acid and base groups inside the supports; therefore, the grafting method was the choice, although the low probability of solid-solid interactions maintains the integrity of the opposing functional catalysts, thus allowing the homogeneously self-quenching catalysts to remain active in the presence of the opposing catalyst.

### 3.4. Experimental

#### 3.4.1. Materials

Silica gel (particle size 40-63  $\mu\text{m}$ ; average pore size 6 nm), (3-mercaptopropyl)trimethoxysilane (MPTMS), (3-aminopropyl)trimethoxysilane (APTMS), ammonia, methylated spirit, cetyltrimethylammonium bromide (CTAB), nitromethane, tetraethoxysilane (TEOS), toluene, sodium hydroxide, acetone, o-xylene, and phosphotungstic acid were purchased from Aldrich. Benzaldehyde was purchased from Acros. Unless noted otherwise, all chemicals were at least 99% pure and used as received. Deionized water was used in all experiments.

#### 3.4.2. Activation of silica gel ( $\text{SiO}_2$ )

Silica gel was treated by different acids where 30 g raw silica gel was refluxed in 150 ml of stock HCl (37%) or  $\text{HNO}_3$  (60%) for 4 h at 100  $^\circ\text{C}$ . The treated silica gel was washed with distilled water and dried under vacuum for 24 h. The activated silica samples were denoted  $\text{SiO}_2$  (HCl) and  $\text{SiO}_2$  ( $\text{HNO}_3$ ). The non-activated silica was denoted  $\text{SiO}_2$ .<sup>[77]</sup>

#### 3.4.3. Synthesis of amorphous mesoporous silica base catalyst ( $\text{SiO}_2\text{-NH}_2$ )

A sample of 10.0 g of silica gel (activated or non-activated) was suspended in 50 ml of dry toluene and (3-aminopropyl)trimethoxysilane APTMS (2.60 ml, 15 mmol) was added to this suspension. The mixture was refluxed under dry nitrogen atmosphere for 72 h at 110  $^\circ\text{C}$  and the modified silica gel was filtered off, washed twice with toluene, and dried under vacuum at room temperature. The catalysts were named as follows:  $\text{SiO}_2\text{-NH}_2$  for non-activated silica gel,  $\text{SiO}_2\text{-NH}_2$  (HCl) and  $\text{SiO}_2\text{-NH}_2$  ( $\text{HNO}_3$ ) for activated silica gel with HCl and  $\text{HNO}_3$  respectively.

#### 3.4.4. Synthesis of silylated mesoporous silica base catalyst ( $\text{SiO}_2\text{-NH}_2\text{-CH}_3$ )

$\text{SiO}_2\text{-NH}_2$  (1g) was added to a dry toluene solution containing trimethoxymethylsilane (0.4 ml, 3 mmol) and the solution left for 12 h at 80  $^\circ\text{C}$  under nitrogen. The solid was filtered and washed with dry toluene and dried in the oven at 120  $^\circ\text{C}$  for 12 h. The new material was named  $\text{NH}_2\text{-SiO}_2\text{-CH}_3$ .

### 3.4.5. Synthesis of supported propylsulfonic acid catalysts (SiO<sub>2</sub>-SO<sub>3</sub>H)

SiO<sub>2</sub> (HCl) (3.0 g) was treated with (3-mercaptopropyl)trimethoxysilane MPTMS (0.8 ml, 4.5 mmol) in toluene as above to form SiO<sub>2</sub>-SH. The SiO<sub>2</sub>-SH samples were oxidized according to different methods.<sup>[23, 25]</sup>

Method A- the sample was contacted with 60% w/w nitric acid at room temperature and stirred for 8 h.<sup>[78]</sup> The solid was then filtered, washed with water, ethanol and ether and dried at room temperature for 12 h. The catalyst was named SiO<sub>2</sub>-SO<sub>3</sub>H (HNO<sub>3</sub>).

Method B- the sample was contacted with a solution of 50% w/w hydrogen peroxide at room temperature and stirred for 24 h.<sup>[12]</sup> The solid was filtered, washed with water and ethanol and dried at 60 °C during 12 h. The catalyst was named SiO<sub>2</sub>-SO<sub>3</sub>H (H<sub>2</sub>O<sub>2</sub>).

### 3.4.6. Synthesis of mesoporous ordered silica (MCM-41)

Mesoporous silica MCM-41 (S) was synthesized using cetyltrimethylammonium bromide (CTAB) template following a literature report.<sup>[79]</sup> NH<sub>4</sub>OH (62 ml, 35% solution) was mixed with 231 g of distilled water. The mixture was heated to 80 °C under vigorous stirring; then 1.0 g cetyltrimethylammonium bromide (CTAB) was added to the mixture and the mixture was stirred for 30 min at 80 °C. Five ml of tetraethoxysilane (TEOS) was added to the above mixture drop-wise. The mixture was stirred at 400 rpm for 2 h at 80 °C. The solution was filtered and the precipitate was washed with distilled water and ethanol. The precipitate was left to dry at 80 °C for 18 h followed by calcination in air at 540 °C for 6 h. The molar ratios of the reactants were as follows:

535 (H<sub>2</sub>O) : 65 (NH<sub>4</sub>OH) : 0.1 (CTAB) : 1.0 (TEOS)

### 3.4.7. Synthesis of MCM-41-NH<sub>2</sub> (G) by grafting method

MCM-41 was grafted with 3-aminopropyltrimethoxysilane (APTMS) by stirring 1 g of dried MCM-41 in 250 mL toluene containing APTMS (0.26 ml, 1.5 mmol) at 78 °C for 12 h under nitrogen. The solution was filtered and the precipitate was washed with dichloromethane (200 mL) and ethanol (500 mL) and then dried in air. The resulting mesoporous material was denoted MCM-41-NH<sub>2</sub> (G).

### 3.4.8. Direct synthesis of MCM-41-NH<sub>2</sub> (C) by co-condensation method

MCM-41-NH<sub>2</sub> (C) was prepared according to the method described by Iliade,<sup>[80]</sup> whereby 1.0 g of CTAB was dissolved in 240 mL of distilled water; then 7 mL of a fresh NaOH solution (1 M) were added and the temperature was raised to 80 °C. Afterwards, 5 mL of TEOS and 1 mL of APTMS were slowly and simultaneously added drop-wise to the reaction solution and the mixture was stirred for 18 h. The obtained white precipitate was filtered, washed with abundant deionized water and methanol and dried in the oven at 80 °C. The removal of the organic template was achieved by reflux of the product for 24 h in a solution of 1.5 ml HCl (37%) and ethanol followed by extensive washing with deionized water and methanol. The solution was filtered and the precipitate was washed with distilled water and ethanol and then dried. The resulting mesoporous material was denoted as MCM-41-NH<sub>2</sub> (C).

### 3.5. Catalyst characterization

Powder XRD patterns were recorded on a Bruker D-8 diffractometer using Cu K $\alpha$  radiation (1.5418 Å) at 40 kV and 20 mA. The patterns were collected over the range 1.5-10 for 2 $\theta$  with a step size of 0.02° at a scanning speed of 2° per min.

Nitrogen adsorption–desorption isotherms were measured at 77 K on a Micromeritics ASAP-2020 after evacuation at 423 K for 5 h. The surface areas and the average pore sizes were calculated from the adsorption isotherm using the BET method and the desorption isotherm using the BJH method respectively.

Levels of functionalization of base catalysts were assessed by acid-base back titration where a sample of 100 mg of dried base catalyst was stirred in 20 ml 0.01M HCl for 4 h. Then 1 ml of the HCl solution was added to 10 ml distilled water along with 2 drops of phenolphthalein as indicator. The mixture was titrated with standardized 0.01 M NaOH solutions. A comparison between the volume of NaOH solution required to neutralize HCl which had not been in contact with the catalyst and HCl which had been in contact with the catalyst allowed the concentration of NH<sub>2</sub> groups on the catalyst surface to be determined.

Catalyst basicity and acidity for some samples were quantified by  $\text{SO}_2$  and  $\text{NH}_3$  adsorption calorimetry, respectively. These experiments were performed using a system based on a flow-through Setaram 111 differential scanning calorimeter (DSC) and an automated gas flow and switching system, with a mass spectrometer (MS) detector for the down-stream gas flow, described elsewhere.<sup>[81-82]</sup> In a typical adsorption experiment, the catalyst (30 mg) was activated at 120 °C under dry nitrogen flow at 10 ml min<sup>-1</sup>. Following activation, and maintaining the sample at 120 °C, pulses of the probe gas (1% ammonia in nitrogen or 1% sulfur dioxide in nitrogen) at atmospheric pressure were injected at regular intervals into the carrier gas stream from a gas-sampling valve.

The concentration of the probe gas downstream of the sample was monitored continuously. The amount of the probe gas irreversibly adsorbed from each pulse was determined by comparing the MS signal during each pulse with a signal recorded during a control experiment. The net heat released for each pulse was calculated from the DSC thermal curves. From this, the molar enthalpies of adsorption of sulfur dioxide or ammonia ( $\Delta H^\circ_{\text{ads}}$ ) were obtained for the amount adsorbed from each successive pulse. The  $\Delta H^\circ_{\text{ads}}$  values are plotted against the amount of irreversibly adsorbed probe gas per gram of the catalyst to give a profile that can be interpreted in terms of the abundance and strength distribution of active sites.

Infrared spectra of the solid samples were recorded on a Nicolet 380 FTIR single reflection Nicolet spectrometer recording attenuated total reflectance infrared (ATR IR) spectra over the range 400-4000  $\text{cm}^{-1}$  under atmospheric conditions. Water vapour adsorption isotherms were measured by a Surface Measurement Systems Dynamic Vapor Sorption apparatus (Advantage<sup>TM</sup>), using a method described by Hill et al.<sup>[83]</sup> Adsorption isotherms of water vapour were recorded at 25 °C, following activation of the catalysts at 100 °C.

### 3.6. Catalytic activity measurement

#### 3.6.1. Aldol reaction

Catalysts were activated before use under static air at 120 °C for 2 h. A mixture of benzaldehyde (1 mmol), nitromethane (10 mL), and the selected catalyst were kept at 70 °C under magnetic stirring. The amount of the catalyst used in each experiment was determined on the basis of the functional group loading value in order to introduce the same supported propylamine equivalents in the different experiments. The reaction mixture was stirred under nitrogen and aliquots of the sample mixture were removed with a filter syringe and analyzed by gas chromatography GC (FID, 25 m BPI column), which was calibrated. The final product was fully identified by mass spectrometry (MS).

Catalyst reusability was tested by two methods: 1) Recycle method: the catalyst was removed from the reaction, washed with nitromethane and acetone, and then dried at 80 °C for 12 h. The catalyst was then introduced to another reactor containing the reactants to start another reaction cycle; 2) Continuous method: the reaction was carried out for 8 h with the same reaction mixture and catalyst, adding extra benzaldehyde (1 mmol) when the amount of benzaldehyde concentration reached the minimum. During the experiment, benzaldehyde concentration was monitored by GC.

#### 3.6.2. Deacetalization reaction and deacetalization-nitroaldol reaction

Catalysts were activated before use under static air at 120 °C for 2 h. Catalyst (30 mg), benzaldehyde dimethylacetal (1 mmol), and xylene (0.1 mL) as internal standard in nitromethane (10 ml) were placed into a 50 mL glass vessel. The mixture was heated at 50 °C under nitrogen with constant stirring. Reaction conversion was monitored by gas chromatography (GC) (FID, 25 m BPI column).

### 3.7. Results and discussion

#### 3.7.1. Characterization of base catalysts

The nitrogen adsorption–desorption isotherms of amorphous silica gel ( $\text{SiO}_2$ ),  $\text{SiO}_2\text{-NH}_2$ , MCM-41, MCM-41- $\text{NH}_2$  (G) and MCM-41- $\text{NH}_2$  (C) are shown in Figure 3.4.

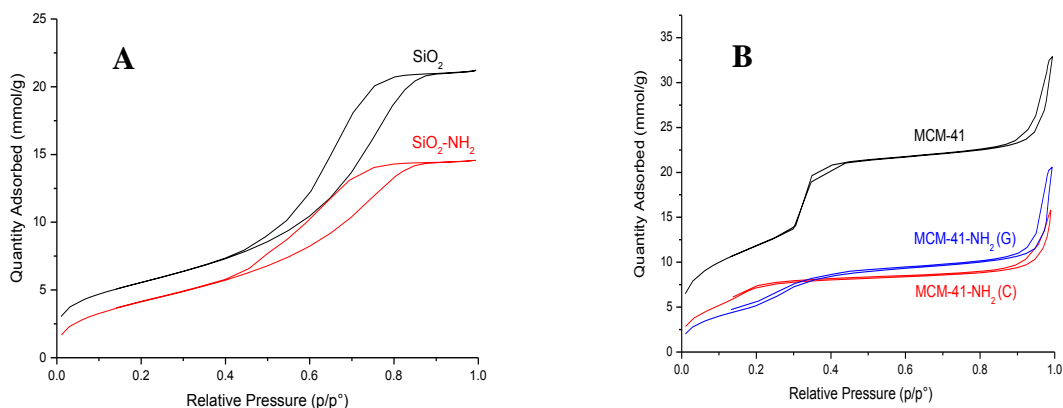


**Figure 3.4** –  $\text{N}_2$  adsorption isotherms at 77 K for  $\text{SiO}_2$  and  $\text{SiO}_2\text{-NH}_2$  (A) and MCM-41, MCM-41- $\text{NH}_2$  (G) and MCM-41- $\text{NH}_2$  (C) (B).

The isotherms of MCM-41 and  $\text{SiO}_2$  show a type IV shape according to the classification of IUPAC<sup>[84]</sup>, indicating the presence of tubular pores of relatively large sizes. Adsorption at low pressures ( $P/P^\circ < 0.25$ ) is accounted for monolayer–multilayer adsorption of  $\text{N}_2$  on the walls of the mesopores. Both figures show a steep capillary condensation in the mesopore region ( $P/P^\circ = 0.3\text{--}0.4$ ). However, MCM-41 shows a sharp increase, suggesting a narrower pore size distribution in MCM-41 than in functionalized MCM-41 and  $\text{SiO}_2$  samples.

A well-defined step in the adsorption isotherm indicates a narrow and uniform pore size distribution, while its height is related to the pore volume. The poorly-defined step in the MCM-41- $\text{NH}_2$  (C) isotherm compared to that of MCM-41 is indicative of a certain disorder in the mesostructure.

The specific (BET) surface area, the average pore diameter and the total pore volume calculated from the corresponding nitrogen sorption isotherms along with amine content on the material calculated from titration data are summarized in Table 3.2.

**Table 3.2** – Textural parameters and level of functionalization for supported base catalysts.

Sample	Surface area /m <sup>2</sup> g <sup>-1</sup>	Pore volume /cm <sup>3</sup> g <sup>-1</sup>	Average pore diameter /nm	Level of base sites <sup>a</sup> /mmol g <sup>-1</sup>
MCM-41	962	1.2	4.5	-
MCM-41-NH <sub>2</sub> (G)	653	0.5	4.4	1.5
MCM-41-NH <sub>2</sub> (C)	540	0.2	4.2	1.3
SiO <sub>2</sub>	528	0.8	5.9	-
SiO <sub>2</sub> (HNO <sub>3</sub> )	506	0.8	5.8	-
SiO <sub>2</sub> (HCl)	452	0.8	6.5	-
SiO <sub>2</sub> -NH <sub>2</sub>	272	0.4	4.1	1.3
SiO <sub>2</sub> -NH <sub>2</sub> (HNO <sub>3</sub> )	312	0.4	4.1	0.9
SiO <sub>2</sub> -NH <sub>2</sub> (HCl)	352	0.5	4.3	0.7

a. Determined by titration.

MCM-41 shows the largest surface area, in line with previous reports.<sup>[85]</sup> Silica gel SiO<sub>2</sub> surface area decreases when treated with concentrated HNO<sub>3</sub> and HCl. Pore size increases by 16% and 5% respectively, suggesting that acid treatment results in wider pores on the silica surface.

With the introduction of organic functional groups, the specific surface areas and pore volumes (Table 3.2) decrease in similar ways for both SiO<sub>2</sub>-NH<sub>2</sub> and MCM-41-NH<sub>2</sub> catalysts. This implies the successful grafting of functional groups in the pores of the silica support. A comparison of results for MCM-41-NH<sub>2</sub> (G) and MCM-41-NH<sub>2</sub> (C) shows that the grafting apparently results in higher amine content and higher surface area and pore volume. Surprisingly, the effect of acid treatment on amorphous silica appears to reduce the extent to which it can be functionalized.

The p-XRD patterns of MCM-41, MCM-41-NH<sub>2</sub> (G) and MCM-41-NH<sub>2</sub> (C) are shown in Figure 3.5.

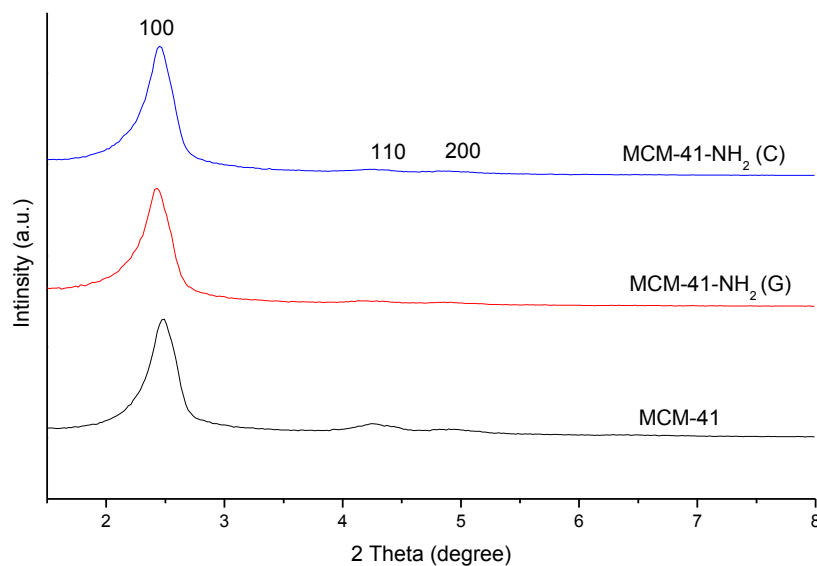


**Figure 3.5** – XRD patterns of MCM-41, MCM-41-NH<sub>2</sub> (G), MCM-41-NH<sub>2</sub> (C)

The XRD patterns of MCM-41, MCM-41-NH<sub>2</sub> (G) and MCM-41-NH<sub>2</sub> (C) show three peaks that can be indexed on a hexagonal unit cell to (100), (110) and (200) by analogy with literature reports.<sup>[85]</sup> Both samples of MCM-41-NH<sub>2</sub> show slightly less well resolved reflections than MCM-41, suggesting a lower degree of order or regularity in the arrangement of the hexagonal pores. This is expected in the co-condensation method because of destructive interference from the diffraction planes associated with the propylamine groups in the framework, while in the grafting method this lower degree of order could be due to the effect of pore filling or the coating of the outer surface of MCM-41 crystals. However, Scaroni<sup>[86]</sup> reported that amine coating on the outer surface of MCM-41 crystals hardly influences the diffraction pattern of MCM-41 support. Therefore, the slight reduction in resolution is probably due to the pore filling effect. This was clearly seen in the significant fall in pore volume and surface area described above and shown in Table 3.2.

The FT-IR spectra of MCM-41-NH<sub>2</sub> and SiO<sub>2</sub>-NH<sub>2</sub> are shown in Figure 3.6.

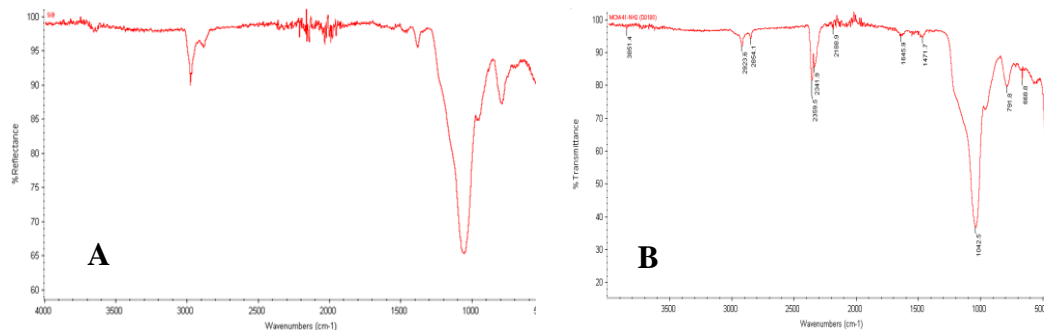


**Figure 3.6** – The FT-IR spectrum of SiO<sub>2</sub>-NH<sub>2</sub> (A) and MCM-41-NH<sub>2</sub> (G) (B)

The FTIR spectra confirm amine functionalization on SiO<sub>2</sub> (A) and MCM-41 (B). Both samples show three bands characteristic of the CH<sub>2</sub> groups of the propyl chain of the silylating agent: a stretching vibration band at 2923 cm<sup>-1</sup>, a bending vibration band at 1471 cm<sup>-1</sup>, and a rocking vibration band (791 cm<sup>-1</sup>). The weak band at 3851 cm<sup>-1</sup> is characteristic of the NH<sub>2</sub> group (NH vibrations). The vibrations of Si–O–Si can be seen at 1042 cm<sup>-1</sup> (asymmetric stretching), 791 cm<sup>-1</sup> (symmetric stretching) and 437 cm<sup>-1</sup> (bending). The C-N bond-stretching signal from the primary amine at is seen at around 1100 cm<sup>-1</sup>. The C-N band, however, overlaps with the broad Si-O-Si band, making it hard to distinguish. The band at 1630 cm<sup>-1</sup> is assigned to the vibrations of physically adsorbed water.<sup>[87-88]</sup> Thus, overall the IR spectra are reflecting the functional groups on the support.

### 3.7.2. Study of surface basicity by calorimetric adsorption of SO<sub>2</sub>

Surface basicity was studied by calorimetric adsorption of SO<sub>2</sub>. Adsorption data are shown in Figure 3.7 as  $-\Delta H^{\circ}_{\text{ads}}(\text{SO}_2)$  versus amount of SO<sub>2</sub> adsorbed for representative catalysts. These data can be broadly interpreted as basic site strength distribution profiles. The relative strengths of base sites are reflected in the values of  $-\Delta H^{\circ}_{\text{ads}}(\text{SO}_2)$ . It is generally assumed that significant basicity corresponds to values greater than 80 kJ mol<sup>-1</sup>.<sup>[89]</sup> The concentration of basic sites is related to the amount of SO<sub>2</sub> that adsorbs with enthalpy above this value. However, it is not possible to determine more than relative

values for the concentrations of basic sites from this data because the  $\text{RNH}_2:\text{SO}_2$  stoichiometry for tethered amine groups interacting with  $\text{SO}_2$  is not known, although it is very likely greater than one.<sup>[90]</sup> Stoichiometries of between 3:1 and 4:1 have been reported by others for  $\text{SO}_2$  complex formation with amine-functionalized silica.<sup>[90]</sup>

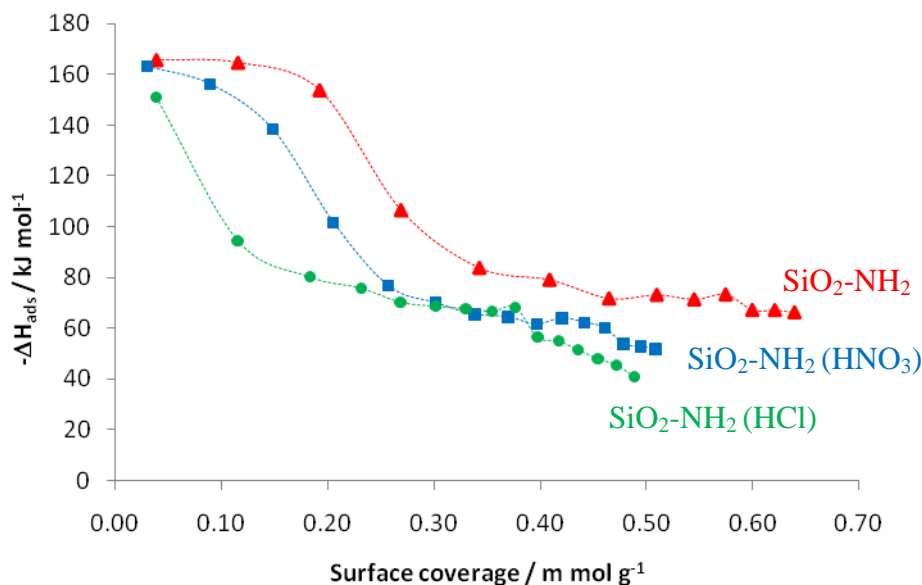


**Figure 3.7** –  $\Delta H_{\text{ads}}^{\circ}(\text{SO}_2)$  vs. amount adsorbed at 120 °C

The figure shows that  $\text{SiO}_2\text{-NH}_2$  has a relatively high concentration of basic sites, in line with previous reports on similar materials. The sample made from silica treated with  $\text{HNO}_3$  shows a small decrease in the basicity while the sample made from silica treated with  $\text{HCl}$  shows a further decrease in the basicity.

### 3.7.3. Characterization of solid acid catalysts

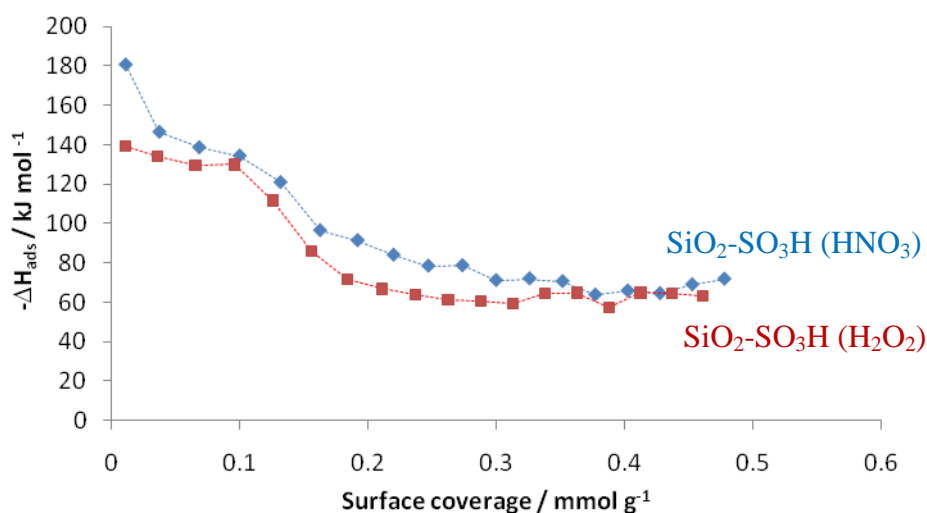
Nitrogen adsorption–desorption isotherms (not shown) are all of type IV, indicating mesoporous structures.<sup>[91]</sup> Table 3.3 shows surface area, pore volume and pore size data for  $\text{SiO}_2$ ,  $\text{SiO}_2\text{-SH}$ ,  $\text{SiO}_2\text{-SO}_3\text{H}(\text{H}_2\text{O}_2)$  and  $\text{SiO}_2\text{-SO}_3\text{H}(\text{HNO}_3)$ .

**Table 3.3** – Textural parameters and level of functionalization for supported acid catalysts.

Catalyst	Surface area /m <sup>2</sup> g <sup>-1</sup>	Pore volume /cm <sup>3</sup> g <sup>-1</sup>	Average pore size /nm
SiO <sub>2</sub>	452	0.75	5.1
SiO <sub>2</sub> -SH	388	0.55	4.7
SiO <sub>2</sub> -SO <sub>3</sub> H (H <sub>2</sub> O <sub>2</sub> )	380	0.55	4.2
SiO <sub>2</sub> -SO <sub>3</sub> H (HNO <sub>3</sub> )	378	0.52	3.9

With the introduction of organic functional groups, the specific surface areas and pore volumes decrease. A small decrease in surface area and pore size after the oxidation of thiol groups by both oxidants is consistent with the presence of sulfonic acid groups.

The concentration of sulfonic acid in the solid product was determined by ammonia adsorption microcalorimetry and not by direct titration in order to obtain the strength of active sites. Calorimetric NH<sub>3</sub> adsorption data are shown as  $-\Delta H^{\circ}_{\text{ads}}(\text{NH}_3)$  versus amount of NH<sub>3</sub> adsorbed profiles in Figure 3.8 for the supported acid catalysts. These data can be broadly interpreted as acid site strength distribution profiles.

**Figure 3.8** –  $\Delta H^{\circ}_{\text{ads}}(\text{NH}_3)$  vs. amount adsorbed at 120 °C, for supported acid catalysts.

The figure shows that SiO<sub>2</sub>-SO<sub>3</sub>H (HNO<sub>3</sub>) has a slightly higher concentration of acid sites than SiO<sub>2</sub>-SO<sub>3</sub>H (H<sub>2</sub>O<sub>2</sub>). It is possible to quantify these profiles by assuming that the concentration of acid sites on a catalyst is equal to the concentration of NH<sub>3</sub> that adsorbs with enthalpies numerically greater than 80 kJ mol<sup>-1</sup>.<sup>[89]</sup>

The first pulse adsorbed (Initial -ΔH<sup>o</sup><sub>ads</sub> (NH<sub>3</sub>)) relates to the strongest sites on the catalysts. These data on surface acidity are shown in Table 3.4.

**Table 3.4** – Summary calorimetric NH<sub>3</sub> adsorption data.

Catalyst	NH <sub>3</sub> adsorbed (-ΔH <sup>o</sup> <sub>ads</sub> > 80 kJ mol <sup>-1</sup> ) <sup>a</sup> /mmol g <sup>-1</sup>	Initial -ΔH <sup>o</sup> <sub>ads</sub> (NH <sub>3</sub> ) <sup>b</sup> /kJ mol <sup>-1</sup>
SiO <sub>2</sub> -SO <sub>3</sub> H (HNO <sub>3</sub> )	0.21	180
SiO <sub>2</sub> -SO <sub>3</sub> H (H <sub>2</sub> O <sub>2</sub> )	0.15	140

[a] ± 0.01 [b] ± 5

From Table 3.4, the calorimetric data suggest that SiO<sub>2</sub>-SO<sub>3</sub>H (HNO<sub>3</sub>) prepared by the nitric acid route exhibit both a higher concentration of acid groups and stronger acid groups than the equivalent material prepared using H<sub>2</sub>O<sub>2</sub> in line with other reports.<sup>[78]</sup>

### 3.8. Catalytic activity of base catalysts

#### 3.8.1. Nitroaldol reaction (Henry reaction)

The comparison of the catalytic efficiency determined as the conversion of benzaldehyde versus time in the nitroaldol condensation reaction is performed in the presence of the three catalysts under the same experimental conditions (Figure 3.9).

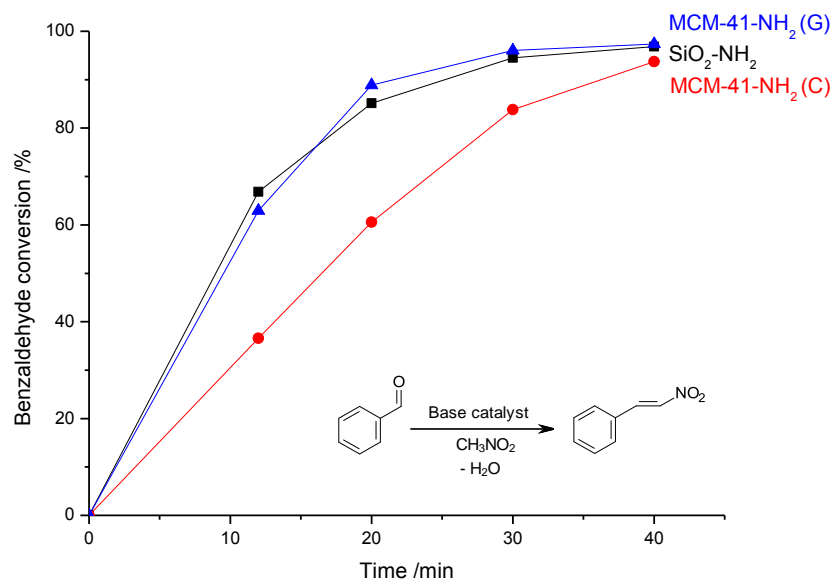


**Figure 3.9** – Reactivity of nitromethane (5 mL) with benzaldehyde (1.0 mmol) over SiO<sub>2</sub>-NH<sub>2</sub>, MCM-41-NH<sub>2</sub> (G) and MCM-41-NH<sub>2</sub> (C) (all with equivalent number of supported propylamine, 0.08 mmol) at 70 °C as a function of time.

As shown in Figure 3.10, the catalysts prepared by the grafting method (SiO<sub>2</sub>-NH<sub>2</sub> and MCM-41-NH<sub>2</sub> (G)) were more active than the catalyst prepared by a sol-gel co-condensation method (MCM-41-NH<sub>2</sub> (C)) independently of whether the amorphous or the mesoporous silica is utilized as the solid support, suggesting that active site accessibility may be relatively poor when the amine group is introduced at the support synthesis stages. For all tested catalysts, nitrostyrene was recognized as the sole reaction product. Nitroalcohol was not observed during the reaction, suggesting an imine mechanism. Indeed, imine stretching peak was observed on the infrared spectrum of used amine-supported catalyst at 1652 cm<sup>-1</sup>. Asefa<sup>[92]</sup> proposed that primary amine preferentially works through an imine mechanism to yield nitrostyrene, while secondary and tertiary amines exclusively proceed via the classical ion-pair mechanism to yield nitroalcohol.

It is also reported that nitrostyrene forming during the reaction could become 2-phenyl-1,3-dinitropropane by Michael addition to nitromethane in the medium as the two reactants were gradually depleted. Ruiz<sup>[93]</sup> found that, with a nitromethane/benzaldehyde

ratio lower than 3, nitrostyrene forming during the reaction became 2-phenyl-1,3-dinitropropane. However, 2-phenyl-1,3-dinitropropane was not detected in this work as an excess of nitromethane was used.

### 3.8.2. Activity of solid base catalyst ( $\text{SiO}_2\text{-NH}_2$ ) in repeat reactions

Silica supported base catalyst was tested in a continuous method in which, each time the benzaldehyde concentration reached a plateau, an extra amount of benzaldehyde was added to the reaction three times; then the catalyst was removed, washed and reused. The data are shown in Figure 3.10.

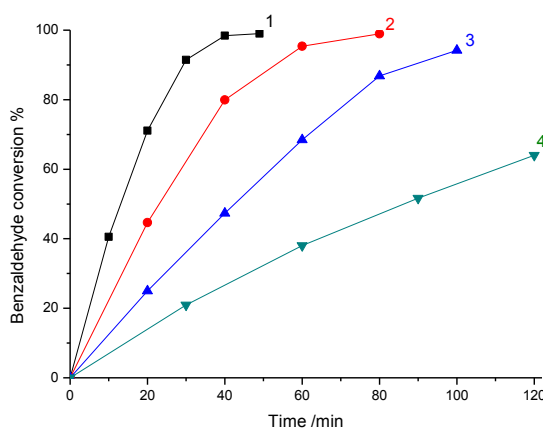


**Figure 3.10** – Reactivity of nitromethane with benzaldehyde in the presence of nitrostyrene over  $\text{SiO}_2\text{-NH}_2$  with repeated addition of the reactants.

Activity is lost as the reaction is repeated. One possible explanation is the competitive interaction of nitrostyrene with the supported propylamine; it is in fact reported that propylamine undergoes addition to nitrostyrene, producing an unstable nitramino intermediate which gives back the starting reagents via a retro-Michael reaction.<sup>[94]</sup> After 8 h, the catalyst was removed, washed with nitromethane and acetone, and then left to dry at 120 °C for 12 h. The catalyst was then reused twice. Activity was similar to the activity in the first cycle (recycle method). These observations support the nitrostyrene effect, and offer a possible explanation for why the reaction rate decreases during the reaction. The effect of nitrostyrene on the catalytic efficiency of such catalysts in nitroaldol reaction was observed by Macquarrie.<sup>[95]</sup>

### 3.8.3. Effect of acid treatment of SiO<sub>2</sub> on the activity of supported amine catalysts

Catalytic activities of SiO<sub>2</sub>-NH<sub>2</sub> (HCl), SiO<sub>2</sub>-NH<sub>2</sub> (HNO<sub>3</sub>) and SiO<sub>2</sub>-NH<sub>2</sub> in the nitroaldol reaction at 50 °C were measured and the kinetic data were recorded as shown in Figure 3.11.

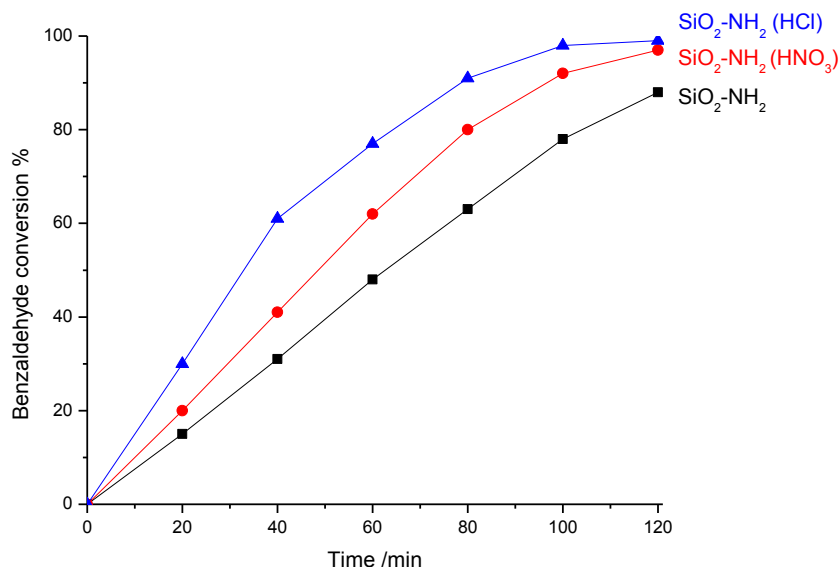


**Figure 3.11** – Activity of SiO<sub>2</sub>-NH<sub>2</sub> in nitroaldol reaction at 50 °C.

The kinetic data show that the catalyst prepared with SiO<sub>2</sub> subjected to HCl treatment is the most active material, followed by the catalyst prepared with HNO<sub>3</sub> and the catalyst prepared without any treatment. The amount of active sites in SiO<sub>2</sub>-NH<sub>2</sub> (HCl) measured by titration (Table 3.2) was lower than the other catalysts. A possible explanation for why this catalyst was the most active is linked to the possibility that more silanol groups are on the surface than other catalysts. Therefore, a cooperative acid-base mechanism may be involved.

Introducing aminopropyl groups to the silica surface naturally consumes surface silanols. If this idea is valid, i.e. that silanol groups can take part in a cooperative mechanism, then the level of functionalization would be critical. Whether or not this is the case, there are additional problems with high amine loading in that they can cause the formation of

multilayer aminopolymer networks that can affect mass transfer on the catalyst surface.<sup>[96]</sup>

### 3.8.4. Effect of silanol groups on the catalytic activity of solid base catalysts

To investigate the possible role of the silanol groups in the nitroaldol reaction, catalytic experiments were carried out with catalysts whose surface silanols had been capped with methyl groups by reaction with trimethoxymethylsilane (TMMS). This decreases the surface hydrophilicity. To investigate the hydrophilicity characteristics of  $\text{SiO}_2\text{-NH}_2$  and  $\text{NH}_2\text{-SiO}_2\text{-CH}_3$ , the catalyst was tested by dynamic vapour sorption data (DVS) where the catalyst was subjected to different levels of humidity at room temperature (Figure 3.12).

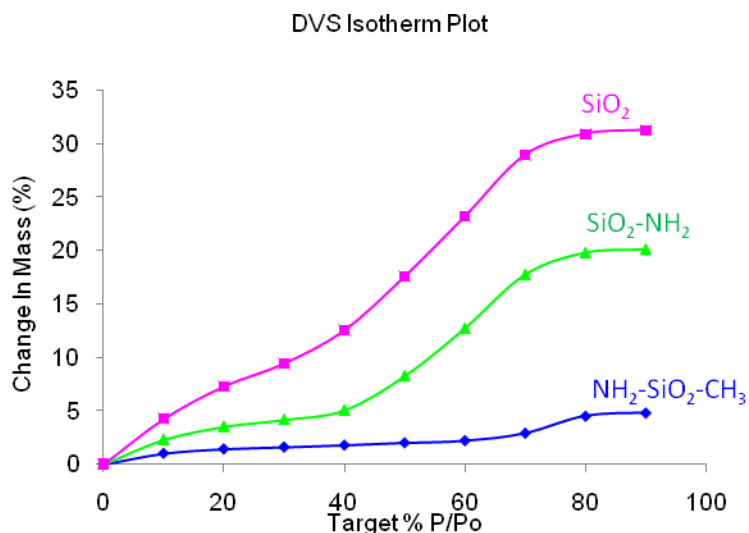


**Figure 3.12** – Water sorption isotherm obtained at 298 K on  $\text{SiO}_2$ ,  $\text{SiO}_2\text{-NH}_2$  and  $\text{NH}_2\text{-SiO}_2\text{-CH}_3$ .

Water sorption yielded a type IV isotherm, which is indicative of weak adsorbate–adsorbent interactions. The lower uptake of water in  $\text{SiO}_2\text{-NH}_2$  than in  $\text{SiO}_2$  is indicative of the expected hydrophobicity of this material. A further decrease in water uptake is observed when  $\text{SiO}_2\text{-NH}_2$  is silylated to form  $\text{NH}_2\text{-SiO}_2\text{-CH}_3$ .

When catalyst  $\text{SiO}_2\text{-NH}_2$  is silylated ( $\text{NH}_2\text{-SiO}_2\text{-CH}_3$ ), its catalytic activity decreases (Figure 3.13).

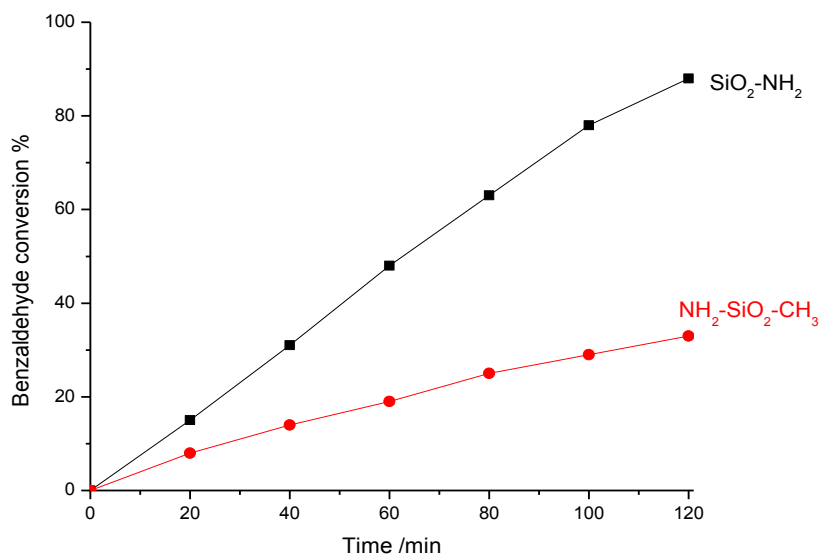
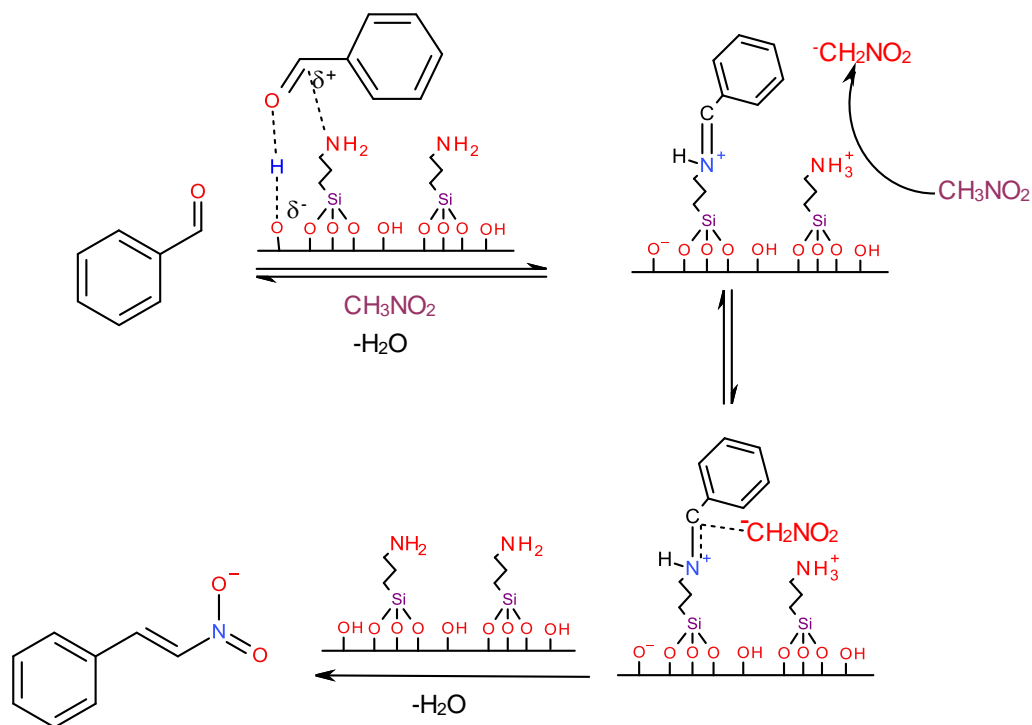


**Figure 3.13** – Activity of SiO<sub>2</sub>-NH<sub>2</sub> (0.03 g) and NH<sub>2</sub>-SiO<sub>2</sub>-CH<sub>3</sub> (0.03 g) in nitroaldol reaction at 50 °C.

This may be the simple consequences of the hydrophobic nature of the catalyst, or it may suggest a significant role of silanol groups in accelerating the nitroaldol reaction. Imine catalytic mechanism has been suggested for acid–base cooperation for nitroaldol reaction.<sup>[97-98]</sup> It is suggested that Bronsted silanol acid groups interact with the lone pair of electrons on the carbonyl oxygen to give the protonated form ( $\alpha$ -hydroxy carbocation), which is more stable than ordinary carbocation. Then, the grafted amine nucleophilically attacks the acid stabilized aldehyde carbonyl, producing an iminium ion intermediate. At the same time, grafted amine groups deprotonate nitromethane to give the nucleophilic  $\text{CH}_2\text{NO}_2^-$  which condenses with the iminium ion through an ion pairing mechanism to produce the final product (Scheme 3.5).<sup>[97]</sup>



**Scheme 3.5** – Imine catalytic mechanism for Henry reaction catalyzed by amines on silica

### 3.9. Catalytic activity of acid catalysts

The catalytic activities of acid catalysts prepared by both oxidation routes were studied in order to determine which oxidation process is more efficient. The catalytic activity of both catalysts was tested in the deacetalization reaction where the conversion of benzaldehyde dimethyl acetal to benzaldehyde was monitored by gas chromatography (Figure 3.14).

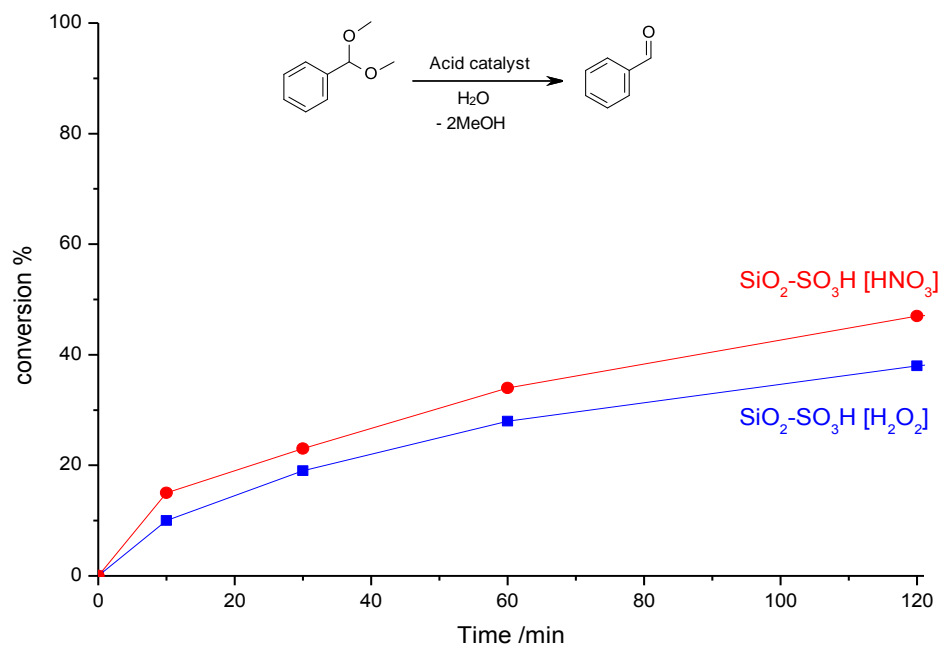


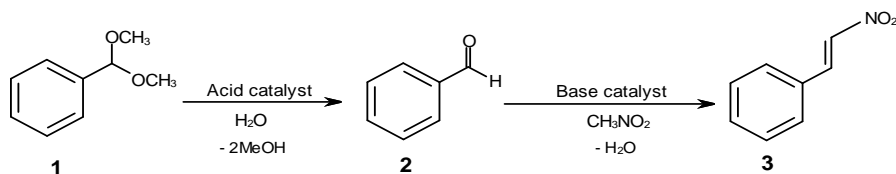
**Figure 3.14** – Reactivity of SiO<sub>2</sub>-SO<sub>3</sub>H [HNO<sub>3</sub>] and SiO<sub>2</sub>-SO<sub>3</sub>H [H<sub>2</sub>O<sub>2</sub>] in deacetalization of benzaldehyde dimethyl acetal reaction at 90°C for 2 hr.

As shown in Figure 3.14, SiO<sub>2</sub>-SO<sub>3</sub>H [HNO<sub>3</sub>] shows slightly higher activity than SiO<sub>2</sub>-SO<sub>3</sub>H [H<sub>2</sub>O<sub>2</sub>] in line with the ammonia adsorption calorimetry results and other literature.<sup>[78]</sup> Therefore, in all the following work the acid catalysts are prepared by the HNO<sub>3</sub> oxidation route.

### 3.10. Physical mixture of acid and base solid catalysts as bifunctional catalyst

The simplest manner in which acid–base catalysts for tandem one-pot organic reactions can be achieved is by simply mixing a heterogeneous acid and base together to identify potentially interesting pairs. Comparing these results with the results of reactions with the acid and base separately gives an indication of the potential compatibility. This strategy allows considerable flexibility, as the individual components can be modified to tune the acidity, basicity, and nucleophilicity, but can also lead to acid and base neutralization that quenches the catalytic activity. In the last two sections, acid and base solid catalysts have been investigated separately in deacetalization and nitroaldol reaction (Henry reaction)

respectively. In this section, solid acid, solid base and physical mixtures of solid acids and solid bases are investigated in a tandem deacetalization-Henry reaction (Scheme 3.6).



**Scheme 3.6** – Tandem deacetalization-Henry reaction.

Activity of the mixture of  $\text{SiO}_2\text{-NH}_2$  and  $\text{SiO}_2\text{-SO}_3\text{H}$  is reported in terms of the conversion of benzaldehyde dimethyl acetal (1) to benzaldehyde (2) and to nitrostyrene (3). Data are shown in Figure 3.15.

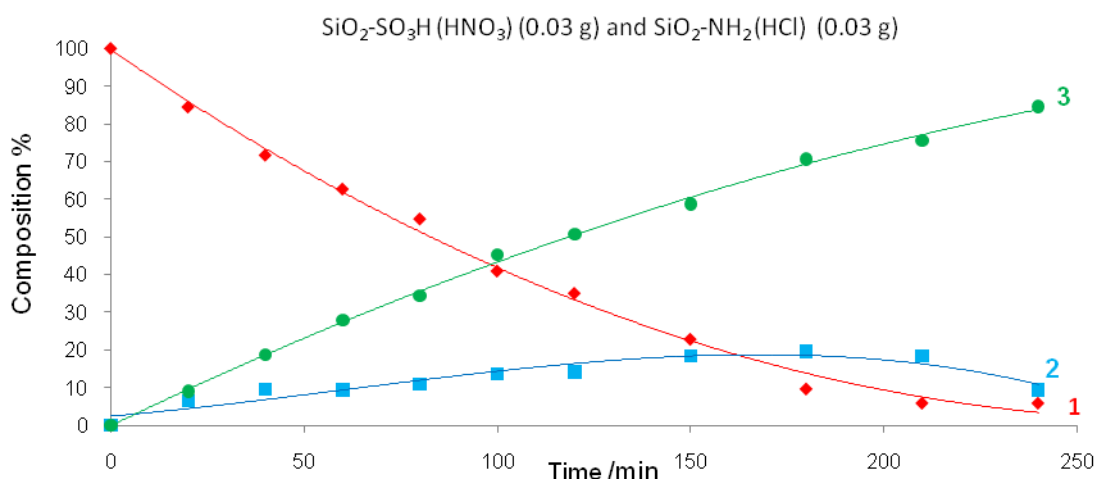


**Figure 3.15** – Composition of the reaction mixture vs. time for the deacetalization-Henry reaction, catalyzed by a physical mixture of  $\text{SiO}_2\text{-SO}_3\text{H}$  (0.03 g) and  $\text{SiO}_2\text{-NH}_2$  (0.03 g) at 90 °C.

The first conversion, from 1 to 2, is acid-catalyzed and conversion to 3 is base-catalyzed. The initial results prove the ability of the physical mixture to work as acid and base catalysts.

One of the advantages of using a physical mixture of acid and base solid catalysts is the ability to adjust the amount of acid and base solid catalysts to give the optimum activity.

In the following experiment, the amounts of acid and base catalyst were varied. The kinetic results of the tandem deacetalization-Henry reaction catalyzed by a physical mixture of solid acid and solid base catalysts with different compositions are shown in Figures 3.16, 3.17 and 3.18.

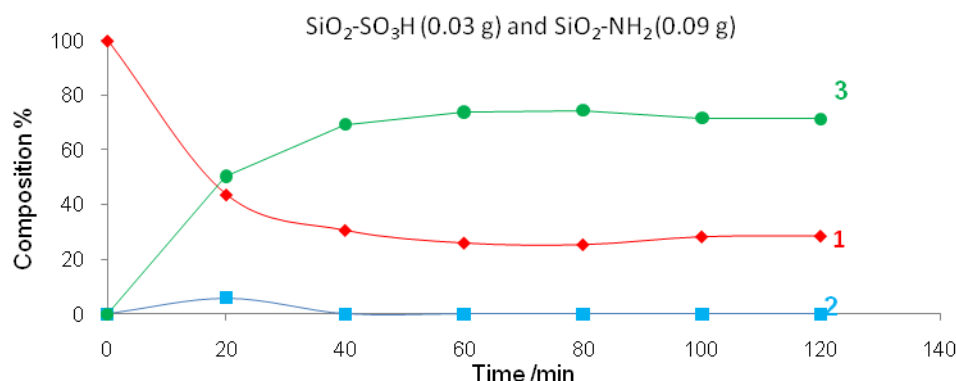


**Figure 3.16** – Composition of the reaction mixture vs. time for the deacetalization-Henry reaction, catalyzed by a physical mixture of  $\text{SiO}_2\text{-SO}_3\text{H}$  (0.03 g) and  $\text{SiO}_2\text{-NH}_2$  (0.09 g) at 90 °C.

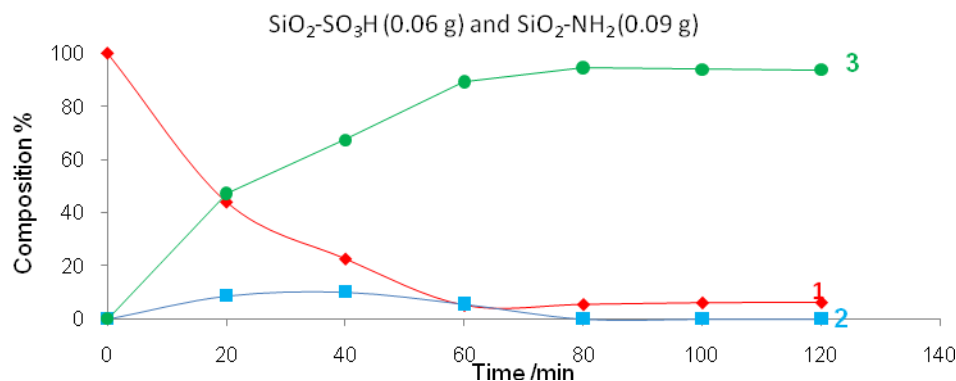


**Figure 3.17** – Composition of the reaction mixture vs. time for the deacetalization-Henry reaction, catalyzed by a physical mixture of  $\text{SiO}_2\text{-SO}_3\text{H}$  (0.06 g) and  $\text{SiO}_2\text{-NH}_2$  (0.09 g) at 90 °C.

The first tested mixture contained 0.03 g acid and 0.09 g base catalysts. In this case, the benzaldehyde that is produced is quickly converted to nitrostyrene, as would be expected. Surprisingly, the acid-catalyzed conversion of benzaldehyde dimethyl acetal stops after

71%. It appears that the acid catalytic centres are prone to poisoning. When a physical mixture with 0.06 g acid catalyst and 0.09 g base catalyst was used, 94% conversion of benzaldehyde dimethyl acetal and 94% nitrostyrene yield were achieved in 2 hr (Figure 3.17). This result confirms that the rate of the base-catalyzed second step is highly dependent on the rate of the acid-catalyzed first step.

Earlier, it was shown that  $\text{SiO}_2\text{-NH}_2$  in which the free silanol groups had been capped with  $-\text{CH}_3$  groups exhibited reduced activity compared to the uncapped catalyst. In the next section, the “capped” catalysts are used along with  $\text{SiO}_2\text{-SO}_3\text{H}$ . The catalyst activity of physical mixtures of 0.03 g  $\text{NH}_2\text{-SiO}_2\text{-CH}_3$  and 0.03 g  $\text{SiO}_2\text{-SO}_3\text{H}$  in a tandem deacetalization-Henry reaction is shown in Figure 3.18.

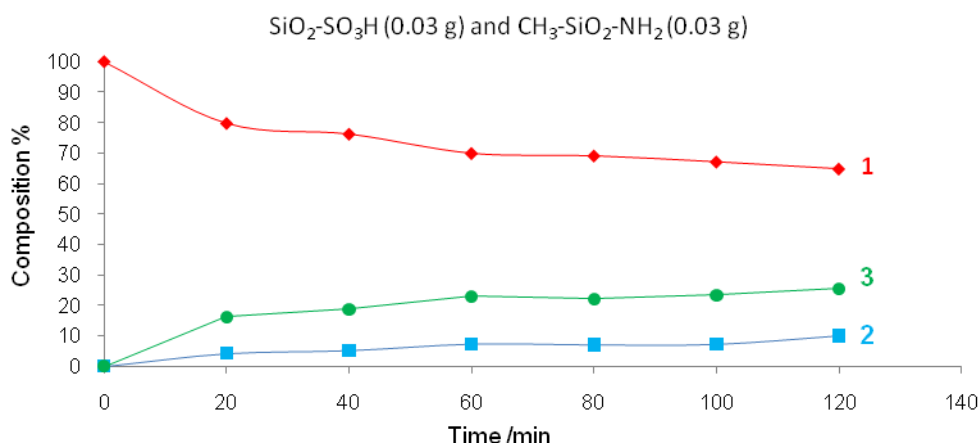


**Figure 3.18** – Composition of the reaction mixture vs. time for the deacetalization-Henry reaction, catalyzed by physical mixtures of  $\text{SiO}_2\text{-SO}_3\text{H}$  (0.03 g) and  $\text{CH}_3\text{-SiO}_2\text{-NH}_2$  (0.03 g) at 90 °C.

The kinetic data in Figure 3.18 show that the acid-catalyzed conversion of benzaldehyde dimethyl acetal reaches 35% after 2 h when  $\text{SiO}_2\text{-SO}_3\text{H}$  (0.03 g) and  $\text{NH}_2\text{-SiO}_2\text{-CH}_3$  (0.03 g) catalysts were used, compared to 65% when same amounts of  $\text{SiO}_2\text{-SO}_3\text{H}$  and  $\text{SiO}_2\text{-NH}_2$  catalysts were used. The decrease in the rate of the acid-catalyzed step is a result of the decrease in the rate of base-catalyzed step, which is expected with  $\text{NH}_2\text{-SiO}_2\text{-CH}_3$  catalyst. The catalytic activity of physical mixtures of 0.09 g  $\text{NH}_2\text{-SiO}_2\text{-CH}_3$

and 0.06 g  $\text{SiO}_2\text{-SO}_3\text{H}$  in a tandem deacetalization-Henry reaction is shown in Figure 3.19.

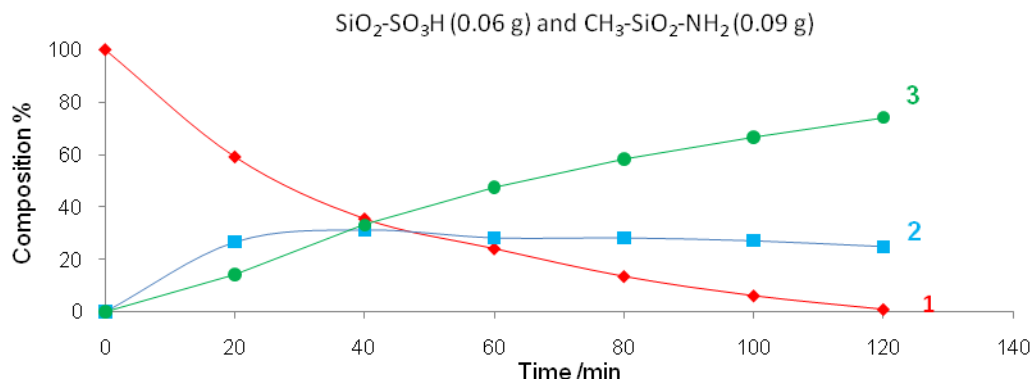


**Figure 3.19** – Composition of the reaction mixture vs. time for the deacetalization-Henry reaction, catalyzed by physical mixtures of  $\text{SiO}_2\text{-SO}_3\text{H}$  (0.06 g) and  $\text{CH}_3\text{-SiO}_2\text{-NH}_2$  (0.09 g).

In Figure 3.19, when the weight of the acid catalyst is increased by factor two the rate of the first step is still only half that recorded with the same amount of the uncapped supported amine catalyst (Figure 3.17). This is consistent with the idea of cooperation between silanol and amine, as discussed before.

The catalytic activities of all studied catalysts in tandem deacetalization-Henry reaction in this chapter are summarized in Table 3.5.

**Table 3.5** – One-pot deacetalization–Henry reaction over different catalysts.

Catalyst	Acid sites <sup>a</sup> /mmol	Base sites <sup>b</sup> /mmol	Conv. of 1 /%	Yield of 2 /%	Yield of 3 /%
SiO <sub>2</sub>	-	-	Trace	Trace	Trace
SiO <sub>2</sub> -NH <sub>2</sub>	-	0.039	Trace	Trace	Trace
SiO <sub>2</sub> -SO <sub>3</sub> H	0.006	-	40	40	Trace
SiO <sub>2</sub> -NH <sub>2</sub>	-	0.039	Trace	Trace	Trace
SiO <sub>2</sub> -SO <sub>3</sub> H + SiO <sub>2</sub> -NH <sub>2</sub>	0.006	0.039	65	14	51
SiO <sub>2</sub> -SO <sub>3</sub> H + SiO <sub>2</sub> -NH <sub>2</sub>	0.006	0.039	100	22	71
SiO <sub>2</sub> -SO <sub>3</sub> H (1) + SiO <sub>2</sub> -NH <sub>2</sub> (3)	0.006	0.117	71	-	71
SiO <sub>2</sub> -SO <sub>3</sub> H (2) + SiO <sub>2</sub> -NH <sub>2</sub> (3)	0.012	0.117	94	-	94
SiO <sub>2</sub> -SO <sub>3</sub> H + NH <sub>2</sub> -SiO <sub>2</sub> -CH <sub>3</sub>	0.006	0.039	35	10	25
SiO <sub>2</sub> -SO <sub>3</sub> H (2) + NH <sub>2</sub> -SiO <sub>2</sub> -CH <sub>3</sub> (3)	0.012	0.117	99	25	74
SiO <sub>2</sub> -SO <sub>3</sub> H + SiO <sub>2</sub> -NH <sub>2</sub> + p-TSA	0.109	0.039	100	100	Trace
SiO <sub>2</sub> -SO <sub>3</sub> H + SiO <sub>2</sub> -NH <sub>2</sub> + APTMS	0.006	0.139	Trace	Trace	Trace

Reaction conditions: Benzaldehyde dimethyl acetal 0.1 ml, water 0.06 ml, nitromethane 5 ml, catalyst 0.05 g, 90 °C, 6 h reaction time. (a) from calorimetric adsorption of NH<sub>3</sub>. (b) from titration. p-TSA is para-toluenesulfonic acid, and APTMS is aminopropyltrimethoxysilane

As shown in Table 3.6, no conversion of benzaldehyde dimethyl acetal was observed when SiO<sub>2</sub>, SiO<sub>2</sub>-NH<sub>2</sub> and SiO<sub>2</sub>-NH<sub>2</sub> (H<sub>2</sub>O) catalysts were used, due to the absence of acid catalytic centres, which are needed for the first step. Likewise, the physical mixture showed no activity when treated with aminopropyltrimethoxysilane (APTMS), which neutralizes acid sites, thus leaving only the amine base sites. When SiO<sub>2</sub>-SO<sub>3</sub>H and SiO<sub>2</sub>-SO<sub>3</sub>H were used without solid base catalyst, the results showed only 100% conversion in the first step and no conversion in the second step. The physical mixture showed only 100% conversion in the first step and no conversion in the second step when treated with para-toluenesulfonic acid (p-TSA), which neutralizes the amine functional groups, thus leaving only the sulfonic acid sites. These results illustrate the cooperative activity of the physical mixture of SiO<sub>2</sub>-NH<sub>2</sub>/ SiO<sub>2</sub>-SO<sub>3</sub>H and the coexistent acidity and basicity.

### 3.11. Conclusion

In summary, we have shown that base catalysts exhibit different activities in nitroaldol reaction depending on the methodology followed for their preparation. In fact, a catalyst

prepared by co-condensation procedure (MCM-41-NH<sub>2</sub> (C)) is less active than those obtained by the grafting strategy (SiO<sub>2</sub>-NH<sub>2</sub> and MCM-41-NH<sub>2</sub> (C)); this is ascribable to the fact that, in the former catalyst, the propylamines are incorporated within the siliceous framework and cannot show catalytic activity. In the latter, despite a reduction in the pore size, the aminopropyl groups are directly linked to the surface of a preformed material and, consequently, the majority of them are accessible by the reactants. The effect of pre-treatment of amorphous silica with concentrated acid apparently reduces its capacity to be functionalized with aminopropyl groups through the grafting method but it nevertheless results in higher activity of the silica supported amine catalyst. When the silanol groups are produced by acid treatment, the key consequence appears to be their ability to take part in a cooperative mechanism in the nitroaldol reaction.

Solid acid catalysts have also been prepared by grafting mercaptopropyltrimethoxysilane; then -SH groups were oxidized to -SO<sub>3</sub>H. The oxidation method seems to influence the number of acid sites in the final catalysts. The catalytic activity of acid catalysts showed that the catalysts prepared by HNO<sub>3</sub> oxidation method are more active than the catalysts prepared by H<sub>2</sub>O<sub>2</sub> oxidation method, in line with the data obtained from ammonia adsorption calorimetry, which shows that more acid sites are generated on the material prepared by concentrated HNO<sub>3</sub> as oxidant results.

Activity of the physical mixture of SiO<sub>2</sub>-NH<sub>2</sub>/ SiO<sub>2</sub>-SO<sub>3</sub>H was studied in tandem with deacetalization-Henry reaction, and the coexistent acidity and basicity was confirmed by the results. Solid immobilization of catalytic sites allows them to be used in cooperative catalysis, which would self-quench in homogeneous media. Regulation of the reaction rate by manipulating and controlling the catalysts' amount, type and additives was presented. The amount of solid acid catalyst seems to control the point at which reaction ceases. In the absence of water the reaction is hindered in the early stages. However, water is produced in the second step of the reaction (base-catalyzed step), and it can sustain the process at a certain limit. The cooperation between silanol-amine groups in the second step is necessary to accelerate the production of water and thus the completion of the reaction.

The combination of recoverable catalysts allowed a successful application of opposing catalysts to multistep, one-pot catalytic reactions including the ability to push the rate of the reaction at each step. A library of physical mixtures of solid catalysts could thus be generated and used in a variety of one-pot multistep catalytic reactions.

### 3.12. References

- [1] I. Fecheté, Y. Wang, J. C. Védrine, *Catalysis Today* **2012**, 189, 2-27.
- [2] K. Tanabe, W. F. Holderich, *Applied Catalysis A: General* **1999**, 181, 399-434.
- [3] Y. Kudoh, T. Kojima, M. Abe, M. Oota, T. Yamamoto, *Solid State Ionics* **2013**, 253, 189-194.
- [4] N. R. Cameron, A. Barbetta, *Journal of Materials Chemistry* **2000**, 10, 2466-2471.
- [5] J. Helminen, E. Paatero, *Reactive and Functional Polymers* **2006**, 66, 1021-1032.
- [6] D. Macquarrie, *Topics in Catalysis* **2009**, 52, 1640-1650.
- [7] D. J. MacQuarrie, D. J. MacQuarrie, in *Nanoporous Materials* (Eds.: X. S. Zhao, X. S. Zhao), Imperial College Press, **2005**.
- [8] X. S. Zhao, G. Q. Lu, G. J. Millar, *Industrial & Engineering Chemistry Research* **1996**, 35, 2075-2090.
- [9] M. Bandyopadhyay, N. R. Shiju, D. R. Brown, *Catalysis Communications* **2010**, 11, 660-664.
- [10] J. Machado, J. E. Castanheiro, I. Matos, A. M. Ramos, J. Vital, I. M. Fonseca, *Microporous and Mesoporous Materials* **2012**, 163, 237-242.
- [11] J. Patarin, B. Lebeau, R. Zana, *Current Opinion in Colloid & Interface Science* **2002**, 7, 107-115.
- [12] K. Wilson, A. F. Lee, D. J. Macquarrie, J. H. Clark, *Applied Catalysis A: General* **2002**, 228, 127-133.
- [13] D. Das, J.-F. Lee, S. Cheng, *Journal of Catalysis* **2004**, 223, 152-160.
- [14] D. Das, J.-F. Lee, S. Cheng, *Chemical Communications* **2001**, 2178-2179.
- [15] K.-i. Shimizu, E. Hayashi, T. Hatamachi, T. Kodama, T. Higuchi, A. Satsuma, Y. Kitayama, *Journal of Catalysis* **2005**, 231, 131-138.
- [16] B. Sow, S. Hamoudi, M. Hassan Zahedi-Niaki, S. Kaliaguine, *Microporous and Mesoporous Materials* **2005**, 79, 129-136.
- [17] V. Dufaud, M. E. Davis, *Journal of the American Chemical Society* **2003**, 125, 9403-9413.
- [18] I. K. Mbaraka, B. H. Shanks, *Journal of Catalysis* **2005**, 229, 365-373.
- [19] M. Alvaro, A. Corma, D. Das, V. Fornes, H. Garcia, *Chemical Communications* **2004**, 956-957.
- [20] M. A. Stanescu, R. S. Varma, *Tetrahedron Letters* **2002**, 43, 7307-7309.
- [21] V. Antochshuk, M. Jaroniec, *Chemistry of Materials* **2000**, 12, 2496-2501.
- [22] I. Díaz, F. Mohino, J. Pérez-Pariente, E. Sastre, *Applied Catalysis A: General* **2001**, 205, 19-30.
- [23] M. H. Lim, C. F. Blanford, A. Stein, *Chemistry of Materials* **1998**, 10, 467-470.
- [24] W. D. Bossaert, D. E. De Vos, W. M. Van Rhijn, J. Bullen, P. J. Grobet, P. A. Jacobs, *Journal of Catalysis* **1999**, 182, 156-164.
- [25] W. Van Rhijn, D. De Vos, W. Bossaert, J. Bullen, B. Wouters, P. Grobet, P. Jacobs, *Vol. 117*, **1998**, pp. 183-190.
- [26] Y. Ono, T. Baba, *Catalysis Today* **1997**, 38, 321-337.
- [27] H. Pines, H. E. Eschinazi, *Journal of the American Chemical Society* **1955**, 77, 6314-6321.
- [28] H. Hattori, *Chemical Reviews* **1995**, 95, 537-558.
- [29] A. Corma, S. Iborra, in *Advances in Catalysis, Vol. Volume 49* (Eds.: C. G. Bruce, K. Helmut), Academic Press, **2006**, pp. 239-302.
- [30] G. Centi, S. Perathoner, in *Comprehensive Inorganic Chemistry II (Second Edition)* (Eds.: J. Reedijk, K. Poepelmeier), Elsevier, Amsterdam, **2013**, pp. 153-184.
- [31] H. Tsuji, F. Yagi, H. Hattori, H. Kita, in *Studies in Surface Science and Catalysis, Vol. Volume 75* (Eds.: F. S. L. Guzzi, T. P.), Elsevier, **1993**, pp. 1171-1183.
- [32] A. Corma, R. M. Martín-Aranda, *Journal of Catalysis* **1991**, 130, 130-137.
- [33] A. Islam, Y. H. Taufiq-Yap, C.-M. Chu, P. Ravindra, E.-S. Chan, *Renewable Energy* **2013**, 59, 23-29.
- [34] X. Wu, M. Tamm, *Coordination Chemistry Reviews* **2014**, 260, 116-138.
- [35] K. A. Utting, D. J. Macquarrie, *Applied Catalysis A: General* **2002**, 232, 7-12.
- [36] H. Fei, D. L. Rogow, S. R. J. Oliver, *Journal of the American Chemical Society* **2010**, 132, 7202-7209.
- [37] G. Nagendrappa, *Applied Clay Science* **2011**, 53, 106-138.
- [38] R. Lin, Y. Ding, *Materials* **2013**, 6, 217-243.
- [39] W. Lang, B. Su, Y. Guo, L. Chu, *Sci. China Chem.* **2012**, 55, 1167-1174.
- [40] H. Hattori, *Applied Catalysis A: General* **2001**, 222, 247-259.

- [41] N. A. Comelli, M. L. Ruiz, N. A. Merino, I. D. Lick, E. Rodríguez-Castellón, A. Jiménez-López, M. I. Ponzi, *Applied Clay Science* **2013**, 80–81, 426-432.
- [42] S. Bonollo, D. Lanari, T. Angelini, F. Pizzo, A. Marrocchi, L. Vaccaro, *Journal of Catalysis* **2012**, 285, 216-222.
- [43] H. Deleuze, X. Schultze, D. C. Sherrington, *Polymer* **1998**, 39, 6109-6114.
- [44] N. G. Khaligh, T. Mihankhah, *Chinese Journal of Catalysis* **2013**, 34, 2167-2173.
- [45] D. J. MacQuarrie, D. Brunel, D. J. MacQuarrie, D. Brunel, in *Fine Chemicals Through Heterogeneous Catalysis* (Eds.: H. van Bekkum, H. van Bekkum), Wiley-VCH, **2001**.
- [46] D. J. Macquarrie, J. H. Clark, A. Lambert, J. E. G. Mdoe, A. Priest, D. J. Macquarrie, J. H. Clark, A. Lambert, J. E. G. Mdoe, A. Priest, *REACTIVE* **1997**, 35, 153-158.
- [47] F. C. Jentoft, in *Comprehensive Inorganic Chemistry II (Second Edition)* (Eds.: J. Reedijk, K. Poeppelmeier), Elsevier, Amsterdam, **2013**, pp. 205-230.
- [48] J. Weitkamp, M. Hunger, U. Ryma, *Microporous and Mesoporous Materials* **2001**, 48, 255-270.
- [49] A. Corma, S. Iborra, Rodri, amp, x, I. guez, F. Sánchez, *Journal of Catalysis* **2002**, 211, 208-215.
- [50] D. J. Macquarrie, R. Maggi, A. Mazzacani, G. Sartori, R. Sartorio, *Applied Catalysis A: General* **2003**, 246, 183-188.
- [51] R. K. Zeidan, S.-J. Hwang, M. E. Davis, *Angewandte Chemie International Edition* **2006**, 45, 6332-6335.
- [52] K. C. Nicolaou, T. Montagnon, S. A. Snyder, *Chemical Communications* **2003**, 551-564.
- [53] B. J. Cohen, M. A. Kraus, A. Patchornik, *Journal of the American Chemical Society* **1981**, 103, 7620-7629.
- [54] B. Voit, *Angewandte Chemie International Edition* **2006**, 45, 4238-4240.
- [55] M. J. Astle, J. A. Zaslowsky, *Industrial & Engineering Chemistry* **1952**, 44, 2867-2869.
- [56] G. Manecke, W. Storck, *Angewandte Chemie International Edition in English* **1978**, 17, 657-670.
- [57] F. Gelman, J. Blum, D. Avnir, *Angewandte Chemie* **2001**, 113, 3759-3761.
- [58] F. Gelman, J. Blum, D. Avnir, *New Journal of Chemistry* **2003**, 27, 205-207.
- [59] J. B. Laughlin, J. L. Sarquis, V. M. Jones, J. A. Cox, *Journal of Chemical Education* **2000**, 77, 77.
- [60] R. Makote, M. M. Collinson, *Analytica Chimica Acta* **1999**, 394, 195-200.
- [61] F. Gelman, J. Blum, H. Schumann, D. Avnir, *Journal of Sol-Gel Science and Technology* **2003**, 26, 43-46.
- [62] K. Motokura, D. Nishimura, K. Mori, T. Mizugaki, K. Ebitani, K. Kaneda, *Journal of the American Chemical Society* **2004**, 126, 5662-5663.
- [63] K. Motokura, N. Fujita, K. Mori, T. Mizugaki, K. Ebitani, K. Kaneda, *Journal of the American Chemical Society* **2005**, 127, 9674-9675.
- [64] B. Helms, S. J. Guillaudeu, Y. Xie, M. McMurdo, C. J. Hawker, J. M. J. Fréchet, *Angewandte Chemie* **2005**, 117, 6542-6545.
- [65] N. T. S. Phan, C. S. Gill, J. V. Nguyen, Z. J. Zhang, C. W. Jones, *Angewandte Chemie International Edition* **2006**, 45, 2209-2212.
- [66] R. K. Zeidan, S.-J. Hwang, M. E. Davis, *Angewandte Chemie* **2006**, 118, 6480-6483.
- [67] J. Alauzun, A. Mehdi, C. Reyé, R. J. P. Corriu, *Journal of the American Chemical Society* **2006**, 128, 8718-8719.
- [68] Y. Shao, H. Liu, X. Yu, J. Guan, Q. Kan, *Materials Research Bulletin* **2012**, 47, 768-773.
- [69] F. Shang, J. Sun, S. Wu, Y. Yang, Q. Kan, J. Guan, *Microporous and Mesoporous Materials* **2010**, 134, 44-50.
- [70] Y. Huang, S. Xu, V. S. Y. Lin, *Angewandte Chemie International Edition* **2011**, 50, 661-664.
- [71] E. Gianotti, U. Diaz, A. Veltz, A. Corma, *Catalysis Science & Technology* **2013**, 3, 2677-2688.
- [72] S. Huh, H.-T. Chen, J. W. Wiench, M. Pruski, V. S. Y. Lin, *Angewandte Chemie International Edition* **2005**, 44, 1826-1830.
- [73] N. R. Shiju, A. H. Alberts, S. Khalid, D. R. Brown, G. Rothenberg, *Angewandte Chemie International Edition* **2011**, 50, 9615-9619.
- [74] K. Suzuki, M. Sugawa, Y. Kikukawa, K. Kamata, K. Yamaguchi, N. Mizuno, *Inorganic Chemistry* **2012**, 51, 6953-6961.
- [75] M. Zhang, P. Zhao, Y. Leng, G. Chen, J. Wang, J. Huang, *Chemistry – A European Journal* **2012**, 18, 12773-12782.
- [76] Q. Zhao, H. Wang, H. Zheng, Z. Sun, W. Shi, S. Wang, X. Wang, Z. Jiang, *Catalysis Science & Technology* **2013**, 3, 2204-2209.

- [77] J.-W. Park, Y. J. Park, C.-H. Jun, *Chemical Communications* **2011**, 47, 4860-4871.
- [78] I. Díaz, F. Mohino, J. n. Pérez-Pariente, E. Sastre, *Thermochimica Acta* **2004**, 413, 201-207.
- [79] J. Qi, B. Qin, J. Liu, Y. Yu, Z. Zhang, W. Zhang, Q. Cai, W. Zhu, *CrystEngComm* **2011**, 13, 4666-4675.
- [80] P. Iliade, I. Miletto, S. Coluccia, G. Berlier, *Res Chem Intermed* **2012**, 38, 785-794.
- [81] H. E. Cross, D. R. Brown, *Catalysis Communications* **2010**, 12, 243-245.
- [82] P. F. Siril, A. D. Davison, J. K. Randhawa, D. R. Brown, *Journal of Molecular Catalysis A: Chemical* **2007**, 267, 72-78.
- [83] C. S. Hill, A. Norton, G. Newman, *Wood Sci Technol* **2010**, 44, 497-514.
- [84] K. S. W. Sing, D. H. Everett, R. A. Haul, W. L. Moscou, R. A. Pierotti, J. Rouquérol, T. Siemieniewska, **1985**, 57, 603.
- [85] M. Mokhonoana, N. Coville, *Journal of Sol-Gel Science and Technology* **2010**, 54, 83-92.
- [86] X. Xu, C. Song, J. M. Andresen, B. G. Miller, A. W. Scaroni, *Energy & Fuels* **2002**, 16, 1463-1469.
- [87] G. Sartori, F. Bigi, R. Maggi, R. Sartorio, D. J. Macquarrie, M. Lenarda, L. Storaro, S. Coluccia, G. Martra, *Journal of Catalysis* **2004**, 222, 410-418.
- [88] M. Etienne, A. Walcarius, *Talanta* **2003**, 59, 1173-1188.
- [89] A. L. Petre, J. A. Perdigón-Melón, A. Gervasini, A. Auroux, *Topics in Catalysis* **2002**, 19, 271-281.
- [90] F. Rezaei, C. W. Jones, *Industrial & Engineering Chemistry Research* **2013**, 52, 12192-12201.
- [91] K. K. Sharma, A. V. Biradar, S. Das, T. Asefa, *European Journal of Inorganic Chemistry* **2011**, 2011, 3174-3182.
- [92] A. Anan, R. Vathyam, K. Sharma, T. Asefa, *Catal Lett* **2008**, 126, 142-148.
- [93] M. Mora, M. Ángeles Carmona, C. Jiménez-Sanchidrián, M. Isabel López, J. Rafael Ruiz, *React Kinet Mech Cat* **2010**, 99, 303-309.
- [94] M. A. Sturgess, D. J. Yarberr, *Tetrahedron Letters* **1993**, 34, 4743-4746.
- [95] D. Macquarrie, *Applied Catalysis A: General* **2003**, 246, 183-188.
- [96] P. Bollini, N. A. Brunelli, S. A. Didas, C. W. Jones, *Industrial and Engineering Chemistry Research* **2012**, 51, 15153-15162.
- [97] J. D. Bass, A. Solovyov, A. J. Pascall, A. Katz, *Journal of the American Chemical Society* **2006**, 128, 3737-3747.
- [98] D. Zorn, V. S. Y. Lin, M. Pruski, M. S. Gordon, *Journal of Physical Chemistry A* **2008**, 112, 10635-10649.

## Chapter 4

# Co-operative acid base bifunctional catalyst

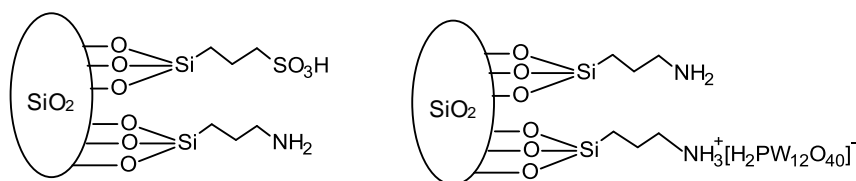
---

In this chapter, catalysts with acid and base groups on the same support are prepared, tested and compared.

#### 4. Introduction

There are many reactions where both acid and base catalysis are required, often in sequential steps, and there are obvious advantages in being able to use a bifunctional solid catalyst which carries both acid and base groups on the same support.<sup>[1-3]</sup> Preparing materials of this type is difficult, not least because of the possibility of mutual neutralization of the active groups. Although some catalysts have been prepared in which the supported acid and base groups retain activity,<sup>[4-7]</sup> the challenge remains to develop solid bifunctional acid-base catalysts with stabilities and activities of practical use.

Despite the large number of papers recently published on this topic, results from the literature are somewhat conflicting and do not allow an easy choice of the best acid-base bifunctional heterogeneous catalyst. This may be because completely different model reactions were analyzed under different experimental conditions. In this chapter, simple and straightforward routes to such bifunctional solids are presented. Two approaches to preparing such bifunctional catalysts are introduced. In the first, the acid and base groups are added by functionalizing the silica support with (3-aminopropyl)trimethoxysilane, and with (3-mercaptopropyl)trimethoxysilane. The thiol groups are then oxidized to sulfonic acid groups (labelled  $\text{NH}_2\text{-SiO}_2\text{-SO}_3\text{H}$ ) (Scheme 4.1). Remarkably, during the synthesis process of  $\text{NH}_2\text{-SiO}_2\text{-SO}_3\text{H}$ , the post-synthesis protection and deprotection procedure to preserve the base functionality was found to be unnecessary. In the second approach, the silica is functionalized with (3-aminopropyl) trimethoxysilane which is then partially neutralized with phosphotungstic acid. The bi-functional acid/base catalysts prepared by this route are labelled  $\text{NH}_2\text{-SiO}_2\text{-PTA}$  (Scheme 4.1).<sup>[8]</sup>

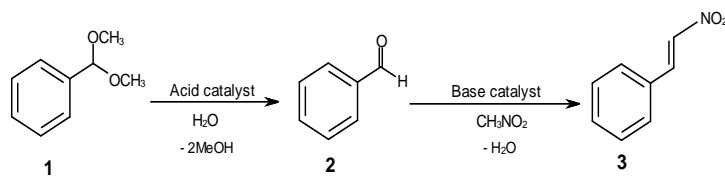


**Scheme 4.1** –  $\text{NH}_2\text{-SiO}_2\text{-SO}_3\text{H}$  and  $\text{NH}_2\text{-SiO}_2\text{-PTA}$  bifunctional catalysts.

A potential difficulty associated with preparation of the aminopropyl/propylsulfonic acid bi-functional catalysts ( $\text{NH}_2\text{-SiO}_2\text{-SO}_3\text{H}$ ) is that the acid group is grafted to the silica using (3-mercaptopropyl)trimethoxysilane (MPTMS) and an oxidation step is required to convert the thiol (-SH) to sulfonic acid (-SO<sub>3</sub>H) groups. This oxidation step can, in principle, oxidize or affect, in some other way, the grafted aminopropyl groups. The two main routes reported for this step are based on hydrogen peroxide followed by sulfuric acid, and on nitric acid (as both oxidant and acidifier).<sup>[9-10]</sup> The method and reagents used for the oxidation step must be chosen to effectively oxidize thiol<sup>[10]</sup> but with minimal side reaction with the base groups. Complete conversion of thiol is particularly important where levels of thiol grafting are low, as in this case of bi-functional materials, and nitric acid has been shown to be effective under these conditions.<sup>[11]</sup> Crucially, co-functionalized amine groups have been shown to be more resistant to oxidation by nitric acid than by hydrogen peroxide, possibly because they are largely in the  $\text{-NH}_3^+$  form.<sup>[11]</sup> Zeidan et al.<sup>[12]</sup> have used this approach with similar catalysts and report that extensive washing of the (acid) oxidized materials regenerates basicity. For this reason, nitric acid, rather than hydrogen peroxide, is used as the oxidant in the work reported here.

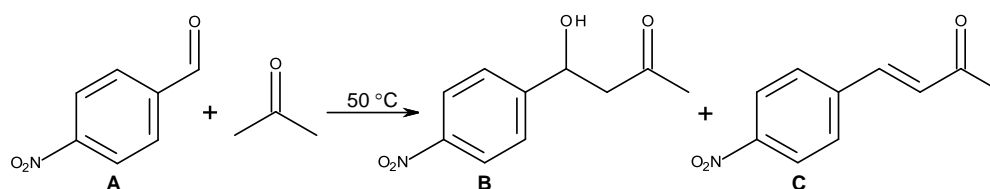
An amorphous silica gel has been used as the catalyst support, rather than other ordered mesoporous silica (e.g. MCM-41<sup>[13-15]</sup> or SBA-15<sup>[8, 12, 16]</sup>) as used in much of the published work on this topic. Silica gel does not exhibit the friability and low bulk density of ordered silica, making it easier to handle<sup>[17-19]</sup>, while the surface properties and stability of amorphous silica gel are similar to those of the ordered silica, and it can be functionalized in the same way. The silica gel used here has been chosen to have an average pore diameter similar to that of an ordered mesoporous silica.

The catalytic activities of these bifunctional catalysts are compared in two reactions. The first is a tandem deacetalization-Henry reaction. This reaction starts with the acid-catalyzed deacetalization of benzaldehyde dimethyl acetal in the presence of water, giving benzaldehyde. The benzaldehyde then reacts with nitromethane in a base-catalyzed step, giving nitrostyrene (scheme 4.2).



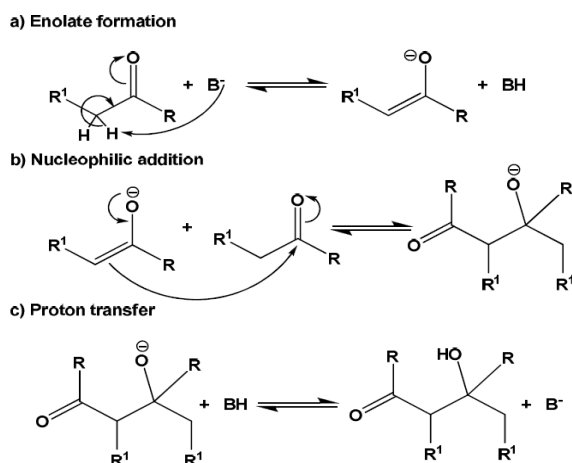
**Scheme 4.2** – Tandem deacetalization-Henry reaction.

The second reaction is the aldol condensation between 4-nitrobenzaldehyde and acetone, catalyzed by acid, base and bifunctional acid-base pairs (scheme 4.3).



**Scheme 4.3** – Cross-aldol reaction between 4-nitrobenzaldehyde (A) and acetone to give 4-hydroxy-4-(p-nitrophenyl)butan-2-one (B) and (E)-4-(4-nitrophenyl)but-3-en-2-one (C) products.

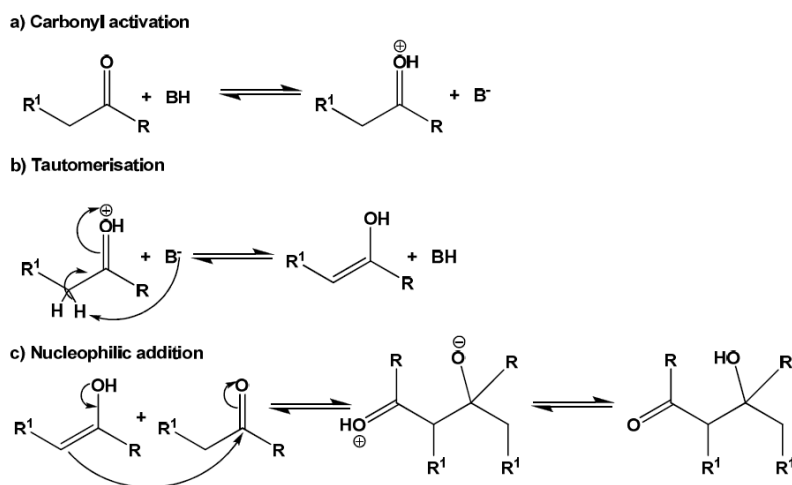
The aldol reaction may be either acid- or base-catalyzed; however, base catalysts are generally preferred. The mechanism of the base-catalyzed condensation reaction of acetaldehyde to form aldol is given below (Scheme 4.4).



**Scheme 4.4** – Reaction mechanism for base-catalyzed aldol reaction.

The first step is the removal of an alpha proton to give a resonance-stabilized enolate anion. In the second step, the enolate anion attacks the carbonyl carbon of a second molecule of acetaldehyde to form a carbon-carbon bond and an alkoxide anion. In the third step, the alkoxide anion abstracts a proton from water to regenerate the hydroxide catalyst. Since all of these steps are reversible, a successful synthesis is contingent on the product being more stable than the reactants, or on some technique for driving the equilibrium towards products.

The acid-catalyzed aldol addition (Scheme 4.5) involves the protonation of the donor, which then tautomerizes to enol by losing a proton. This active species attacks an acceptor carbonyl, generating the corresponding protonated aldol, which is transformed in the neutral aldol by a proton transfer



**Scheme 4.5** – Reaction mechanism for base-catalyzed aldol reaction.

However, it has been proposed that the aldol formation can be accelerated through a second mechanism involving adjacent acid and base catalytic sites acting in concert.<sup>[13]</sup> In this mechanism, acetone is activated by reaction with the acid. The activated acetone is then subject to nucleophilic attack by the amine to form an imine. The imine is then deprotonated to regenerate the acid and form the corresponding enamine. The nitromethane is activated by the acid centre and is then subject to nucleophilic addition by the enamine. The aldol is then formed by reaction with water. The usefulness of this

reaction lies in the fact that, if such acid-base pairs are present and their cooperative mechanism is in place, the yield of B, the aldol product, should be increased relative to C, the dehydration product. In other words, high activity and selectivity towards B is an indicator of the presence of catalytic acid-base pairs.<sup>[13]</sup>

## 4.1. Experimental Section

### 4.1.1. Materials

Silica gel (particle size 40-63  $\mu\text{m}$ ; average pore size 6 nm), (3-mercaptopropyl)trimethoxysilane, (3-aminopropyl)trimethoxysilane, nitromethane, benzaldehyde dimethyl acetal, 4-nitrobenzaldehyde, acetone, o-xylene, dichloromethane, ethanol, and phosphotungstic acid were purchased from Aldrich. Benzaldehyde was purchased from Acros and nitric acid from Fischer. Unless noted otherwise, all chemicals were at least 99 % pure and used as received. Deionized water was used in all experiments. The silica gel was activated before use by refluxing 30 g in 150 ml HCl solution (37 %) for 4 h at 100  $^{\circ}\text{C}$ . It was washed thoroughly with water to remove all acid residues, and dried in still air at 120  $^{\circ}\text{C}$  for 12 h.<sup>[20]</sup>

## 4.2. Catalyst synthesis

### 4.2.1. Supported propylamine catalysts (Scheme 4.4)

$\text{SiO}_2\text{-NH}_2$ : Activated silica gel (3.0 g) was suspended in 50 ml dry toluene, and 3 ml (3-aminopropyl)trimethoxysilane added. The mixture was refluxed under dry nitrogen for 2 h at 80  $^{\circ}\text{C}$ . The liquid was filtered, and the cake washed with toluene, and then dried at 120  $^{\circ}\text{C}$  in still air for 2 h.<sup>[21]</sup> The basicity of  $\text{SiO}_2\text{-NH}_2$  was determined by  $\text{SO}_2$  adsorption calorimetry.

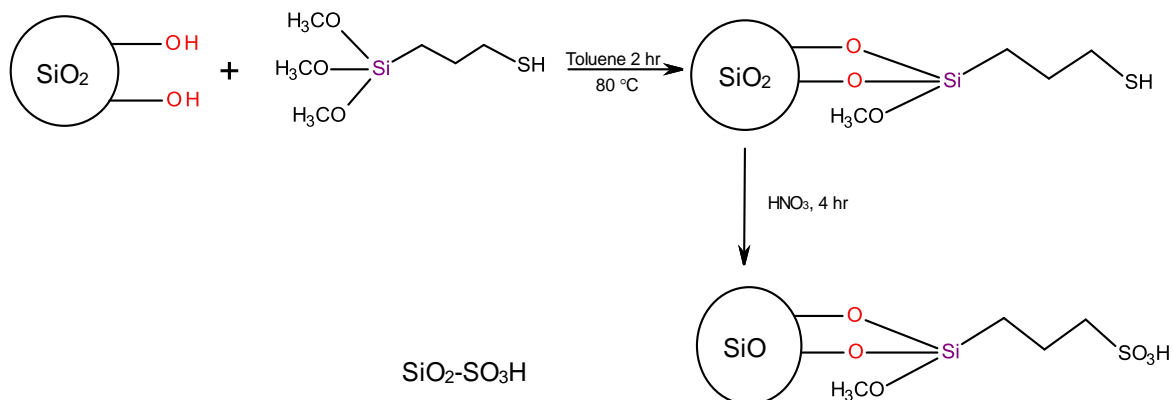


**Scheme 4.6** – Synthesis of supported base catalyst.

### 4.2.2. Supported propylsulfonic acid catalysts (Scheme 4.5)

$\text{SiO}_2\text{-SO}_3\text{H}$ : Activated silica gel (3.0 g) was treated as above but with 3 ml (3-mercaptopropyl)trimethoxysilane<sup>[21-22]</sup> to form  $\text{SiO}_2\text{-SH}$ . To convert thiol groups to

sulfonic acid groups, 0.5 g of  $\text{SiO}_2\text{-SH}$  was suspended in 20 ml 70% nitric acid solution (oxidant) at room temperature for 4 h.<sup>[9]</sup> The modified silica gel was filtered and washed with water until the pH of the washings was 7. The acidity of  $\text{SiO}_2\text{-SO}_3\text{H}$  was determined by  $\text{NH}_3$  adsorption calorimetry.



**Scheme 4.7** – Synthesis of supported acid catalyst.

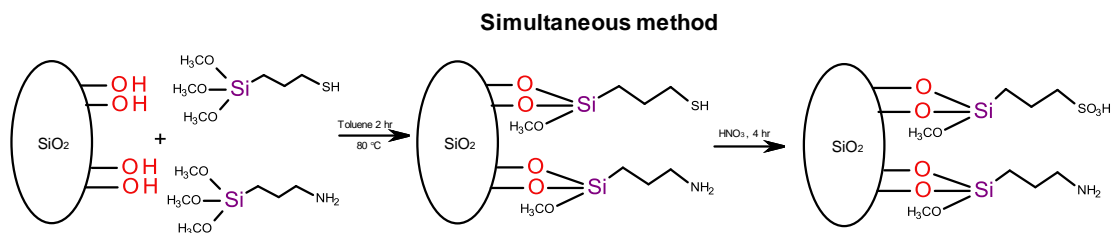
#### 4.2.3. Supported propylsulfonic acid-propylamine bifunctional catalysts

Two new and simple routes were used. In the first, the two functionalization steps were carried out simultaneously from the same solution (“simultaneous” method). In the second, the support was first functionalized with propylamine groups and then with propylthiol groups; then thiol groups were oxidized to sulfonic acid groups (“sequential” method). The reason for this was to study the ideal methodology to obtain the maximum efficiency of the cooperating groups which have the right arrangement of functional groups on the surface.

#### 4.2.4. Simultaneous method (Scheme 4.6)

$\text{NH}_2\text{-SiO}_2\text{-SO}_3\text{H}$  (simultaneous): Activated silica gel (1.0 g) was suspended in 50 ml toluene at 80 °C followed by the addition of 1 ml of (3-aminopropyl)trimethoxysilane and 1 ml of (3-mercaptopropyl)trimethoxysilane. The mixture was refluxed under nitrogen for 2 h at 80 °C. The modified silica gel was filtered, washed with toluene and left to dry at room temperature, to yield  $\text{NH}_2\text{-SiO}_2\text{-SH}$  (simultaneous). This material (0.5 g) was then suspended in 20 ml of 70% nitric acid at room temperature for 4 h to convert

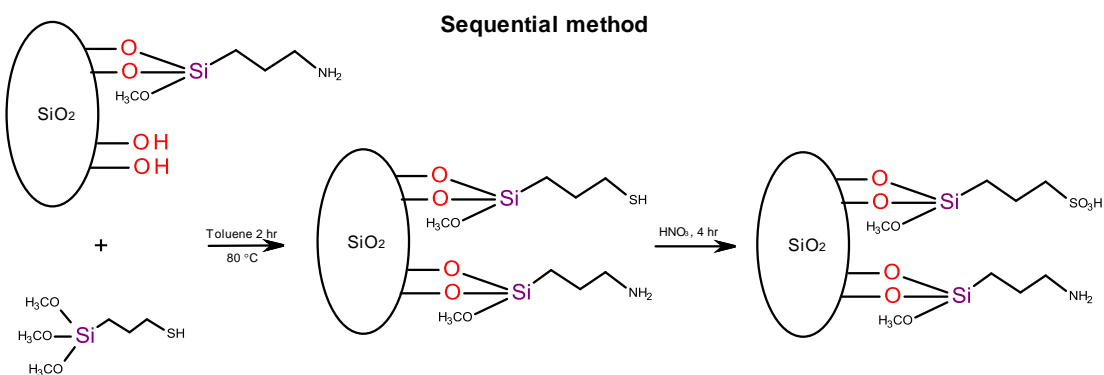
thiol to sulfonic acid groups. The product was filtered and washed with water until the pH of the washings was 7. The acidity and basicity of the catalyst were determined by  $\text{NH}_3$  and  $\text{SO}_2$  adsorption calorimetry respectively.



**Scheme 4.8** – Synthesis of acid-base bifunctional catalyst by the simultaneous method.

#### 4.2.5. Sequential methods (Scheme 4.7)

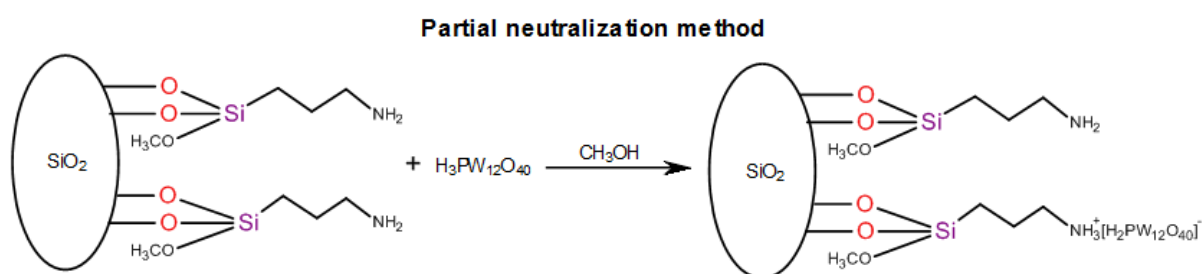
$\text{NH}_2\text{-SiO}_2\text{-SO}_3\text{H}$  (sequential: propylamine functionalised silica gel ( $\text{SiO}_2\text{-NH}_2$ )) was first prepared by the grafting method described above. 1.0 g of  $\text{SiO}_2\text{-NH}_2$  was then suspended in 50 ml dry toluene containing 5 mmol (3-mercaptopropyl)trimethoxysilane, and refluxed under nitrogen for 2 h at 80 °C. The product,  $\text{NH}_2\text{-SiO}_2\text{-SH}$  (sequential), was filtered, washed with toluene and left to dry at room temperature. To obtain the final material, 0.5 g of  $\text{NH}_2\text{-SiO}_2\text{-SH}$  (sequential) was suspended in 20 ml of 70% nitric acid at room temperature for 4 hour. The modified silica gel washed and dried.



**Scheme 4.9** – Synthesis of acid-base bifunctional catalyst by the sequential method.

#### 4.2.6. Supported propylamine/phosphotungstic acid bifunctional catalysts (Scheme 4.8)

NH<sub>2</sub>-SiO<sub>2</sub>-PTA: SiO<sub>2</sub>-NH<sub>2</sub> (1.0 g), containing approximately 1 mmol of amine, prepared as described above,<sup>[8]</sup> was stirred with a methanolic solution of 0.05 mmol phosphotungstic acid for 20 h. The solid was washed with warm water (60 °C) and dried, to yield NH<sub>2</sub>-SiO<sub>2</sub>-PTA 0.05. Similar materials were prepared with 0.1, 0.5 and 1.0 mmol of phosphotungstic acid, and are labelled accordingly as: NH<sub>2</sub>-SiO<sub>2</sub>-PTA 0.1, NH<sub>2</sub>-SiO<sub>2</sub>-PTA 0.5 and NH<sub>2</sub>-SiO<sub>2</sub>-PTA 0.9.



**Scheme 4.10** – Synthesis of acid-base bifunctional catalyst by the partial neutralization method.

#### 4.3. Catalyst characterization

Nitrogen adsorption–desorption isotherms were measured at 77 K on a Micromeritics ASAP-2020 after evacuation at 423 K for 5 h. The surface areas and the average pore sizes were calculated from the adsorption isotherms using the BET method and the desorption isotherms using BJH method respectively. Levels of functionalization were initially assessed through nitrogen, sulfur and carbon elemental analysis (MEDAC Ltd).

Catalyst basicity and acidity were quantified by SO<sub>2</sub> and NH<sub>3</sub> adsorption calorimetry, respectively. These experiments were performed using a system based on a flow-through Setaram 111 differential scanning calorimeter (DSC) and an automated gas flow and switching system, with a mass spectrometer (MS) detector for the downstream gas flow.<sup>[23-24]</sup>

In a typical adsorption experiment, the catalyst (30 mg) was activated at 120 °C under dry nitrogen flow at 10 ml min<sup>-1</sup>. Following activation, and maintaining the sample

temperature at 120 °C, pulses of the probe gas (1% ammonia in nitrogen or 1% sulfur dioxide in nitrogen) at atmospheric pressure were injected at regular intervals into the carrier gas stream from a gas-sampling valve. The concentration of the probe gas downstream of the sample was monitored continuously. The amount of the probe gas irreversibly adsorbed from each pulse was determined by comparing the MS signal during each pulse with a signal recorded during a control experiment. The net heat released for each pulse was calculated from the DSC thermal curves. From this, the molar enthalpies of adsorption of sulfur dioxide or ammonia ( $\Delta H_{\text{ads}}^{\circ}$ ) were obtained for the amount adsorbed from each successive pulse. The  $\Delta H_{\text{ads}}^{\circ}$  values were plotted against the amount of adsorbed probe gas per gram of the catalyst, to give a  $\Delta H_{\text{ads}}^{\circ}$ /coverage profiles for each catalyst.

Infrared spectra of the solid samples were recorded on a Nicolet 380 FT-IR instrument as KBr pellets over the range 400-4000  $\text{cm}^{-1}$  under atmospheric conditions. Water vapour adsorption isotherms were measured by a Surface Measurement Systems Dynamic Vapor Sorption apparatus (AdvantageTM), using a method described by Hill et al.<sup>[25]</sup> Adsorption isotherms were recorded at 25 °C, following activation of the catalysts at 100 °C.

#### 4.4. Catalytic activities

##### 4.4.1. Nitroaldol (Henry) reaction

Catalysts were activated before use at 120 °C for 2 h. A mixture of benzaldehyde (1 mmol), nitromethane (10 mL), and the selected catalyst (0.08 mmol) were kept at 70 °C under magnetic stirring. The reaction mixture was then stirred under an atmosphere of nitrogen and aliquots of the sample mixture were removed with a filter syringe and analyzed by gas chromatography GC (FID, 25 m BPI column) which was calibrated previously. The final product was fully identified by GC-MS. Nitrostyrene was the only product, accounting for 100% of the converted benzaldehyde. The possibility of catalyst leaching from the silica surface was tested by monitoring the reaction mixture after removal of the catalyst by filtration at the reaction temperature after a suitable reaction time. In all cases, the reaction ceased on removal of the catalyst.

#### 4.4.2. One-pot deacetalization–Henry reaction

Catalysts were activated before use at 120 °C. Benzaldehyde dimethylacetal (0.15 ml) and nitromethane (10 ml) were added to a glass reactor. The mixture was heated to 90 °C under nitrogen and catalyst (0.05 g) and water (0.06 ml) added. The stirrer speed was set to ensure that the reaction was not under diffusion control. Control experiments confirmed that the reaction did not proceed in the absence of catalyst. Aliquots of the sample mixture were removed with a filter syringe regularly and analyzed by gas chromatography (FID, 25 m BPI column).

#### 4.4.3. Aldol condensation reaction

The aldol condensation reaction was performed in a flask under nitrogen. First, 4-nitrobenzaldehyde (76 mg, 0.5 mmol) was dissolved in acetone (10 mL). Then each catalytic reaction was carried out over 0.20 g catalyst at 50 °C for 20 h. The catalysts were then separated by filtration, and the supernatants were concentrated under reduced pressure. Reaction yields were measured by <sup>1</sup>H NMR.

The study analyzed the disappearance of the signal of the aldehyde proton at δH 10.09 ppm and the concomitant increase of intensity of the signal associated with the single protons in the aldol products B at 5.20 ppm and C at 6.75 ppm. The percentage of the aldol products (B and C) were calculated by dividing the integral of the product proton signals by the sum of the integrals of the aldehyde proton signals plus the product proton signals considered as 100% (NMR spectra with interpretation in appendix A-2).

$$B(\%) = \frac{H(B)}{H(A) + H(B) + H(C)}, \quad C(\%) = \frac{H(C)}{H(A) + H(B) + H(C)}$$

## 4.5. Results and discussion

### 4.6. Characterization of the silica structures

Nitrogen adsorption–desorption isotherms for the SiO<sub>2</sub> support and for the catalysts SiO<sub>2</sub>-NH<sub>2</sub>, NH<sub>2</sub>-SiO<sub>2</sub>-SH (sequential) and NH<sub>2</sub>-SiO<sub>2</sub>-SO<sub>3</sub>H (sequential) are shown in Figure 4.1, illustrating the effect of functionalization on surface properties.

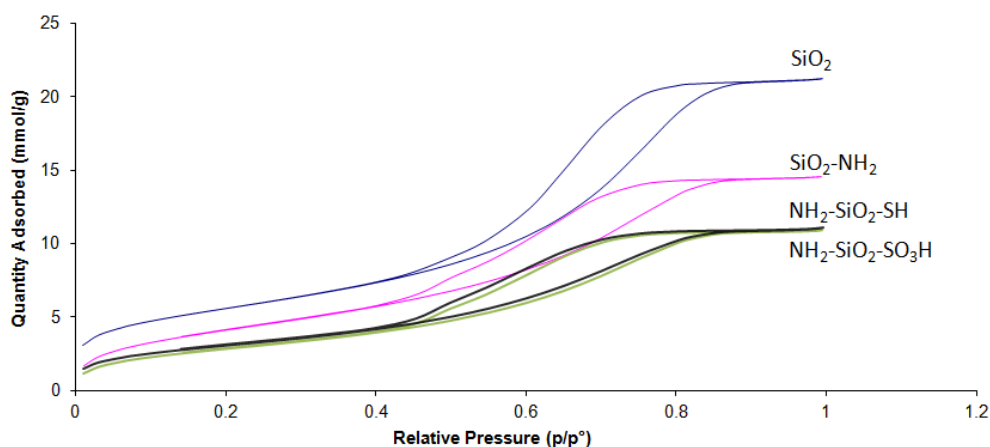


**Figure 4.1** – N<sub>2</sub> adsorption–desorption isotherms at 77 K for SiO<sub>2</sub>, SiO<sub>2</sub>-NH<sub>2</sub>, NH<sub>2</sub>-SiO<sub>2</sub>-SH (sequential) and NH<sub>2</sub>-SiO<sub>2</sub>-SO<sub>3</sub>H (sequential).

All samples display type IV isotherms, indicating the presence of mesopores.<sup>[6]</sup> With the introduction of organic functional groups, the specific surface area and pore volume progressively decrease, implying successful grafting of these groups in the pores of the support. Table 4.1 summarizes the data for all the catalysts in this series.

**Table 4.1** – Textural parameters for supported acid, supported base and amine/sulfonic acid samples.

Sample	Surface area /m <sup>2</sup> g <sup>-1</sup>	Pore volume /cm <sup>3</sup> g <sup>-1</sup>	Average pore diameter /nm
SiO <sub>2</sub>	452	0.75	5.1
SiO <sub>2</sub> -SO <sub>3</sub> H	418	0.57	4.4
SiO <sub>2</sub> -NH <sub>2</sub>	351	0.52	4.3
NH <sub>2</sub> -SiO <sub>2</sub> -SO <sub>3</sub> H (Sequential)	256	0.39	4.3
NH <sub>2</sub> -SiO <sub>2</sub> -SO <sub>3</sub> H (Simultaneous)	353	0.50	4.5

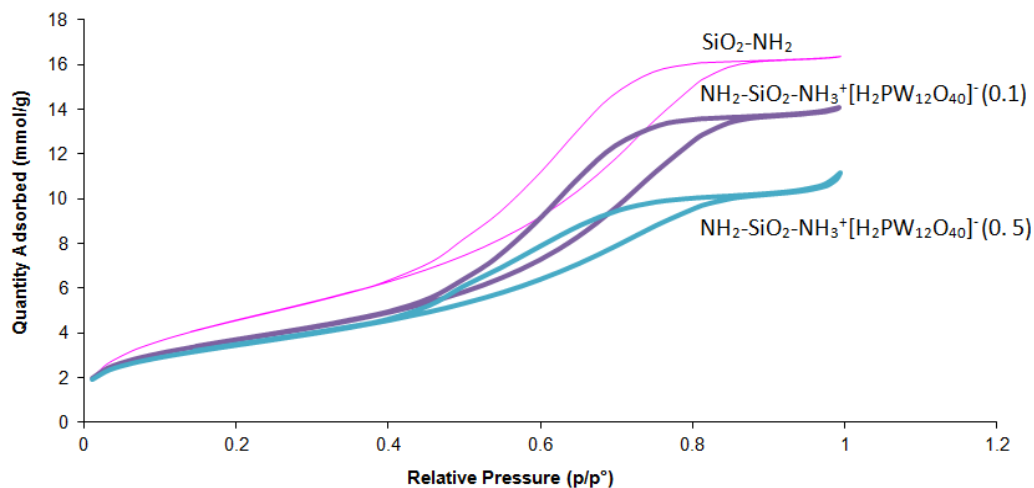


**Figure 4.2** –  $N_2$  adsorption–desorption isotherms at standard temperature of catalysts ( $SiO_2-NH_2$ ,  $NH_2-SiO_2-PTA$  0.1 and  $NH_2-SiO_2-PTA$  0.5).

$N_2$  adsorption–desorption isotherms at 77 K of catalysts  $SiO_2-NH_2$ ,  $NH_2-SiO_2-PTA$  0.1 and  $NH_2-SiO_2-PTA$  0.5 are shown in Figure 4.2. As the amount of phosphotungstic acid is increased, the surface area and porosity of the catalyst decrease, supporting the idea that the acid reacts with amine groups on the surface and in the pores. Table 4.2 gives the data for  $SiO_2-NH_2$  and all four  $NH_2-SiO_2-PTA$  catalysts. The decrease in the average pore volume and average pore size suggests that some of organic moieties apparently blocked the pore entrances, even for small probe molecules such as nitrogen (estimated hard sphere diameter of 0.39 nm and a cross-sectional area of  $0.162 \text{ nm}^2$ ).

**Table 4.2** – Textural parameters for supported amine and supported amine/phosphotungstic acid catalysts.

Sample	Surface area $/\text{m}^2 \text{ g}^{-1}$	Pore volume $/\text{cm}^3 \text{ g}^{-1}$	Average pore diameter $/\text{nm}$
$SiO_2-NH_2$	351	0.52	4.3
$NH_2-SiO_2-PTA$ 0.05	326	0.54	4.8
$NH_2-SiO_2-PTA$ 0.1	302	0.50	4.8
$NH_2-SiO_2-PTA$ 0.5	282	0.40	4.6
$NH_2-SiO_2-PTA$ 1	218	0.35	4.9

The elemental analysis data for the supported amine and amine/sulfonic acid catalysts are shown in Table 4.3, expressed as molar concentrations. The carbon data are useful in confirming that the functional groups are covalently bonded to the silica surface. The carbon to nitrogen (or sulfur) molar ratios depend on the number of methoxy groups condensed and, hence, the number of oxygen bridges to the silica surface. If all three react, the ratio is 3:1. If two react, the ratio is 4:1, etc. The data presented show that both the aminopropylsilane and the mercaptopropylsilane bind to the surface through three oxygen bridges in most catalysts.

**Table 4.3** – Elemental analysis data for supported amine, supported sulfonic acid and bifunctional catalysts.

Catalyst	C /mmol g <sup>-1</sup>	N /mmol g <sup>-1</sup>	S /mmol g <sup>-1</sup>	C /(N+S)
SiO <sub>2</sub> -SO <sub>3</sub> H	2.20	0.00	0.63	3.4
SiO <sub>2</sub> -NH <sub>2</sub>	3.40	1.10	0.00	3.0
NH <sub>2</sub> -SiO <sub>2</sub> -SH (Simultaneous)	3.50	0.89	0.27	3.0
NH <sub>2</sub> -SiO <sub>2</sub> -SO <sub>3</sub> H (Simultaneous)	3.40	0.86	0.26	3.0
NH <sub>2</sub> -SiO <sub>2</sub> -SH (Sequential)	3.37	1.12	0.47	3.0
NH <sub>2</sub> -SiO <sub>2</sub> -SO <sub>3</sub> H (Sequential)	3.35	1.11	0.27	3.0

The nitrogen and the sulfur contents can be taken as measures of the maximum concentrations of amine and thiol or sulfonic acid groups on the catalysts. The nitrogen levels are similar in SiO<sub>2</sub>-NH<sub>2</sub> and in NH<sub>2</sub>-SiO<sub>2</sub>-SH (sequential) but slightly lower in NH<sub>2</sub>-SiO<sub>2</sub>-SH (simultaneous), as might be expected. Nitrogen levels fall through the thiol oxidation step. It is possible that there is some leaching to the nitric acid.

Sulfur concentrations are all lower than nitrogen. It is possible that the relatively low level of reaction of MPTMS compared to APTMS with the silica surface may simply be due to stronger interactions between the amine groups on APTMS and the weakly acidic hydroxyl groups on the silica surface than the interactions between the mildly acidic thiol groups on MPTMS and the same hydroxyl groups on the silica.<sup>[26]</sup>

Let us now consider the area on the silica support that might be occupied by added functional groups. One aminopropylsilane group, bound by three oxygen bridges covers approximately  $0.50 \text{ nm}^2$ .<sup>[27]</sup> A level of functionalization of  $1.48 \text{ mmol g}^{-1}$  (from elemental analysis of  $\text{SiO}_2\text{-NH}_2$ ) corresponds to a nominal surface area covered by the added functional groups of  $445 \text{ m}^2 \text{ g}^{-1}$ . This is very close to the specific surface area of the silica support ( $452 \text{ m}^2 \text{ g}^{-1}$ ). We therefore conclude that functionalization with the aminopropyl groups is essentially complete, forming effectively a monolayer of aminopropyl groups on the silica surface.

A similar calculation based on mercaptopropylsilane, one molecule of which covers approximately  $0.30 \text{ nm}^2$ ,<sup>[28]</sup> suggests that the coverage of  $0.63 \text{ mmol g}^{-1}$  on  $\text{SiO}_2\text{-SO}_3\text{H}$  accounts for  $114 \text{ m}^2 \text{ g}^{-1}$  on the  $\text{SiO}_2\text{-SO}_3\text{H}$  catalyst. This suggests that MPTMS reacts with a much smaller fraction of available surface sites.

On  $\text{NH}_2\text{-SiO}_2\text{-SH}$  catalysts, the areas covered jointly by aminopropyl and mercaptopropyl groups calculated in the same way are  $415 \text{ m}^2 \text{ g}^{-1}$  for the catalyst prepared by the simultaneous route, and  $559 \text{ m}^2 \text{ g}^{-1}$  for the catalyst prepared by the sequential route. Functionalization on the second of these catalysts evidently occurs at a level greater than that corresponding to the available surface area. It is not clear how this might occur. Presumably it is due to some form of multilayer adsorption. MPTMS is known to undergo self-polymerization under some conditions, forming sub-micrometer-sized particles, and it is possible that such clusters are the explanation for adsorption beyond a monolayer.<sup>[29]</sup> Despite this uncertainty over the precise nature of the functionalized surface in some cases, our results show that functionalization with both mercaptopropyl and aminopropyl groups can occur at significant levels on the same support.

The  $^{13}\text{C}$  NMR spectra of the catalysts provide further evidence for the nature of the functional groups. The spectrum of  $\text{SiO}_2\text{-NH}_2$  is shown in Figure 4.3. Three peaks at 11, 22 and 43 ppm are assigned to the three carbon atoms on the aminopropyl group.<sup>[30]</sup> The absence of a signal at 51 ppm confirms that there are no free methoxy groups.<sup>[31]</sup> The spectrum for  $\text{NH}_2\text{-SiO}_2\text{-SH}$  in Figure 4.3b shows an additional peak for the mercaptopropyl carbons at 27 ppm.<sup>[32]</sup> The expected peaks at 11 and 18 ppm are most

probably present but hidden by the aminopropyl peaks. There is no peak at 51 ppm, again showing that there are no unreacted methoxy groups.

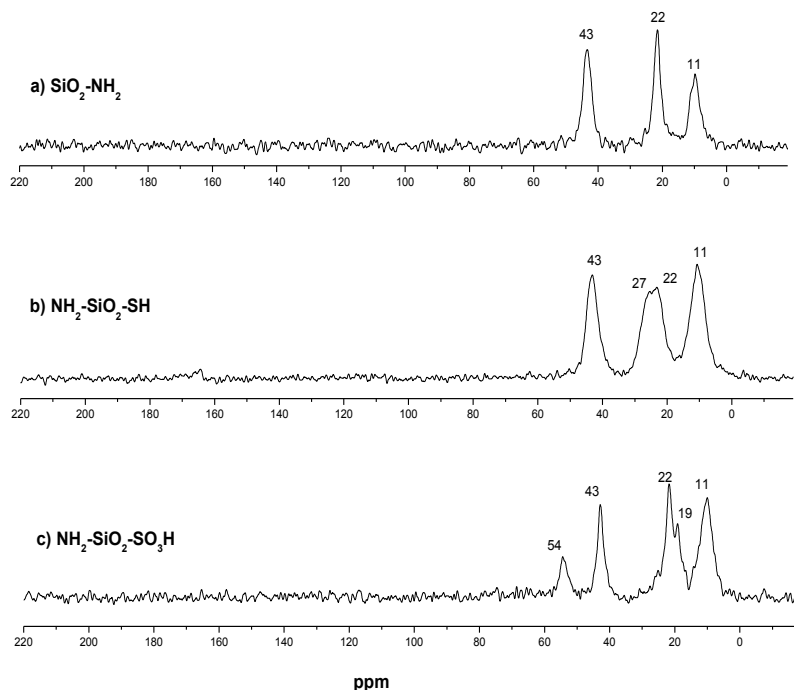
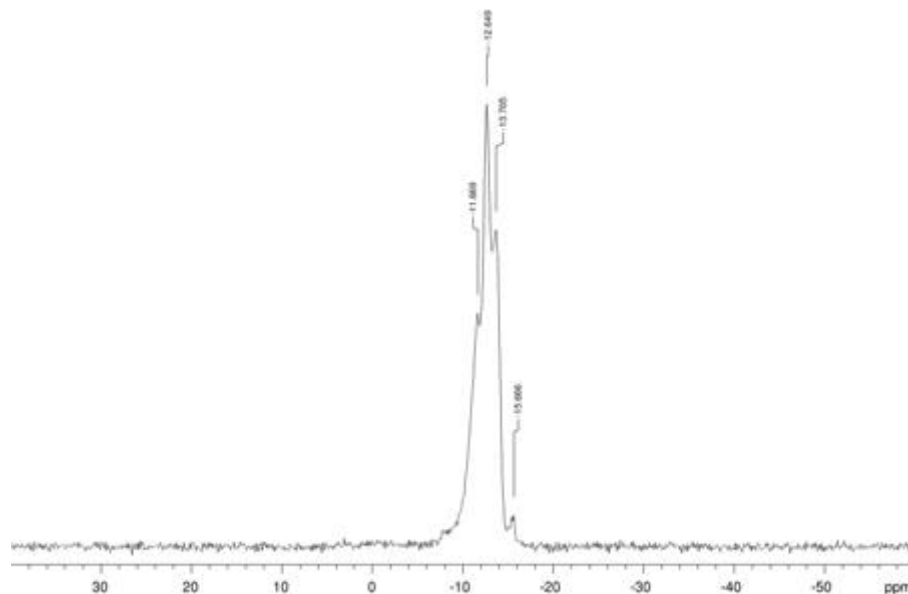


Figure 4.3 –  $^{13}\text{C}$  CP MAS NMR spectra of silica catalysts bearing a) aminopropyl groups, b) aminopropyl and mercaptopropyl groups and c) aminopropyl and mercaptopropyl groups following nitric acid oxidation.

For the bi-functional  $\text{NH}_2\text{-SiO}_2\text{-SO}_3\text{H}$  catalyst (Figure 4.3c), signals associated with aminopropyl groups are still present at 11, 22 and 43 ppm. The new peak at 54 ppm is due to the  $\alpha$ -carbon atom on the propylsulfonic acid, with peaks at 19 ppm and 11 ppm expected for the  $\beta$ - and  $\gamma$ -carbons.<sup>[32]</sup> The absence of the  $\text{CH}_2\text{-SH}$  peak at 27 ppm is evidence of effective conversion of thiol to sulfonic acid<sup>[32]</sup>, and the unchanged sequence of peaks for the aminopropyl group at 11, 22 and 43 ppm suggests that the amine group has been retained intact.

The spectra for  $\text{NH}_2\text{-SiO}_2\text{-PTA}$  (0.9) similarly support the proposed structure of this bi-functional catalyst. The  $^{13}\text{C}$  NMR spectrum exhibits the characteristic signals for the

aminopropyl group at 11, 22 and 43 ppm. The  $^{31}\text{P}$  spectrum of  $\text{NH}_2\text{-SiO}_2\text{-PTA}$  (0.9) is shown in Figure 4.4



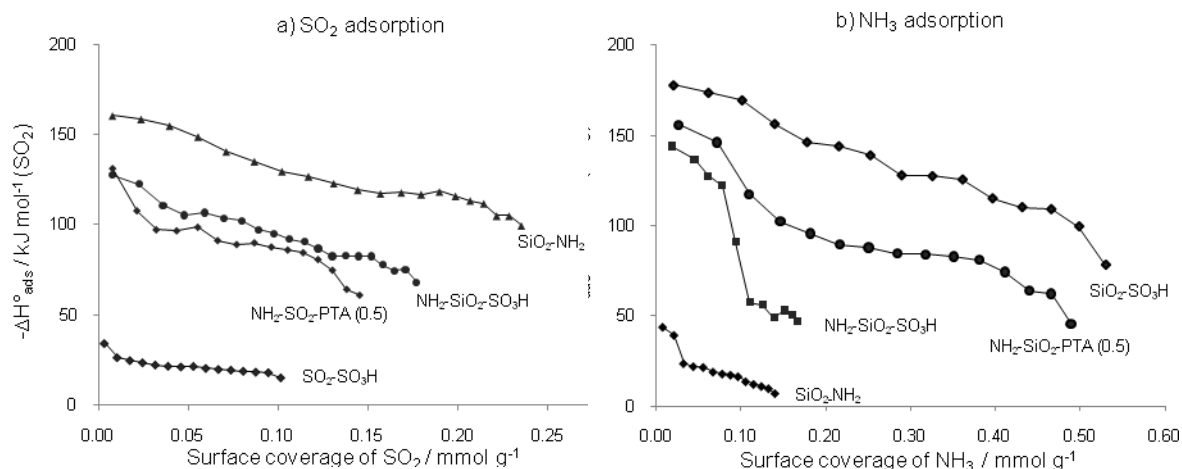
**Figure 4.4** –  $^{31}\text{P}$  MAS-NMR spectrum of  $\text{NH}_2\text{-SiO}_2\text{-NH}_3^+[\text{H}_2\text{PW}_{12}\text{O}_{40}^-]$  (0.9).

Figure 4.4 shows a set of signals (three resolved but possibly more) at -11.7 to -13.7 ppm. This compares with the expected peak position for bulk, unsupported phosphotungstic acid (Keggin structure) at -15.3 ppm.<sup>[33-34]</sup> In fact a small peak can be seen at this position. The signals at -11.7 to -13.7 ppm are characteristic of immobilized phosphotungstic acid, with shifts from -15.3 ppm caused by interaction with the silica support and by possible water loss from the Keggin ion structure as it is loaded on the surface.<sup>[35]</sup> The detection of several peaks in this range suggests multiple environments for phosphorus. This is not unusual when the normal symmetry of the bulk structure is disrupted.<sup>[33-34]</sup>

Surface basicity was studied by calorimetric adsorption of  $\text{SO}_2$ . Adsorption data are shown in Figure 4.5a as  $-\Delta H_{\text{ads}}^\circ(\text{SO}_2)$  versus amount of  $\text{SO}_2$  adsorbed for representative catalysts. These data can be broadly interpreted as basic site strength distribution profiles. The relative strengths of base sites are reflected in the values of  $-\Delta H_{\text{ads}}^\circ(\text{SO}_2)$ . It is

generally assumed that significant basicity corresponds to values greater than  $80 \text{ kJ mol}^{-1}$ .<sup>[36]</sup> The concentration of basic sites is related to the amount of  $\text{SO}_2$  that adsorbs with enthalpy above this value. However, it is not possible to determine more than relative values for the concentrations of basic sites from these data because the  $\text{RNH}_2:\text{SO}_2$  stoichiometry for tethered amine groups interacting with  $\text{SO}_2$  is not known, although it is very likely to be greater than one.<sup>[37]</sup> Stoichiometries of between 3:1 and 4:1 have been reported by others for  $\text{SO}_2$  complex formation with amine-functionalized silica.<sup>[37]</sup>

Figure 4.5a shows that the basicities of the two bi-functional catalysts,  $\text{NH}_2\text{-SiO}_2\text{-SO}_3\text{H}$  and  $\text{NH}_2\text{-SiO}_2\text{-PTA}(0.5)$ , are between those of  $\text{SiO}_2\text{-NH}_2$  and  $\text{SiO}_2\text{-SO}_3\text{H}$ . Significant basicity is retained in both bi-functional materials with  $\text{NH}_2\text{-SiO}_2\text{-PTA}(0.5)$  showing slightly fewer and weaker base sites than  $\text{NH}_2\text{-SiO}_2\text{-SO}_3\text{H}$ , in line with other reports.<sup>[37-38]</sup>



**Figure 4.5** – a)  $\Delta H^{\circ}_{\text{ads}}(\text{SO}_2)$  vs. amount adsorbed at  $120 \text{ }^{\circ}\text{C}$  and b)  $\Delta H^{\circ}_{\text{ads}}(\text{NH}_3)$  vs. amount adsorbed at  $120 \text{ }^{\circ}\text{C}$ , for supported catalysts.

Equivalent  $\text{NH}_3$  calorimetric adsorption data for the supported sulfonic acid catalysts are shown in Figure 4.5b. In the same way as above, adsorption on significantly acidic sites is taken as that with enthalpy greater than  $80 \text{ kJ mol}^{-1}$ . With  $\text{NH}_3$  it is generally assumed that adsorption on acid sites is stoichiometric (1:1); therefore, acid site concentrations can in principle be determined from the amount of  $\text{NH}_3$  that adsorbs with enthalpy greater

than  $80 \text{ kJ mol}^{-1}$ . On this basis,  $\text{SiO}_2\text{-SO}_3\text{H}$  exhibits about  $0.55 \text{ mmol g}^{-1}$  acid sites and this compares with a sulfur content of  $0.63 \text{ mmol g}^{-1}$ . For the bi-functional catalysts, the acid site concentrations are much lower. In the case of  $\text{NH}_2\text{-SiO}_2\text{-SO}_3\text{H}$  there are ca.  $0.1 \text{ mmol g}^{-1}$  detectable acid sites, based on Figure 4.5b, compared to  $0.26 \text{ mmol g}^{-1}$  sulfur, suggesting a degree of acid site loss, presumably by neutralization. The acidity of  $\text{NH}_2\text{-SiO}_2\text{-PTA}(0.5)$  reflects the phosphotungstic acid content and is significantly higher, in terms of both concentration and strength of acid sites, than for  $\text{NH}_2\text{-SiO}_2\text{-SO}_3\text{H}$ . However, in this case, the concentration of phosphotungstic acid added to the  $\text{SiO}_2\text{-NH}_2$  was  $0.55 \text{ mmol g}^{-1}$  ( $0.5 \times$  amine concentration based on elemental analysis); therefore, a higher concentration of acid sites from the  $\text{H}_2\text{PW}_{12}\text{O}_{40}^-$  ions on the neutralized amine sites than the  $0.3\text{-}0.4 \text{ mmol g}^{-1}$  detected by ammonia adsorption from Figure 4.5b might have been expected. Despite the relatively low acid site concentration found in  $\text{NH}_2\text{-SiO}_2\text{-PTA}(0.5)$ , it is worth noting that the molar enthalpies of  $\text{NH}_3$  adsorption are relatively high and similar to those measured typically for this heteropolyacid supported on silica in the absence of other surface functional groups.<sup>[39]</sup>

As further proof of the existence of free amines, infrared spectra were recorded for  $\text{SiO}_2$ ,  $\text{SiO}_2\text{-NH}_2$ ,  $\text{H}_2\text{N-SiO}_2\text{-SH}$  (sequential) and  $\text{H}_2\text{N-SiO}_2\text{-SO}_3\text{H}$  (sequential) (Figure 4.6).

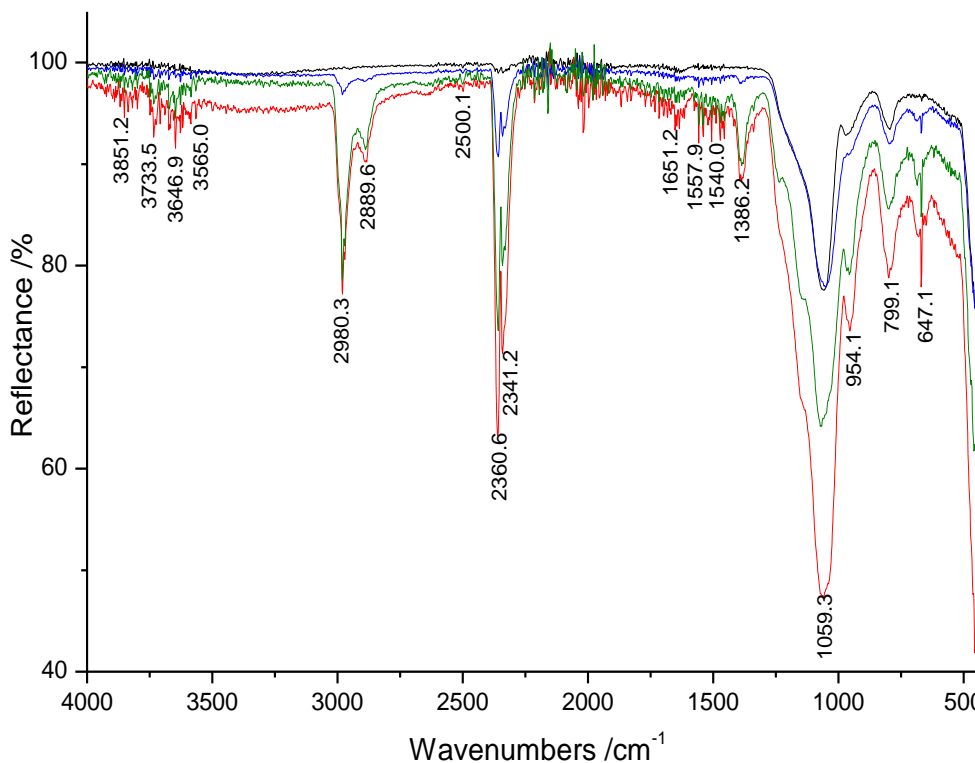


**Figure 4.6** – IR spectra of samples SiO<sub>2</sub> (black line), SiO<sub>2</sub>-NH<sub>2</sub> (green line), NH<sub>2</sub>-SiO<sub>2</sub>-SH (sequential) (blue line) and NH<sub>2</sub>-SiO<sub>2</sub>-SO<sub>3</sub>H (red line).

The FTIR spectrum confirms the presence of propyl groups on the silica surface. SiO<sub>2</sub>-NH<sub>2</sub>, NH<sub>2</sub>-SiO<sub>2</sub>-SH and NH<sub>2</sub>-SiO<sub>2</sub>-SO<sub>3</sub>H showed three bands, stretching vibration bands at 2980.3 and 2889.6 cm<sup>-1</sup> characteristic of the CH<sub>2</sub> groups of the propyl chain of the silylating agent. The vibrations for CH bending can be observed at 1386.2 cm<sup>-1</sup>.<sup>[40-41]</sup> The bands at 3851 and 3565 cm<sup>-1</sup> are characteristic of the NH<sub>2</sub> (NH vibrations). The bands at 1558 and 1540 cm<sup>-1</sup> belong as well to -NH<sub>2</sub> vibration<sup>[42]</sup> NH<sub>3</sub><sup>+</sup> bending respectively<sup>[43]</sup>. The bands at 2360 and 2341 cm<sup>-1</sup> are assigned to CO<sub>2</sub> gas adsorbed on the surface, which could be used as an indicator of presence of base sites; these bands disappeared when the sample was heated at 150 °C. The band at 1651 cm<sup>-1</sup> is assigned to scissoring mode of physically adsorbed water on the surface. The band at 2500 cm<sup>-1</sup> is assigned to SH stretching vibration.<sup>[44]</sup>

Bands at 3733 and 3664  $\text{cm}^{-1}$  are assigned to the terminal Si-OH. However, their low frequencies are acceptable since the spectra were taken in the solid phase. The vibrations of Si-O-Si can be seen at 1059  $\text{cm}^{-1}$  (asymmetric stretching) and 799  $\text{cm}^{-1}$  (symmetric stretching) and 437  $\text{cm}^{-1}$  (bending). The band at 1651  $\text{cm}^{-1}$  is assigned to the deformation vibrations of water.<sup>[44]</sup> IR spectra confirm the presence of free and protonated amine on the catalysts' surfaces.

## 4.7. Catalytic activity

### 4.7.1. One-pot deacetalization–Henry reaction

#### 4.7.1.1. Silica-supported amine/sulphonic acid catalysts

We studied the one-pot tandem conversion of benzaldehydedimethylacetal (1) to nitrostyrene (3) over the catalysts (Scheme 4.2). This reaction involves the acid-catalyzed deprotection of the starting material to give the intermediate benzaldehyde (2), and the subsequent base-catalyzed nitroaldol (Henry) reaction with nitromethane to yield nitrostyrene (3).

**Table 4.4** – Catalytic activity of solid materials.

Sr	Catalyst	Conv. of 1 (%)	Yield of 2 (%)	Yield of 3 (%)
1	SiO <sub>2</sub>	Trace	Trace	Trace
2	SiO <sub>2</sub> -SO <sub>3</sub> H	~100%	~100%	Trace
3	SiO <sub>2</sub> -NH <sub>2</sub>	Trace	Trace	Trace
4	NH <sub>2</sub> -SiO <sub>2</sub> -SO <sub>3</sub> H (Simultaneous)	98%	1%	97%
5	NH <sub>2</sub> -SiO <sub>2</sub> -SO <sub>3</sub> H (Sequential)	79%	19%	60%
7	SiO <sub>2</sub> -NH <sub>2</sub> / SiO <sub>2</sub> -SO <sub>3</sub> H <sup>a</sup>	99%	14%	86%

Benzaldehydedimethylacetal (1 mmol), nitromethane (5 ml), catalyst (0.05 g), 90 °C, 6 h reaction time. (a = 30 mg SiO<sub>2</sub>-SO<sub>3</sub>H +30 mg SiO<sub>2</sub>-NH<sub>2</sub>).

From Table 4.4, SiO<sub>2</sub> cannot catalyze the reactions (entry 1). While when SiO<sub>2</sub>-SO<sub>3</sub>H was used as the catalyst in the absence of any amino groups, benzaldehyde was the only product (entry 2). In contrast, when SiO<sub>2</sub>-NH<sub>2</sub> was used as the catalyst in the absence of any sulfonic acid groups, no product was found (entry 3). Therefore, each catalyst

individually was not able to promote the conversion of 1 to 3. Remarkably, bifunctional heterogeneous catalysts showed high activity in one-pot tandem deacetalization–Henry reaction (entry 4 and 5). Their results illustrate the bifunctionality of the catalysts and the coexistence of acidity and basicity. In all cases, the concentrations of the starting material, the intermediate benzaldehyde and the product nitrostyrene were monitored. Kinetic data are shown for  $\text{NH}_2\text{-SiO}_2\text{-SO}_3\text{H}$  (sequential) and  $\text{NH}_2\text{-SiO}_2\text{-SO}_3\text{H}$  (simultaneous) in Figure 4.7.

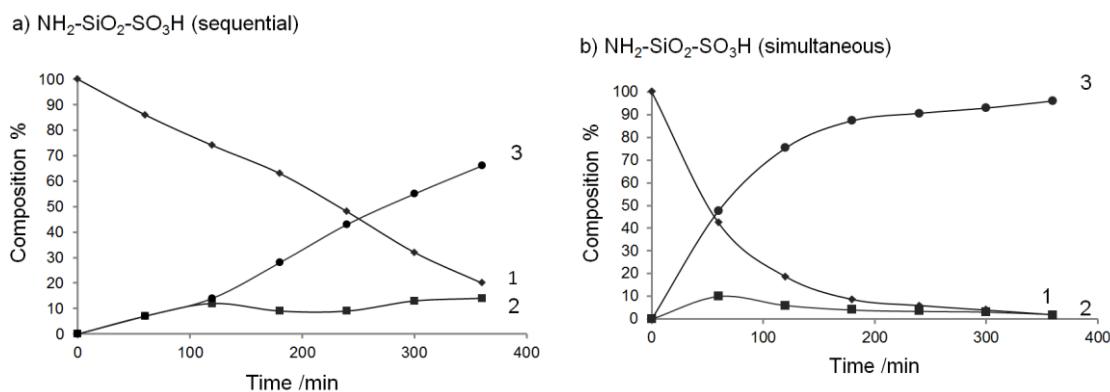


**Figure 4.7** – Composition of the reaction mixture versus time for the deacetalization Henry reaction between benzaldehyde dimethyl acetal and nitromethane at 90 °C to form nitrostyrene, catalyzed by a)  $\text{NH}_2\text{-SiO}_2\text{-SO}_3\text{H}$  (sequential) and b)  $\text{NH}_2\text{-SiO}_2\text{-SO}_3\text{H}$  (simultaneous).

The sulfonic acid catalyzes the conversion of 1 to 2, and then the amine catalyzes the second step to the product 3. The activity of the acid is clearly much higher for the “simultaneous” catalyst. The basic sites appear to convert the benzaldehyde intermediate immediately in both cases. The difference between the activities of the two acid functionalities is consistent with the relative acidities as measured by adsorption calorimetry.

Also tested was a physical mixture of  $\text{SiO}_2\text{-NH}_2$  and  $\text{SiO}_2\text{-SO}_3\text{H}$  (entry 7). Amounts of the two components were chosen to give the same overall weight of catalyst. This means that the overall acid and base concentrations for the mixture were higher than for the bifunctional catalysts. Based on calorimetric data, the mixture contains 60% more acid

sites and 95% more basic sites than the same weight of  $\text{NH}_2\text{-SiO}_2\text{-SO}_3\text{H}$  (simultaneous). The activity of the mixture is lower than the activity of  $\text{NH}_2\text{-SiO}_2\text{-SO}_3\text{H}$  (simultaneous) in both first and second step. The lower activity in the first, acid-catalyzed step and second, base-catalyzed, step is surprising given the much higher acid and base concentrations and strengths for catalysts. There may be a distinct catalytic advantage offered by the bifunctional catalysts. It is possible that base groups adjacent to acid groups, on the same surface, may be particularly active in rapidly converting newly formed benzaldehyde to nitrostyrene.

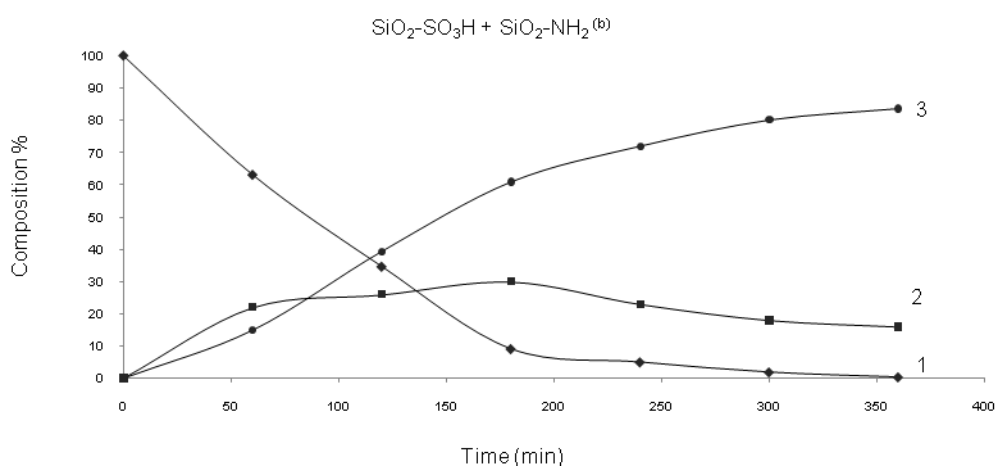


**Figure 4.8** – Composition of the reaction mixture versus time for the deacetalization Henry reaction between benzaldehyde dimethyl acetal and nitromethane at 90 °C to form nitrostyrene, catalyzed by a physical mixture of  $\text{SiO}_2\text{-SO}_3\text{H}$  and  $\text{SiO}_2\text{-NH}_2$ .

#### 4.7.1.2. Silica-supported amine/phosphotungstic acid catalysts

The group of  $\text{NH}_2\text{-SiO}_2\text{-PTA}$  catalysts with phosphotungstic acid: amine stoichiometric ratios of 0.9, 0.5, 0.1 and 0.05 were tested in the same two-step reaction, and the data appear in Figure 4.9. For the catalysts with nominal 0.9 and 0.5 phosphotungstic acid contents, the first step is faster than for  $\text{NH}_2\text{-SiO}_2\text{-SO}_3\text{H}$ , which is consistent with the relative acidities as measured by adsorption calorimetry. However, the rate of the second step, relying on residual amine groups, is very sensitive to the amount of acid used and is slower than for  $\text{NH}_2\text{-SiO}_2\text{-SO}_3\text{H}$ .

An additional observation here is that, for the catalysts with the two lower acid contents,  $\text{NH}_2\text{-SiO}_2\text{-PTA}(0.1)$  and  $\text{NH}_2\text{-SiO}_2\text{-PTA}(0.05)$ , the acid-catalyzed conversion of benzaldehyde dimethyl acetal stops after 61% and 20% conversion respectively. (The benzaldehyde that is produced is fairly quickly converted to nitrostyrene, as would be expected.) The acid sites in these catalysts are prone to poisoning, and the amount of phosphotungstic acid used in the synthesis of these materials seems to control the point at which reaction ceases.

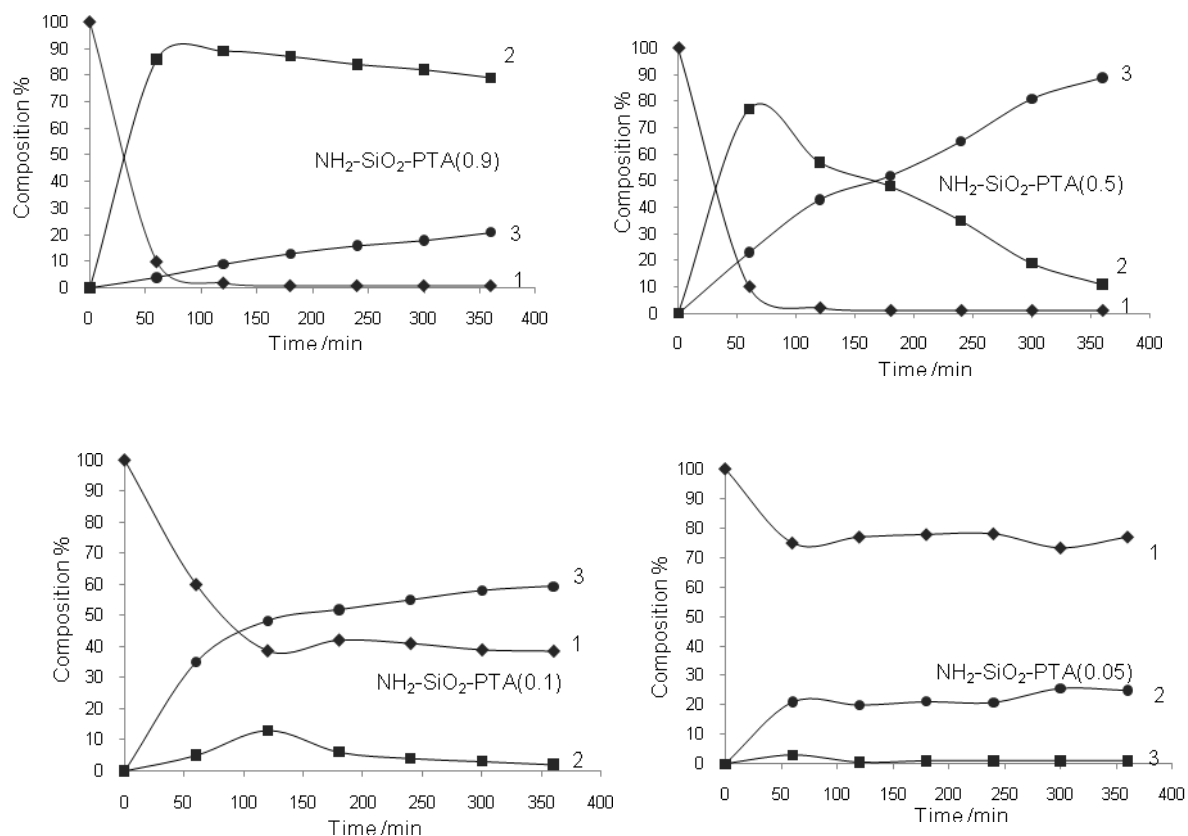


**Figure 4.9** – Composition of the reaction mixture vs. time for the reaction between benzaldehyde dimethyl acetal (1) and water to form benzaldehyde (2) and the subsequent reaction with nitromethane to form nitrostyrene (3), catalyzed by  $\text{NH}_2\text{-SiO}_2\text{-PTA}$  with acid/amine ratios of 0.9, 0.5, 0.1 and 0.05 at 90 °C .

As stated above, a significant observation from Figure 4.7 is that the  $\text{NH}_2\text{-SiO}_2\text{-SO}_3\text{H}$  (simultaneous) bi-functional catalyst shows relatively high base-catalytic activity in the

Henry reaction between benzaldehyde and nitromethane, higher even than the mono-functional  $\text{SiO}_2\text{-NH}_2$  catalyst. This suggests that the mode of operation of  $\text{NH}_2\text{-SiO}_2\text{-SO}_3\text{H}$  incorporates a degree of cooperative catalysis, such that the acid, as well as the base, catalytic centres are involved in the reaction. The mechanism for this reaction involves the base catalyst (tethered amine) abstracting a proton from nitromethane to form  $\text{CH}_2\text{NO}_2^-$ , which then takes part in nucleophilic attack on the benzaldehyde carbonyl carbon. It seems quite possible that the role of the sulfonic acid site is to hydrogen bond to the carbonyl oxygen, activating the carbonyl carbon. Based on the lower base catalytic activity of  $\text{NH}_2\text{-SiO}_2\text{-PTA}(0.5)$ , which is directly comparable to  $\text{NH}_2\text{-SiO}_2\text{-SO}_3\text{H}$  in terms of acid and base site concentrations, such a cooperative mechanism appears to be impossible where the acid site is an  $[\text{H}_2\text{PW}_{12}\text{O}_{40}]^-$  ion.

A cooperative mechanism of this type requires the acid and base sites to be adjacent. One important feature of the bi-functional catalysts which is difficult to study is the extent to which the acid and the base groups are inter-dispersed on the surface, rather than existing in groups of sites of the same type. One test which was carried out to investigate this was based on the premise, mentioned above, that  $\text{SO}_2$  requires several amine groups in close proximity in order to chemisorb on the surface. If this is the case, as it is thought to be,<sup>[37]</sup> and certainly is for the somewhat similar adsorption of  $\text{CO}_2$  on surface amines,<sup>[38, 45]</sup> then  $\text{SO}_2$  should differentiate between well-dispersed and bunched amine groups. To test this, catalysts  $\text{SiO}_2\text{-NH}_2$  and  $\text{NH}_2\text{-SiO}_2\text{-SO}_3\text{H}$  were first saturated with  $\text{SO}_2$  in a calorimetric adsorption experiment and then their catalytic activities in the Henry reaction between benzaldehyde and nitromethane were measured. The saturated  $\text{SiO}_2\text{-NH}_2$  and  $\text{NH}_2\text{-SiO}_2\text{-SO}_3\text{H}$  (sequential) showed no activity, showing that  $\text{SO}_2$  is indeed able to passivate amine groups. In contrast, the saturated  $\text{NH}_2\text{-SiO}_2\text{-SO}_3\text{H}$  (simultaneous) showed significant activity. This suggests that some amine groups on  $\text{NH}_2\text{-SiO}_2\text{-SO}_3\text{H}$  are immune to reaction with  $\text{SO}_2$ . This may be because those amine groups are well dispersed (amongst surface sulfonic acid groups) on the catalyst surface and are unable to act jointly to chelate  $\text{SO}_2$  molecules. If so, then this could explain why this catalyst is able to participate in acid/base cooperative catalysis.

Finally, calculations above suggest that silica functionalization with (aminopropyl)trimethoxysilane covers a high percentage of the support surface area. This implies, unsurprisingly, that the surface area and porosity of the support are important features in controlling the possible concentrations of basic and acidic groups, and therefore the catalytic activity.

#### 4.8. Aldol condensation – 4-nitrobenzaldehyde and acetone

The second reaction studied was the aldol condensation between 4-nitrobenzaldehyde and acetone. Summary data for the activities of the catalysts identified as most active in the previous section are shown in Table 4.5.

**Table 4.5** – Catalytic activities in the aldol condensation between 4-nitrobenzaldehyde (A) and acetone to form 4-hydroxy-4-(p-nitrophenyl)butan-2-one (B) and 4-(4-nitrophenyl)but-3-en-2-one (C).

Catalyst	Conversion of A /%	Yield of B /%	Yield of C/%	Selectivity B/C
SiO <sub>2</sub>	Trace	Trace	Trace	-
SiO <sub>2</sub> -SO <sub>3</sub> H	7	5	2	-
SiO <sub>2</sub> -NH <sub>2</sub>	78	55	23	1.9
NH <sub>2</sub> -SiO <sub>2</sub> -SO <sub>3</sub> H (simultaneous)	99	78	20	4.0
NH <sub>2</sub> -SiO <sub>2</sub> -PTA 0.5	85	69	16	4.6
SiO <sub>2</sub> -NH <sub>2</sub> + SiO <sub>2</sub> -SO <sub>3</sub> H <sup>a</sup>	98	50	48	1.0

A = 4-nitrobenzaldehyde. B = 4-hydroxy-4-(p-nitrophenyl)butan-2-one. C = (E)-4-(4-nitrophenyl)but-3-en-2-one. Reaction condition: 4-nitrobenzaldehyde (76 mg), acetone (10 mL), catalyst (0.20 g), 50 °C for 20 h. a. physical mixture of 0.1 g of SiO<sub>2</sub>-NH<sub>2</sub> and 0.1 g SiO<sub>2</sub>-SO<sub>3</sub>H.

Pure silica gel and the acid catalyst SiO<sub>2</sub>-SO<sub>3</sub>H give very low conversions, as expected. The base catalyst SiO<sub>2</sub>-NH<sub>2</sub> alone, and the physical mixture of SiO<sub>2</sub>-NH<sub>2</sub> and SiO<sub>2</sub>-SO<sub>3</sub>H, are active but with low selectivity towards the aldol product B. In contrast the bi-functional NH<sub>2</sub>-SiO<sub>2</sub>-SO<sub>3</sub>H (simultaneous) catalyst shows B/C selectivity of 4.0, supporting the idea that this catalyst is particularly active towards the aldol reaction (forming B) via the cooperative acid-base mechanism. With NH<sub>2</sub>-SiO<sub>2</sub>-PTA(0.5), overall activity is relatively low, presumably because of the relatively low basicity. Even so it too shows high selectivity towards the aldol over the dehydration product (B/C = 4.6).

The B/C selectivity ratio is an indicator of the relative cooperative activity of acid-base pairs compared to acid sites alone.<sup>[13]</sup> Kan reported that proper matching between the acid and the base can both efficiently activate the substrate through cooperative activation and inhibit dehydration without diminishing the yield. On this basis, both NH<sub>2</sub>-SiO<sub>2</sub>-SO<sub>3</sub>H (simultaneous) and NH<sub>2</sub>-SiO<sub>2</sub>-PTA 0.5 show evidence of cooperative catalysis when compared to the other catalysts, all of which are based on isolated acid or base groups. The overall activities of NH<sub>2</sub>-SiO<sub>2</sub>-SO<sub>3</sub>H (simultaneous) and NH<sub>2</sub>-SiO<sub>2</sub>-PTA 0.5 are similar in this reaction. The limiting factor in controlling activity in the first, deacetalization–Henry reaction was thought to be the base properties of the catalyst. In this aldol reaction these base properties appear less important, and this further supports the idea that it is the combined, acid-base, centres and not simply basic sites that are responsible for the activity towards the aldol formation. This results confirm the presence of acid and base groups in their active form. If neutralization of the acid and base sites occurred due to the pairing of the sulfonic acid and amine base on the silica support, this will lead to a completely inactive catalyst. Therefore the high catalytic activity of NH<sub>2</sub>-SiO<sub>2</sub>-SO<sub>3</sub>H (simultaneous) and NH<sub>2</sub>-SiO<sub>2</sub>-PTA 0.5 must therefore be due to isolated acid and base groups that are far apart to neutralize one another. A possible mechanism for the acid–base cooperative activation of the aldol reaction according to a prior report<sup>[13]</sup> is shown in Figure 4.10.

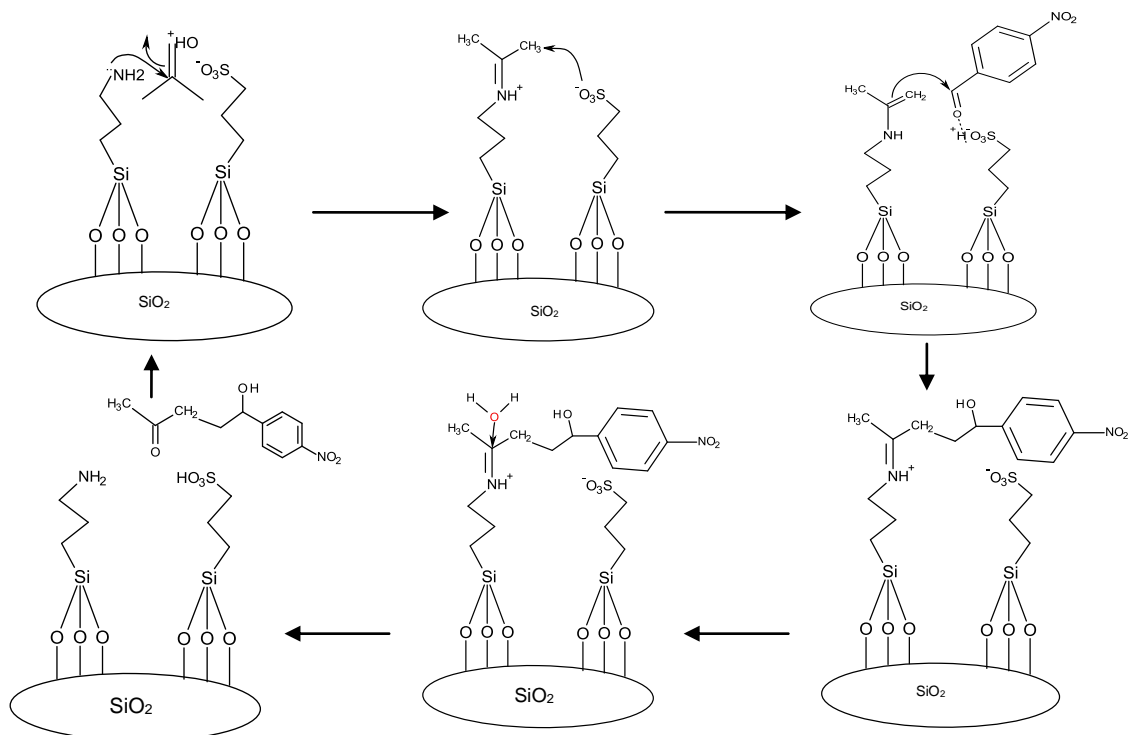


**Figure 4.10** – Proposed catalytic cycle for aldol condensation.

As shown in steps (A and B), the nucleophilic primary amine attacks acetone to provide the corresponding imine. Step (C), imine is deprotonated to generate a nucleophilic enamine. Step (D) involves nucleophilic addition of an enamine to the activated carbonyl group of 4-nitrobenzaldehyde. Steps (D) show the following proton-transfer reaction.

#### 4.9. Conclusion

This work demonstrates that bi-functional acid-base catalysts can exhibit particularly high activities in reactions where near-neighbour acid and base sites can take part in either tandem reactions or in reactions involving cooperative catalytic processes. In comparing the bi-functional catalysts prepared in this study it appears that the nature of the reaction may dictate the relative advantages and disadvantages of catalysts made in different ways. Where grafted aminopropyl and grafted propylsulfonic acid groups are used, the most active catalysts are prepared by carrying out the two functionalization steps simultaneously rather than sequentially. The importance of the relative coverage of the support material by functional groups and, hence, the dependence of ultimate activity

on the surface area and porosity of the catalyst support is demonstrated. It seems that an amorphous silica gel, as opposed to the ordered mesoporous molecular sieve materials such as SBA-15, can be used as an effective catalyst support.

Comparison has been made with bifunctional acid-base silica-supported acid-base catalysts prepared by functionalizing with amines as above and then adding phosphotungstic acid. By controlling the ratio of acid added to amine, both surface acidity and basicity are achieved. These catalysts show lower activity than supported amine/sulfonic acids in the test reactions. Addition of even small amounts of phosphotungstic acid disproportionately reduces the base catalytic activity of the amine groups. Furthermore, the phosphotungstic acid rapidly loses activity in the test reactions.

We envisage that a successful cohabitation of antagonist groups like acids and bases within a material will open the way to new routes for the rational design of morphology-controlled novel nanomaterials for multifunctional applications.

#### 4.10. References

- [1] I. Fechete, Y. Wang, J. C. Védrine, *Catalysis Today* **2012**, *189*, 2-27.
- [2] T. Setoyama, *Catalysis Today* **2006**, *116*, 250-262.
- [3] K. Tanabe, W. F. Hölderich, *Applied Catalysis A: General* **1999**, *181*, 399-434.
- [4] Y. Huang, B. G. Trewyn, H.-T. Chen, V. S. Y. Lin, *New Journal of Chemistry* **2008**, *32*, 1311-1313.
- [5] K. Motokura, M. Tomita, M. Tada, Y. Iwasawa, *Chemistry – A European Journal* **2008**, *14*, 4017-4027.
- [6] K. K. Sharma, A. V. Biradar, S. Das, T. Asefa, *European Journal of Inorganic Chemistry* **2011**, *2011*, 3174-3182.
- [7] S. Shylesh, A. Wagner, A. Seifert, S. Ernst, W. R. Thiel, *Chemistry – A European Journal* **2009**, *15*, 7052-7062.
- [8] N. R. Shiju, A. H. Alberts, S. Khalid, D. R. Brown, G. Rothenberg, *Angewandte Chemie International Edition* **2011**, *50*, 9615-9619.
- [9] M. H. Lim, C. F. Blanford, A. Stein, *Chemistry of Materials* **1998**, *10*, 467-470.
- [10] W. D. Bossaert, D. E. De Vos, W. M. Van Rhijn, J. Bullen, P. J. Grobet, P. A. Jacobs, *Journal of Catalysis* **1999**, *182*, 156-164.
- [11] I. Díaz, F. Mohino, J. n. Pérez-Pariente, E. Sastre, *Thermochimica Acta* **2004**, *413*, 201-207.
- [12] R. K. Zeidan, S.-J. Hwang, M. E. Davis, *Angewandte Chemie* **2006**, *118*, 6480-6483.
- [13] F. Shang, J. Sun, S. Wu, H. Liu, J. Guan, Q. Kan, *Journal of Colloid and Interface Science* **2011**, *355*, 190-197.
- [14] Y. Shao, H. Liu, X. Yu, J. Guan, Q. Kan, *Materials Research Bulletin* **2012**, *47*, 768-773.
- [15] X. Yu, Y. Zou, S. Wu, H. Liu, J. Guan, Q. Kan, *Materials Research Bulletin* **2011**, *46*, 951-957.
- [16] R. Gao, Q. Zhu, W.-L. Dai, K. Fan, *Green Chemistry* **2011**, *13*, 702-708.
- [17] I. P. Alimarin, V. I. Fadeeva, G. V. Kudryavtsev, I. M. Loskutova, T. I. Tikhomirova, *Talanta* **1987**, *34*, 103-110.
- [18] A. R. Sarkar, P. K. Datta, M. Sarkar, *Talanta* **1996**, *43*, 1857-1862.
- [19] L. N. H. Arakaki, L. M. Nunes, J. A. Simoni, C. Airoidi, *Journal of Colloid and Interface Science* **2000**, *228*, 46-51.
- [20] A. N. Kursunlu, E. Guler, H. Dumrul, O. Kocyigit, I. H. Gubbuk, *Applied Surface Science* **2009**, *255*, 8798-8803.
- [21] K. K. Sharma, T. Asefa, *Angewandte Chemie* **2007**, *119*, 2937-2940.
- [22] H. C. Zeng, *Nanotechnology* **1988**, 2539-2551.
- [23] H. E. Cross, D. R. Brown, *Catalysis Communications* **2010**, *12*, 243-245.
- [24] P. F. Siril, A. D. Davison, J. K. Randhawa, D. R. Brown, *Journal of Molecular Catalysis A: Chemical* **2007**, *267*, 72-78.
- [25] C. S. Hill, A. Norton, G. Newman, *Wood Sci Technol* **2010**, *44*, 497-514.
- [26] C.-H. Kuo, H.-Y. Chang, C.-P. Liu, S.-H. Lee, Y.-W. You, J.-J. Shyue, *Physical Chemistry Chemical Physics* **2011**, *13*, 3649-3653.
- [27] M. Etienne, A. Walcarius, *Talanta* **2003**, *59*, 1173-1188.
- [28] D. G. Kurth, T. Bein, *Journal Name: Langmuir; (United States); Journal Volume: 9:11* **1993**, Medium: X; Size: Pages: 2965-2973.
- [29] M. Hu, S. Noda, T. Okubo, Y. Yamaguchi, H. Komiyama, *Applied Surface Science* **2001**, *181*, 307-316.
- [30] H.-M. Kao, C.-H. Liao, A. Palani, Y.-C. Liao, *Microporous and Mesoporous Materials* **2008**, *113*, 212-223.
- [31] A. J. Crisci, M. H. Tucker, M.-Y. Lee, S. G. Jang, J. A. Dumesic, S. L. Scott, *ACS Catalysis* **2011**, *1*, 719-728.
- [32] S. Shylesh, S. Sharma, S. P. Mirajkar, A. P. Singh, *Journal of Molecular Catalysis A: Chemical* **2004**, *212*, 219-228.
- [33] S. Uchida, K. Inumaru, M. Misono, *The Journal of Physical Chemistry B* **2000**, *104*, 8108-8115.
- [34] C. J. Dillon, J. H. Holles, R. J. Davis, J. A. Labinger, M. E. Davis, *Journal of Catalysis* **2003**, *218*, 54-66.
- [35] S. Damyanova, J. L. G. Fierro, I. Sobrados, J. Sanz, *Langmuir* **1998**, *15*, 469-476.

- [36] A. L. Petre, J. A. Perdigón-Melón, A. Gervasini, A. Auroux, *Topics in Catalysis* **2002**, *19*, 271-281.
- [37] F. Rezaei, C. W. Jones, *Industrial & Engineering Chemistry Research* **2013**, *52*, 12192-12201.
- [38] I. J. Uyanga, R. O. Idem, *Industrial & Engineering Chemistry Research* **2007**, *46*, 2558-2566.
- [39] A. D. Newman, D. R. Brown, P. Siril, A. F. Lee, K. Wilson, *Physical Chemistry Chemical Physics* **2006**, *8*, 2893-2902.
- [40] Ş. Sert, M. Eral, *Journal of Nuclear Materials* **2010**, *406*, 285-292.
- [41] M. R. Mello, D. Phanon, G. Q. Silveira, P. L. Llewellyn, C. M. Ronconi, *Microporous and Mesoporous Materials* **2011**, *143*, 174-179.
- [42] M. Rieger, G. Schaumann, Y. Mouvenchery, R. Niessner, M. Seidel, T. Baumann, *Analytical and Bioanalytical Chemistry* **2012**, *403*, 2529-2540.
- [43] G. G. Ristori, P. Fusi, M. Franci, *Clay Minerals* **1981**, *16*, 125-137.
- [44] D. Méhn, Z. Kónya, J. Halász, J. B. Nagy, B. Rác, A. Molnár, I. Kiricsi, *Applied Catalysis A: General* **2002**, *232*, 67-76.
- [45] P. Bollini, N. A. Brunelli, S. A. Didas, C. W. Jones, *Industrial and Engineering Chemistry Research* **2012**, *51*, 15153-15162.

## Chapter 5

# Cooperative acid-base catalysis using amine/ carboxylic acid-functionalized silica with potential for chiral synthesis

---

In this chapter, the background and the objectives of this research are described. The structure of this thesis and a brief overview of individual chapter are also summarized.

## 5. Introduction

In earlier chapters, it has been shown that the presence of acids in addition to amine bases on a silica support can accelerate the rate of aldol reaction between acetone and benzaldehyde. In this chapter, chiral functionality has been added to these materials by supporting L-proline on the silica in which the secondary amine and carboxylic acid moieties are both available for activity and enantioselectivity.

Chiral materials containing a single enantiomer are of importance for chemists as they can be used in a range of fields including flavour and aroma chemicals<sup>[1-3]</sup>, non-linear optical properties<sup>[4-6]</sup>, agricultural chemicals<sup>[7-8]</sup> and, especially, the manufacture of pharmaceuticals.<sup>[9-11]</sup> There are only two ways of preparing such materials: by separating the components of a racemic mixture, which is wasteful, or by chiral synthesis. For decades, practical access to pure enantiomers relied largely on biochemical or biological methods. However, the scope of such methods using enzymes, cell cultures, or whole microorganisms is limited because of the inherent single-handed, lock-and-key specificity of biocatalysts.<sup>[12]</sup> On the other hand, a chemical approach allows the flexible synthesis of a wide array of enantiopure organic substances from achiral precursors. The chemical synthesis of chiral materials essentially implies asymmetric catalysis, and this can involve heterogeneous or homogeneous enantioselective catalysis.

Concerning practical performance, asymmetric catalysis currently lies mostly in the area of homogeneous catalysis.<sup>[13]</sup> Highly selective homogeneous chiral transition metal catalysts were the first catalysts introduced for the synthesis of pure enantiomers from achiral precursors. This type of chiral catalyst transformed synthetic chemistry, recognized by the award of the 2001 Nobel Prize for chemistry to Knowles and Noyori.<sup>[12]</sup> Another type of chiral catalysis, asymmetric organocatalysis, has become of interest recently, and involves small organic molecules. These compounds are robust and show cost, availability and environmental benefits. They can be used in the construction of complex and enantiopure molecular skeletons.<sup>[14]</sup>

## 5.1. Organocatalysis

The expression “organocatalysis” is quite new. Organocatalysis refers to organic molecules capable of catalyzing organic reactions with no need for expensive and potentially toxic metals or protein-based catalysts.<sup>[15]</sup> In the last ten years, the organocatalysis field has grown very rapidly. Now, it provides a significant toolbox for synthetic chemists, who can rely on organocatalysts to catalyze a number of reactions (around 130 thus far).<sup>[16]</sup>

Organocatalysts which display secondary amine functionality can perform either enamine catalysis (by forming catalytic quantities of an active enamine nucleophile) or iminium catalysis (by forming catalytic quantities of an activated iminium electrophile). Such types of organocatalysis offer several advantages. There is no need for metal-based catalysis, thus contributing to green chemistry. When the organocatalyst is chiral, there is a possibility of asymmetric catalysis. A variety of secondary amine organic molecules has been employed as asymmetric organocatalysts but proline and its derivatives are among the most successful catalysts studied to date.<sup>[17-19]</sup>

## 5.2. Proline as a powerful chiral catalyst

Proline is one of the twenty naturally occurring amino acids. It is a secondary cyclic amino acid, with a carboxylic acid group on the alpha carbon, which is a chiral centre (Figure 5.1). The most important feature of this amino acid is its availability in both enantiomeric forms. Proline can be characterized as a bifunctional catalyst since the amine moiety and the carboxylic acid can act simultaneously (Figure 5.1).

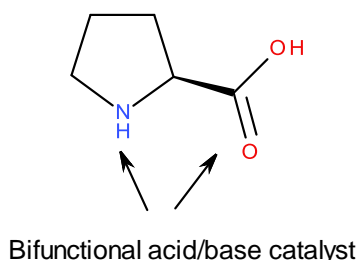
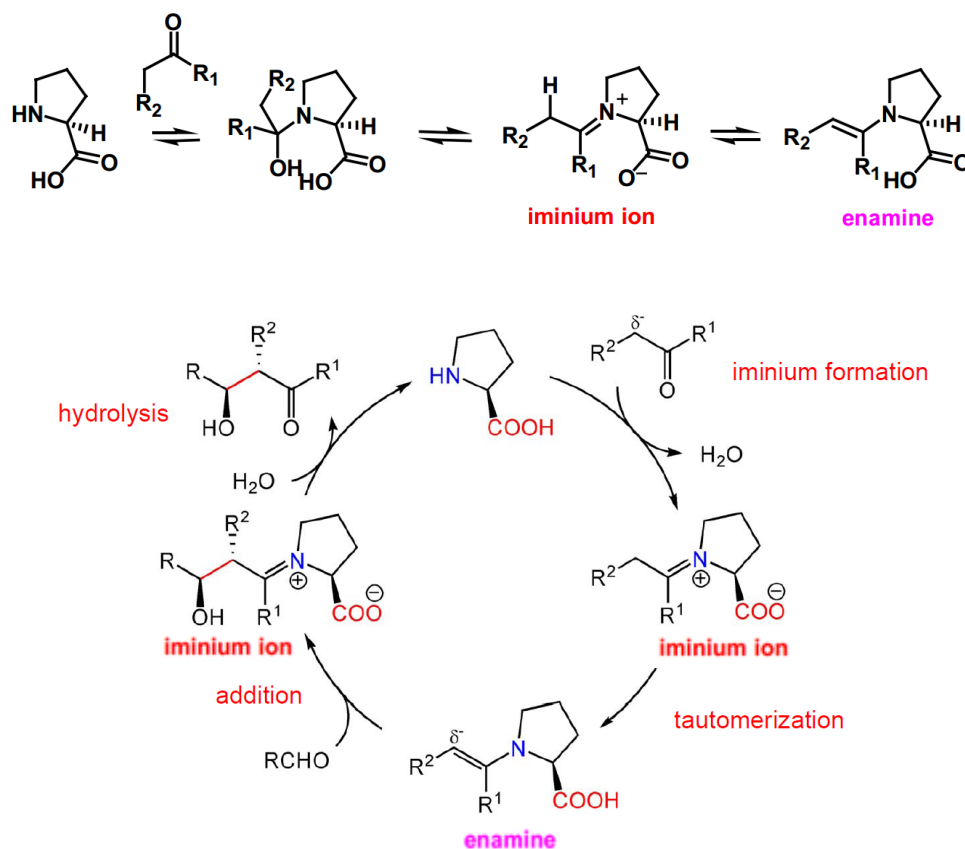


**Figure 5.1** – Structure of the bifunctional organocatalyst L-proline

The high  $pK_a$  value of the secondary amine functional group ( $\sim 10.6$ ) enhances the nucleophilicity, allowing proline to react easily with carbonyl compounds, and leading to the formation of iminium ions or enamines.<sup>[20]</sup> The general catalytic cycle of proline-mediated aldol reactions starts with the secondary amine acting as a nucleophilic enamine catalyst in order to form a positive iminium ion (Scheme 5.1).<sup>[15-16, 21]</sup> As a result, the acidity of the adjacent  $\alpha$ -proton increases, leading to the formation of the enamines which attack the carbonyl group of the acceptor with high enantiofacial selectivity due to the carboxylic acid acting as a Brønsted catalyst. Finally, hydrolysis of the iminium ion affords the aldol product and regeneration of proline.



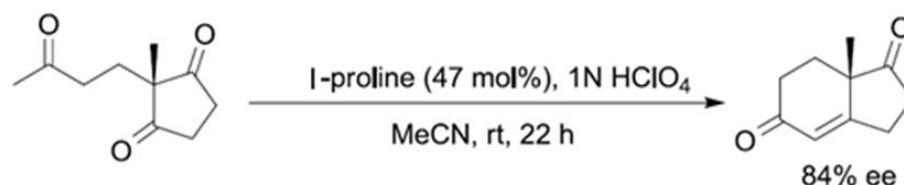
**Scheme 5.1** – Proposed mechanism of the proline-catalyzed asymmetric aldol reaction.<sup>[22]</sup>

The bifunctional character of proline is critical to the enantio-determining transition state. Houk et al.<sup>[23]</sup> and List et al.<sup>[24]</sup> proposed that the proton transfer from the proline,

carboxylic acid moiety and the nucleophilic addition of the neutral enamine to the carbonyl group occurs simultaneous.

The ability of proline not only to catalyze organic reactions but also to favour the formation of a single enantiomer was first noted more than 40 years ago.<sup>[25-26]</sup> Limited interest was observed until 2000 when its potential was rediscovered by Barbas and List.<sup>[22]</sup> Since then, an impressive number of catalytic applications have been reported. It has been successfully applied to many other reactions such as Michael reactions,<sup>[27]</sup> Mannich reactions,<sup>[28-29]</sup> Robinson annulation,<sup>[30]</sup> Diels–Alder reactions,<sup>[31]</sup> direct electrophilic  $\alpha$ -aminations,<sup>[32]</sup> Baylis–Hillman reactions,<sup>[33]</sup>  $\alpha$ -selenenylation,<sup>[34]</sup> aza-Morita-Baylis–Hillman reactions,<sup>[35]</sup> chlorination,<sup>[36]</sup> oxidation<sup>[37]</sup> and others.<sup>[38]</sup>

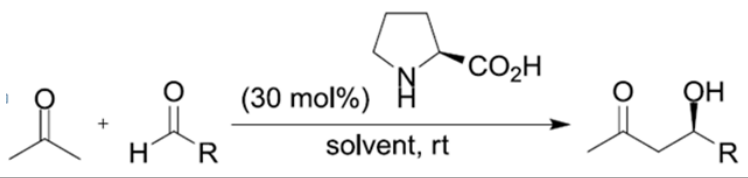
In the early 1970s, in an attempt to develop new methods for the synthesis of steroids, two industrial groups independently discovered that a small amount of (*S*)-proline can catalyze an asymmetric intramolecular aldol reaction (Scheme 5.2).<sup>[25-26]</sup>

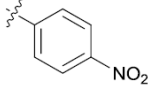
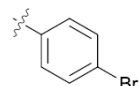
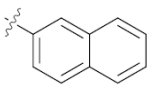


**Scheme 5.2** – First proline-catalyzed intramolecular aldol reaction

A number of experimental and theoretical studies have followed. Nevertheless, the only synthetic utility of this methodology before the beginning of the new century was illustrated by the synthesis of a variety of steroids and terpenes.<sup>[39-41]</sup>

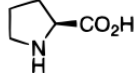
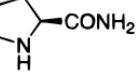
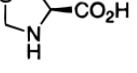
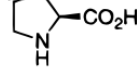
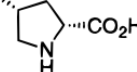
As stated earlier, the first proline-catalyzed direct intermolecular aldol reaction between acetone and a variety of aldehydes was reported by List and Barbas.<sup>[22]</sup> Data are shown in Table 5.1.

**Table 5.1** – Enantioselective aldol reaction catalyzed by L-proline, between acetone and a variety of aldehydes.<sup>[22]</sup>


Entry	R	Solvent	Yield [%]	ee [%]
1		DMSO	68	76
2		DMSO	62	60
3		DMSO	74	65
4		DMSO	54	77

This work was remarkable since it is known that proline can undergo a variety of reactions with aldehydes. For example, aliphatic aldehydes react with proline to give oxazolidinone and other compounds, including products of self-aldolization.<sup>[42]</sup> Aromatic aldehydes (including 4-nitrobenzaldehyde) can condense with proline to form azomethine ylides that undergo further 1,3-dipolar cycloaddition reaction.<sup>[43]</sup> List and Barbas claimed that high concentrations of acetone in the reaction mixtures suppress these side reactions. The only significant side product was the  $\alpha,\beta$ -unsaturated ketone, formed by aldol dehydration. Anhydrous DMSO was found to be the most suitable solvent regarding reaction times and enantioselectivity at room temperature. List and Barbas also studied the catalytic activity of different commercially available proline derivatives to overcome the high catalyst concentration required (Table 5.2). Interestingly, none of the commercially available proline derivatives showed a significantly improved yield of enantioselectivity compared to proline itself except, perhaps, 4-hydroxy-L-proline.<sup>[22]</sup>

**Table 5.2** – Amino acid derivatives tested as catalysts for the asymmetric aldol reaction of acetone with 4-nitrobenzaldehyde

Compound	Yield	ee
	68%	76%
	< 10%	n. d.
	67%	73%
 <div style="display: inline-block; vertical-align: middle; margin-left: 10px;"> R = OH    85%  R = O<i>t</i>Bu &gt; 50%  R = OAc    70% </div>		78% 62% 74%
	> 50%	62%

The rediscovery of the proline-catalyzed strategy has initiated the growth of research on chiral synthesis reactions using homogenous and heterogeneous proline catalysts. [16-19, 38, 44]

### 5.3. Immobilization of proline

Immobilization of proline is relatively expensive because a proline derivative is used as a starting material, usually a hydroxy-N-substituted-L-proline, and several synthetic steps may be necessary for its immobilization.<sup>[38]</sup> To counterbalance this point, the supported proline material can be easily recovered and, in principle, reused many times. Proline is used at up to 30 mol% compared to reactants, when used in homogeneous solution, so reusability is important.<sup>[22, 28, 30, 37]</sup> Moreover, immobilization allows the use of many different solvents and does not rely on the catalyst being soluble. Finally, immobilization gives the possibility of exploring modifications of the properties of the supported catalysts by employing specific characteristics via the support material.

Two different approaches can be summarized from the literature for L-proline immobilization. Covalently supported catalyst, in this case L-proline, or a proline derivative, has been covalently anchored to solid supports such as polyethylene glycol (PEG),<sup>[45-46]</sup> dendrimer,<sup>[47]</sup> polystyrene<sup>[48-50]</sup> and silica supports.<sup>[51-53]</sup> Non-covalently

supported catalyst, in this case L-proline, or a proline derivative, has been adsorbed or linked by electrostatic interactions (e.g. Layered double hydroxides (LDH)<sup>[54]</sup>) in the support.

A potential difficulty with immobilization of proline is the reactivity of the amine and the carboxylic groups. Whether or not these groups require chemical protection prior to immobilization is somewhat uncertain. Generally, proline derivatives such as 4-hydroxy-L-proline were used for immobilization where the hydroxyl group was used to attach the proline to the support. During these procedures, amine and, occasionally, carboxylic acid groups were protected. The protecting group for the amine group can be any of the many available for the protection of the amine group, such as tert-butoxycarbonyl-(Boc), carbobenzoxy-(Cbz), 9-fluorenyl-methoxycarbonyl-(Fmoc) or allyloxycarbonyl-(alloc) protecting group. Meanwhile, the carboxylic acid group was protected by converting it to methyl carboxylate. The purpose of such protection is to mask these functionalities during subsequent synthetic transformations. The removal of the protecting group that has been utilized may be undertaken after the immobilization. The deprotection protocol must be carried out according to which protecting group/groups are present. However, protection/deprotection methods present disadvantages such as extra steps (at least 2 - protection and deprotection), lowered yield, low atom economy, added mass, the use of expensive reagents and more excessive amounts of catalysts and organic solvents, low chemoselectivity, and high temperature in some cases. These disadvantages reduce the potential for translating these catalysts into industrial applications. In recent years, supported proline and other chiral organic catalysts have been the subject of many reviews.<sup>[16-19, 38-39, 44, 55-58]</sup> In this introduction, only covalently supported proline and proline derivatives are covered.

### 5.3.1. Polymer-supported proline

Polymer supported organocatalysts have recently been reviewed by Gruttadauria et al.<sup>[38]</sup> These immobilized catalysts are reputed to be successful at inducing asymmetry in products in much the same way as when the catalysts are used in homogeneous solution. Proline can be modified with an appropriate functional group, capable of binding the catalyst onto a solid polymer. This approach has been described by Benaglia et al.,<sup>[45]</sup>

who used polyethylene glycol (PEG) of average molecular weight 5000 to immobilize proline by esterification of the 4-hydroxy group of trans 4-hydroxy-L-proline with PEG via a succinate spacer using carbodiimide reagent, without the protection of amine or carboxylic acid groups in the proline molecule. The immobilized catalyst (Figure 5.2 (1)) was used to induce asymmetry in the preparation of  $\beta$ -hydroxy ketones and  $\beta$ -amino ketones. More recently, similar PEG-proline catalysts (Figure 5.2 (2)) were prepared starting with PEG (MW=2000 or 5000) and other proline derivatives.<sup>[59]</sup>

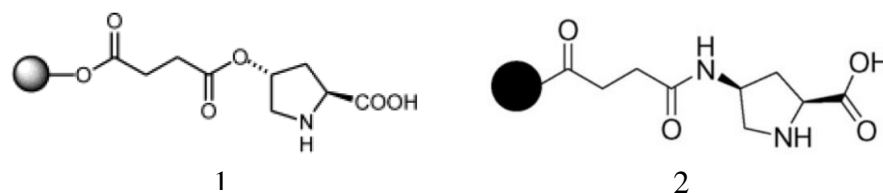
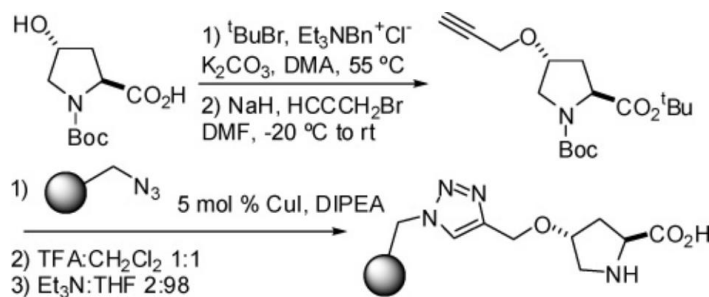


**Figure 5.2** – Structures of polymer-supported proline

These polymers are homogeneously soluble in the reaction medium and can be precipitated after the reaction by the addition of a suitable non-solvent for the polymer. Especially good results have been obtained with the type of cross-linked polystyrene-anchored proline supports introduced by the groups of Perica and Gruttadauria, from 2006 onwards.<sup>[49]</sup> The chiral resin catalyst was synthesized through several steps starting with N-Boc-trans-4-hydroxy-L-proline to prepare o-propargyl hydroxy proline which underwent 1,3-dipolar cycloaddition of an azide substituted Merrifield resin; this was followed by deprotection of the amine to yield the final catalyst, as shown in Scheme 5.3.



**Scheme 5.3** – Preparation of Polystyrene-Supported Hydroxyproline

This resin was used in the aldol reaction between several ketones (cyclohexanone, cyclopentanone, acetone and hydroxy acetone and arylaldehydes). However, as shown in Scheme 5.3, the methodology used to synthesize the catalyst was complicated and was not suitable for large-scale production. Generally, the use of polymers as support has many disadvantages such as their poor thermal and chemical stability when compared with other solid catalysts such as silica.

### 5.3.2. Silica-supported proline

Silica is an attractive support because of its thermal and mechanical stability as well as its chemical inertness. After the 2000 report that L-proline could catalyze aldol reactions with enantioselectivity, examples of grafted proline on inorganic supports (MCM-41,<sup>[51-52]</sup> SBA-15,<sup>[60]</sup> silica gel<sup>[51]</sup>, and zeolites<sup>[61]</sup>) appeared, initially in 2003.<sup>[51]</sup> Proline was immobilized on MCM-41 in eight steps starting from (2S,4R)-4-hydroxyproline and passing through complex chemistry to give the final catalyst (Figure 5.3). The protection and deprotection of amine and carboxylic acid groups was necessary during the catalyst preparation.

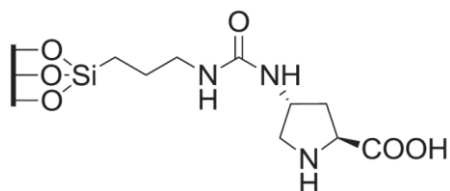
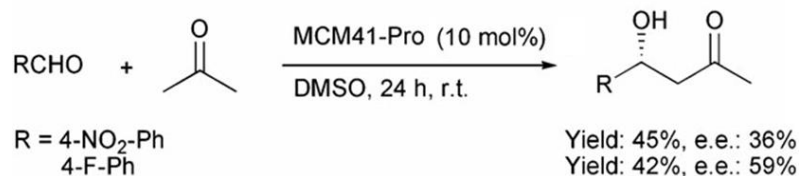


**Figure 5.3** – Structure of MCM-41 supported proline.<sup>[51]</sup>

Only two aldol reactions were investigated. Both yields and enantioselectivities were poor (Scheme 5.4). Recycling investigations (3 cycles) showed a decrease in both activities and enantioselectivities.



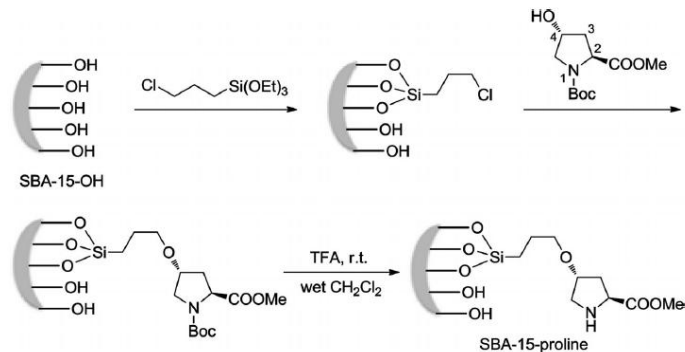
**Scheme 5.4** – Direct aldol reaction of acetone with aromatic aldehydes using MCM-41-Pro.<sup>[51]</sup>

Other groups modified the method to obtain better catalysts. However, they used similar grafting strategies where the linkage of the proline was done through the formation of urea, carbamate or ether groups, starting with the readily available *trans* 4-hydroxy-L-proline. This strategy enables the conservation of the NH function that is involved in the formation of enamines and the COOH that directs the positioning of the electrophile.<sup>[62]</sup> Recently a similar strategy was used for immobilizing L-proline on silica, but using a co-condensation sol-gel synthesis.<sup>[63]</sup>

These materials prepared with the co-condensation sol-gel method catalyzed the asymmetric aldolization between *p*-nitrobenzaldehyde and acetone at room temperature with moderate performances and low enantiomeric excess (20-37 ee%). Interestingly, the performance of the material with ether linkage was significantly better than the one with the carbamate linker. However, both catalysts showed very low activity in their second run.

All of the above-mentioned systems were devised by organic chemists to be effective in promoting asymmetric induction. However, they suffer from one or more disadvantages. Their preparation is inherently complicated, often using lengthy procedures. Accordingly, these catalysts are for the most part only useful for academic pursuits. In fact, considering the extensive interest that organocatalysis has received and the importance of proline in particular, it is surprising that so few genuinely effective procedures for simple immobilization of L-proline in solid support have been reported. Recently, two new, successful concepts for immobilization of L-proline on solid support have been reported that are different. Li et al.<sup>[64]</sup> have reported the preparation of a proline-modified porous SBA-15 catalyst through three steps where a (3-chloropropyl)trimethoxysilane tether was

grafted on silica, and then N-Boc-trans-4-hydroxy-L-proline methyl ester was added. Then the tert-butyloxycarbonyl protecting group (BOC group) was removed as shown in Scheme 5.5.



**Scheme 5.5** – Preparation of porous SBA-15-proline.<sup>[64]</sup>

This heterogeneous catalyst showed high activity and durability in promoting intermolecular conjugated addition between nitroalkenes and enones. It gave excellent yields even after multiple recycles (measured up to 7 times). However this study didn't investigate the enantioselectivity of their catalyst.

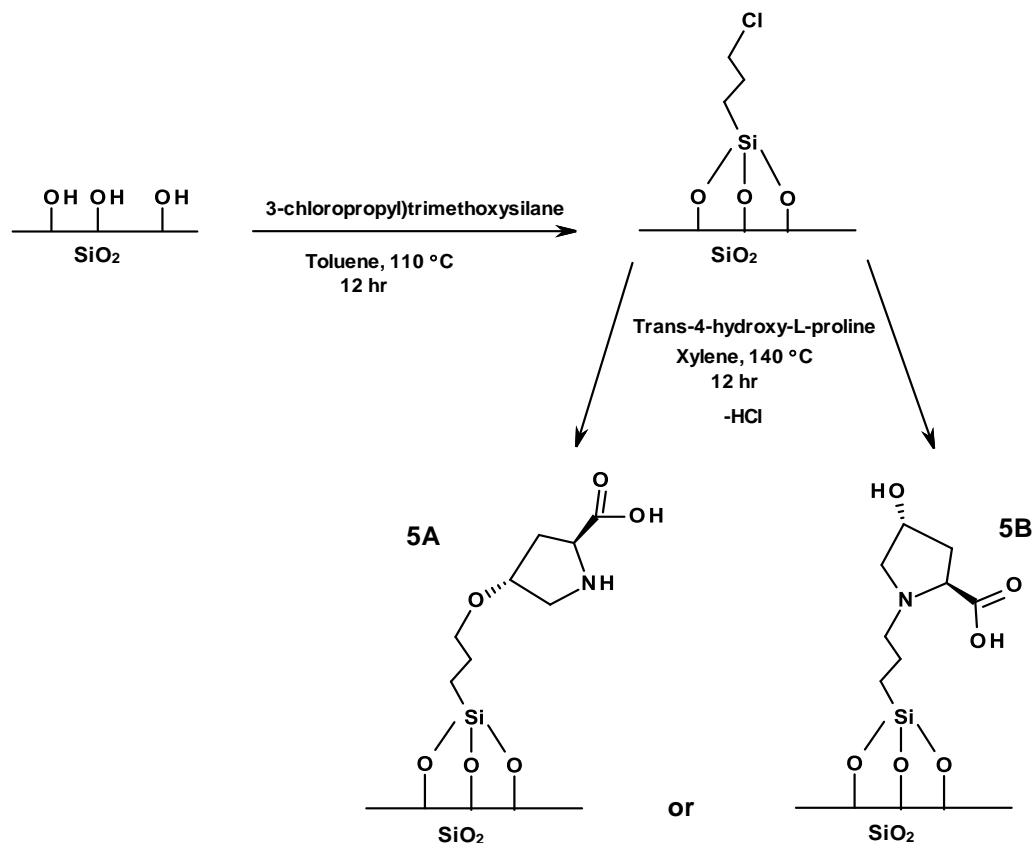
Hansen<sup>[65]</sup> introduced another approach to the synthesis of acrylic polymer beads containing proline on a large scale. Monomeric proline (meth)acrylates were prepared from hydroxyproline in one step. Free-radical copolymerization then gave solid-supported proline organocatalysts directly in as few as two steps overall. These acrylic beads have highly favourable and adjustable swelling characteristics and are excellent reusable catalysts for organocatalytic reactions.

What makes this method interesting is not only the ease of preparation but also the fact that there is selective acylation of the hydroxyl group on the proline molecule in the presence of the amine group, without protecting the amine group. In general, amines react more rapidly with carbonyl electrophiles than do alcohols; therefore, this preferential reaction with the hydroxyl group is possibly not what might have been expected (although it is fortuitous). A noteworthy amount of research has been dedicated to the chemoselective reaction of the hydroxyl moiety. The first, in 1964, was the preparation of

o-acetyl derivatives of hydroxyamino acids (hydroxyproline among them) by dissolution of hydroxyamino acids in a mixture of aqueous HCl and acetic acid.<sup>[66]</sup> Hansen<sup>[65]</sup> found that acylation in concentrated sulfuric acid is possible, but is also unpredictable, violent and unsafe. Trifluoroacetic acid has been used as a medium for selective acylation of hydroxyl groups in gelatin and serine.<sup>[67]</sup> All these reports show the possibility of selective reactivity of the hydroxyl group over the amine group of hydroxyproline in acidic medium. In fact it may be that the acid medium provide some protection of the amine.

In the work described in this thesis, it was proposed that choosing a support such as silica gel with slightly acidic characteristics could protect amines by protonation. To a certain degree, there may also be protection of carboxylic acids by ensuring that they remain in the protected, undisassociated form. Using (3-chloropropyl)trimethoxysilane as a linker for hydroxyproline with amine protonated could result in selective OH reaction with a linker releasing HCl in the solution, which could enhance the protection of the remaining hydroxyproline in the solution. Therefore, immobilization could then be provided in one step without using the traditional protection.

In order to investigate the possibility of this concept, three catalysts were prepared using a modified version of the method described by Li et al.,<sup>[64]</sup> where 4-hydroxyproline was added to three silica supports with different textural parameters, grafted by (3-chloropropyl)trimethoxysilane. In this case, it was hoped that the 4-hydroxyproline would attach to the linker through the hydroxyl group (Scheme 5.6, 5A). Catalyst 5A would be active in aldol reaction while catalyst 5B would not be active in aldol reaction, as the tertiary nitrogen cannot form an iminium intermediate.



**Scheme 5.6** – Preparation of porous silica-supported proline

Another two catalysts were prepared by the conventional protection-deprotection process<sup>[64]</sup> by using N-Boc-trans-4-hydroxy-L-proline, in which the amine group is protected by tert-butyl carbamates (Boc) (Figure 5.4a), or N-Boc-trans-4-hydroxy-L-proline methyl ester (Figure 5.4b), where the amine is protected by Boc and the acid is present as the methyl ester.

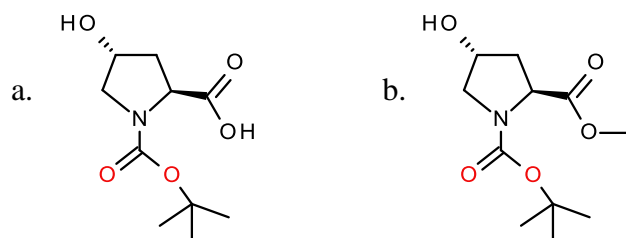
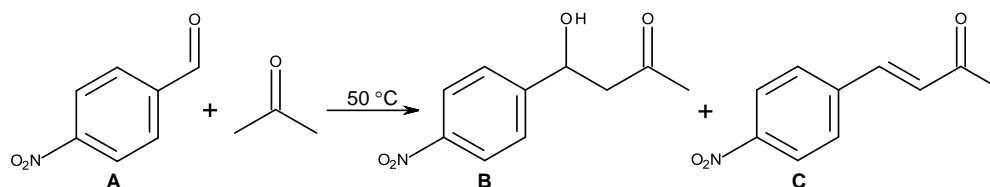


**Figure 5.4** – Structures of a) N-Boc-trans-4-hydroxy-L-proline and b) N-Boc-trans-4-hydroxy-L-proline methyl ester.

In this work, a crossed-aldol reaction between 4-nitrobenzaldehyde (A) and acetone was used to test the catalysts (Scheme 5.7). It is well known that this reaction is catalyzed by the natural amino acid (L)-proline to give the aldol product B, which is chiral.



**Scheme 5.7** – Cross-aldol reaction between 4-nitrobenzaldehyde (A) and acetone to give the aldol addition (B) and aldol condensation (C) products.

In the above reaction, (L)-proline reacts first with acetone to form an enamine. This enamine adds to the carbonyl group of preferentially from one face, leading mainly to (S) configuration of the newly formed asymmetric centre. The iminium intermediate is subsequently hydrolyzed to produce the (S) aldol product as a major product, as the proline catalyst is released.

All catalysts were fully characterized and tested in an aldol reaction. The effect of the synthesis method, support textural parameters and reaction conditions on the catalytic activities, reusabilities and enantioselectivities were studied.

## 5.4. Experimental section

### 5.4.1. Materials

Tetraethyl orthosilicate (TEOS, 98%), (3-chloropropyl)trimethoxysilane, trans-4-hydroxy-L-proline, N-Boc-trans-4-hydroxy-L-proline, N-Boc-trans-4-hydroxy-L-proline methyl ester, cetyltrimethylammonium bromide (CTABr, as a structure-directing agent for synthesis of MCM-41), toluene and xylene were purchased from Sigma Aldrich and used as received. 4-nitro benzaldehyde and benzyl alcohol were purchased from Acros. Deionized water was used in all experiments. Two commercial mesoporous silica gels of high-purity grade, (SiO<sub>2</sub> (H), 516 m<sup>2</sup>/g and SiO<sub>2</sub> (L), 312 m<sup>2</sup>/g), were purchased from

Aldrich. Both silicas were activated prior to any functionalization by stirring them in concentrated HCl at 100 °C for 4 hours; they were then filtered and washed with water several times until pH 7 to remove all acid residues before being dried for 24 h at 120 °C under air.<sup>[68]</sup>

#### 5.4.2. Synthesis of catalyst materials

##### 5.4.3. Chloropropyl functionalized silica gel (SiO<sub>2</sub>-Cl)

Activated silica gel (4 g) was added to toluene (40 mL) in a round-bottomed flask. The mixture was heated to 110 °C and stirred for 1 h under nitrogen. Then, 3-chloropropyltrimethoxysilane (20.0 mmol, 4.0 g) was added, under stirring at the same temperature under nitrogen. After 12 h the solid was filtered, washed with toluene and then dried in the oven at 120 °C in air for 12 h. The obtained solid was labelled with reference to the type of silica gel. In the case of silica gel with the higher surface area, the solid was labelled SiO<sub>2</sub>-Cl (H), while in the case of silica gel with the lower surface area the solid was labelled SiO<sub>2</sub>-Cl (L).

##### 5.4.4. Proline-functionalized silica gel (SiO<sub>2</sub>-Pr) by direct route

SiO<sub>2</sub>-Cl (1.0 g) was suspended in 20 mL xylene at 140 °C under nitrogen and stirred for 1 h. Trans-4-hydroxy-L-proline (2 mmol, 0.26 g) was added under stirring at the same temperature under nitrogen. After 12 h, the proline catalyst was filtered, washed with water and then ethanol, and dried in an oven at 120 °C in air for 12 h to give SiO<sub>2</sub>-Pr. The catalyst prepared from silica gel with low surface area (312 m<sup>2</sup>/g) was named SiO<sub>2</sub>-Pr (L) while the catalyst with higher surface area (516 m<sup>2</sup>/g) was named SiO<sub>2</sub>-Pr (H).

##### 5.4.5. Proline-functionalized silica gel by amine protecting/deprotecting route

SiO<sub>2</sub>-Cl (L) (1.0 g) was suspended in 20 mL xylene at 140 °C under nitrogen and stirred for 1 h. Then Boc-L-hydroxyproline (2 mmol, 0.46 g) was added under stirring at the same temperature under nitrogen. After 12 h the proline catalyst was filtered, washed with water and then ethanol, and dried as before to give SiO<sub>2</sub>-Pr-Boc. To remove the Boc group, 0.5 g of SiO<sub>2</sub>-Pr-Boc was suspended in 5 mL of CH<sub>2</sub>Cl<sub>2</sub> for 10 min; then 10 mL of trifluoroacetic acid (99%) was added to the solution.<sup>[69]</sup> The mixture was left for 12 h at

room temperature; then the solid was filtered, washed with water and then ethanol, and dried at 120 °C to give  $\text{SiO}_2\text{-Pr (Boc)}_{\text{deprotected}}$ .

#### **5.4.6. Proline-functionalized silica gel by both amine and carboxylic acid groups protecting/deprotecting route**

$\text{SiO}_2\text{-Cl (L)}$  (1.0 g) was suspended in 20 mL xylene at 140 °C under nitrogen and stirred for 1 h. Then N-Boc-trans-4-hydroxy-L-proline methyl ester (2 mmol, 0.5 g) was added under stirring at the same temperature under nitrogen. After 12 h, the proline catalyst was filtered, washed with water and then ethanol, and then dried at 120 °C to give  $\text{SiO}_2\text{-Pr-Boc-Me}$ . For deprotection, 0.5 g of  $\text{SiO}_2\text{-Pr-Boc-Me}$  was suspended in 10 mL of 30% HBr in acetic acid.<sup>[51]</sup> The mixture was left for 12 h at room temperature; then the solid was filtered, washed with water, then ethanol and then dried in the oven at 120 °C in air for 12 h to give  $\text{SiO}_2\text{-Pr (Boc, Me)}_{\text{deprotected}}$ .

#### **5.4.7. Proline-functionalized MCM-41 silica by direct route (MCM-41-Pr)**

Mesoporous silica (MCM-41) was synthesized according to the original literature procedure using cetyl trimethylammonium bromide as a template. For a typical synthesis, 65%  $\text{NH}_4\text{OH}$  (69 mL) was mixed with 525 mL of distilled water. CTAB (0.125 g) was added with stirring at 80 °C. When the solution became homogenous, TEOS (1.0 g) was added. After 2 h, the resulting product was filtered, washed with distilled water, dried at ambient temperature, and calcined in air at 540 °C for 4 h to obtain MCM-41 structure, verified using XRD and  $\text{N}_2$  adsorption.<sup>[70]</sup> Covalent grafting of the chiral proline derivative onto MCM-41 was carried out as outlined for the amorphous silica by grafting (3-chloropropyl) trimethoxysilane on the surface in toluene at 110 °C for 12 h, followed by direct reaction with trans-4-hydroxy-L-proline in xylene at 140 °C for 12 h. The solid was filtered, washed and dried as before to give MCM-41-Pr.

### **5.5. Catalyst characterization:**

X-ray diffraction (XRD) patterns were measured on a Rigaku miniflex diffractometer. Data were recorded over the  $2\theta$  range 1.5°–10° with a step size of 0.05° and a counting time of 30 s/degree. The  $\text{N}_2$  adsorption–desorption isotherms were measured at 77 K on a Micromeritics ASAP-2020, after evacuation at 473 K for 5 h. Surface areas were

calculated by the BET method on the adsorption branch. Thermogravimetric Analysis (TGA) was conducted using a thermogravimetric analyzer (Perkin-Elmer TGA). The heating rate was 10 °C/min in a nitrogen atmosphere and the materials were heated to 150 °C and held at this temperature for 2 h to ensure the evaporation of all surface adsorbed water. Then the temperature was increased to 500 °C at 10 °C/min under nitrogen to estimate the concentration of organic molecules attached to the silica surface. Nitrogen and chlorine levels in the catalysts were determined by elemental analysis (MEDAC Ltd.). Infrared spectra of the solid samples were recorded on a Nicolet 380 FTIR single reflection spectrometer recording attenuated total reflectance infrared (ATR IR) spectra over the range 400-4000  $\text{cm}^{-1}$  under atmospheric conditions, to investigate the chemical nature of the catalyst surface.

### 5.6. Catalytic activities

Catalytic activity was examined in the cross-aldol reaction. Two methods were used to test the catalyst. First, 4-nitrobenzaldehyde (1 mmol), 10 mL acetone and 0.1 mL benzyl alcohol as internal standards were placed in a 50 mL round-bottomed flask and stirred at 50 °C for 6 h under nitrogen. Then the catalyst (0.05 g) was added to the reactor after being activated at 120 °C for 2 h. Samples were taken at regular intervals, and the percentage conversion of 4-nitrobenzaldehyde and aldol product yields were estimated using the reverse phase HPLC method. At the same time, the enantiomeric excess (%) of aldol product was determined by the normal phase HPLC method.

In the second method, a solution of 2 mmol of 4-nitrobenzaldehyde in 2 mL acetone and 8 mL DMSO was used in each experiment. Then each catalytic reaction was carried out over 0.05 g activated catalyst at room temperature for 20 h. Next, filtration was used to remove the solid catalyst. After washing with acetone and then chloroform (3 x 10 mL each), the resulting product was obtained and analyzed by  $^1\text{H}$  NMR in  $\text{CDCl}_3$ . The activity of catalysts was studied by  $^1\text{H}$ -NMR. The study analyzed the disappearance of the signal of the aldehyde proton (A) at  $\delta\text{H}$  10.09 ppm and the concomitant increase of intensity of the signal associated with the same proton in the aldol products [B at 5.20 ppm and C at 6.75 ppm. The percentages of the aldol products (B) were calculated by

dividing the integral of the product proton by the sum of the integrals of the aldehyde proton plus the product protons considered as 100%.

$$B(\%) = \frac{H(B)}{H(A) + H(B) + H(C)}$$

To screen the recyclability of silica-supported proline, two methods were used. In the first, the catalyst was separated from the reaction mixture after reaction, washed with acetone, dried, and reintroduced to the reaction vessel where fresh starting materials were charged. In the second method, the leaching of proline was tested by stirring the catalyst in acetone at 50 °C for 12 h then removing the catalyst and testing the filtrate solution for activity in the reaction.

### 5.6.1. Development of a suitable analytical method for reactants and products

The use of UV-Vis spectroscopy is advantageous because it is very quick and accurate and it allows the generation of a considerable amount of kinetic data in a relatively short timeframe. In this project, this was not possible because the UV-Vis spectra of the starting reactants and products were too similar to provide reliable data. It was then decided to use high-performance liquid chromatography with a reverse phase column (HPLC-RP) and a double channel UV-Vis detector, which allows simultaneous identification and monitoring of all the components of the reaction mixture and any undesired side products.

The development of the analytical method started with the evaluation of retention times of each component of the reaction mixture - acetone, 4-nitrobenzaldehyde (A), aldol product (hydroxyketone) (B), condensation product (C) (Scheme 5.9) - using an isocratic mixture 50/50 of acetonitrile (ACN) and water. The ratio of the two solvents was varied to optimize the resolution of the components, leading to a 55/45 ratio. Unfortunately, after the initial experiments, it became apparent that the retention times of the 4-nitrobenzaldehyde and aldol product were always too similar, making it difficult to use an isocratic elution to carry out the analysis. The conditions for the elution were then further improved by introducing gradient elution.

The accuracy of any HPLC methodology relies on the use of an internal standard. The chemicals tried as internal standard in this project were polar compounds not too different from those of the reactants, to minimize the length of the run, but with more polar groups, such as benzoic acid, benzyl alcohol and 4-nitrophenol. Among them, the best results were obtained with the benzyl alcohol, which came out before the aldol product; this was subsequently used in all runs. The solvent gradient of ACN/water 30/70, reaching 85/15 after 14 minutes, was used. Chromatograms for reactants and products are shown in Figure 5.6.

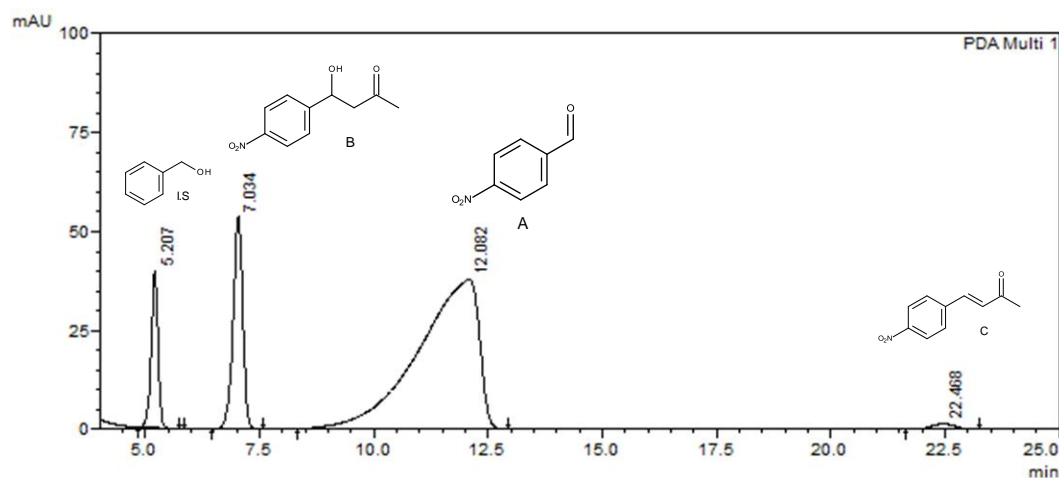


**Figure 5.6** – Standard HPLC chromatogram with the components deriving from a cross-aldol reaction between 4-nitro-benzaldehyde and acetone plus the internal standard (I.S).

Enantiomeric excesses (ee%) of aldol reactions were determined using a chiral analytical normal phase column Lux Cellulose-3, where solvent A was hexane Hipersolv (BDH) with 0.1% formic acid and solvent B was 2-propanol Hipersolv (BDH). This method allowed full separation of enantiomers as shown in Figure 5.7.

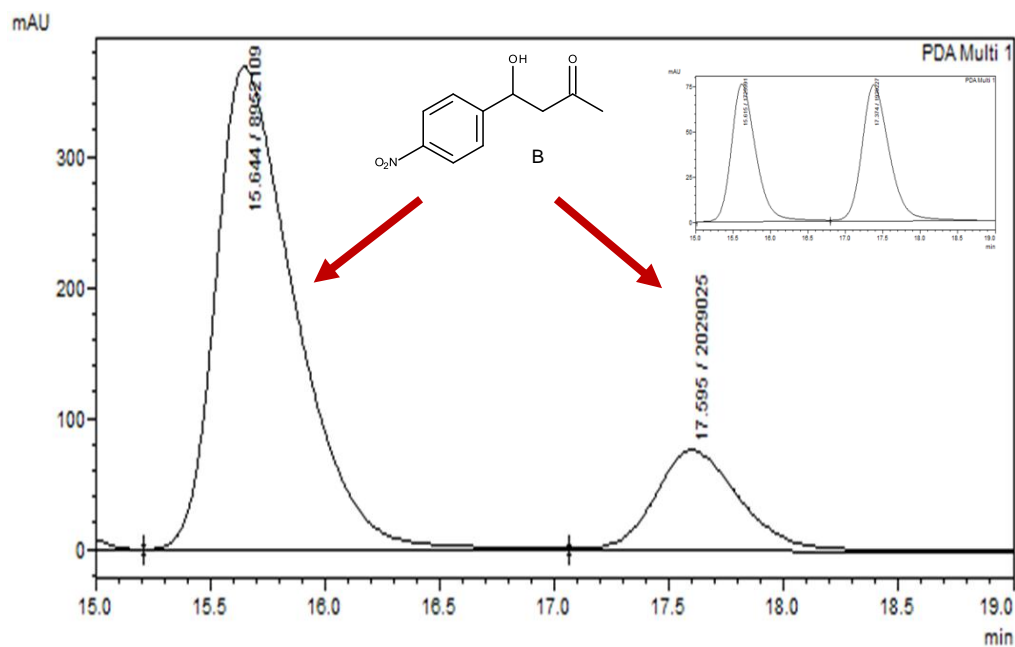


**Figure 5.7** – Chiral HPLC chromatogram of hydroxyl aldol product (B) deriving from a cross-aldol reaction between 4-nitro-benzaldehyde and acetone in presence of SiO<sub>2</sub>-Pr (H). In the top right are standard HPLC chromatograms of B as racemic mixture.

Enantiomeric excess (ee%) was calculated from the chromatographic data by the following equation:

$$(\text{ee}\%) = \left[ \frac{\text{Peak area 1} - \text{Peak area 2}}{\text{Peak area 1} + \text{Peak area 2}} \right] \times 100$$

## 5.7. Results and discussion

### 5.7.1. Characterization of L-proline functionalized silica materials

The XRD data for MCM-41, MCM-41-Cl and MCM-41-Pr were collected. Figure 5.8 shows their X-ray diffraction patterns.

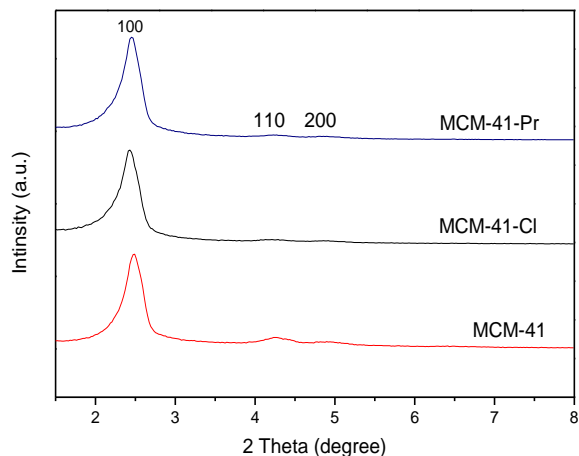


**Figure 5.8** – X-ray diffraction pattern of MCM-41, MCM-41-Cl and MCM-41-Pr.

The XRD patterns show well-resolved peaks with intense peaks at  $2\theta = 2.3\text{--}2.5$  and two or more peaks at higher angles, which were indexed to the 100, 110, and 200 planes characteristic of the long-range order and good textural uniformity of mesoporous material with a mesostructure of hexagonal space group symmetry by analogy with literature reports.<sup>[51, 71]</sup>

Notably, the mild modification conditions applied in the synthesis procedure did not disturb the porous nature of MCM-41. The XRD data confirm the preservation of the ordered structure throughout the Cl-CH<sub>2</sub>-CH<sub>2</sub>-CH<sub>2</sub>- grafting and proline molecule modification. However, the 100 reflection became slightly less well resolved, suggesting an effect on long-range order. The shift to a slightly lower angle of the principal peak demonstrates the enhanced wall thickness from MCM-41, MCM-41-Cl to MCM-41-proline, possibly suggesting that both the 3-chloropropyl and the proline groups are mainly incorporated into the pore channels.

Nitrogen adsorption–desorption isotherms for MCM-41, MCM-41-Cl and MCM-41-proline are shown in Figure 5.9 (left), while nitrogen adsorption–desorption isotherms for SiO<sub>2</sub> (L), SiO<sub>2</sub>-Cl (L), SiO<sub>2</sub>-Pr (L), SiO<sub>2</sub>-Pr-BOC and SiO<sub>2</sub>-Pr-BOC,Me are shown in Figure 5.9 (right). All samples indicate typical IV nitrogen adsorption-desorption isotherms with the H1 hysteresis loops characteristic of mesoporous structures.<sup>[72-73]</sup>

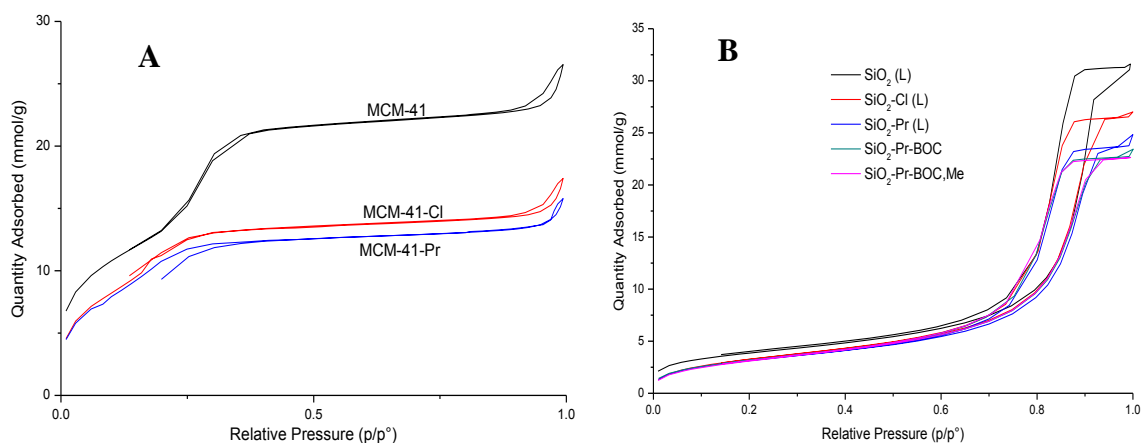


**Figure 5.9** – N<sub>2</sub> adsorption–desorption isotherms at 77 K for MCM-41, MCM-41-Cl and MCM-41-Pr (A) and SiO<sub>2</sub> (L), SiO<sub>2</sub>-Cl (L), SiO<sub>2</sub>-Pr (L), SiO<sub>2</sub>-Pr-BOC and SiO<sub>2</sub>-Pr-BOC,Me (B).

As shown in Figure 5.9 (A), MCM-41 shows a sharp increase of nitrogen uptake at  $p/p_0 \approx 0.4$ . This step is caused by condensation of nitrogen inside the mesopores. Below this pressure, the formation of an adsorbed monolayer of N<sub>2</sub> takes place. The further increase in N<sub>2</sub> pressure leads to the formation of a multilayer until capillarity occurs. In this way, an increase in the volume of adsorbed N<sub>2</sub> is observed. Once the pores are filled, the adsorption carries on on the external surface of the solids. This step decreases in height for MCM-41-Cl and MCM-41-Pr, indicating that the grafting occurred inside the mesopores. The poorly defined step in the MCM-41-Pr isotherm is indicative of broad pore size distribution. As shown in Figure 5.9 (B), SiO<sub>2</sub> (L) shows a sharp increase of nitrogen uptake at  $p/p_0 \approx 0.7$ , which indicates that SiO<sub>2</sub> (L) contains larger pores than MCM-41. It is clear that grafting leads to a decrease in surface area and pore volume as in the case of SiO<sub>2</sub>-Cl (L). The surface area was decreased further by grafting the

hydroxyproline on the surface and the protected form of the hydroxyproline (SiO<sub>2</sub>-Pr-BOC and SiO<sub>2</sub>-Pr-BOC,Me), as shown in Figure 5.9 (B).

Based on the nitrogen adsorption-desorption isotherms, the surface area (BET), the average pore sizes (DP), and the pore volumes (VP) were calculated by applying the BET and BJH models on the adsorption and desorption branches respectively. Table 5.3 summarizes the data for the prepared materials.

**Table 5.3** – Textural parameters for studied catalysts.

Sample	Surface area /m <sup>2</sup> g <sup>-1</sup>	Pore volume /cm <sup>3</sup> g <sup>-1</sup>	Average pore diameter /nm
SiO <sub>2</sub> (L)	313	1.1	11.1
SiO <sub>2</sub> -Cl (L)	278	0.9	9.9
SiO <sub>2</sub> -Pr (L)	265	0.8	9.6
SiO <sub>2</sub> -Pr-Boc	260	0.8	8.9
SiO <sub>2</sub> -Pr-Boc,Me	257	0.8	8.8
SiO <sub>2</sub> (H)	517	0.8	4.6
SiO <sub>2</sub> -Cl (H)	361	0.5	3.9
SiO <sub>2</sub> -Pr (H)	357	0.4	3.9
MCM-41	1100	1.0	2.9
MCM-41-Cl	998	0.5	2.6
MCM-41-Pr	959	0.4	2.1

Thermogravimetric analysis curves for SiO<sub>2</sub>-Cl (L) and SiO<sub>2</sub>-Pr (L) are shown in Figure 5.10. In this analysis, 10 mg of the sample were heated up to 500 °C at 10 °C/min ramp in nitrogen atmosphere, and weight loss was measured as a function of temperature.

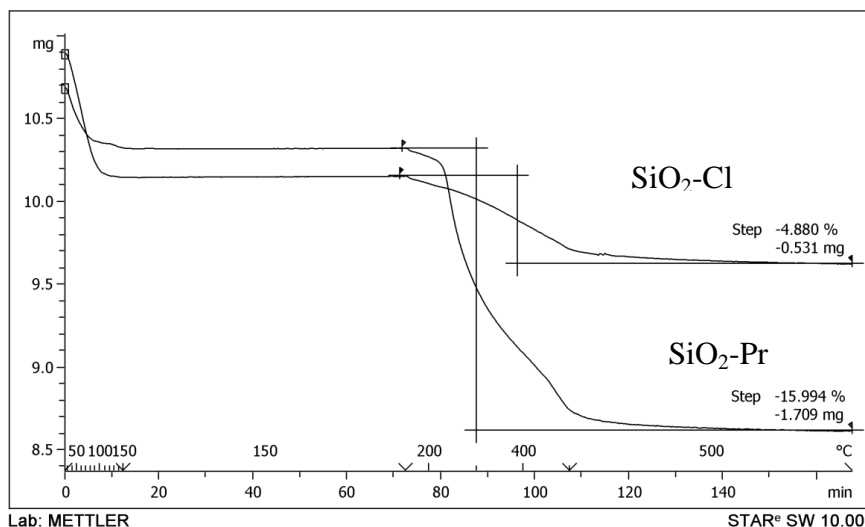


**Figure 5.10** – TGA-curves of hybrid silica samples with different organic groups in nitrogen atmosphere.

There are two weight loss steps, at 20–200 °C and at 200–500 °C. The first is related to the drying of silica. The second, which is the more important, is attributed to the decomposition of the organic groups grafted on the surface. Elemental analysis data for nitrogen and for chlorine (Table 5.4) are taken as indicators of the relative concentrations of the supported proline and the unreacted chloropropyl groups on the silica surface. On the basis of these two tethered groups, the overall mass losses measured over 200–500 °C are converted to molar concentrations (Table 5.4). It is worth noting that the overall concentration of surface functional groups from elemental analysis (N plus Cl concentrations) agrees very well with the overall concentration based on TGA. However, the weight loss obtained from TGA was converted to mmol by the aid of elemental analysis data.

**Table 5.4.** TGA and elemental analysis for the synthesized materials.

Sample	Organic content <sup>a</sup> /mmol g <sup>-1</sup>	N content <sup>b</sup> /mmol g <sup>-1</sup>	Cl content <sup>b</sup> /mmol g <sup>-1</sup>
SiO <sub>2</sub> -Cl (L)	0.62	-	0.64
SiO <sub>2</sub> -Pr (L)	0.61	0.43	0.20
SiO <sub>2</sub> -Pr-Boc	0.63	0.42	0.21
SiO <sub>2</sub> -Pr-Boc,Me	0.61	0.39	0.22
SiO <sub>2</sub> -Pr (Boc) <sub>deprotected</sub>	0.58	0.41	0.19
SiO <sub>2</sub> -Pr (Boc,Me) <sub>deprotected</sub>	0.33	0.17	0.14
SiO <sub>2</sub> -Cl (H)	1.31	-	1.32
SiO <sub>2</sub> -Pr (H)	1.30	1.30	-
MCM-41-Cl	1.12	-	1.05
MCM-41-Pr	1.10	0.71	0.29

a. Thermogravimetric data, b. Elemental analysis data.

Some significant trends can be seen in the data in Table 5.4. Not unreasonably, there seems to be a link between the specific surface area of the support and the level of functionalization when comparing the related SiO<sub>2</sub>-Pr (L) and SiO<sub>2</sub>-Pr (H) catalysts. The fact that the much higher surface area of MCM-41 does not correspond to a proportionally higher level of functionalization may reflect a less accessible surface in the deep pores in this material, or it may be a consequence of a less reactive surface arising from high temperature calcination and a relatively low concentration of surface silanol groups.

The extent to which chloropropyl groups can be converted to supported proline is also significant. This is quantitative for SiO<sub>2</sub>-Cl (H) but only about 70% conversion occurs for SiO<sub>2</sub>-Cl (L) and MCM-41-Cl. It is tempting to link this to pore size and the facility with which 4-hydroxyproline can access the surface chloropropyl groups. The data are, on the face of it, inconsistent with this idea, however, since the support with the largest average pore diameter, SiO<sub>2</sub> (L), only supports partial conversion, and the only support that allows full conversion by proline exhibits an intermediate pore diameter. There is no other obvious explanation for the differences in conversion and it is possible that a more subtle dependence on porosity is controlling the reaction, possibly worthy of further study.

The data in Table 5.4 lend weight to the overall objective of bypassing the need to protect the proline functional group for tethering on silica. The table shows that the act of protecting and then de-protecting results in significant losses of functional group concentrations, especially through the esterification of the carboxylic acid group and its subsequent hydrolysis.

The FT-IR spectra of SiO<sub>2</sub>-Pr (L), SiO<sub>2</sub>-Pr-Boc and SiO<sub>2</sub>-Pr-Boc,Me were recorded (Figure 5.11).

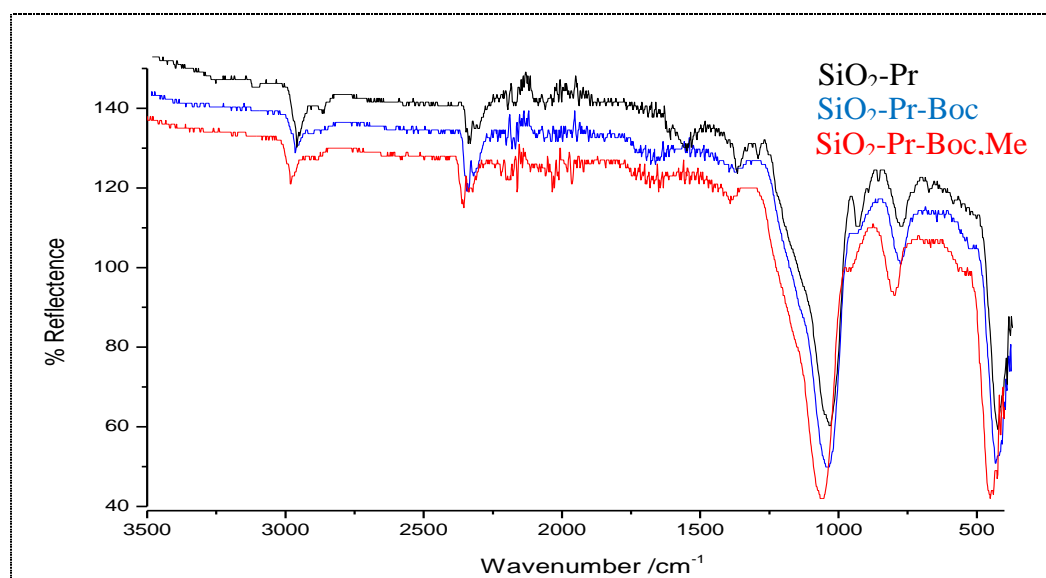


**Figure 5.11** – FTIR spectra of hybrid silica samples.

As shown in Figure 5.11, SiO<sub>2</sub>-Pr (L), SiO<sub>2</sub>-Pr-Boc and SiO<sub>2</sub>-Pr-Boc,Me have nearly the same spectra with only a few differences. The stretching vibration band at 2923 cm<sup>-1</sup> and the rocking vibration band at 799 cm<sup>-1</sup> are characteristic of the CH<sub>2</sub> groups of the propyl chain of the silylating agent in all samples. The vibrations of Si–O–Si can be seen at 1058 cm<sup>-1</sup> (asymmetric stretching), 799 cm<sup>-1</sup> (symmetric stretching), 452 cm<sup>-1</sup> (bending) and 957 cm<sup>-1</sup> (for Si–O<sup>-</sup> stretching) which are characteristic of the silica support. SiO<sub>2</sub>-Pr (L) shows three weak vibration bands at 3273, 3145 and 1570 cm<sup>-1</sup> which are not present in SiO<sub>2</sub>-Pr-Boc and SiO<sub>2</sub>-Pr-Boc,Me. The band at 3273 cm<sup>-1</sup> is assigned to N–H stretching. The band at 3145 is assigned to the hydrogen-bonded N–H stretching mode and the vibration band at 1570 cm<sup>-1</sup> is assigned to the COO<sup>-</sup> group. These three vibration bands

suggest the presence of the key functional groups in proline and confirm the presence of free amine and carboxylic moiety that are vital for the catalytic activity of this material. The C=O stretching vibration of the Boc group can be observed at  $1701\text{ cm}^{-1}$  for SiO<sub>2</sub>-Pr-Boc and SiO<sub>2</sub>-Pr-Boc,Me. It is noticeable that the intensities of the bands near  $3000\text{ cm}^{-1}$ , which are due to C–H stretching of alkyl chain, increase with increasing of concentration of tethered groups.

### 5.8. Catalytic activity

The reaction of 4-nitrobenzaldehyde (A) with acetone to give 4-hydroxy-4-(p-nitrophenyl)butan-2-one (product B) was tested. Following the preliminary work on the kinetic analysis described in the previous chapters, it was decided to perform the kinetic analysis under pseudo-first-order conditions by using one of the reagents in large excess. The large excess of acetone also ensures that the formation of the activated enamine was favoured. Figure 5.12 shows a typical kinetic experiment performed to determine the initial rate of aldol reaction catalyzed by different catalysts.

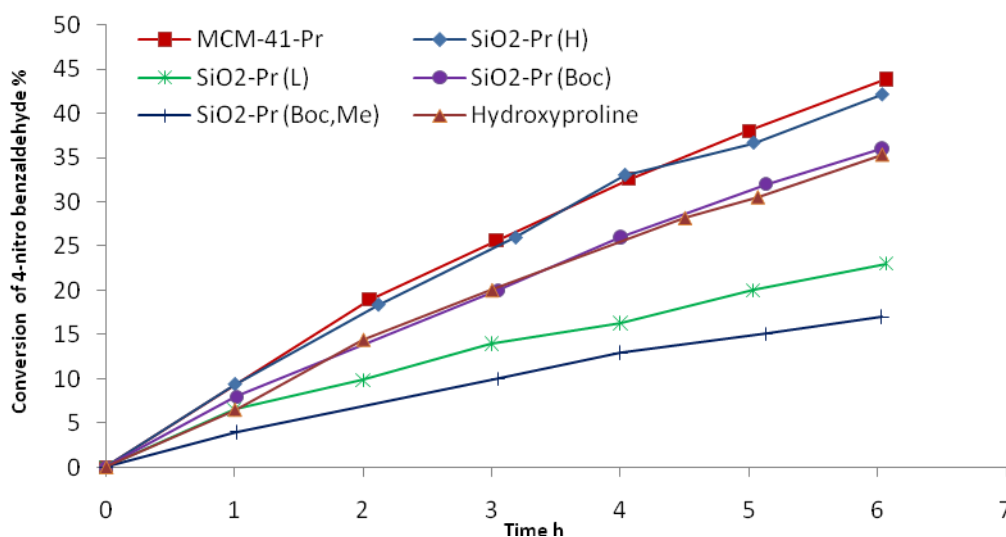


**Figure 5.12**– Comparison of aldol reaction progress of the studied catalysts over time.

Figure 5.12 shows the reaction progress curves for different catalysts, which can be used as an indicator of the activity of the catalyst. The rate of the reaction ( $k$ ) can be estimated by applying the pseudo-first-order kinetic model  $[A = A_0 e^{-kt}]$  as shown in Figure 5.13.

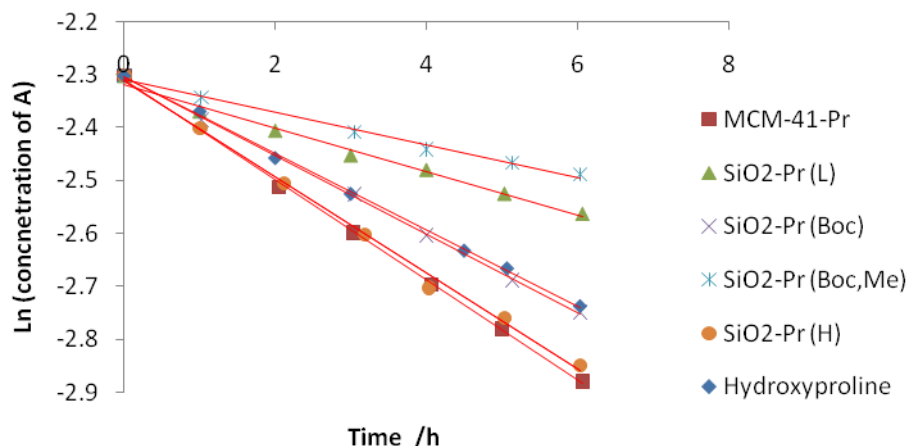


**Figure 5.13** – First-order kinetic model of aldol reaction for the studied catalysts.

From data shown in Figure 5.13, it appears clear that the linear fittings are good for all catalysts in our reaction conditions. These data were then analyzed using the linear regression and the results are used to estimate the rate of the reaction. The results are summarized in Table 5.5.

**Table 5.5** – Pseudo-first-order rate constant the studied catalysts at pseudo-first-order condition aldol condensation reaction.

Catalyst	Active sites concentrations <sup>a</sup> /mmol	1 <sup>st</sup> order rate constant (k) <sup>b</sup> /h <sup>-1</sup>	1 <sup>st</sup> order rate constant/number of active sites /mmol <sup>-1</sup> h <sup>-1</sup>
3 MCM-41-Pr	0.036	0.095	2.6
4 SiO <sub>2</sub> -Pr (H)	0.065	0.091	1.4
5 SiO <sub>2</sub> -Pr (L)	0.022	0.041	1.9
6 SiO <sub>2</sub> -Pr (Boc)	0.021	0.074	3.5
7 SiO <sub>2</sub> -Pr (Boc,Me)	0.009	0.031	3.5
8 Hydroxyproline <sup>c</sup>	0.190	0.072	0.4

a. Calculated from elemental analysis data and the amount of catalyst used in the reaction

b. k – confident limit is  $\pm 0.02 \text{ h}^{-1}$

c. 0.025 g catalyst

Reaction condition: 4-nitrobenzaldehyde (76 mg, 1 mmol), acetone (10 mL), 0.1 mL benzyl alcohol as internal standard, catalyst (0.05 g), 50 °C for 6 h reaction time.

The data show differences between the reaction rate of the free proline catalyst used as a homogeneous catalyst in solution in comparison with the immobilized catalysts, although the proline concentration in homogeneous solution was three to nine times higher than the proline concentration immobilized into silica supports for all catalysts in the reaction. Summary data for the activities of the catalysts with enantiomeric excess results are shown in Table 5.6.

**Table 5.6** – Catalytic activities in the Aldol condensation between 4-nitrobenzaldehyde and acetone.

	Catalyst	Conversion of A%	Yield of B%	ee%	1st order rate constant/number of active sites /mmol <sup>-1</sup> h <sup>-1</sup>
1	MCM-41	Trace	Trace	Trace	-
2	MCM-41-Cl	Trace	Trace	Trace	-
3	MCM-41-Pr	44	41	27	2.6
4	SiO <sub>2</sub> -Pr (H)	42	40	63	1.4
5	SiO <sub>2</sub> -Pr (L)	23	22	51	1.9
6	SiO <sub>2</sub> -Pr (Boc)deprotected	35	34	37	3.5
7	SiO <sub>2</sub> -Pr (Boc,Me)deprotected	17	12	2	3.5
8	Hydroxyproline <sup>a</sup>	35	35	37	0.40
9	Hydroxyproline-Bocprotected <sup>a</sup>	Trace	Trace	Trace	-
10	SiO <sub>2</sub> -Pr (H) <sup>c3</sup>	41	38	65	-

Reaction condition: 4-nitrobenzaldehyde (76 mg, 1 mmol), acetone (10 mL), 0.1 mL benzyl alcohol as internal standard, catalyst (0.05 g), 50 °C for 6 h reaction time.

a. 0.025 g catalyst, c3. re-used three times: activity on fourth cycle.

Data are shown for the support materials with no functionalization, the supported proline catalysts prepared with and without the protecting groups in place for functionalization (both by Boc and by esterification), by hydroxyproline in homogeneous solution at concentration three times higher than the concentration of SiO<sub>2</sub>-Pr (H) in the reaction (with and without Boc protection) and for one of the functionalized catalysts (SiO<sub>2</sub>-Pr (H)) after three re-use cycles.

Firstly, neither MCM-41 nor MCM-41-Cl with no supported proline shows catalytic activity. MCM-41-Pr, SiO<sub>2</sub>-Pr (H) and SiO<sub>2</sub>-Pr (L) catalyze this transformation

effectively (Entries 3, 4 and 5). In all three cases, the catalyst results in an enantiomeric excess in the product. There is variability however, with the MCM-41 functionalized catalyst seeming to show significantly lower enantiomeric selectivity than the functionalized silica gel catalysts.

The highest overall activities are exhibited by MCM-41-Pr, suggesting that, all things being equal, the surface area of the support is a vital factor in controlling activity. SiO<sub>2</sub>-Pr (H) gives the highest enantioselectivity, twice that of the homogeneous hydroxy-L-proline (entry 8).

It is difficult to draw conclusions about the differences in enantioselectivity exhibited by SiO<sub>2</sub>-Pr (H), SiO<sub>2</sub>-Pr (L) and MCM-41-Pr but it is possible that a controlling factor is the size of the pores on the supported catalyst, and it could be constraints imposed by the pores that result in the solid supported proline catalysts exhibiting higher enantioselectivities than homogeneous proline. The enantioselectivity of proline is believed to arise from the positioning of the aldehyde by the COOH group via H-bonding. In these materials, we suggest that the acidic silanol groups present on the surface of the pores might interfere, competing with the carboxylic acid groups for the localisation of the aldehyde. Therefore, in large pores this competition is less than in small pores. A simplified representation of the possible competition between the silanol and COOH groups is shown in Figure 5.14.

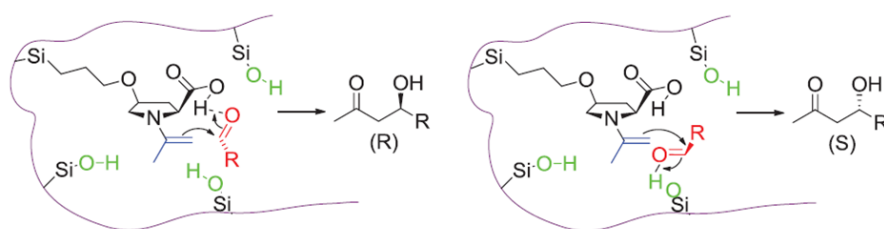


**Figure 5.14** – Simplified representation of the competition between the silanol and COOH groups.<sup>[74]</sup>

The other catalysts prepared by the protection routes (entries 6 and 7) show good activity in line with other reports.<sup>[52-53]</sup> Preparing the supported proline via protected amine only (with Boc) is more successful in terms of enantioactivity than preparing with both amine and acid group protected, The fact that the low enantioactivity associated with the proline

that has had protection at both sites is possible suggests that the ester group used to protect the carboxylic acid may be difficult to remove.

To evaluate our catalyst system against the parent homogeneous catalyst, L-hydroxyproline was used as catalyst (entry 8). This gave 35% conversion with only 37% ee%. As mentioned above, two things are possible: 1) in the case of the supported proline, interaction with the silica surface enhances activity relative to the homogeneous catalyst; and 2) performing the reaction in the pores of the silica, provided they are of the appropriate diameter, contributes to the enantioselectivity of the catalysts.

The protected homogeneous catalyst N-Boc-trans-4-hydroxy-L-proline (hydroxyproline-Boc<sub>protected</sub>) (entry 9) shows no significant activity, confirming that the secondary amine is the key catalyst in this aldol reaction. This observation is consistent with reported work.<sup>[21-22]</sup> According to the commonly accepted mechanism, the reaction begins with the condensation of acetone with the amine fragment of L-proline to form an enamine.

The last entry in Table 5.6 shows that SiO<sub>2</sub>-Pr (H) is readily recycled and loses negligible activity and negligible enantioselectivity over four reaction cycles. Leaching tests were performed in which the same catalyst was stirred in acetone at 50 °C for 12 h and then filtered; the filtrate was then used in the reaction. The activity of both the treated solid catalyst and the supernatant acetone solution showed that SiO<sub>2</sub>-Pr (H) was entirely stable under these conditions.

The important conclusion from these results is that it is possible to prepare a supported chiral proline catalyst without having to protect the amine and carboxylic acid groups through the tethering process. The catalytic evidence suggests that the hydroxyproline reacts with the chloropropyl tether via the hydroxy group, thus leaving the secondary amine and the carboxylic acid free. This is not an obvious reaction route. An explanation for it may be that the mildly acidic silanol groups on the silica surface protonate the amine, effectively protecting it during reaction. And HCl would be released on reaction with chloropropyl groups. It is worth noting that the pK<sub>a</sub> of silanol groups can vary significantly, depending on the nature of the surface (to as low as 3 in some cases).<sup>[75]</sup> In addition, the protonated amino group would also serve as protection against any

racemization at the  $\alpha$ -carbon atom, a major concern in amino acid chemistry.<sup>[76]</sup>

Supported proline is clearly more active towards aldol condensation than in homogeneous solution. It may be the case that the catalytic amine group is activated by hydrogen-bonding to adjacent surface silanol groups, or that these same silanol groups play a role in activating the reactant ketone or aldehyde, or the intermediate enamine. The silanol groups may simply act to concentrate the reactants by surface adsorption.

### 5.8.1. Supported-proline catalytic activity in polar aprotic solvent

Proline-catalyzed aldol reactions are usually carried out in organic solvents such as dimethyl sulfoxide (DMSO), dimethylformamide (DMF) or chloroform. DMSO has been identified as the solvent of choice in many cases.<sup>[45, 51]</sup> In the work reported above, the reactant acetone was also the solvent. We also carried out catalytic experiments in DMSO/acetone (volume ratio 4/1) mixtures at room temperature. Yields and enantiomeric excesses are given in Table 5.7. Both yields and enantioselectivities are very much higher in this solvent than in acetone alone. The trends amongst the three catalysts studied are the same as those observed in acetone. This is consistent with DFT calculations which have shown that the energy barrier to complexation between acetone and proline is 171.4 kJ mol<sup>-1</sup> in acetone solvent but is reduced to 40.7 kJ mol<sup>-1</sup> in the presence of excess DMSO.<sup>[77]</sup>

**Table 5.7** – Catalytic activities in the aldol condensation between 4-nitrobenzaldehyde and acetone in DMSO at room temperature.

	Catalyst	Conversion of A%	Yield of B%	ee%
1	MCM-41-Pr	74	72	77
3	SiO <sub>2</sub> -Pr (H)	90	87	75
2	SiO <sub>2</sub> -Pr (L)	54	51	59

Reaction condition: 4-nitrobenzaldehyde (2 mmol), acetone (2 mL), DMSO (8 mL), catalyst (0.05 g) at RT for 20 h.

### 5.8.2. Supported-proline catalytic activity with various aromatic aldehydes

To examine the generality of the reaction, a variety of aromatic aldehydes were used in the reaction. As shown in Table 5.8, aromatic aldehydes bearing electron-withdrawing

groups, such as chloro- and nitro-groups, undergo aldol condensation smoothly with acetone in the presence of MCM-41-Pr in DMSO/acetone (volume ratio 4/1). The reactions generated the corresponding aldols in good yields (59–74%) and enantioselectivities (73–77% ee).

**Table 5.8** – Catalytic activities in the aldol condensation between acetone and a range of aldehydes.

	Catalyst	Conversion of A%	Yield of B%	ee%
1	4-nitrobenzaldehyde	74	72	77
2	4-isopropylbenzaldehyde	47	43	70
4	Benzaldehyde	69	69	82
5	4-chlorobenzaldehyde	59	56	73

Reaction condition: 4-nitrobenzaldehyde (2 mol), acetone (2 mL), DMSO (8 mL), catalyst (0.05 g) at RT for 20 h.

## 5.9. Conclusion

L-proline-functionalized mesoporous silica has been successfully synthesized by a relatively simple route, and the effect of protecting the amine and the carboxylic acid groups through the synthesis on the ultimate activity and enantiomeric selectivity of the catalyst has been investigated. The results clearly show that the most active and selective catalysts are prepared without protecting the two functional groups on the proline. This new route could be an economical and green step towards chiral catalysts in general and solid-supported proline catalysts in particular. Furthermore, there seems to be a relationship between the nature of the silica support and the ultimate activity and enantioselectivity of the supported proline. It seems that a high surface area for the support is beneficial and it is possible that pore size is also important in terms of imparting enantioselectivity to the catalyst. So far, it seems that two supports with pores in the 4-5 nm diameter range provide better selectivity than supports with pores of 11 nm diameter. Current research is directed at ordered mesoporous silica supports with a range of pore sizes.

## 5.10. References

- [1] R. Zawirska-Wojtasiak, *Food Chemistry* **2004**, *86*, 113-118.
- [2] G. Flores, G. P. Blanch, M. L. Ruiz del Castillo, *Food Chemistry* **2013**, *141*, 2982-2987.
- [3] E. Brenna, C. Fuganti, S. Serra, *Tetrahedron: Asymmetry* **2003**, *14*, 1-42.
- [4] M. Kauranen, T. Verbiest, J. J. Maki, A. Persoons, *Synthetic Metals* **1996**, *81*, 117-120.
- [5] J. Lu, L. Wu, L. Jing, X. Xu, X. Zhang, *Dyes and Pigments* **2012**, *94*, 169-174.
- [6] M. Sylla, M. Giffard, V. Boucher, B. Illien, N. Mercier, X. Nguyen Phu, *Synthetic Metals* **1999**, *102*, 1548-1549.
- [7] R. Celis, B. Gámiz, M. A. Adelino, M. C. Hermosín, J. Cornejo, *Science of The Total Environment* **2013**, *444*, 288-297.
- [8] H. Zhang, M. Spiteller, K. Guenther, G. Boehmler, S. Zuehlke, *Environmental Pollution* **2009**, *157*, 1904-1910.
- [9] R. N. Patel, *Coordination Chemistry Reviews* **2008**, *252*, 659-701.
- [10] N. P. Ramesh, in *Biocatalysis in the Pharmaceutical and Biotechnology Industries*, CRC Press, **2006**.
- [11] G.-Fern n. Vicente, G. Vicente, R. Francisca, in *Biocatalysis in the Pharmaceutical and Biotechnology Industries*, CRC Press, **2006**.
- [12] R. Noyori, *Angewandte Chemie International Edition* **2002**, *41*, 2008-2022.
- [13] K. Schulz, L. Ratjen, J. Martens, *Tetrahedron* **2011**, *67*, 546-553.
- [14] P. G. Bulger, in *Comprehensive Chirality* (Eds.: E. M. Carreira, H. Yamamoto), Elsevier, Amsterdam, **2012**, pp. 228-252.
- [15] H. Pellissier, *Tetrahedron* **2007**, *63*, 9267-9331.
- [16] S. Mukherjee, J. W. Yang, S. Hoffmann, B. List, *Chemical Reviews* **2007**, *107*, 5471-5569.
- [17] E. Marques-Lopez, R. P. Herrera, M. Christmann, *Natural Product Reports* **2010**, *27*, 1138-1167.
- [18] S. Bertelsen, K. A. Jorgensen, *Chemical Society Reviews* **2009**, *38*, 2178-2189.
- [19] B. R. Buckley, *Annual Reports Section "B" (Organic Chemistry)* **2013**, *109*, 189-206.
- [20] M. Gruttadauria, F. Giacalone, P. Lo Meo, A. Mossuto Marculescu, S. Riela, R. Noto, *European Journal of Organic Chemistry* **2008**, *2008*, 1589-1596.
- [21] N. Zotova, L. J. Broadbelt, A. Armstrong, D. G. Blackmond, *Bioorganic & Medicinal Chemistry Letters* **2009**, *19*, 3934-3937.
- [22] B. List, R. A. Lerner, C. F. Barbas, *Journal of the American Chemical Society* **2000**, *122*, 2395-2396.
- [23] S. Bahmanyar, K. N. Houk, *Journal of the American Chemical Society* **2001**, *123*, 11273-11283.
- [24] B. List, L. Hoang, H. J. Martin, *Proceedings of the National Academy of Sciences of the United States of America* **2004**, *101*, 5839-5842.
- [25] U. Eder, G. Sauer, R. Wiechert, *Angewandte Chemie International Edition in English* **1971**, *10*, 496-497.
- [26] Z. G. Hajos, D. R. Parrish, *The Journal of Organic Chemistry* **1974**, *39*, 1615-1621.
- [27] I. K. Mangion, D. W. C. MacMillan, *Journal of the American Chemical Society* **2005**, *127*, 3696-3697.
- [28] N. S. Chowdari, J. T. Suri, C. F. Barbas, *Organic Letters* **2004**, *6*, 2507-2510.
- [29] A. Córdoba, *Accounts of Chemical Research* **2004**, *37*, 102-112.
- [30] T. Bui, C. F. Barbas Iii, *Tetrahedron Letters* **2000**, *41*, 6951-6954.
- [31] G. Sabitha, N. Fatima, E. V. Reddy, J. S. Yadav, *Advanced Synthesis & Catalysis* **2005**, *347*, 1353-1355.
- [32] A. Bøgevig, K. Juhl, N. Kumaragurubaran, W. Zhuang, K. A. Jørgensen, *Angewandte Chemie International Edition* **2002**, *41*, 1790-1793.
- [33] M. Shi, J.-K. Jiang, C.-Q. Li, *Tetrahedron Letters* **2002**, *43*, 127-130.
- [34] J. Wang, H. Li, Y. Mei, B. Lou, D. Xu, D. Xie, H. Guo, W. Wang, *The Journal of Organic Chemistry* **2005**, *70*, 5678-5687.
- [35] N. Utsumi, H. Zhang, F. Tanaka, C. F. Barbas, *Angewandte Chemie International Edition* **2007**, *46*, 1878-1880.
- [36] M. P. Brochu, S. P. Brown, D. W. C. MacMillan, *Journal of the American Chemical Society* **2004**, *126*, 4108-4109.

- [37] Y. Hayashi, J. Yamaguchi, K. Hibino, M. Shoji, *Tetrahedron Letters* **2003**, *44*, 8293-8296.
- [38] M. Gruttadauria, F. Giacalone, R. Noto, *Chemical Society Reviews* **2008**, *37*, 1666-1688.
- [39] M. E. Jung, *Tetrahedron* **1976**, *32*, 3-31.
- [40] C. Agami, C. Puchot, H. Sevestre, *Tetrahedron Letters* **1986**, *27*, 1501-1504.
- [41] D. Rajagopal, M. S. Moni, S. Subramanian, S. Swaminathan, *Tetrahedron: Asymmetry* **1999**, *10*, 1631-1634.
- [42] D. Seebach, M. Boes, R. Naef, W. B. Schweizer, *Journal of the American Chemical Society* **1983**, *105*, 5390-5398.
- [43] G. P. Rizzi, *The Journal of Organic Chemistry* **1970**, *35*, 2069-2072.
- [44] J. Mlynarski, S. Bas, *Chemical Society Reviews* **2014**.
- [45] M. Benaglia, G. Celentano, F. Cozzi, *Advanced Synthesis & Catalysis* **2001**, *343*, 171-173.
- [46] M. Benaglia, M. Cinquini, F. Cozzi, A. Puglisi, G. Celentano, *Advanced Synthesis & Catalysis* **2002**, *344*, 533-542.
- [47] E. Bellis, G. Kokotos, *Journal of Molecular Catalysis A: Chemical* **2005**, *241*, 166-174.
- [48] D. Font, A. Bastero, S. Sayalero, C. Jimeno, M. A. Pericàs, *Organic Letters* **2007**, *9*, 1943-1946.
- [49] D. Font, C. Jimeno, M. A. Pericàs, *Organic Letters* **2006**, *8*, 4653-4655.
- [50] E. Alza, X. C. Cambeiro, C. Jimeno, M. A. Pericàs, *Organic Letters* **2007**, *9*, 3717-3720.
- [51] D. Dhar, I. Beadham, S. Chandrasekaran, *J Chem Sci* **2003**, *115*, 365-372.
- [52] F. Calderón, R. Fernández, F. Sánchez, A. Fernández-Mayoralas, *Advanced Synthesis & Catalysis* **2005**, *347*, 1395-1403.
- [53] E. G. Doyagüez, F. Calderón, F. Sánchez, A. Fernández-Mayoralas, *The Journal of Organic Chemistry* **2007**, *72*, 9353-9356.
- [54] Z. An, W. Zhang, H. Shi, J. He, *Journal of Catalysis* **2006**, *241*, 319-327.
- [55] M. Benaglia, A. Puglisi, F. Cozzi, *Chemical Reviews* **2003**, *103*, 3401-3430.
- [56] M. Benaglia, *New Journal of Chemistry* **2006**, *30*, 1525-1533.
- [57] A. Corma, H. Garcia, *Advanced Synthesis & Catalysis* **2006**, *348*, 1391-1412.
- [58] F. Cozzi, *Advanced Synthesis & Catalysis* **2006**, *348*, 1367-1390.
- [59] L. Gu, Y. Wu, Y. Zhang, G. Zhao, *Journal of Molecular Catalysis A: Chemical* **2007**, *263*, 186-194.
- [60] L.-H. Hsiao, S.-Y. Chen, S.-J. Huang, S.-B. Liu, P.-H. Chen, J. C. C. Chan, S. Cheng, *Applied Catalysis A: General* **2009**, *359*, 96-107.
- [61] K. Arya, U. C. Rajesh, D. S. Rawat, *Green Chemistry* **2012**, *14*, 3344-3351.
- [62] J. Yan, L. Wang, *Chirality* **2009**, *21*, 413-420.
- [63] A. Zamboulis, N. J. Rahier, M. Gehringer, X. Cattoën, G. Niel, C. Bied, J. J. E. Moreau, M. W. C. Man, *Tetrahedron: Asymmetry* **2009**, *20*, 2880-2885.
- [64] W. He, F. Zhang, X. Shi, H. Li, *European Journal of Organic Chemistry* **2012**, *2012*, 3753-3758.
- [65] T. E. Kristensen, K. Vestli, K. A. Fredriksen, F. K. Hansen, T. Hansen, *Organic Letters* **2009**, *11*, 2968-2971.
- [66] M. Wilchek, A. Patchornik, *The Journal of Organic Chemistry* **1964**, *29*, 1629-1630.
- [67] J. Bello, J. R. Vinograd, *Journal of the American Chemical Society* **1956**, *78*, 1369-1372.
- [68] A. N. Kursunlu, E. Guler, H. Dumrul, O. Kocyigit, I. H. Gubbuk, *Applied Surface Science* **2009**, *255*, 8798-8803.
- [69] S. E. Blondelle, R. A. Houghten, *International Journal of Peptide and Protein Research* **1993**, *41*, 522-527.
- [70] J. Qi, B. Qin, J. Liu, Y. Yu, Z. Zhang, W. Zhang, Q. Cai, W. Zhu, *CrystEngComm* **2011**, *13*, 4666-4675.
- [71] E. G. Garrido-Ramírez, B. K. G. Theng, M. L. Mora, *Applied Clay Science* **2010**, *47*, 182-192.
- [72] C. T. Campbell, *Surface Science* **2007**, *601*, ix.
- [73] J. Ross, *Applied Catalysis A: General* **1992**, *92*, N3-N4.
- [74] R. Breslow, *Science* **1982**, *218*, 532-537.
- [75] J. A. Gladysz, *Chemical Reviews* **2002**, *102*, 3215-3216.
- [76] M. D. Andrews, A. G. Brewster, K. M. Crapnell, A. J. Ibbett, T. Jones, M. G. Moloney, K. Prout, D. Watkin, *Journal of the Chemical Society, Perkin Transactions 1* **1998**, 223-236.
- [77] K. N. Rankin, J. W. Gauld, R. J. Boyd, *The Journal of Physical Chemistry A* **2002**, *106*, 5155-5159.

## Chapter 6

### Summary and conclusion

---

My work has demonstrated and studied several new ways of functionalizing solid silica with pairs of disparate organic functional groups. In Chapter 3, the grafting and co-condensation method were used to generate alkylamine groups or alkylsulfonic acid groups attached to silica support. Physical mixtures of base and acid silicas were studied. In Chapter 4, alkylsulfonic acid/amine and phosphotungestic acid/amine pairs were generated using different approaches. And in Chapter 5, bifunctional amino acid with chiral site was pre-formed in an organosilane precursor which grafted onto the silica surface.

In chapter 3, we have shown that aminopropylsilica catalysts exhibit different activity in nitroaldol reaction depending on the methodology followed for their preparation. In fact, catalysts prepared by sol-gel procedure (MCM-41-NH<sub>2</sub> (C)) are less active than those obtained by the grafting strategy (MCM-41-NH<sub>2</sub> (G) and SiO<sub>2</sub>-NH<sub>2</sub>); this is ascribable to the fact that, in the grafting method, the aminopropyl groups are directly linked to the silica and the majority of them are thus easily reachable by the reagents and take part in the reaction. Amines and surface silanols were found to be necessary for good catalytic activity where silanols activate reacting groups through hydrogen bonding interactions.

Heterogeneous silica catalysts functionalized with sulfonic acid groups were prepared by grafting alkylthiol groups into the silica support before oxidizing them to sulfonic acid groups. The oxidation method used to transform the -SH groups to -SO<sub>3</sub>H is a determinant of the number of acid sites in the final catalysts. The adsorption calorimetric studies and catalytic activity reported in this work demonstrate that, in this case, the use of concentrated HNO<sub>3</sub> optimizes the oxidation process.

Isolated catalytically active centres could be created based on silica materials for realization of a variety of acid-base tandem reactions. This protocol has several advantages: (I) the ease of preparing the solid catalysts; (II) high catalytic activities; (III) wide applicability to several acid or base reactions; (IV) simple workup procedure; (V) reusability; and (VI) regulation of the reaction pathway by manipulating the reaction conditions, including control of the concentration of active sites (catalysts) that are

present. The combination of gravimetrically recoverable acid and base catalysts allowed a successful application of opposing catalysts to multistep, one-pot catalytic reactions including the ability to steer the direction of the reaction at each step, all with recovery of catalysts after use. The successful use of the recovered catalysts in combination with other catalysts in subsequent, unrelated reactions showed the versatility of this approach. A library of gravimetrically recoverable catalysts could thus be generated and used in a variety of one-pot multistep catalytic reactions, and this methodology may be further expanded almost without limit through other means of catalyst separation, such as membrane encapsulation.

In chapter 4, a new type of efficient acid-base bifunctional catalyst was synthesized by simply grafting 3-mercaptopropyltriethoxysilane (MPTMS) and 3-aminopropyltriethoxysilane (APTMS) onto a silica gel ( $\text{SiO}_2$ ) surface, followed by nitric acid treatment to convert SH groups to  $\text{SO}_3\text{H}$ . These materials were used as bifunctional acid/base catalysts in tandem with deacetalization-Henry reaction where they showed higher activity compared to the physical mixture. These materials were also tested in aldol condensation reaction, which is known to be catalyzed by acidic and basic groups at the same time. Bifunctional acid/base catalysts prepared in this thesis showed an overall acceleration of the reaction rate higher than using acid or base or a physical mixture of acid and base solid catalysts. This sort of cooperative catalysis cannot be achieved if liquid catalysts are used; therefore, it is an extremely important route by which solid catalysts might be developed to offer equivalent catalytic activities to the polluting liquid acid/base catalysts.

Comparison with silica-supported  $\text{NH}_2/\text{NH}_3^+[\text{H}_2\text{PW}_{12}\text{O}_{40}]^-$  catalysts synthesized by the partial neutralization method shows that bifunctional catalysts with  $\text{SO}_3\text{H}/\text{NH}_2$  groups are more active as acid and base catalysts. The results show the importance of having comparable acid and base site concentrations on the catalyst, at least for the tandem reaction used here.

Bifunctional acid/base silica-supported  $\text{NH}_2/\text{NH}_3^+[\text{H}_2\text{PW}_{12}\text{O}_{40}]^-$  catalysts prepared with relatively low levels of phosphotungstic acid seem prone to poisoning. The reasons for this need further investigation.

In Chapter 5, L-proline-functionalized silica has been successfully synthesized by a relatively simple route, and the effect of protecting the amine and the carboxylic acid groups through the synthesis on the ultimate activity and enantiomeric selectivity of the catalyst has been investigated. The results clearly show that the active and selective catalysts can be prepared without protecting the two functional groups on the proline. This new route could be an economical and green step towards chiral catalysts in general and solid-supported proline catalysts in particular.

In general, I have shown that antagonist organic functional groups, which are mutually incompatible in solution at least, can cohabit on the surface of silica support without mutual neutralization. The type of functional groups on the surface of a bifunctional heterogeneous catalyst plays a role in the catalytic activity of the material. The degree to which the catalytic activity depends on the group-to-group distance depends on the concentration of functional groups and the reaction being catalyzed.

## Chapter 7

### Future consideration

---

The work I have described in the preceding chapters is only one step in the design of cooperative heterogeneous catalysts. The synthetic methodologies developed are versatile and should allow for the synthesis of other paired bifunctional catalysts.

New and better synthetic heterogeneous catalysts will surely emerge in the future which extend the idea of polyfunctional cooperativity to other classes of reactions beyond those that are currently known to benefit from cooperative catalysis. Identifying the appropriate functional groups and optimum concentration and organizing them on the surface are key steps in designing good cooperative materials. There are still many obstacles to be overcome before synthetic materials can approach the catalytic prowess of enzymes.

In order to rival enzymatic catalysts, two aspects of enzymes must be copied: the number of cooperating functional groups should be increased beyond two, and chirality must be introduced to these polyfunctional catalysts. Although this may seem a daunting challenge, the promise of novel catalytic activity is immense.

The introduction of chirality into polyfunctional cooperative catalysts is already underway. The entire field of asymmetric proline catalysis relies on amine/carboxylic acid cooperativity to drive enantioselectivity. Heterogeneous acid/base catalysis using a proline-derived moiety immobilized on silica was recently demonstrated. The body of literature on transcribing chirality from molecular precursors to hybrid silicas also continues to increase. Ultimately, combining asymmetric heterogeneous catalysis with principles of cooperativity should lead to improved catalytic materials using currently available technology. The importance of such a type of catalysts is that, if the reaction products exhibit the same sort of chiral symmetry, it should allow us to make one of the isomers selectively. This is vitally important in drug manufacture, for instance where only one of the related isomers is usually active and selective synthesis of one over the other isomer is required. These types of catalysts could therefore be very important in the synthesis of bioactive compounds, drugs, agrochemicals etc.

## Appendixes

---

## 1- Gas Chromatography Clarus 500 Perkin Elmer

This work utilized gas chromatography technique to monitor sample (reactant and product) for nitoaldol (Henry) reaction and tandem deacetalization-Henry reaction. The GC used for this purpose was Perkin Elmer Clarus 500 with 50 m capillary column (BP1 column), equipped with FID detector.

### a) GC operation conditions

Unit	Operating Conditions
Column	BP1 50 m
Detector	Flame Ionisation Detector (FID) at 250 °C
Oven Temperature	Initial Temp. 60 °C, hold 0 min Ramp 1 10°/ min to 160°, hold for 0 min Ramp 2 20°/ min to 290°, hold for 2 min
Carrier Gas	Helium at 2 ml min <sup>-1</sup> Air at 450 ml min <sup>-1</sup> H2 at 45 ml min <sup>-1</sup>
Injector	On Colum injector
Injection temperature	250 °C
Injection volume	0.5 µml
Channel Run Time	18.5 min



**Gas Chromatography Clarus 500 Perkin Elmer**

## Appendix

b) Characterization of reaction products in test reaction: tandem deacetalisation-henry reaction.

Reactant conversions were determined from peak areas relative to that of internal standard, using calibration plots with standard solutions of o-xylene, nitrostyrene, benzaldehyde and benzaldehyde dimethyl acetal.

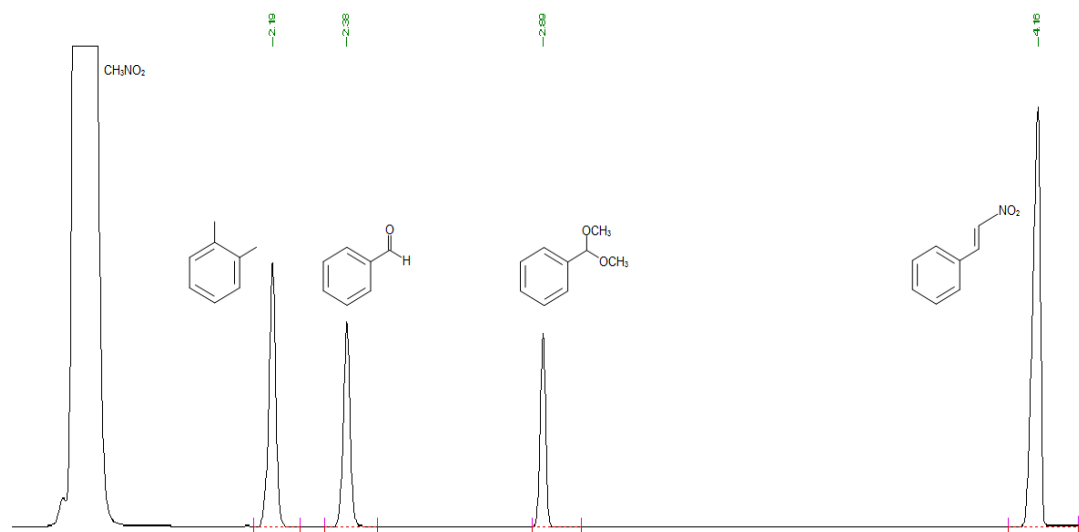


Figure X1. GC chromatograms of tandem deacetalization-henry reaction

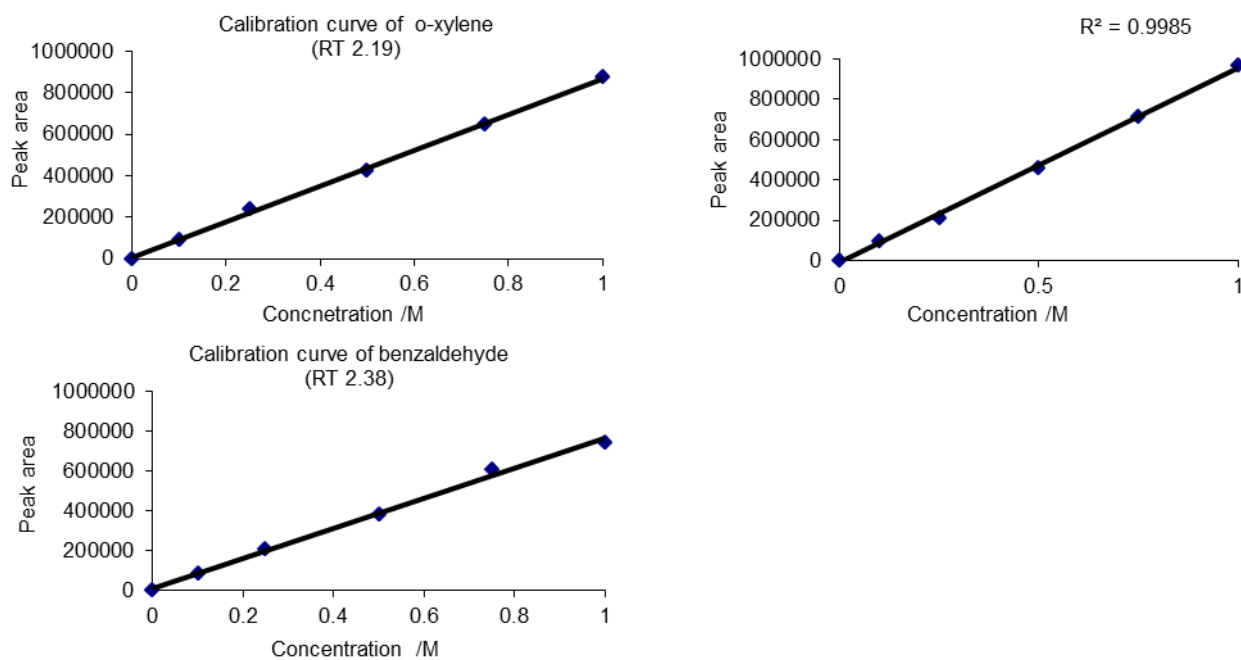


Figure X2. Calibration curves of the reactants in tandem deacetalization-henry reaction and o-xylene as internal standard

## Appendixes

C) The identity of nitrostyrene as product was confirmed using GCMS for the peak in Figure X1. at RI 4.10 min.

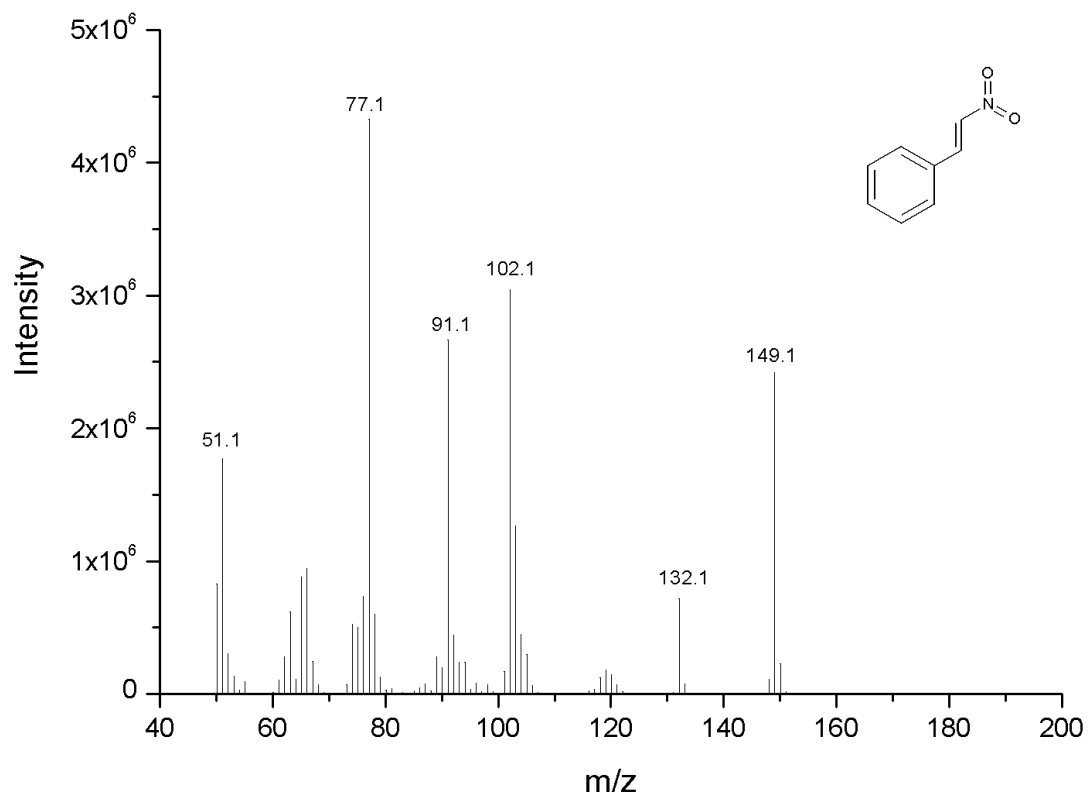
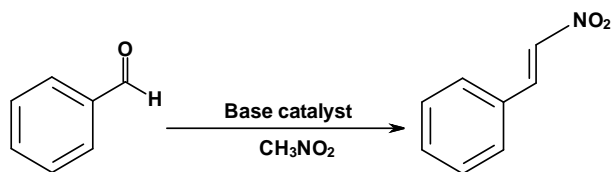


Figure X3. Mass spectrum taken from GC peak at RI 4.10 in Fig 1S, verifying origin as nitrostyrene.

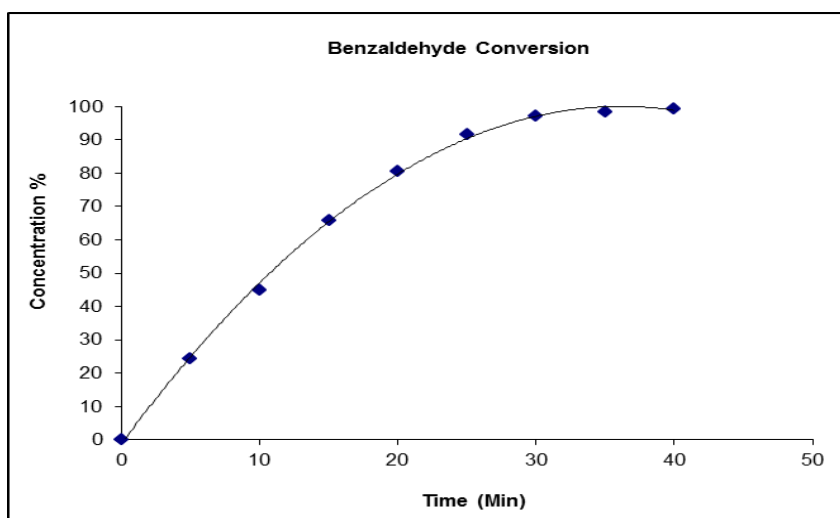
## Appendixes

d) Monitoring the conversion using GC-FID for Henry reaction.

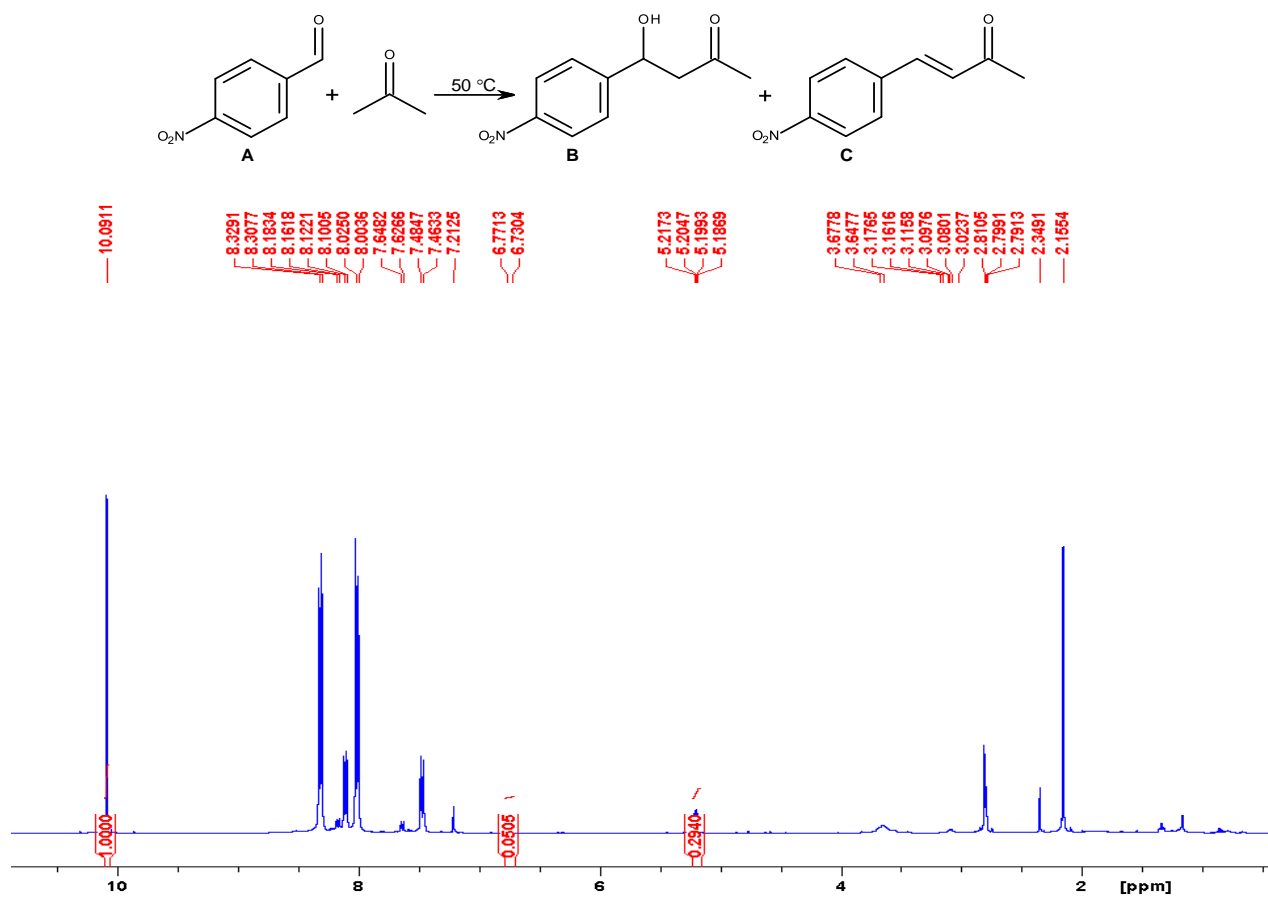


Min	SiO <sub>2</sub> -NH <sub>2</sub> (52.10 mg)	Peak area	Conc. M
0	Benzaldehyde	124913	0.124
	O-xylene	16303	
5	Benzaldehyde	96868	0.094
	O-xylene	16712	
10	Benzaldehyde	53215	0.068
	O-xylene	12624	
15	Benzaldehyde	44295	0.042
	O-xylene	16923	
20	Benzaldehyde	24682	0.024
	O-xylene	16586	
25	Benzaldehyde	10543	0.010
	O-xylene	16619	
30	Benzaldehyde	3040	0.003
	O-xylene	14091	
35	Benzaldehyde	1835	0.002
	O-xylene	16559	
40	Benzaldehyde	1035	0.001
	O-xylene	17585	

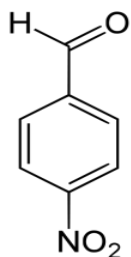
Time min	Conc. M	Conv. %
0	0.124	0
5	0.094	24
10	0.068	45
15	0.042	66
20	0.024	81
25	0.010	92
30	0.003	97
35	0.002	99
40	0.001	99



## 2- NMR spectra for aldol reaction catalyzed by silica supported proline.

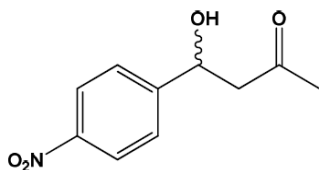


### 4-Nitrobenzaldehyde



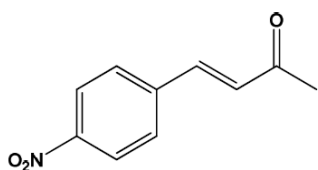
<sup>1</sup>H-NMR (400 MHz, CDCl<sub>3</sub>)= 8.01 (2H, d, J=8.56, Ar-H<sub>-ortho</sub>), 8.32 (2H, d, J=8.56 Ar-H<sub>-meta</sub>), 10.09 (1H, s).

**4-hydroxy-4-(p-nitrophenyl)butan-2-one (A)**



$^1\text{H-NMR}$  (400 MHz,  $\text{CDCl}_3$ )= 8.11 (2H, d,  $J=8.64$ , Ar-H-ortho), 7.47 (2H, d,  $J=8.56$ , Ar-H-meta), 5.20 (1H, q,  $J=4.05$ , -CH-), 3.66 (1H, d,  $J=12.04$ , -OH), 2.80 (2H, d,  $J=3.12$ , -CH<sub>2</sub>-), 2.16 (3H, s, -CH<sub>3</sub>).

**(E)-4-(4-nitrophenyl)but-3-en-2-one (B)**



$^1\text{H-NMR}$  (400 MHz,  $\text{CDCl}_3$ )= 8.17 (2H, d,  $J=8.64$ , Ar-H-ortho), 7.64 (2H, d,  $J=8.64$ , Ar-H-meta), 7.47 (1H, d,  $J=8.56$ , C(4)H-), 6.75 (1H, d,  $J=16.37$ , C(3)H-), 2.35 (3H, s, CH<sub>3</sub>).

### 3- Reproducibility of the results.

It is important to note that throughout this thesis in certain sections, the results shown are summarily formatted to demonstrate the best results obtained based on triplicate reading. Also some experiments were repeated three or two times to ensure reproducibility of the results. Below for reference is a comparison between two MCM-41 supports prepared by same conditions in different dates.

#### MCM-41 (Two patches A1 and A2)

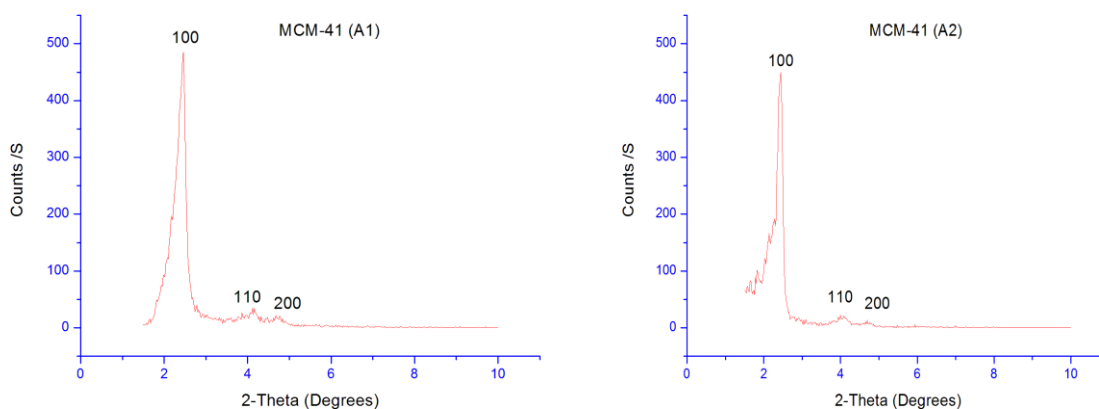
##### Synthesis of the catalysts:

62 ml NH<sub>4</sub>OH (35% solution (d=0.88)) was mixed with 231 g of distilled water. The mixture was heated to 80 °C under vigorous stirring then 1.0 g cetyltrimethylammonium bromide (CTAB) was added to the mixture and the mixture was stirred for 30 min at 80 °C. 5 ml of TEOS was added into the above mixture drop wise. The mixture was stirred (400 rpm) for 2 h at 80 °C. The solution was filtered and the precipitate was washed with distilled water and ethanol. The precipitate was left to dry in the oven at 80 °C for 18 hour and followed by calcination in air at 540 °C for 6 h.

The ratio was as follow:

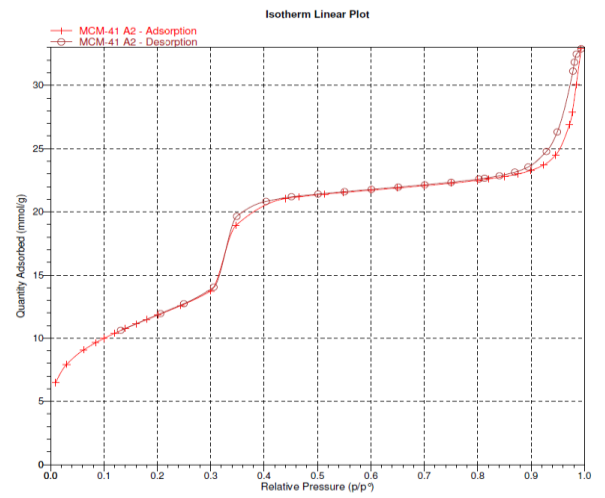
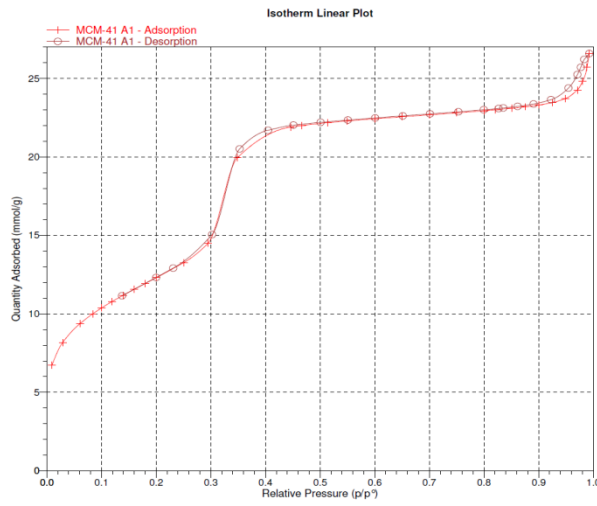
535 (H<sub>2</sub>O) : 65 (NH<sub>4</sub>OH) : 0.1(CTAB) : 1(TEOS)

##### Powder X-ray diffraction



# Appendixes

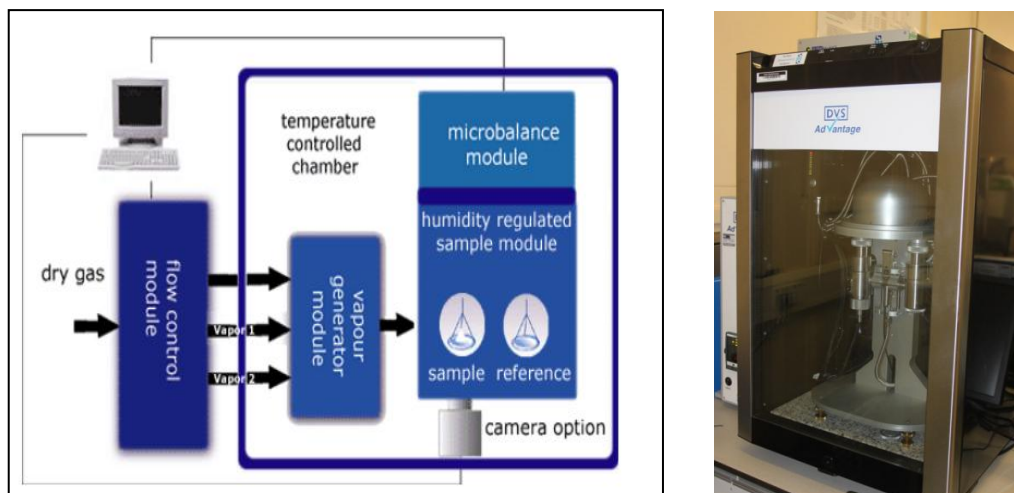
## Surface area and pore size determination



	MCM-41 (A1)	MCM-41 (A2)
BET Surface Area:	1002.2 m <sup>2</sup> /g	991.4 m <sup>2</sup> /g
Average Pore Volume:	0.84 cm <sup>3</sup> /g	0.89 cm <sup>3</sup> /g
Average Pore Size:	3.36 nm	3.58 nm

#### 4- Dynamic Vapor Sorption

Moisture sorption and desorption isotherms were generated at 25 C using Dynamic Vapour Sorption (Surface Measurement Systems Ltd. a schematic of which is shown in Fig. 11).



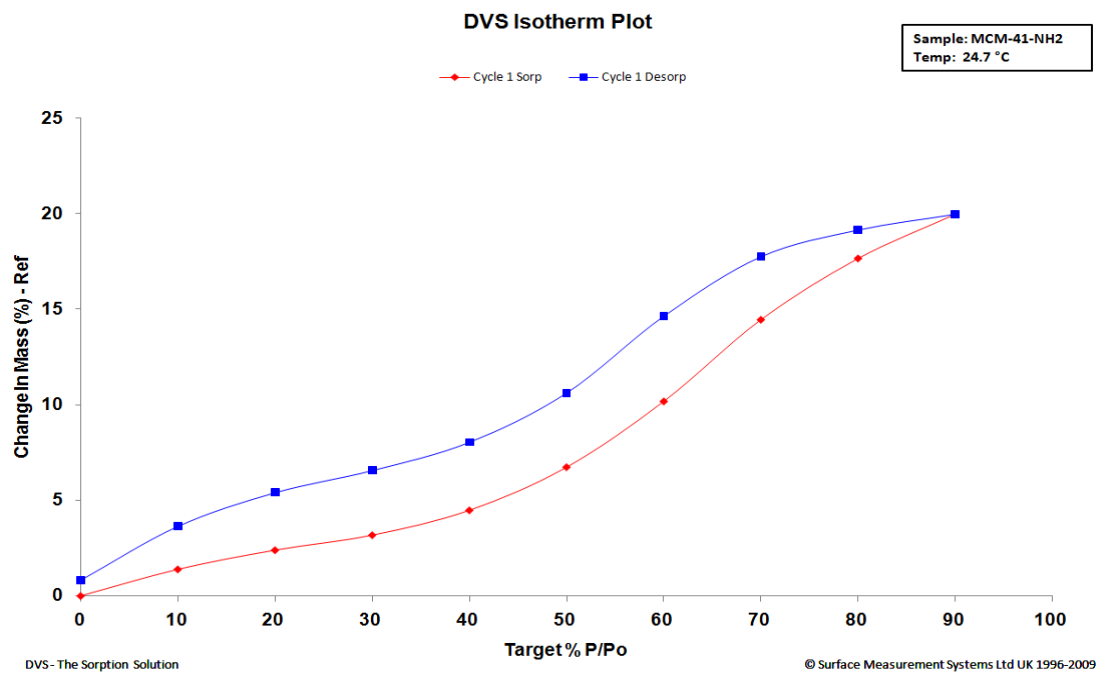
Schematic Diagram of Dynamic Vapour Sorption Instrument

The DVS is equipped with an electronic microbalance for the accurate measurement of weight. The procedure involved 10% steps of relative humidity (RH) between 0–95% RH following an initial drying at 200 °C. Equilibrium was assumed to be established when  $dm/dt$  is equal to 0.02%; The symbol “ $dm/dt$ ” means the criteria of sample weight change ratio (m: mass and t: time). The experimentally measured moisture sorption–desorption data and isotherms for MCM-41-NH<sub>2</sub>

Moisture sorption–desorption data of MCM-41-NH<sub>2</sub>

Target % P/Po	Change In Mass (%)		
	Sorption	Desorption	Hysteresis
0.0	0.00	0.83	
10.0	1.39	3.65	2.25
20.0	2.39	5.40	3.01
30.0	3.18	6.56	3.38
40.0	4.48	8.04	3.56
50.0	6.74	10.62	3.88
60.0	10.18	14.63	4.46
70.0	14.45	17.75	3.30
80.0	17.66	19.14	1.49
90.0	19.97	19.97	

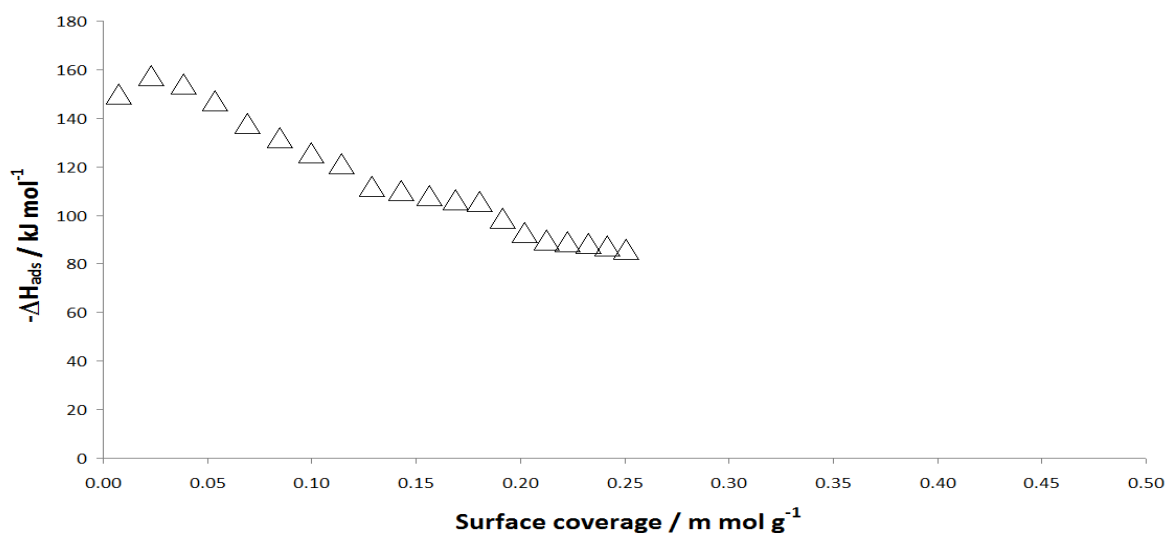
# Appendixes



Moisture sorption–desorption isotherm of MCM-41-NH<sub>2</sub>

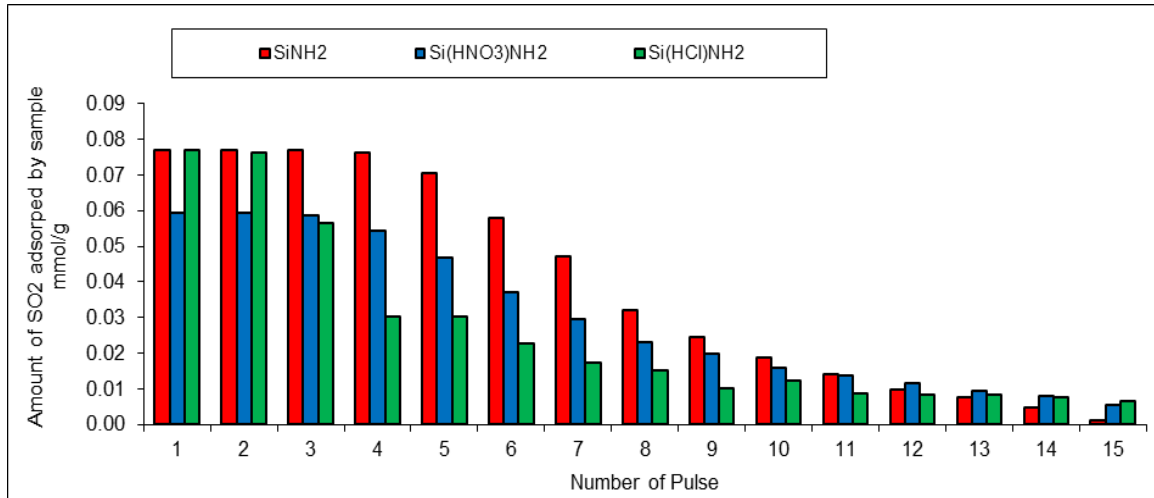
## 5- Calculations for flow adsorption calorimetry measurements

Pulse no	Breakthrough pulse area (MS)	Calibration mean pulse area (MS)	Percentage of pulse adsorbed	Amount of gas adsorbed / mol	Sample adsorption / mol g <sup>-1</sup>	Cumulative adsorption / mol g <sup>-1</sup>	Cumulative adsorption (half pulse width) / m mol g <sup>-1</sup>	- dH / J (DSC)	- dH / kJ mol <sup>-1</sup> adsorbed
1	5.68E-11	6.24E-08	99.91	4.16E-07	1.54E-05	1.54E-05	0.008	0.0623	149.9
2	5.68E-11		99.91	4.16E-07	1.54E-05	3.08E-05	0.023	0.0654	157.4
3	7.49E-11		99.88	4.15E-07	1.54E-05	4.62E-05	0.038	0.064	154.1
4	8.49E-11		99.86	4.15E-07	1.54E-05	6.16E-05	0.054	0.0611	147.1
5	1.89E-10		99.70	4.15E-07	1.54E-05	7.69E-05	0.069	0.0572	137.9
6	4.47E-10		99.28	4.13E-07	1.53E-05	9.22E-05	0.085	0.0545	132.0
7	1.49E-09		97.61	4.06E-07	1.50E-05	1.07E-04	0.100	0.0511	125.9
8	3.61E-09		94.21	3.92E-07	1.45E-05	1.22E-04	0.115	0.0475	121.2
9	3.79E-09		93.93	3.91E-07	1.45E-05	1.36E-04	0.129	0.0438	112.1
10	6.92E-09		88.90	3.70E-07	1.37E-05	1.50E-04	0.143	0.0408	110.3
11	1.03E-08		83.49	3.47E-07	1.29E-05	1.63E-04	0.156	0.0375	108.0
12	1.39E-08		77.75	3.23E-07	1.20E-05	1.75E-04	0.169	0.0344	106.4
13	1.71E-08		72.56	3.02E-07	1.12E-05	1.86E-04	0.180	0.0319	105.7
14	1.80E-08		71.15	2.96E-07	1.10E-05	1.97E-04	0.191	0.0292	98.7
15	1.99E-08		68.02	2.83E-07	1.05E-05	2.07E-04	0.202	0.0263	93.0
16	2.08E-08		66.73	2.78E-07	1.03E-05	2.18E-04	0.213	0.0249	89.7
17	2.14E-08		65.65	2.73E-07	1.01E-05	2.28E-04	0.223	0.0243	89.0
18	2.40E-08		61.49	2.56E-07	9.47E-06	2.37E-04	0.233	0.0226	88.4
19	2.53E-08		59.37	2.47E-07	9.15E-06	2.46E-04	0.242	0.0216	87.5
20	2.85E-08		54.27	2.26E-07	8.36E-06	2.55E-04	0.251	0.0194	85.9

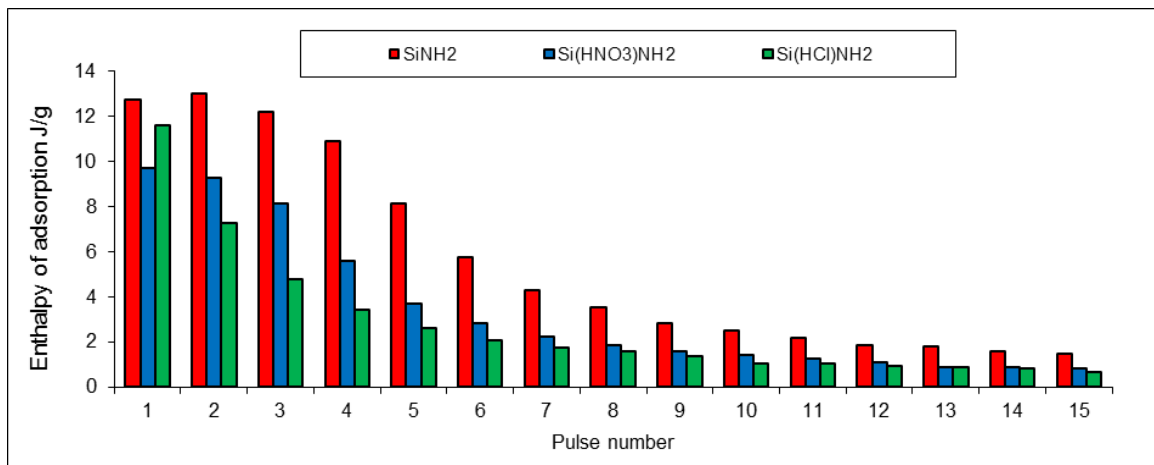


**6- A comparison between three different catalysts by using flow adsorption calorimetry.**

Amount of SO<sub>2</sub> adsorbed by the catalysts



The enthalpy of adsorption of SO<sub>2</sub> for the catalysts

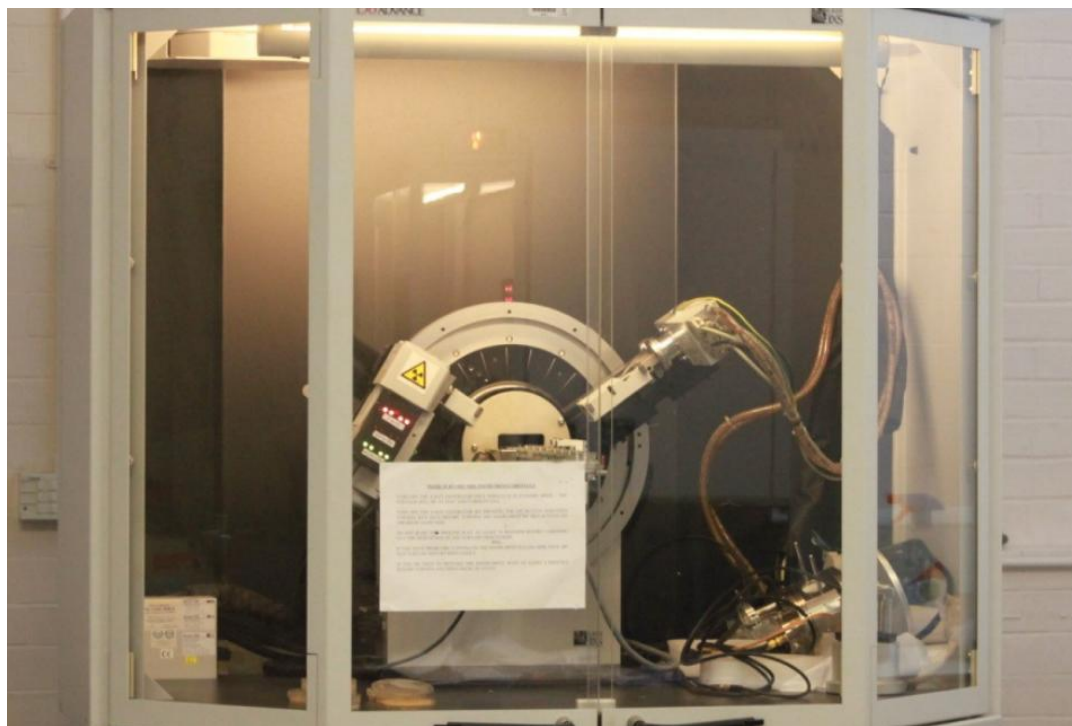


## 7- Powder X-ray Diffraction Bruker D8

### a) Operating conditions

- Operating conditions: 40 kV, 20 mA using nickel-filtered Cu K $\alpha$  radiation (1.5406 Å)
- Scan Axis 2 theta
- Start 1.5 and stop 10°
- Step size : 0.02
- No. of steps : 3250
- Time/step : 1
- Total scan : 0:54:11

### b) XRD –Equipment Bruker D8



## 8- Nitrogen Adsorption : Micrometrics ASAP 2020

This method was used to measure BET surface area, pore volume and pore diameter of the catalyst. The analysis was run at 77 K or -196 °C.

### Micrometrics ASAP 2020



## Appendixes

b) Surface area report on catalyst MCM-41-NH<sub>2</sub> is shown below

---

<b>Full Report Set</b>			
ASAP 2020 V3.00 H	Unit 1	Serial #: 517	Page 1
Sample: SiNH2			
Operator:			
Submitter:			
File: C:\2020\001-081.SMP			
Started: 23/10/2011 12:01:23PM		Analysis Adsorptive: N2	
Completed: 23/10/2011 20:26:34PM		Analysis Bath Temp.: 77.261 K	
Report Time: 03/05/2012 18:19:46PM		Thermal Correction: No	
Sample Mass: 0.2116 g		Warm Free Space: 28.6127 cm <sup>3</sup> Measured	
Cold Free Space: 87.6621 cm <sup>3</sup>		Equilibration Interval: 10 s	
Low Pressure Dose: None		Automatic Degas: Yes	

### Summary Report

#### Surface Area

Single point surface area at  $p/p^0 = 0.200166593$ : 357.2640 m<sup>2</sup>/g

BET Surface Area: 388.6869 m<sup>2</sup>/g

Langmuir Surface Area: 554.6802 m<sup>2</sup>/g

t-Plot External Surface Area: 449.9709 m<sup>2</sup>/g

BJH Adsorption cumulative surface area of pores  
between 17.000 Å and 3000.000 Å width: 477.297 m<sup>2</sup>/g

BJH Desorption cumulative surface area of pores  
between 17.000 Å and 3000.000 Å width: 531.5192 m<sup>2</sup>/g

#### Pore Volume

Single point adsorption total pore volume of pores  
less than 820.096 Å width at  $p/p^0 = 0.975813598$ : 0.565778 cm<sup>3</sup>/g

t-Plot micropore volume: -0.037996 cm<sup>3</sup>/g

BJH Adsorption cumulative volume of pores  
between 17.000 Å and 3000.000 Å width: 0.585571 cm<sup>3</sup>/g

BJH Desorption cumulative volume of pores  
between 17.000 Å and 3000.000 Å width: 0.583135 cm<sup>3</sup>/g

#### Pore Size

Adsorption average pore width (4V/A by BET): 58.2246 Å

BJH Adsorption average pore width (4V/A): 49.074 Å

BJH Desorption average pore width (4V/A): 43.884 Å